TABLE OF CONTENTS

Table of contents I

List of symbols, abbreviations and units VII

Introduction 1

Chapter 1
THEORETICAL DESCRIPTION AND MODELLING OF HEAT, WATER VAPOUR AND CO_2-FLUXES IN FOREST ECOSYSTEMS 7

1.1 Theoretical description of heat, water vapour and CO_2-exchange 7
1.1.1 Water vapour, heat and CO_2-exchange at leaf level 8
1.1.1.1 Leaf transpiration rate 8
1.1.1.2 Heat exchange at leaf level 12
1.1.1.3 Leaf photosynthesis rate 13
The CO_2 response curve 13
The photosynthesis-light response curve (LRC) 19
1.1.2 Momentum, water vapour, heat and CO_2-exchange at canopy level 21
1.1.2.1 Physics of turbulent transfer 21
Momentum transfer 22
Transfer of latent heat 25
Transfer of sensible heat 27
Transfer of CO_2 28
1.1.2.2 Atmospheric stability 29
Stability conditions 29
Flux-profile relationships in non-neutral conditions 32
1.1.2.3 The Bowen ratio 34
1.1.2.4 The Penman-Monteith model for actual evapotranspiration 36
1.1.2.5 The decoupling coefficient 42
1.2 Modelling of CO_2- and water vapour exchange: the FORUG-model 44
1.2.1 Multi-layer CO_2-exchange 45
1.2.1.1 Submodel solar elevation 45
1.2.1.2 Submodel diffuse and direct incident short-wave radiation 47
1.2.1.3 Submodel diffuse and direct incoming PAR 48
1.2.1.4 Submodel LAI of sunlit and shaded leaves 48

1.2.1.5 Submodel extinction coefficient 49
1.2.1.6 Submodel LAI-evolution 50
1.2.1.7 Submodel PAR interception 52
1.2.1.8 Submodel leaf photosynthesis: the CO_2 response curve 54
Temperature dependence 54
Seasonal variation 54
Leaf photosynthesis 55
1.2.1.9 Submodel leaf photosynthesis: the light response curve 57
Temperature dependence of A_{max} 57
Seasonal variation 58
Leaf photosynthesis 58
1.2.1.10 Submodel leaf respiration 60
1.2.1.11 Canopy photosynthesis 61
1.2.1.12 Submodel woody biomass respiration 61
1.2.1.13 Submodel soil respiration 63
1.2.1.14 Net CO_2-exchange of the forest 64
1.2.2 Single-layer water vapour exchange 64
1.2.2.1 General input parameters 65
Virtual temperature, $T_{v,K}$ 65
Atmospheric pressure, P_{atm} 65
Density of the air, $\boldsymbol{r}_a$ 66
Actual vapour pressure, e_a 66
Saturated vapour pressure, e_s 66
Slope of the saturation water vapour pressure curve, D 66
The latent heat of evaporation, l 67
1.2.2.2 Heat inputs 67
Net radiation 67
Soil heat flux 69
1.2.2.3 Physiological inputs 69
Canopy resistance 69
Leaf area index 71
1.2.2.4 Interception of rain 71
1.2.3 Multi-layer water vapour exchange 74
1.2.3.1 Introduction of a net radiation profile 74
1.2.3.2 Resistances and conductances at different layers 75
Leaf boundary layer resistance 75
Soil boundary layer resistance 76
Stomatal conductance 76
Soil resistance 79
1.2.3.3 Interception of rain 79
1.2.3.4 Total multi-layer evapotranspiration 80
1.2.4 Overall structure of the FORUG model 81

Chapter 2
THE EXPERIMENTAL SET-UP IN THE FOREST AELMOESENEIE 85

2.1 Characteristics of the experimental forest 85
2.1.1 Location and history 85
2.1.2 Biotic and abiotic characteristics 87
2.1.2.1 The scientific zone 87
2.1.2.2 The oak-beech forest site 88
2.1.2.3 The ash forest site 90
2.2 The measuring tower, sensors and data acquisition 92
2.2.1 The measuring tower 92
2.2.2 Sensors 94
2.2.2.1 Radiation and soil heat flux 94
2.2.2.2 Temperature 96
2.2.2.3 Wind speed and wind direction 97
2.2.2.4 Precipitation 99
2.2.2.5 Humidity 101
2.2.2.6 Soil water 101
2.2.3 Data acquisition and data editing 102
Appendix to Chapter 2 105

Chapter 3
EXPERIMENTAL DETERMINATION OF THE ACTUAL EVAPOTRANSPIRATION IN THE FOREST AELMOESENEIE 107

3.1 Sap flow dynamics of upperstory and understory species 110
3.1.1 Introduction 110
3.1.2 Material and methods 111
3.1.2.1 Sap flow measurements with the thermal dissipation technique 111
3.1.2.2 Sap flow measurements with the stem heat balance method 114
3.1.3 Results and discussion 122
3.1.3.1 Seasonal sap flow dynamics 122
3.1.3.2 Daytime and nighttime sap flow 125
3.1.3.3 Effect of vapour pressure deficit on sap flow 130
3.2 Hydraulic conductance of the upperstory and understory species 135
3.2.1 Introduction 135
3.2.2 Material and methods 137
3.2.2.1 Measurement of leaf water potential 137
3.2.2.2 Calculation of hydraulic and stomatal conductance 139
3.2.3 Results and discussion 140

3.2.3.1 Diurnal pattern of leaf water potential and sap flow....140
3.2.3.2 Diurnal patterns of hydraulic conductance....143
3.2.3.3 Relation between hydraulic and stomatal conductance....144
3.3 Water storage in stems and branches....148
3.3.1 Introduction....148
3.3.2 Material and methods....149
3.3.3 Results and discussion....150
3.4 Upscaling from single tree to stand level....156
3.4.1 Introduction....156
3.4.2 Material and methods....157
3.4.2.1 Determination of the sapwood cross-sectional area of single trees....157
3.4.2.2 Sapwood area as a scaling factor....159
3.4.2.3 Leaf area index as a scaling factor....160
3.4.2.4 Time integration....161
3.4.3 Results and discussion....162
3.4.3.1 Comparison of both upscaling methods....162
3.4.3.2 Monthly water loss....166
3.4.3.3 Annual water loss....167
3.5 Energy balance storage terms and big-leaf evapotranspiration in a mixed deciduous forest....172
3.5.1 Introduction....172
3.5.2 Materials and Methods....173
3.5.2.1 Heat storage calculation....173
Latent and sensible heat storage....173
Soil heat storage....174
Heat storage in the vegetation....174
Photosynthetic heat capacity....175
3.5.2.2 Forest evapotranspiration....175
3.5.2.3 Measurement period....176
3.5.2.4 Measurement of surface temperature....176
3.5.3 Results and discussion....177
3.5.3.1 Diurnal behaviour of storage components....177
3.5.3.2 Daily and daytime pattern of heat storage....184
3.5.3.3 Seasonal pattern of storage....185
3.5.3.4 Storage and big leaf evapotranspiration....187
3.6 Estimation of the latent heat flux at stand level with the Bowen ratio method
3.6.1 Introduction....190
3.6.2 Material and methods....192
3.6.2.1 Micro-meteorological measurements, instrumentation and data collection....192
3.6.2.2 Theoretical background....193
3.6.2.3 Data analysis....196

3.6.3 Results and discussion....196
3.6.3.1 Data analysis....196
3.6.3.2 Estimation of the latent heat flux....198
3.6.3.3 Comparison between latent heat fluxes obtained from Bowen ratio and sap flow measurements....202

CHAPTER 4
MODELLING APPROACH TO THE ACTUAL EVAPOTRANSPIRATION

4.1 Forest canopy conductance and leaf conductance inverted from sap flow measurements of upperstory and understory species....209
4.1.1 Introduction....209
4.1.2 Material and Methods....210
4.1.2.1 Calculation of canopy and leaf conductance....210
4.1.2.2 The canopy conductance and leaf conductance submodel....213
4.1.3 Results and discussion....215
4.1.3.1 Effects of radiation, vapour pressure deficit and temperature on canopy conductance....215
4.1.3.2 Effects of radiation, vapour pressure deficit and temperature on stomatal conductance....220
4.1.3.3 Stomatal control of transpiration....223
4.2 Comparison of a single-layer and a multi-layer model approach for the calculation of forest evapotranspiration....227
4.2.1 Introduction....227
4.2.2 Methodology....228
4.2.2.1 The single-layer evapotranspiration model....228
4.2.2.2 The multi-layer evapotranspiration model....229
4.2.2.3 Parameterisation of the models....229
4.2.2.4 Estimation of zero plane displacement and roughness length....232
4.2.2.5 Calculation of reference crop evapotranspiration....234
4.2.2.6 Sensitivity analysis....235
4.2.3 Results and discussion....236
4.2.3.1 Estimation of aerodynamic resistance....236
4.2.3.2 Model validation....238
4.2.3.3 Model sensitivity....238
4.2.3.4 Model predictions....241
4.2.3.5 Model results in comparison with literature data....246

General conclusions and research perspectives.....249

Summary.....257

Samenvatting 261

References.....265

Curriculum vitae 287

Chapter 1
THEORETICAL DESCRIPTION AND MODELLING OF HEAT, WATER VAPOUR AND CO_2-FLUXES IN FOREST ECOSYSTEMS

Forests are complex ecosystems, playing a very important role in large scale biogeochemical cycles. As a consequence, a major focus of contemporary ecological research is the understanding of how the carbon, water and nutrient cycles of forest ecosystems respond to environmental and climatic perturbations (Dixon et al., 1990; Agren et al., 1991; Running & Hunt, 1993; McMurtrie & Wang, 1993). One research approach can be the measurement of the overall exchanges of carbon, water and nutrients between the forest and the atmosphere. This is often done using micro-meteorological techniques, such as the eddy covariance method (Verma et al., 1986; Fan et al., 1990; Wofsy et al., 1993; Hollinger et al., 1994; Baldocchi & Harley, 1995; Goulden et al., 1996; Lee et al., 1996; Baldocchi, 1997; Shurpali & Ceulemans, 1997) and the flux-profile method (Rosenberg et al., 1983; Denmead & Raupach, 1993; Vermetten et al., 1994; Bosveld, 1997). The output obtained this way is an integrated response of all biotic and abiotic stresses working on the system. A major drawback, however, is that the knowledge of the overall exchange does not explain the underlying physiological processes. Therefore, in addition to the overall fluxes between vegetation and atmosphere, also intra-canopy fluxes should be described in order to understand the physiological control mechanisms. Knowledge of the intra-canopy fluxes allows modelling of the canopy processes starting from the lower level of ecosystem organisation (on leaf level).
In this chapter, first the H_2O- and CO_2-fluxes in a deciduous forest will be described on both leaf and canopy scale. Then this knowledge will be incorporated in a multi-layer and process based model to simulate these H_2O- and CO_2-fluxes in a deciduous forest.

1.1 Theoretical description of heat, water vapour and CO_2-exchange

In this part the fundamental background of the exchange of H_2O and CO_2 between

vegetation and atmosphere will be described. A distinction will thereby be made between two different space-time scales i.e. the leaf and the canopy level.
The exchange of H_2O (transpiration) at leaf level will be explained in terms of the electric analogon concept. The CO_2-exchange at the leaf level will be described by means of the classical light response curve, and by the more recent, and the nowadays more widespread Farquhar approach (Farquhar et al., 1980). In the FORUG model, which will be described in a second part of this chapter, light response curves are actually used to calculate CO_2 exchange. However, it is the aim, later, to calculate CO_2 exchange according to the Farquhar approach, or to let the user of the model choose, depending on the available data.
The exchange processes at the canopy level will, on the other hand, be described using transport equations for H_2O and CO_2. Based on these flux-profile methods the Bowen ratio will be explained as well. The role of atmospheric stability on the exchange between the vegetation and the atmosphere will be elucidated. Next the Penman-Monteith concept (Monteith, 1965) for canopy evapotranspiration will be clarified, and important parameters for this approach, e.g. surface temperature and canopy resistance, will be analysed.
It is important to remark that the physical processes explained in this chapter are not only applicable to forests, but to other kinds of vegetation as well.

1.1.1 Water vapour, heat and CO_2-exchange at leaf level

1.1.1.1 Leaf transpiration rate

The exchange of heat, water and CO_2 between living organisms (plants and animals) is subject to molecular diffusion processes through a thin skin of air (boundary layer), surrounding each object and organism. This boundary layer defines the region between object and surrounding where the velocity of the flow is between 0 and 99 % of its value in the free stream. However, it is more convenient to work with and average boundary layer depth with an average constant stream velocity. When the streamlines of flow are almost parallel to the surface, then the layer is said to have a laminar flow. When the flow becomes unstable and breaks down to a chaotic pattern of swirling motions, the boundary layer is said to be turbulent.
Boundary layers are also occurring on a larger and regional level, like a meadow, a forest or a city. Even our atmosphere is in fact one enormous boundary layer (the planetary boundary layer). So, more generally spoken, boundary layers can be considered as regions with a specific micro- or macro-climate. This specific climate, as

well as the thickness and behaviour of the boundary layer, depends strongly on the physical properties of the system (e.g. leaf dimension, roughness of the forest,…).
The thickness of the boundary layer depends on several factors such as velocity of the air movement, the viscosity and temperature of the air, the roughness of the surface and the length of the object or organism in the direction of airstream.
Figure 1.1 shows the development of a laminar boundary layer over a smooth flat surface immersed in a moving fluid (i.e. a gas or liquid). The thickness of a laminar boundary layer cannot increase indefinitely because the flow becomes unstable and breaks down to a turbulent boundary layer.

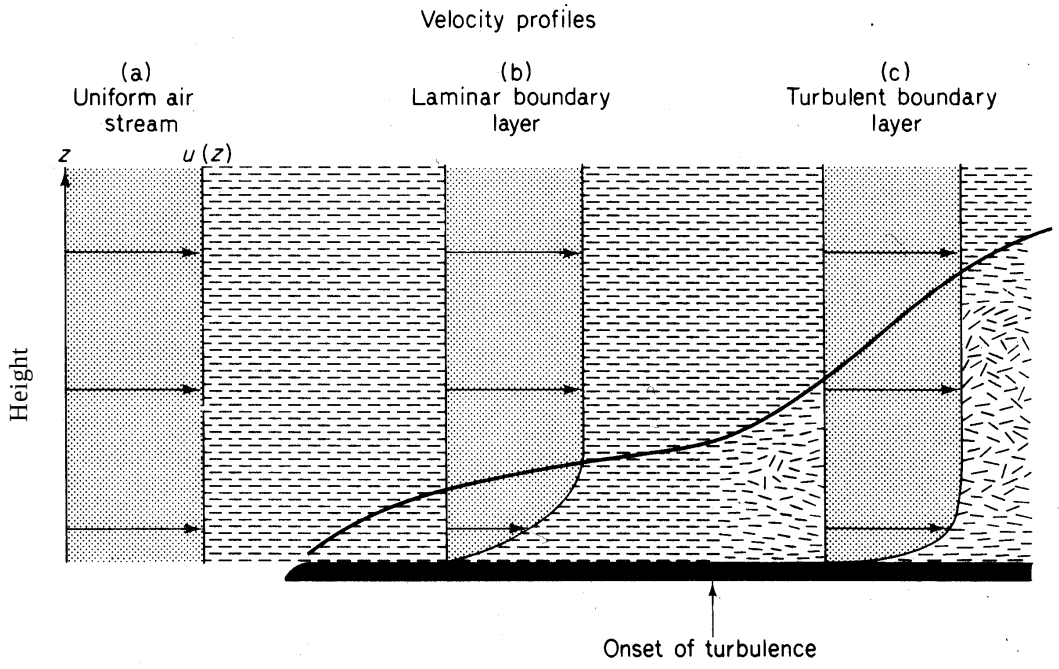

Figure 1.1 Development of laminar and turbulent boundary layers over a smooth flat plate. The vertical scale is greatly exaggerated. (from Monteith, 1973)

Molecular diffusion of heat, water vapour or CO_2 through the laminar boundary layer is very slow compared to turbulent diffusion, the difference being a magnitude of 10^5. The boundary layer surrounding the object or organism causes a very high resistance for molecular diffusion of matter and energy through the boundary layer. One can say there is a resistance to molecular diffusion, its resistance r_d, being defined as:

$$r_d = \frac{\text{pathlength for diffusion}}{\text{diffusion coefficien t}} \qquad (1.1)$$

or

$$r_b = \frac{\text{thickness laminar boundary layer}}{\text{diffusion coefficien t}} \quad (1.2)$$

where r_b is the boundary layer resistance.
Diffusion coefficients ($m^2\ s^{-1}$) are well known for diffusion of water vapour, CO_2 and heat through air layers, but the diffusion length (the depth of the boundary layer) is more difficult to assess. Therefore approximation formulae are used for the calculation of the boundary layer resistance. In case of free convection (absence or very low air displacement), the boundary layer resistance for heat transfer r_h (s m^{-1}) can be defined as (Campbell, 1977):

$$r_h = 840\left(\frac{d_c}{|T_o - T_a|}\right)^{1/4} \quad (1.3)$$

where d_c is the characteristic dimension (m), and T_o and T_a are respectively the temperature of the object or organism and the air temperature, both expressed in °C. The characteristic dimension is equal to the length of the object or organism in the direction of the air stream (or the mean of length and width if the direction of air movement to the object cannot be specified).
Similarly, in case of forced convection r_h is defined as (Campbell, 1977):

$$r_h = 307\sqrt{\frac{d_c}{u}} \quad (1.4)$$

with u the velocity of air movement (m s^{-1}).

A general way of stating Fick's Law of diffusion is:

$$\text{flux density} = \text{diffusion coefficien t} * (\text{concentrat ion gradient}) \quad (1.5)$$

This law can be applied to describe the water vapour transfer between leaves and the environment.

$$E = -D_v \frac{d\rho_v}{dz} \quad (1.6)$$

where E is the flux density of water vapour (g m^{-2} s^{-1}), D_v is the diffusion coefficient of

water vapour or 0.242 10^{-4} m^2 s^{-1} at 20°C, r_v the vapour density (g m^3) and z the distance (m). When the flux density E is constant in the vertical z-direction, Equation 1.6 can be integrated between the distances z_1 and z_2:

$$E = -\frac{D_v}{z_2 - z_1}\left[r_v(z_2) - r_v(z_1)\right] \qquad (1.7)$$

or

$$E = \frac{r^o(T_l) - r_v}{r_v} \qquad (1.8)$$

when z_1 is chosen to be a leaf surface where the water vapour density is assumed to be saturated at the leaf temperature T_l. Further, is $r°(T_l)$ the saturated vapour density at leaf temperature T_l, expressed in g water vapour per m^3 of air in the substomatal cavity, r_v the vapour density outside the boundary layer and r_v the resistance for water vapour transport from the inside of the leaf to outside the boundary layer (s m^{-1})(Figure 1.2). This relation is analogue to Ohm's law in electricity, which states that the electrical resistance of a wire is equal to the potential difference between its ends divided by the current flowing through it: i.e.

current = potential difference / resistance (1.9)

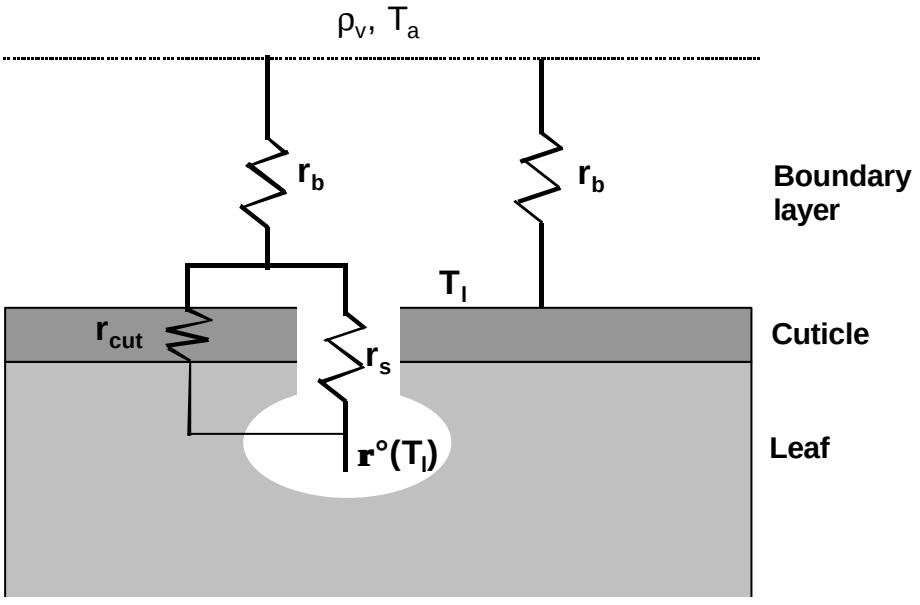

Figure 1.2 Schematic representation of resistances and parameters influencing the sensible and the latent heat exchange between a leaf and the atmosphere. Symbols are T_l:

temperature of the leaf; T_a temperature of the air outside the leaf boundary layer; r_b: leaf boundary layer resistance; r_s: stomatal resistance; r_{cut}: cuticular resistance; r_v: vapour density of the air and $r°(T_l)$:saturated vapour density at leaf temperature.

Indeed, the numerator of Equation 1.8 can be considered as a potential difference, being the difference in vapour density between substomatal cavities inside the leaf and the air outside the boundary layer. The denominator represents the inhibition of the water vapour diffusion by a resistance. This resistance is a combination of a stomatal and a boundary layer resistance. To sum up serial (in this case) or parallel resistances, the same rules as in electricity have to be followed. The calculation of the leaf resistance can be rather complex. If stomata are occurring at both sides of the leaf, and cuticular resistance cannot be neglected, the leaf resistance can be calculated as:

$$r_v = \left(\frac{1}{\left(\frac{1}{r_{s,u}} + \frac{1}{r_{cut,u}} \right)^{-1} + r_h} + \frac{1}{\left(\frac{1}{r_{s,l}} + \frac{1}{r_{cut,l}} \right)^{-1} + r_h} \right)^{-1} \qquad (1.10)$$

with r_s and r_{cut} stomatal and cuticular resistance (s m^{-1}) respectively. The subscripts *u* and *l* denote the upper (adaxial) and lower (abaxial) side of the leaf. In deciduous trees stomata only occur on the lower epidermis (Jones, 1992). Because the diffusion coefficients of water vapour and heat are comparable, the boundary layer resistance for water vapour and heat transfer may be assumed identical (see Jones, 1992).

Another commonly used formula to express the transpiration rate of leaves, is based on the vapour pressure gradient between the saturated air in the substomatal cavities and the air outside the boundary layer:

$$lE = \frac{\rho_a . c_p}{g} \frac{e_s(T_l) - e_a}{r_v} \qquad (1.11)$$

where $e_s(T_l)$ is the saturated vapour pressure (hPa) at leaf temperature (°C), e_a is the vapour pressure (hPa) of the air measured outside the boundary layer, ρ_a the density of the air (1.204 kg m^{-3}), c_p the specific heat of the air at constant pressure (1010 J kg^{-1} $°C^{-1}$), g the psychrometer constant (0.662 hPa $°C^{-1}$), and lE is expressed in W m^{-2}.

1.1.1.2 Heat exchange at leaf level

Fick's Law of diffusion (Equation 1.5) can also be applied to describe the heat transfer between leaves and the environment

$$H = -D_H \frac{d(\rho_a c_p T)}{dz} \quad (1.12)$$

where H is the flux density of sensible heat (W m^{-2}), D_H is the diffusion coefficient for heat or 0.215 10^{-4} m^2 s^{-1} at 20°C and T is temperature (°C). When the flux H is constant in the vertical z-direction, the above formula can be integrated between the distances z_1 and z_2:

$$H = -\frac{D_H}{z_2 - z_1}\left[\rho_a c_p T_2 - \rho_a c_p T_1\right] \quad (1.13)$$

or

$$H = \rho_a c_p \frac{T_l - T_a}{r_h} \quad (1.14)$$

when z_1 is chosen to be a leaf surface at leaf temperature T_l (Figure 1.2).

1.1.1.3 Leaf photosynthesis rate

The rate of photosynthetic carbon assimilation is determined by both the supply and demand for CO_2. The supply of CO_2 to the chloroplast is governed by diffusion in both the gas and liquid phases. This process can be limited at several points along the pathway from the air surrounding the leaf to the sites of carboxylation inside. The demand for CO_2 is determined by the rate of CO_2 processing in the chloroplasts, being influenced by the structure and biochemistry of the chloroplast, by environmental factors such as irradiance, and by plant factors that affect the demand for carbohydrates. Limitations imposed by either supply or demand will regulate the overall rate of carbon assimilation.

The CO_2 response curve

The response of photosynthesis rate to CO_2 concentration is the principal tool to analyse the demand for CO_2 (Farquhar & Sharkey, 1982)(Figure 1.3). The graph giving CO_2 assimilation (A) as a function of intercellular CO_2 partial pressure (p_i) is generally referred to as the A-p_i curve (or A-c_i when CO_2 concentration is expressed as mole

fraction of CO_2 in air). There is no net CO_2 uptake until the production of CO_2 in respiration (mainly photorespiration, but also maintenance or dark respiration that occurs in the light) is fully compensated by the fixation of CO_2 in photosynthesis. The CO_2 pressure at which this is reached is called the CO_2-compensation point (*G*).

Two separate regions of the CO_2 response curve above the compensation point can be distinguished. At low p_i, which is below values normally found in leaves (approximately 25 Pa), photosynthesis increases steeply with increasing partial pressure of CO_2. This is the region where CO_2 limits the rate of functioning of the Rubisco enzyme, whereas RuBP is present in saturating quantities (RuBP-saturated or CO_2-limited region). This part of the A-p_i curve is quantified by the initial slope and is also referred to as the carboxylation efficiency. At light saturation and with a fully activated enzyme, the initial slope governs the carboxylation capacity of the leaf, which in turn depends on the amount of active Rubisco.

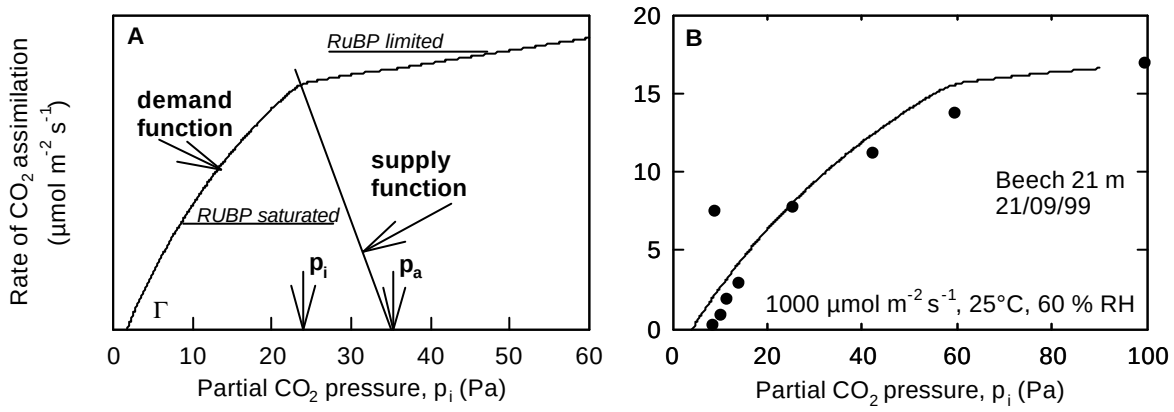

Figure 1.3 The relationship between the rate of CO_2 assimilation and the partial pressure of CO_2 in the intercellular spaces, p_i, represented as a "demand function": (left) a typical theoretical response, (right)(from Vande Walle et al., 2000) a measured response for a beech leaf at a canopy height of 21 m, measured on 21 September 1999. The measurement conditions are shown in the graph. The dots indicate measurements, whereas the line represents the fitted relationship. *G* represents the CO_2-compensation point. In the "linear" region at low values of p_i, the CO_2 concentration is limiting. At higher values of p_i, the concentration of CO_2 is saturating the activity of Rubisco, whereas the regeneration of ribulose-1,5-biphosphate (RuBP) limits carboxylation. The rate of diffusion of CO_2 from the atmosphere to the intercellular spaces is indicated by the "supply function". The slope of this corresponds with the leaf conductance. The intersection of the "supply function" with the "demand function" is the operating point and gives the actual rate of net CO_2 assimilation at a value of p_i that occurs in the leaf at the

value for p_a in the air.

In the regions of high p_i, the increase in A with rising p_i levels off. At this point CO_2 will no longer restrict the carboxylation reaction, but the rate at which the substrate RuBP becomes available will limit the activity of Rubisco (RuBP-limited region). This rate, in turn, depends on the activity of the Calvin cycle, which ultimately depends on the rate at which ATP and NADPH are produced in the light reactions. In this region, photosynthetic rates are limited by the rate of the electron transport. This may either be due to limitation by light or, at light saturation, by a limited capacity of electron transport. Even at a high p_i, being a situation where the rate of electron transport J no longer increases with increasing p_i, the rate of net CO_2 assimilation will continue to increase slightly. This is because the oxygenation reaction of Rubisco is increasingly suppressed with increasing partial pressure of CO_2 in favour of the carboxylation reaction. At the normal atmospheric partial pressures of CO_2 and O_2 (35 and 21000 Pa, respectively) and at a temperature of 20 °C, the ratio between the reaction constants for carboxylation and oxygenation is about 4:1

Based on known biochemical characteristics of Rubisco and the requirement of $NADPH_2$ and ATP for CO_2 assimilation, Farquhar & Von Caemmerer (1982) have developed a model of photosynthesis of C_3-plants. This model is now widely used in ecophysiological research and is introduced briefly here.

Net CO_2 assimilation rate A_n (µmol m^{-2} s^{-1}) is the result of the rate of carboxylation V_c (µmol m^{-2} s^{-1}) minus the losses by photorespiration and other respiratory processes. In photorespiration, one CO_2 is produced per two oxygenation reactions (V_o in µmol m^{-2} s^{-1}). The rate of dark respiration during photosynthesis may differ from normal dark respiration (night respiration) and is called 'day respiration' R_{day} (µmol m^{-2} s^{-1}). Hence:

$$A_n = V_c - 0.5V_o - R_{day} \qquad (1.15)$$

CO_2-limited and O_2-limited rates of carboxylation and oxygenation can be described with standard Michaelis-Menten kinetics. However, when both substrates are present they will inhibit each other competitively. An effective Michaelis-Menten constant of Rubisco for the carboxylation reaction K' (µmol mol^{-1}) that takes into account competitive inhibition by O_2 is described as:

$$K' = K_c\left(1 + \frac{O}{K_o}\right) \qquad (1.16)$$

where K_c and K_o are respectively the Michaelis-Menten constants for the carboxylation and oxygenation reaction. Both are expressed in Pa, and O is the partial pressure of

oxygen (0.21 mol mol^{-1}).
The rate of carboxylation in the CO_2-limited part of the CO_2-response curve can then be described as:

$$V_c = \frac{V_{c\,\max}\ p_i}{p_i + K_m} \tag{1.17}$$

where $V_{c\ max}$ (µmol m^{-2} s^{-1}) is the rate of CO_2 assimilation at saturating intercellular partial pressure of CO_2 (p_i). The specificity of Rubisco for CO_2 relative to O_2 ($S_{c/o}$) is remarkably similar among higher plants (Lambers et al., 1998). Increasing temperature, however, decreases the specificity, because K_o decreases faster with increasing temperature than K_c does.

The CO_2-compensation point in the absence of R_{day} (Γ^*) is determined experimentally and used to calculate the rates of carboxylation and oxygenation from photosynthesis rates using:

$$\frac{V_o}{V_c} = \frac{2\Gamma^*}{p_i} \tag{1.18}$$

In the RuBP-limited part of the CO_2-response curve, the rate of electron transport J is constant. Increasing the partial pressure of CO_2 increases the rate of carboxylation at the expense of the rate of oxygenation. There is a minimum requirement of four electrons per carboxylation or oxygenation reaction. Hence, the minimum J required for particular rates of carboxylation and oxygenation is:

$$J = 4(V_c + V_o) \tag{1.19}$$

Using Equations 1.18 and 1.19, the rate of carboxylation can be expressed as:

$$V_c = \frac{J}{4\left(1 + \frac{2\Gamma^*}{p_i}\right)} \tag{1.20}$$

The CO_2-limited and RuBP-saturated rate of photosynthesis $A_n(c)$ (µmol m^{-2} s^{-1}) can then be calculated using Equations 1.15, 1.17 and 1.18 as:

$$A_n(c) = \frac{V_{c\,\max}(p_i - \Gamma^*)}{p_i + K_m} - R_{day} \tag{1.21}$$

The RuBP-limited rate of photosynthesis $A_n(j)$ (µmol m^{-2} s^{-1}) can be calculated using Equations 1.15, 1.18 and 1.20 as:

$$A_n(j) = \frac{J(p_i - \Gamma*)}{4(p_i + 2\Gamma*)} - R_{day} \quad (1.22)$$

The minimum of the Equations 1.21 and 1.22 describes the full CO_2-response curve:

$$A_n = \min\{A_n(c), A_n(j)\} \quad (1.23)$$

Parameter values for the preceding formulas are normally given for an air temperature of 25 °C. Values for other temperatures can be determined from the temperature dependence of the parameter values. The following relations are derived from Farquhar & Von Caemmerer (1982), Kirshbaum & Farquhar (1984), Brooks & Farquhar (1985), and Von Caemmerer et al. (1994).

$$K_c = K_c(25)\exp^{59356x}$$
$$K_o = K_o(25)\exp^{35948x} \quad (1.24)$$

where $K_c(25)$ and $K_o(25)$ are respectively 40.4 and 24800 Pa, and

$$x = 0.000404\frac{T - 25}{T + 273} \quad (1.25)$$

where T is temperature (ideally leaf temperature otherwise air temperature) in °C.
The CO_2-compensation point at 25 °C equals 3.7 Pa, and

$$\Gamma* = \Gamma*(25) + 0.188(T - 25) + 0.0036(T - 25)^2 \quad (1.26)$$

$$V_{c\max} = V_{c\max(25)}\left[1 + 0.0505(T - 25) - 0.248\cdot10^{-3}(T - 25)^2 - 8.09\cdot10^{-5}(T - 25)^3\right] \quad (1.27)$$

$$J_{\max} = J_{\max(25)}\left[1 + 0.0409(T - 25) - 1.24\cdot10^{-3}(T - 25)^2 - 9.42\cdot10^{-5}(T - 25)^3\right] \quad (1.28)$$

The above values and temperature relations for K_o, K_c, and $\Gamma*$ do not vary much between species and growth conditions, but the temperature dependence of V_{cmax}, and particularly J_{max}, may vary considerably (Lambers et al., 1998). Electron-transport rate varies due to variation in irradiance. Harley et al. (1992) used, to describe

photosynthesis of cotton, the following relation to assess the electron transport rate J (µmol m^{-2} s^{-1}):

$$J = \frac{\alpha_F I}{\left(1 + \frac{\alpha_F{}^2 I^2}{J_{max}{}^2}\right)^{0.5}} \qquad (1.29)$$

where α_F (-) is the curvature of the response of electron transport to irradiance, and I is the intercepted photosynthetically active radiation (PAR)(µmol m^{-2} s^{-1}).
Plants typically operate at a p_i where CO_2 and electron transport co-limit the rate of CO_2 assimilation. This is the point where the RuBP-saturated and the RuBP-limited part of the CO_2-respons curve intersect. This allows effective utilisation of all components of the light and dark reactions.

In contrast with the biochemical approach, the rate of supply of CO_2 to the chloroplast can also be considered as a physical process of diffusion ("supply function" in Figure 1.3).
Hence, as was also done above for the case of leaf transpiration, the rate of CO_2 assimilation (A_n) can also be described by Fick's law, and equals the rate of CO_2 diffusion into the leaf (Figure 1.4). Hence:

$$A_n = \frac{c_a - c_i}{r_{CO2}} = g_{CO2}\frac{p_a - p_i}{P} \qquad (1.30)$$

where r_{CO2} is the total resistance for CO_2 transport, c_a and c_i are the mole or volume fractions of CO_2 in the atmosphere and the intercellular spaces respectively, g_{CO2} is the total conductance for CO_2 transport and the inverse of r_{CO2}, p_a and p_i are respectively the partial pressures of CO_2 in the atmosphere and the intercellular spaces, and P is the atmospheric pressure. The total resistance for CO_2 transport is composed of several components which can be added:

$$r_{CO2} = r_{b,CO2} + r_{s,CO2} \qquad (1.31)$$

where $r_{b,CO2}$ and $r_{s,CO2}$ are respectively the boundary layer and stomatal resistance for CO_2 transport; both resistances being expressed in s m^{-1}. The resistance for CO_2 transport is thus a similar concept as was done for water vapour transport, but now taking into account the different diffusion coefficients of both molecules. The ratio of the diffusion coefficients for H_2O and CO_2 diffusion in air is approximately 1.6. The smaller water molecule indeed diffuses more rapidly than CO_2. This value refers only to the

movement of CO_2 inside the leaf and through the stomata. For the boundary layer above the leaf, where both turbulence and diffusion influence the flux, the ratio is approximately 1.37. An internal resistance, r_i, also influences the transport of CO_2 from the substomatal cavity to the chloroplast. The internal resistance varies widely between species and is a complicated trait related to morphological and biochemical aspects that involve diffusion of CO_2 in the gas phase, dissolving of CO_2 in the liquid phase, and conversion of CO_2 into HCO_3^- catalysed by carbonic anhydrase and diffusion in the liquid phase.

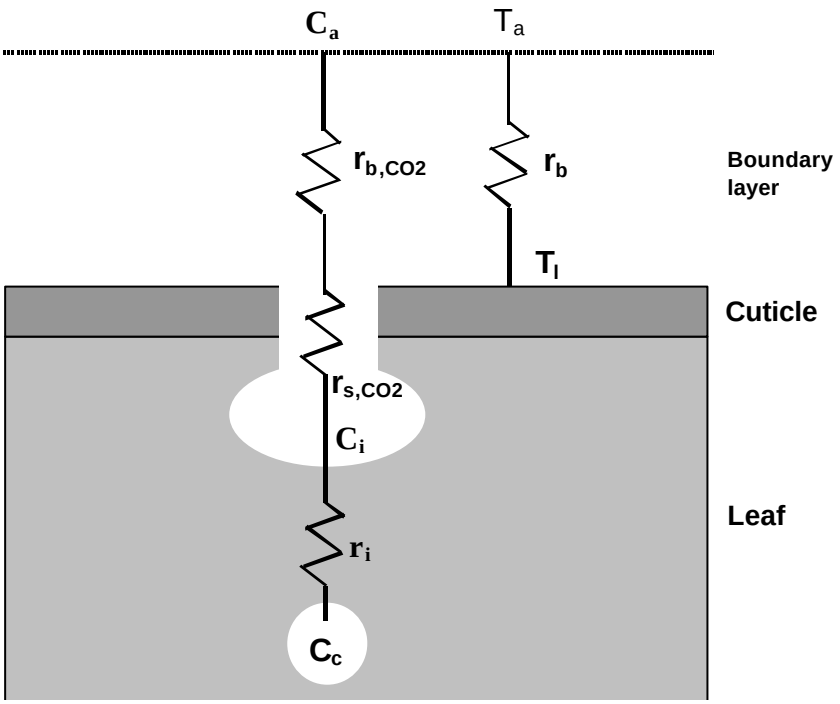

Figure 1.4 Schematic representation of resistances and parameters influencing the sensible heat and the CO_2 exchange between a leaf and the atmosphere. Symbols are c_i, c_a, c_c: mole fraction of CO_2 in the intercellular spaces, atmosphere and chloroplast respectively; $r_{b,CO2}$ leaf boundary layer for CO_2 diffusion; $r_{s,CO2}$: stomatal resistance for CO_2; T_l: temperature of the leaf; T_a: temperature of the air outside the leaf boundary layer and r_b: leaf boundary layer resistance.

The photosynthesis-light response curve (LRC)

The level of irradiance is an important ecological factor on which all photoautotrophic plants depend. Only the photosynthetically active part of the spectrum (photosynthetically active radiation or PAR, wavelength interval 400 to 700 nm) directly drives photosynthesis. It is found that the rate of CO_2 assimilation increases asymptotically with increasing irradiance. Below the light compensation point I_c (LCP)(Figure 1.5), there is insufficient light to compensate for respiratory carbon dioxide release due to

photorespiration and dark respiration. At low light intensities, A_n increases linearly with irradiance, with the light driven electron transport limiting the photosynthetic assimilation. The initial slope of the light-response curve (LRC) is the quantum yield (α). This parameter describes the efficiency with which light is converted into fixed carbon. According to Lambers et al. (1998) the quantum yield for higher plants is typically about 0.06 moles CO_2 fixed per mole of quanta (under favourable conditions and for a normal atmospheric CO_2 concentration). At high irradiance, photosynthesis becomes light-saturated and is limited by the carboxylation rate, which is governed by some combination of limited CO_2 diffusion into the leaf and the carboxylation capacity or regeneration of the substrate. The shape of the LRC can be satisfactorily described by an exponential equation (Goudriaan, 1982)(Figure 1.5):

$$A_n = A_{\max}\left[1 - e^{\frac{-\alpha . I}{A_{\max}}}\right] - R_d \qquad (1.32)$$

where A_n is the net CO_2 assimilation rate (µmol m^{-2} s^{-1}), A_{max} is the light-saturated rate of gross CO_2 assimilation (net rate of CO_2 assimilation plus dark respiration) at infinitely high irradiance (µmol m^{-2} s^{-1}), α is the quantum yield (µmol CO_2 μmol^{-1} PAR), R_d is the dark respiration (µmol CO_2 m^{-2} s^{-1}), and I is the intercepted photon flux density (µmol PAR m^{-2} s^{-1}).

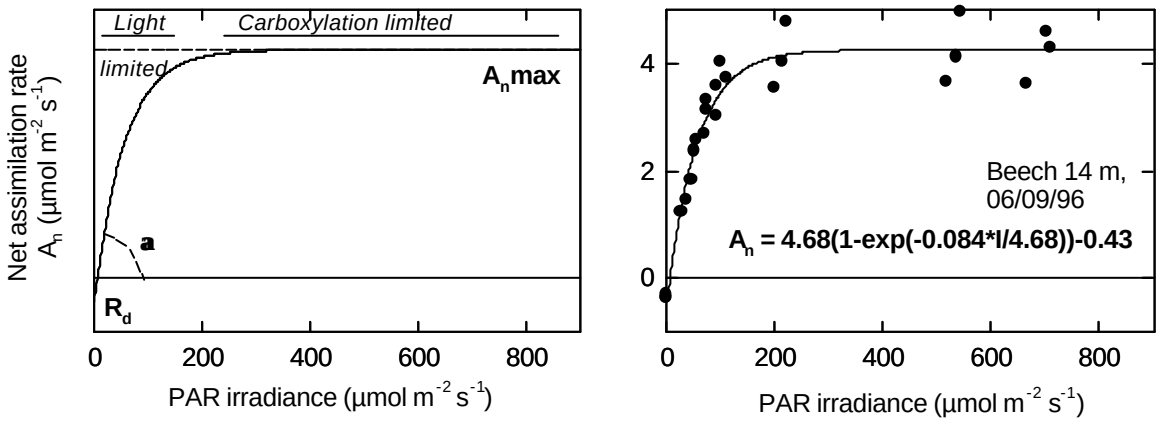

Figure 1.5 The relationship between the net rate of CO_2 assimilation (A_n) and the PAR irradiance intercepted by a leaf, called the light response curve (LRC): (left) a typical response of photosynthesis to irradiance as defined by Equation 1.32, and a measured response (right) for a beech leaf at a canopy height of 14 m, measured on 6 September 1996. The dots indicate measurements, whereas the

line represents the fitted LRC (r^2 = 0.95; n = 24). The initial slope of the curve gives the quantum yield (a), and the intercept with the vertical axis corresponds with the rate of dark respiration (R_d). The plateau value is the maximal net assimilation rate ($A_n max$), which is an indication of the assimilation potential of the leaf.

1.1.2 Momentum, water vapour, heat and CO_2-exchange at canopy level

In this part the exchange of water vapour, heat and CO_2 at canopy level will be described. First, the physics of turbulent transfer, based on the transport equations, will be considered. Based on this the flux-profile concept the Bowen ratio method will be explained as well. An other micro-meteorological method, i.e. the eddy covariance technique, will not be touched, as it will not be used in this study. The effective exchange of e.g. CO_2, heat and water vapour between the vegetation and the atmosphere is also influenced by the stability of the atmosphere. As such, the parameters qualifying this atmospheric stability will be described as well. Also, some attention will be given to footprint analysis, which allows evaluation of the quality and the source of the measured flux data.
Further the Penman and Penman-Monteith concept for actual evapotranspiration will be elucidated, including relevant parameters such as surface temperature and surface or canopy resistance. This theoretical description will focus on the exchange of water vapour, heat and CO_2 between a forest stand and the atmosphere, but most of this theory can also be applied to other atmospheric constituents and vegetation types.

1.1.2.1 Physics of turbulent transfer

Diffusion is the process by which constituents of a fluid (momentum, heat, water vapour) are transferred from one position to another within the fluid. Such transfers occur whenever there are differences in concentrations of the constituent in different parts of the fluid as expressed by Fick's law which was mentioned before. The rate of transfer of a constituent X in the direction z is directly proportional with the gradient of concentration of X in that direction:

$$F_z(X) = -D_x \frac{dC(X)}{dz} \qquad (1.33)$$

where $F_z(X)$ is the rate of transfer of X in the z-direction (m) expressed as a quantity per unit time and per unit area (called the flux density of X), $C(X)$ is the concentration of X, and D_x is the molecular diffusion coefficient of X in the fluid (m^2 s^{-1}). The diffusion

coefficient is here a characteristic of the flow, whereas for molecular diffusion the diffusion coefficient is a characteristic of the fluid.

Momentum transfer

When wind blows over a surface, the surface produces frictional drag and turbulence. Turbulent eddies carry latent (water vapour) and sensible heat, CO_2 and other atmospheric constituents. In order to quantitatively express the effectiveness of these, the vertical transfer of momentum must be examined. Momentum (*M*) equals a mass times a velocity. The concentration of momentum (momentum per unit volume) at any vertical level equals the mass density of the air times the velocity, as the mass density of the air can be considered constant in the lowest levels of the atmosphere, Equation 1.33 becomes:

$$F_z(M) = -\rho_a K_M \frac{du}{dz} \qquad (1.34)$$

where $F_z(M)$ is the flux density of momentum transfer expressed in kg m^{-1} s^{-2}, K_M (m^2 s^{-1}) is the turbulent diffusivity for momentum in turbulent air. As velocity always increases with height, the derivative *du/dz* is always positive. This is because frictional drag slows down the air movement near the ground. Consequently $F_z(M)$ is always negative, reflecting that momentum is being transferred downward from levels where velocities are higher to levels where they are lower. The physical significance of $F_z(M)$ is the horizontal shear stress τ due to differences of wind velocity at adjacent vertical levels.

The relation between wind speed and height can be expressed formally by the equation

$$u = a \ln\left(\frac{z-d}{z_0}\right) \qquad (1.35)$$

where *u* (m s^{-1}) is the wind velocity at height *z* above the ground surface, *d* (m) is the zero plane displacement, z_0 (m) is the roughness length, and *a* is a parameter with the dimensions of velocity. If the boundary is defined as a region in which τ is constant with height, and ρ_a is also constant, the product $K_m du/dz$ must be independent of *z*. But from Equation 1.35, *du/dz* is proportional to *a/(z-d)* so K_M must be proportional to *(z-d).* This is a fundamental feature of momentum transfer in a turbulent boundary layer, the coefficient of momentum transfer increases linearly with height above *d*. Now suppose

$$K_M = b(z - d) \tag{1.36}$$

where *b*, like *a*, is a parameter with the dimensions of velocity. Then Equation 1.34 becomes

$$\tau = \rho_a (ab) \tag{1.37}$$

The factor *(ab)* has the dimension of (velocity)^2 and is usually written as u_*^2 where u_* is called the friction velocity (m s^{-1}) because it is closely related to τ. The friction velocity is a measure of the effectiveness of turbulent eddies (considered as the velocity of the eddies). Both *a* and *b* must be proportional to u_* and if $a = u_*/k$ say, then $b = k\,u_*$. Substituting for *a* and *b* in Equation 1.37 gives:

$$\tau = \rho_a u_*^2 \tag{1.38}$$

which defines the friction velocity as

$$u_* = \sqrt{\frac{\tau}{\rho_a}} \tag{1.39}$$

Substituting for *a* in Equation 1.35; gives

$$u = \frac{1}{k} u_* \ln\left(\frac{z-d}{z_0}\right) \tag{1.40}$$

which is the conventional form of the wind profile for $z>d+z_0$, and where *k* is the dimensionless von Karman constant (0.41). A typical diurnal pattern of wind speed measured at several heights above the canopy of the forest Aelmoeseneie, and of the corresponding friction velocity is shown in Figure 1.6.

Equation 1.40 is known as the Prandtl-von Karman universal velocity distribution for turbulent flows. The zero plane displacement is an apparent reference height, and the roughness length expresses the aerodynamic roughness of the vegetation, and thus its ability for turbulent transfer of constituents (Jones, 1992). The plane at a height $d+z_0$ may be regarded as an apparent sink for momentum. Values of *d* and z_0 are approximately proportional to the average height of the roughness elements covering the ground surface, e.g. for a range of dense vegetations one can write after Stanhill (1969):

$$\begin{aligned} d &= 0.64 h_c \\ z_0 &= 0.13 h_c \end{aligned} \tag{1.41}$$

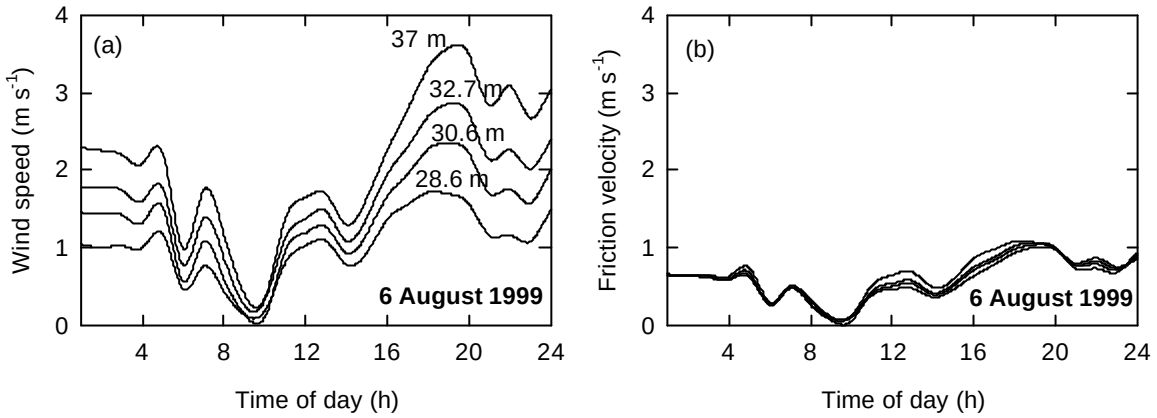

Figure 1.6 Wind speed measurements at four different heights above the canopy of the forest Aelmoeseneie (Figure (a)). Friction velocity calculated according to Equation 1.40 for the wind speed measurements shown in Figure (a)(Figure (b)). Shown data are measured at 6 August 1999. Figures indicate measurement heights.

where h_c (m) is the crop height. More appropriate values for a deciduous oak forest are given by Dolman (1986):

$$d = 0.75h_c$$
$$z_0 = 0.10h_c \qquad (1.42)$$

And substituting b in Equation 1.36

$$K_M = ku_*(z-d) \qquad (1.43)$$

Thus the turbulent diffusivity for momentum increases in proportion to the height above the zero-plane displacement, the factor of proportionality being the eddy velocity u_*. This friction velocity, also called the eddy velocity u_*, can be determined when measurements of wind speed are available:

$$u_* = \frac{ku}{\ln[(z-d)/z_0]} \qquad (1.44)$$

Combining Equations 1.34 and 1.38 also yields the following expression for K_M:

$$K_M = \frac{u_*^2}{du/dz} \tag{1.45}$$

Transfer of latent heat

The theory explained above can also be used to describe the water vapour or latent heat transfer.
The concentration of water vapour is given by the absolute humidity of the air, and its gradient defines the flux density of water vapour:

$$F_z(WV) = -K_{LE}\frac{d\rho_v}{dz} \tag{1.46}$$

where $F_z(WV)$ is flux density of water vapour transfer, K_{LE} (m^2 s^{-1}) is the turbulent diffusivity of water vapour in turbulent air, and ρ_v is the vapour density of the air (kg m^{-3}). The upward flux of water vapour is equivalent with the evapotranspiration rate, E (g m^{-2} s^{-1}), which can also be expressed in terms of the water vapour pressure of the air e_a:

$$E = -K_{LE}\frac{0.622\,\rho_a}{P_{atm}}.\frac{de_a}{dz} \tag{1.47}$$

when the following relationship is used:

$$\frac{e_a}{\rho_v} = \frac{P_{atm}}{0.622\,\rho_a} \tag{1.48}$$

where e_a (Pa) is the water vapour pressure in air, ρ_v (kg m^{-3}) the vapour density or absolute humidity, P_{atm} (Pa) is the atmospheric pressure and ρ_a (kg m^{-3}) is the air density.
The upward flux density of latent heat, λE (W m^{-2}), is then:

$$\lambda E = -K_{LE}\,\lambda\frac{0.622\,\rho_a}{P_{atm}}.\frac{de_a}{dz} \tag{1.49}$$

with λ the latent heat of evaporation (J g^{-1}).
Latent heat and momentum are transported vertically by the same turbulent eddies. In

order to develop a practical formula for calculating the rate of latent heat transfer, the Equation 1.44, and the Equation 1.45 can be combined with the diffusion equation for latent heat (Equation 1.49), yielding:

$$lE = -\frac{K_{LE}}{K_M} l \frac{0.622 \rho_a}{P_{atm}} \cdot \frac{k^2 u^2}{\{\ln[(z-d)/z_0]\}^2} \cdot \frac{de_a}{du} \qquad (1.50)$$

The derivative in Equation 1.50 can be replaced by finite differences, reflecting the measurements of vapour pressure and wind speed at two height levels. One of these levels can be taken at the so-called effective surface for evapotranspiration. It is thereby assumed that evapotranspiration originates from a single hypothetical surface. This surface can be located at height $z_e = d + z_0$ where the horizontal wind velocity theoretically becomes zero. The vapour pressure at this level is designated e_{ze}. The second level can be chosen at the height, z_m, at which the wind speed and the vapour pressure are measured. Equation 1.50 then becomes ($u = u_m$ and $u_{ze} = 0$):

$$lE = \frac{K_{LE}}{K_M} l \frac{0.622 \rho_a}{P_{atm}} \cdot \frac{k^2 u_m}{\{\ln[(z_m - d)/z_0]\}^2} (e_{ze} - e_{zm}) \qquad (1.51)$$

We can define the following coefficient χ_{LE} (-):

$$c_{LE} = \frac{K_{LE}}{K_M} l \frac{0.622 \rho_a}{P_{atm}} \cdot \frac{k^2}{\{\ln[(z_m - d)/z_0]\}^2} \qquad (1.52)$$

Equation 1.51 can now be rewritten as:

$$lE = c_{LE} u_m (e_{ze} - e_{zm}) \qquad (1.53)$$

The above equation shows that the latent heat flux is proportional with the product of the wind speed at a particular measuring height and the difference between the vapour pressure at the effective surface and the vapour pressure at that height.
During the summer of 1998 (August 15- November 9) the latent heat flux was measured above the forest Aelmoeseneie with the flux profile method. Peak values of latent heat exchange during this period were 0.3 and 0.6 mm h^{-1} for cloudy and sunny days respectively (Dhondt, 1999). The mean daily value of latent heat exchange during this measurement period was 3 mm d^{-1}.

Transfer of sensible heat

Analogous to the latent heat flux, the sensible heat flux can be described in a similar way.
In comparison with $F_z(WV)$, one can write:

$$F_z(SH) = -K_H \frac{dh_s}{dz} \tag{1.54}$$

with h_s being the concentration of sensible heat expressed in J m^{-3}. This heat concentration is equal to $\rho_a c_p T$ with ρ_a the density of the air, c_p its heat capacity at constant pressure and T the air temperature. Assuming constant values of ρ_a and c_p close to the ground, the flux density for sensible heat $F_z(SH)$ now becomes:

$$F_z(SH) = -K_H \rho_a c_p \frac{dT}{dz} \tag{1.55}$$

The same eddies that were responsible for the latent heat and momentum flux are also involved for the sensible heat flux. Therefore an equation, analogous to the one for latent heat transfer (Equation 1.51) can be derived in the same way as was done before:

$$H = \frac{K_H}{K_M} c_p \rho_a \frac{k^2 u_m}{\{\ln[(z_m - d)/z_0]\}^2}(T_{ze} - T_{zm}) \tag{1.56}$$

where H represents the flux density of sensible heat (W m^{-2}), and T_{ze} and T_{zm} are the temperature at the reference level $z_e = z_0+d$ and at the measurement height z_m respectively.
We again define a coefficient γ_H (J m^{-3} °C^{-1}):

$$\gamma_H = \frac{K_H}{K_M} c_p \rho_a \frac{k^2}{\{\ln[(z_m - d)/z_0]\}^2} \tag{1.57}$$

The equation for the flux density of sensible heat (W m^{-2}) can now be rewritten as:

$$H = \gamma_H u_m (T_{ze} - T_{zm}) \tag{1.58}$$

where χ_H is effectively constant for a given situation. This equation shows that the sensible heat flux is proportional with the product of the wind speed at a particular measuring height and the temperature difference between the effective surface and the measuring height.

Transfer of CO_2

Analogous to the vertical flux of water vapour, the flux density of CO_2, indicated as $F_z(C)$ and expressed as µmol m^{-2} s^{-1} can described as:

$$F_z(C) = -K_c \frac{d\rho_C}{dz} \tag{1.59}$$

where K_c is the turbulent diffusivity of CO_2 in air (m^2 s^{-1}), and ρ_C is the CO_2 concentration (µmol m^{-3}).
The same eddies that were responsible for the latent and sensible heat and momentum flux are also involved for the flux density of CO_2. Therefore an equation, analogous to the one for sensible and latent heat transfer (Equation 1.51 and 1.56) can be derived in the same way as was done before:

$$C = \frac{K_C}{K_M} \cdot \frac{k^2 u_m}{\{\ln[(z_m - d)/z_0]\}^2} \cdot (\rho_{C,ze} - \rho_{C,zm}) \tag{1.60}$$

where C represents the flux density of CO_2 (µmol m^{-2} s^{-1}), and $\rho_{C,ze}$ and $\rho_{C,zm}$ are the CO_2 concentration at the reference level $z_e = z_0 + d$ and at the measurement height z_m respectively. We again define a coefficient γ_C (-):

$$\gamma_C = \frac{K_C}{K_M} \cdot \frac{k^2}{\{\ln[(z_m - d)/z_0]\}} \tag{1.61}$$

The equation for the flux density of CO_2 can now be rewritten as:

$$C = \gamma_C u_m (\rho_{C,ze} - \rho_{C,zm}) \tag{1.62}$$

where γ_C is effectively constant for a given situation. This equation shows that the flux density of CO_2 is proportional with the product of the wind speed at a particular measuring height and the difference in CO_2 concentration between the effective surface and the measuring height.

The CO_2 flux between the forest Aelmoeseneie and the atmosphere was, as well during the summer of 1997 as during the summer of 1998, measured with the flux profile method. During the summer of 1998 peak uptake of CO_2 decreased from –23 to -10 µmol m^{-2} s^{-1} for a period without soil water stress to a period with soil water stress (Dhondt, 1999). Nighttime respiration was between 0 and 5 µmol m^{-2} s^{-1}. Day sums varied between –4 and 4 g C m^{-2} d^{-1}, indicating that the forest sometimes acted as source and sometimes as a sink for CO_2.

1.1.2.2 Atmospheric stability

The turbulent transfer of momentum, water vapour, sensible heat and CO_2 can be described as formulated before. If the turbulent diffusivities are assumed to be identical, then knowledge of any one in conjunction with the appropriate gradient measurements permits the estimation of any and all of the fluxes. This assumption of identity of the turbulent diffusivities is called the similarity hypothesis or Reynolds analogy. Observations suggest that the assumption of identity in turbulent diffusivities is valid only when the atmosphere is in a condition of nearly neutral stability. Such conditions normally prevail for only limited periods of the day. Therefore, the effect of atmospheric stability on the relationship between the turbulent diffusivities is described below, following Debruyckere (1998).

Stability conditions

When a parcel of air is transported upward in a turbulent eddy and this parcel of air cools adiabatically (-1.0 °C per 100 m vertical displacement in dry conditions and -0.6 °C per 100 m in wet atmospheric conditions), neutral conditions occur. Under these circumstances, the turbulent diffusivity values for water vapour, heat and CO_2 are identical to the turbulent diffusivity of momentum. This is because the same turbulent eddies are responsible for the transport of all four quantities. Therefore:

$$\frac{K_{LE}}{K_M} = \frac{K_H}{K_M} = \frac{K_C}{K_M} = 1 \qquad (1.63)$$

However, if the actual lapse rate is steeper than adiabatic lapse rate, the air in the rising eddy is warmer and, hence, it is less dense than the surrounding air. The eddy will then continue to rise due to buoyancy, enhancing vertical transport (Figure 1.7). With such unstable conditions, the vertical movement of eddies is enhanced beyond that due to

momentum transfer. In this case there can be significant vertical transport of water vapour, sensible heat and CO_2 but less transport of momentum. Hence:

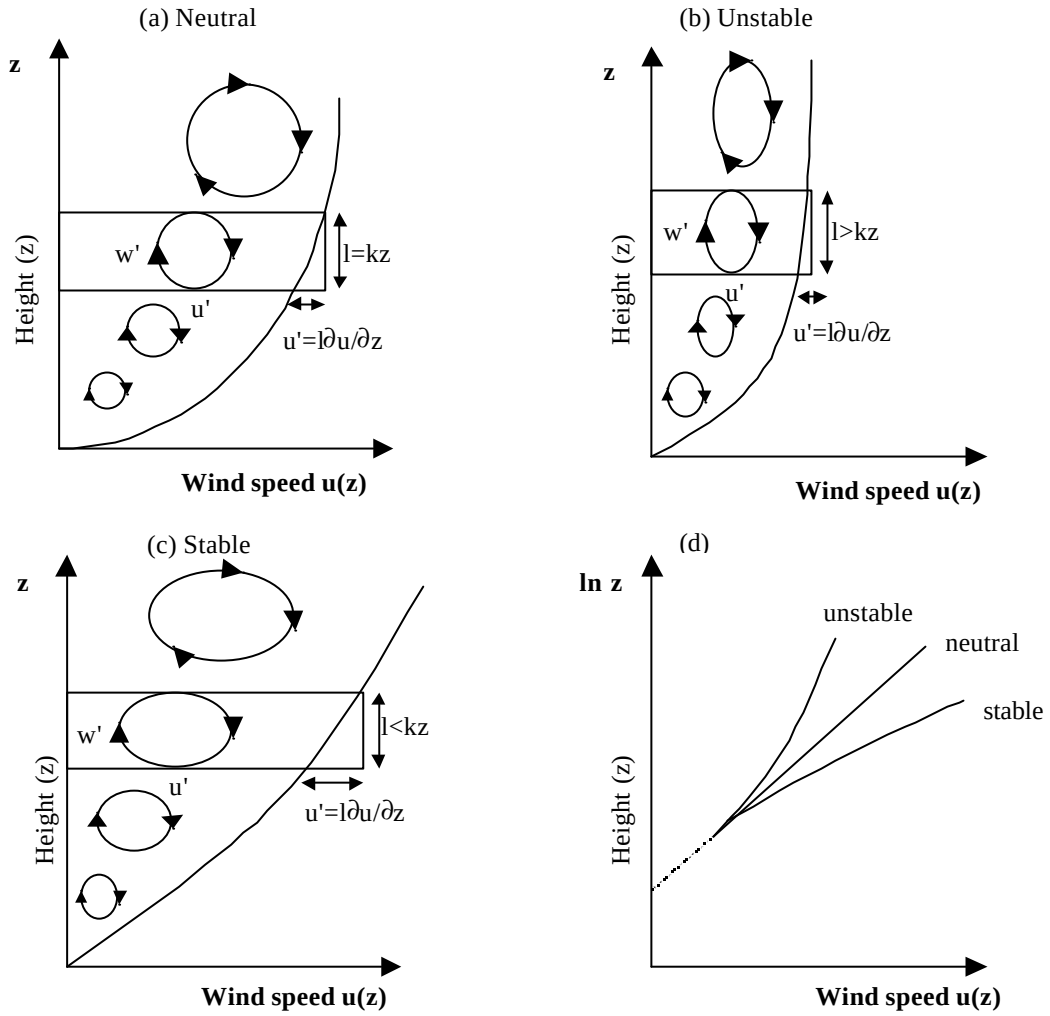

Figure 1.7 Vertical wind speed profiles *u(z)* and simplified eddy characteristics of the wind turbulence near the ground for neutral, stable and unstable atmospheric conditions (afterThom, 1975). Symbols are *l*: mixing length; *k* is von Karman constant; *z* is height above the reference level and *u',w'*: respectively horizontal and vertical turbulent velocity fluctuations.

$$\frac{K_{LE}}{K_M} > 1, \frac{K_H}{K_M} > 1 \text{ and } \frac{K_C}{K_M} > 1 \qquad (1.64)$$

On the contrary, when the actual lapse rate is less steep than the adiabatic one, the air in the eddy will be cooler and denser than that of the surrounding air. Hence, the eddy will sink toward the surface, reducing vertical transport of atmospheric constituents. With such stable conditions the turbulence is suppressed, yielding:

$$\frac{K_{LE}}{K_M} < 1, \frac{K_H}{K_M} < 1 \text{ and } \frac{K_C}{K_M} < 1 \qquad (1.65)$$

Unstable conditions typically occur when wind speed is low and the surface is strongly heated by the sun, inducing strong vertical convection. A stable condition is typical when warm air overlies a cold surface such as a snowpack, or a ground surface cooled by emission of longwave radiation.
Neutral conditions are, on the other hand, more rare in nature. Atmospheric stability is one of the most important issues in micro-meteorology and turbulent exchange.

Turbulence is enhanced by buoyancy forces under unstable conditions and is suppressed under stable conditions. The effects of atmospheric stability on the shape of the vertical wind speed profile and on the turbulent exchange are generally expressed in terms of two non-dimensional parameters: the Richardson number *Ri* and the Monin-Obukhov length *z/L*.
The Richardson number, which is also called the gradient Richardson number, is given by:

$$Ri = \frac{g\left(d\boldsymbol{q}/dz\right)}{T_K\left(du/dz\right)^2} \qquad (1.66)$$

where *g* is the acceleration due to gravity, *dq/dz* and *du/dz* are the vertical gradients of mean potential temperature and mean horizontal wind speed, and T_K is the mean absolute temperature (K) over the vertical distance *dz*. The potential temperature is the temperature that a parcel of dry air would have if it was brought adiabatically from its initial state to a standard sea-level pressure of 1000mb. *Ri* can be interpreted as a parameter describing the relative importance of buoyancy in comparison with mechanical forces: that is, the relative importance of free versus forced convection. The sign of *Ri* is determined by the gradient of potential temperature which is negative in lapse (or unstable)(*Ri*<-0.01) and positive under inversion (or stable)(0.01<*Ri*<0.2) conditions. *Ri* approaching zero implies near neutral conditions (-0.01<*Ri*<0.01). When *Ri*>0.2 convection is inhibited. For practical reasons, the Richardson number may be calculated with *dT/dz* substituted for *dq/dz* in Equation 1.66.
During September 1997 *Ri* at daytime was around +0.1, indicating stable atmospheric conditions (De Bie, 1998). During October of the same year *Ri* was negative during daytime, inicating unstable conditions. During the summer of 1998 *Ri* at daytime was mainly negative (Dhondt, 1999).

The Monin-Obukhov length or stability parameter *z/L* is given by:

$$z/L = \frac{-kzgH}{\rho_a c_p T_K u_*^3} \quad (1.67)$$

The parameter is derived as the ratio of the buoyant turbulent production to the mechanical production, where H is the sensible heat flux density (W m^{-2}), c_p is the specific heat of air at constant pressure (J kg^{-1} °C^{-1}), ρ_a is the atmospheric density (kg m^{-3}), k is the von Karman constant (-) and g is the gravity acceleration (9.81 m s^{-2}).
Measurements of sensible heat flux H and friction velocity u_* are thus needed to evaluate this parameter. Theoretically, z/L is considered a more precise indicator of thermal stability than Ri (Rosenberg et al., 1983). The Richardson number, however, requires measurement of wind speed and air temperature gradients only, and it is much easier to evaluate in practice (Rosenberg et al., 1983).
As moist air is less dense than dry air, the effect of moisture on buoyancy should be accounted for. For this purpose a virtual temperature $T_{v,K}$ (K) can be introduced, and is defined by:

$$T_{v,K} = T_{a,K}(1 + 0.6q) \quad (1.68)$$

where $T_{a,K}$ is the absolute temperature of the air (K) and q is the specific humidity. The use of virtual temperature ($T_{v,K}$) instead of the actual temperature makes it possible to apply the ideal gas law for moist air in the same way as for dry air. Therefore, when buoyancy forces are involved, gradients of $T_{v,K}$ rather than T_K should be considered.
The specific humidity q is defined as the mass of water vapour to the mass of moist air. Thus, the specific humidity is:

$$q = \frac{\rho_v}{\rho_v + \rho_{da}} \quad (1.69)$$

where ρ_v is the absolute humidity or water vapour density (g m^{-3}), and ρ_{da} is the mass density of dry air (g m^{-3}). The specific humidity can be expressed in units of kg of water vapour per kg of moist air.
The specific humidity is related to the vapour pressure e_a by:

$$q = \frac{0.622 e_a}{P - 0.378 e_a} \quad (1.70)$$

Flux-profile relationships in non-neutral conditions

It was mentioned above that the similarity hypothesis states that the turbulent exchange coefficients (e.g. K_M, K_{LE}, K_H, K_C) are identical. If indeed these turbulent diffusivities are assumed to be equal, then knowledge of any one K-value in conjunction with a measured concentration gradient permits the estimation of any and/or all of the corresponding fluxes. Many observations suggest that the assumption of identity in turbulent diffusivity is valid only when the atmosphere is in a condition of near neutral stability. Such conditions normally prevail for only a limited period of the day, say early morning or late afternoon. The effect of atmospheric stability on the relationship between turbulent diffusivity under non-neutral conditions has been determined experimentally in several micro-meteorological investigations. The value of K_C is thereby generally assumed to be equal to K_H and K_{LE} (Rosenberg et al., 1983). While the following relationships with K_M hold:

(for unstable conditions)

$$\frac{K_H}{K_M} \approx \frac{K_{LE}}{K_M} \approx \frac{K_C}{K_M} = \left(1-16Ri\right)^{0.25} \qquad \text{(Dyer \& Hicks, 1970)} \qquad (1.71)$$

$$\frac{K_{LE}}{K_M} = 1.13\left(1-60Ri\right)^{0.074} \qquad \text{(Pruitt et al., 1973)} \qquad (1.72)$$

(for stable conditions)

$$\frac{K_H}{K_M} \approx \frac{K_{LE}}{K_M} \approx \frac{K_C}{K_M} = 1 \qquad \text{(Webb, 1970)} \qquad (1.73)$$

$$\frac{K_{LE}}{K_M} = 1.13\left(1+95Ri\right)^{-0.11} \qquad \text{(Pruitt et al., 1973)} \qquad (1.74)$$

For Ri values between –1 and –0.01, values often observed above the forest Aelmoeseneie during daytime (Dhondt, 1999), the ratio of K_H, K_{LE} and K_C over K_M varied between 2.03 and 1.04 respectively, according to Equation 1.71.
It should also be mentioned that the logarithmic wind profile equation (Equation 1.40) is only valid in neutral atmospheric conditions. When non-neutral conditions exist, the shape of the wind profile deviates significantly from the logarithmic ideal. The change in shape of the wind profile due to thermal stability effects is accounted for by introducing a dimensionless stability function f_m in the derivative of Equation 1.40:

$$\frac{du}{dz} = \frac{u_*}{k\left(z-d\right)} f_m \qquad (1.75)$$

where f_m is generally expressed as a function of Ri. In neutral conditions f_m equals 1, and Equation 1.75 converts into the logarithmic wind profile (Equation 1.40). There have been many efforts in the past to precisely define the functional relationships between f_m and Ri, and some results are given below:

(for unstable conditions)

$$f_m = (1 - 16Ri)^{-0.25} \quad \text{(Dyer \& Hicks, 1970)} \quad (1.76)$$

$$f_m = (1 - 16Ri)^{-1/3} \quad \text{(Pruitt et al., 1973)} \quad (1.77)$$

(for stable conditions)

$$f_m = (1 - 5.2Ri)^{-1} \quad \text{(Webb, 1970)} \quad (1.78)$$

$$f_m = (1 + 16Ri)^{1/3} \quad \text{(Pruitt et al., 1973)} \quad (1.79)$$

For calculating CO_2-exchange between the forest Aelmoeseneie and the atmosphere the formulas of Dyer & Hicks (1970) combined with the formulas of Webb (1970) are preferred (De Bie, 1998). This is because at an Ri of 0.2, high CO_2-fluxes were calculated using the formulas of Pruitt et al. (1973), while the fluxes should have been low because at an Ri of 0.2 convection is assumed to be inhibited.

1.1.2.3 The Bowen ratio

The Bowen ratio b (-) is defined as the ratio of sensible to the latent heat flux in the vertical direction (Bowen, 1926):

$$b = \frac{H}{lE} \quad (1.80)$$

Before it was assumed that the heat exchange took place between an effective surface at height z_e and a measuring height z_m. Because the theory of the Bowen ratio also assumes a constant diffusion flux of heat along its vertical gradient, the heat flux can also be measured between two heights above the canopy different from z_e and z_m, namely z_1 and z_2. Referring to Equations 1.53 and Equation 1.58 for latent and sensible heat transfer respectively, the following equations can be obtained:

$$\lambda E = \chi_{LE}(u_2 - u_1)(e_2 - e_1) \quad (1.81)$$

$$H = \chi_H(u_2 - u_1)(T_2 - T_1) \quad (1.82)$$

The variables are now defined at two height levels, z_1 and z_2 (m) above the surface, where u_1 and u_2 (m s^{-1}) are the wind speed, e_1 and e_2 (Pa) are the vapour pressure and T_1 and T_2 (°C) are the temperature at the two levels respectively. The modified eddy diffusivities χ_{LE} and χ_H for neutral conditions can be written as (see Equation 1.52 and 1.57)

$$\chi_{LE} = \frac{K_{LE}}{K_M}\lambda\frac{0.622\,\rho_a}{P_{atm}}\frac{k^2}{\{\ln[(z_2-d)/(z_1-d)]\}^2} \quad (1.83)$$

$$\chi_H = \frac{K_H}{K_M}c_p\rho_a\frac{k^2}{\{\ln[(z_2-d)/(z_1-d)]\}^2} \quad (1.84)$$

Under normal conditions, K_{LE} equals K_H, and the Bowen ratio, obtained from Equations 1.80-1.84 is:

$$\beta = \frac{c_p P_{atm}}{0.622\,\lambda}\frac{(T_2-T_1)}{(e_2-e_1)} = \gamma\frac{(T_2-T_1)}{(e_2-e_1)} \quad (1.85)$$

where γ is called the psychrometer constant, with a typical value of 66.1 Pa $°C^{-1}$ for a well-ventilated surface at 100 kPa air pressure and 20 °C. Note that γ is not strictly a constant.
Thus, if measurements of temperature and vapour pressure at two levels are available, the Bowen ratio can be calculated. Atmospheric pressure, P_{atm}, is also necessary, but seldom varies by more than a few percent.

The actual evapotranspiration λE can be estimated from combining the Bowen ratio and the energy balance of a given surface layer:

$$R_n - S = H + \lambda E \quad (1.86)$$

where R_n is net radiation to the surface layer, S is the net change in energy storage within the layer, all terms are expressed in W m^{-2}. The net available energy R_n-S is partitioned into a sensible (H) and a latent heat flux (λE) component. Combining Equation 1.80 and 1.86 and solving for λE yields:

$$\lambda E = \frac{R_n - S}{1 + \beta} \qquad (1.87)$$

The disadvantage of the Bowen ratio approach is that there are periods during the day, such as at sunrise and sunset when $(e_2\text{-}e_1)$ and $(T_2\text{-}T_1)$ are small, causing β to give unrealistic results. The Bowen ratio then approaches the value -1, causing the calculated fluxes to approach infinity. However, when β is close to -1, λE and H are both assumed to be negligible and are not calculated.
The Bowen ratio method has proved its usefulness in many studies concerning forest evapotranspiration (e.g. Aston, 1985a,b; Herbst, 1995; Ogink-Hendriks, 1995), and is relatively cheap and accurate for direct estimation of actual evapotranspiration if the instrumental set-up is performed by skilled hands and the collected data are analysed, judged and evaluated in a critical way (see later Chapter 3).

1.1.2.4 The Penman-Monteith model for actual evapotranspiration

Before, the sensible and latent heat flux of an individual leaf was described based on an electrical analogon approach (see § 1.1.1.1). In this approach the flow, potential difference and resistance were described between the individual leaf and the air outside the laminar boundary layer. A forest, however, is much more complex, and exists out of many different leaves. Considering the forest as being one "big leaf", the exchange of sensible and latent heat flux can again be described based on the electrical analogon concept. In this "big leaf" approach the flow, potential difference and resistance will be described between the height at which this "big leaf" is assumed to be located and the air outside the turbulent boundary layer.
As mentioned in the preceding paragraph the energy balance of a layer, e.g. a forest canopy can be written as:

$$R_n - S = H + \lambda E \qquad (1.86)$$

where R_n is net radiation to the forest canopy, S is the net change in energy storage within the canopy, H and λE are the sensible and latent heat flux respectively: all terms being expressed in W m^{-2}.
According to Equation 1.34 the horizontal shear stress τ can be defined as:

$$\tau = \frac{r_a du}{r_{am}} \tag{1.88}$$

where u is wind speed (m s^{-1}) at height z, and r_{am} is the aerodynamic resistance for momentum (s m^{-1}). If Equation 1.88 is integrated between the effective surface $z_e = d + z_0$ and a measurement level z_m, the next expression is obtained:

$$\tau = \frac{r_a (u_m - u_e)}{r_{am}} \tag{1.89}$$

Taking into account that u_e = 0 (from Equation 1.40), and combining Equations 1.89, 1.38 and 1.44, yields the following expression for r_{am} (s m^{-1}):

$$r_{am} = \frac{\left[\ln\left(\frac{z-d}{z_0}\right)\right]^2}{k^2 u} \tag{1.90}$$

Because the apparent sink for momentum in a canopy is above those for sensible or latent heat exchange, there is a small extra resistance required when converting from r_{am} to the corresponding resistance for sensible or latent heat exchange. This extra resistance refers to transfer between the level of the momentum sink ($d + z_0$) and the alternate sink (Thom, 1975). The aerodynamic resistance for sensible heat flux (r_{ah}) is defined as (Brutsaert, 1982):

$$r_{ah} = \frac{\left[\ln\left(\frac{z-d}{z_0}\right)\right]\left[\ln\left(\frac{z-d}{z_{0h}}\right)\right]}{k^2 u} \tag{1.91}$$

where z_{0h} is the roughness length for sensible heat (m). On average $ln(z_0/z_{0h})$ or kB^{-1} is about 2.4 (Garrat, 1978). It is assumed that the aerodynamic resistance for sensible heat flux r_{ah} equals that of the aerodynamic resistance for latent heat flux r_{av}.
A diurnal course of r_{am} and r_{ah}, calculated from wind speed measured above the canopy of the forest Aelmoeseneie, is shown in Figure 1.8.
Combining Equations 1.11 and 1.14 with Equation 1.91, H and λE can be reformulated as:

$$H = \rho_a c_p \frac{T_s - T_a}{r_{ah}} \tag{1.92}$$

$$lE = \frac{\rho_a c_p}{\gamma} \frac{e_s(T_s) - e_a}{r_{av} + r_c} \quad (1.93)$$

where T_s and T_a are respectively the surface and air temperature (°C), and $e_s(T_s)$ and e_a are the saturated vapour pressure of the surface and actual vapour pressure of the air (hPa) respectively, and r_c is the bulk resistance describing both the physiological control by the vegetation and the control exerted by the soil moisture (Monteith, 1965), called the surface or canopy resistance (see Chapter 4). The surface is the theoretical apparent sink for sensible and latent heat exchange, represented by the "big leaf" (Figure 1.9).

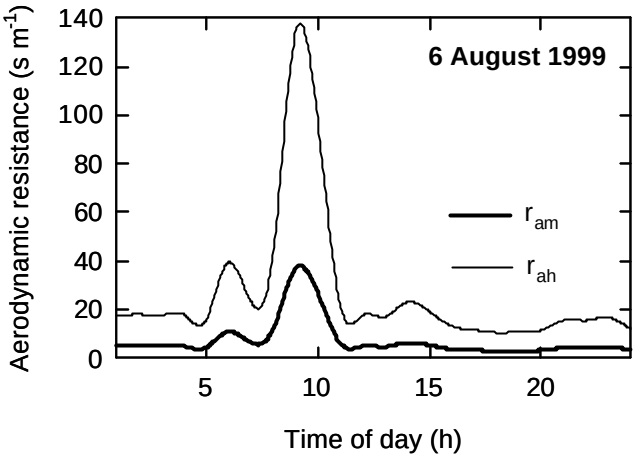

Figure 1.8 Diurnal course of the aerodynamic resistance for momentum (r_{am}) and sensible heat flux (r_{ah}) calculated from wind speed measurements above the forest Aelmoeseneie at 28.6 m for 6 August 1999 (see Figure 1.6).

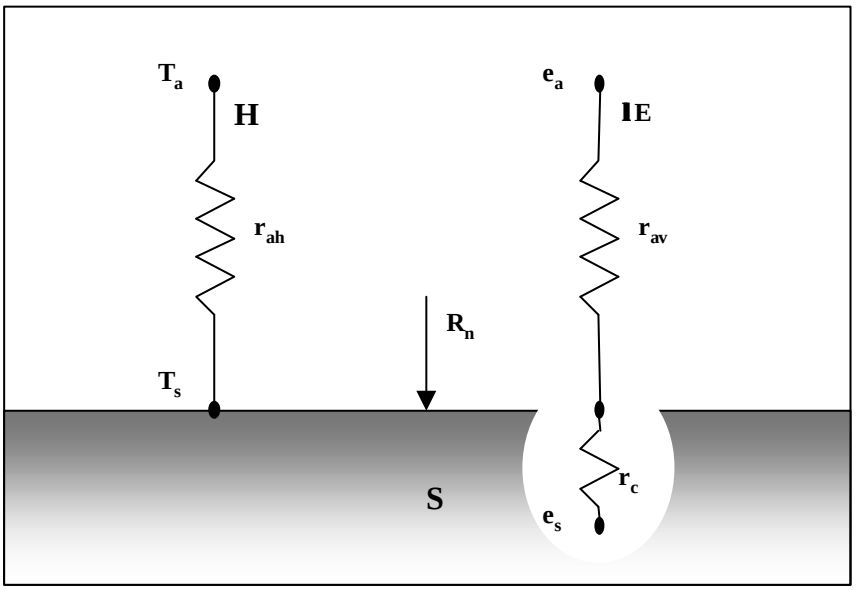

Figure 1.9 Schematic diagram of the "big-leaf" approach. Symbols are R_n: net radiation; lE: latent heat flux; H: sensible heat flux; S: heat storage; r_{ah} and r_{av}: aerodynamic resistance for sensible and latent heat; r_c: canopy or surface resistance; e_s: saturated vapour pressure at surface temperature T_s; e_a: vapour pressure of the air at air temperature T_a (after Zhang et al. 1995).

The problem in this approach is that data for surface temperature T_s, and thus also $e_s(T_s)$, are difficult to obtain experimentally. So, in order to eliminate this variable T_s, one can apply the Penman-transformation based on the slope D (hPa °C^{-1}) of the saturation

water vapour pressure curve. This slope is defined as:

$$\Delta = \frac{e_s(T_s) - e_s(T_a)}{T_s - T_a} \tag{1.94}$$

Reformulation of Equation 1.94 gives:

$$e_s(T_s) - e_a = \Delta(T_s - T_a) + [e_s(T_a) - e_a] \tag{1.95}$$

Combining this formula with Equation 1.93, yields:

$$\lambda E \frac{g(r_{av} + r_c)}{\rho_a c_p} = \Delta(T_s - T_a) + [e_s(T_a) - e_a] \tag{1.96}$$

The surface temperature T_s can be further eliminated by combining Equation 1.92 and 1.96:

$$\lambda E \frac{g(r_{av} + r_c)}{\rho_a c_p} = \Delta H \frac{r_{ah}}{\rho_a c_p} + [e_s(T_a) - e_a] \tag{1.97}$$

or, after implementation of Equation 1.86:

$$\lambda E \frac{g(r_{av} + r_c)}{\rho_a c_p} = \Delta(R_n - S - \lambda E) \frac{r_{ah}}{\rho_a c_p} + [e_s(T_a) - e_a] \tag{1.98}$$

Rearrangement gives:

$$\lambda E = \frac{\Delta(R_n - S) + \frac{\rho_a c_p}{r_{ah}}[e_s(T_s) - e_a]}{\Delta + g\,(r_{av} + r_c)/r_{ah}} \tag{1.99}$$

If we assume that r_c=0, and that r_{av} equals r_{ah}, then:

$$\lambda E = \lambda E_p = \frac{\Delta}{\Delta + g}(R_n - S) + \frac{1}{\Delta + g}\frac{\rho_a c_p}{r_{ah}}[e_s(T_a) - e_a] \tag{1.100}$$

or, replacing vapour pressure by vapour density:

$$\lambda E = \lambda E_p = \frac{\Delta}{\Delta + g}(R_n - S) + \frac{g}{\Delta + g}\frac{\lambda}{r_{ah}}[\rho_{v,s}(T_a) - \rho_v]$$

(1.101)

The assumption of r_c=0 indicates total wet canopy (e.g. after rain), without any physiological control of transpiration rate.
These last two equations (Equation 1.100 and 1.101) are called the Penman equations (Penman, 1948) and they express the potential evapotranspiration (λE_p). Burman & Pochop (1994) define λE_p as the rate at which water is removed from the soil surface or profile if available. λE_p has always been referred to plants well supplied with water and usually not impaired by disease.

The essence of the Penman equation can be expressed as:

$$\lambda E = \frac{\Delta}{\Delta + g}(Energy) + \frac{g}{\Delta + g}(Aerodynamic) \qquad (1.102)$$

This notation illustrates that the evapotranspiration is driven by both an energy term and by an aerodynamic or mass transfer term. The partitioning between both terms depends on the available energy (R_n-S) and on the vapour pressure deficit $[e_s(T_a) - e_a]$.

Monteith (1965) used Equation 1.99 to develop a modified Penman formula which represents the actual evapotranspiration λE_a rate from the vegetated surface. Re-arrangement of Equation 1.99 gives:

$$\lambda E_a = \frac{\Delta}{\Delta + g(1 + r_c/r_{ah})}(R_n - S) + \frac{1}{\Delta + g(1 + r_c/r_{ah})}\frac{\rho_a c_p}{r_{ah}}[e_s(T_a) - e_a] \qquad (1.103)$$

or, after introducing the modified psychrometer coefficient g^* as:

$$g^* = g\left(1 + \frac{r_c}{r_{ah}}\right) \qquad (1.104)$$

the equation can then be reformulated in a form analogous to the Penman equation (Equation 1.100) for potential evapotranspiration:

$$\lambda E_a = \frac{\Delta}{\Delta + g^*}(R_n - S) + \frac{1}{\Delta + g^*}\frac{\rho_a c_p}{r_{ah}}[e_s(T_a) - e_a] \qquad (1.105)$$

λE_a is now the actual evapotranspiration, including the physiological control of the water vapour losses through the canopy resistance r_c.

This formula is known as the Penman-Monteith equation (Monteith, 1965). It is interesting to note that Equation 1.103 reduces to Equation 1.100 when r_c equals 0 (indicating a wet canopy surface). This formula is widely used to calculate evapotranspiration from vegetated land surfaces.

The canopy or surface resistance r_c can be defined as:

$$r_c = \frac{r_s}{LAI} \tag{1.106}$$

where r_s is the stomatal resistance of leaves with stomatal pores located at one leaf surface only, as is the case for the tree species in the forest Aelmoeseneie. The resistances r_s and r_c have units of s m^{-1}, and LAI (m^2 m^{-2}) is the total leaf area per unit ground surface. However, this approach is an oversimplification surely for dense vegetations (see later § 4.1). When the surface temperature is known, r_c can be determined by substituting Equations 1.92 and 1.93 into Equation 1.86:

$$r_c = \frac{e_s(T_s) - e_a}{g\left[(R_n - S)/\rho_a c_p - (T_s - T_a)/r_{ah}\right]} - r_{av} \tag{1.107}$$

When surface temperature T_s is not know, r_c can be determined from rearrangement or inversion of the Penman-Monteith equation (Equation 1.105):

$$r_c = \frac{r_{ah}}{g\lambda E}\left[\Delta(R_n - S) + \frac{\rho_a c_p\left(e_s(T_a) - e_a\right)}{r_{ah}} - \lambda E(\Delta + g)\right]$$

(1.108)

The surface temperature can be obtained from rearranging Equation 1.107:

$$T_s = T_a + r_{ah}\left[\frac{(R_n - S)}{\rho_a c_p} - \frac{\left(e_s(T_s) - e_a\right)}{g\left(r_{av} + r_c\right)}\right] \tag{1.109}$$

As the surface temperature is also implicitly enclosed in the term $e_s(T_s)$, it is clear that T_s can only be obtained from the equation above by an iteration procedure.
Where the surface is completely dry, so that there is no latent heat exchange ($r_c = \infty$), Equation 1.109 reduces to:

$$T_s = T_a + r_{ah}\left[\frac{(R_n - S)}{\rho_a c_p}\right]$$

(1.110)

In this case T_s is proportional to $(R_n\text{-}S)$ with the surface being warmer than air when $(R_n\text{-}S)$ is positive (as it is usually during the day), and cooler than air when $(R_n\text{-}S)$ is negative.

When the surface is perfectly wet, as might occur when it is covered with dew or after a rain shower, then, r_c=0. In this case the latent heat cooling is maximal for any aerodynamic resistance, and Equation 1.109 becomes:

$$T_s = T_a + r_{ah}\left[\frac{(R_n - S)}{\rho_a c_p} - \frac{(e_s(T_s) - e_a)}{\gamma r_{av}}\right] \qquad (1.111)$$

As r_c=0 and r_{ah} tends to zero, the value of T_s tends to theoretical wet bulb temperature:

$$T_s = T_a - \frac{e_s(T_s) - e_a}{\gamma} \qquad (1.112)$$

1.1.2.5 The decoupling coefficient

The effect of stomatal regulation on transpiration can be described using the decoupling coefficient Ω, as was introduced for the first time by Jarvis & McNaughton (1986). This parameter expresses the coupling between the canopy and the atmosphere. An Ω value close to 0 indicates a strong coupling of the canopy to the surrounding air, with the rate of transpiration being controlled mainly by the degree of opening by the stomata. A value for Ω close to 1, on the other hand, indicates a canopy which is decoupled from the atmosphere by a thick boundary layer, leading to local equilibrium values of air humidity near the evaporating surfaces. In this circumstance transpiration is no longer controlled by the stomatal aperture but by the net amount of absorbed energy. Following the theory of Jarvis & McNaughton (1986), Ω is calculated from:

$$\Omega = \frac{\Delta/\gamma + 1}{\Delta/\gamma + 1 + r_c/r_{ah}} \qquad (1.113)$$

where r_{ah} and r_c are the aerodynamic resistance for sensible heat transfer and canopy resistance respectively, both expressed in s m^{-1}.

Martin (1989) redefined the decoupling coefficient Ω in terms of a radiative transfer resistance of the canopy r_r, defined as:

$$\frac{1}{r_r} = \left(\frac{4\varepsilon\sigma T_{a,K}^3 LAI}{\rho_a c_p} \right) \qquad (1.114)$$

where σ is the Stefan-Boltzmann constant, in W m^{-2} K^{-4}, ε is the emissivity (-) and $T_{a,K}$ is air temperature in K. The radiative decoupling coefficient Ω_r can then be defined as:

$$\Omega_r = \frac{\Delta/\gamma + 1 + r_{ah}/r_r}{\Delta/\gamma + (1 + r_c/r_{ah})(1 + r_{ah}/r_r)} = \frac{\Delta/\gamma + 1 + r_{ah}/r_r}{\Delta/\gamma + 1 + r_c/r_{ah} + r_c/r_r + r_{ah}/r_r} \qquad (1.115)$$

The radiative decoupling coefficient Ω_r describes how closely the vegetation is coupled convectively and radiatively to the air around it. Ω_r is between 0 and 1. When the surface is in radiative equilibrium with the air around it (T_s=T_a), i.e. when it is well coupled radiatively ($r_r \rightarrow \infty$), the behaviour of decoupling coefficient with radiative coupling converges towards that of the decoupling coefficient without radiative coupling ($\Omega_r \rightarrow \Omega$). When the (long-wave) radiative loss from the surface is large, i.e., when the surface is poorly coupled radiatively to air around it ($r_r \rightarrow 0$), vegetation control is solely determined by the relative importance of aerodynamic control ($\Omega_r \rightarrow r_{ah}/(r_{ah}+r_c)$).
Typical values for Ω and Ω_r for the forest Aelmoeseneie are given in § 4.3. These values indicate that the forest Aelmoeseneie is strongly coupled to the atmosphere.

1.2 Modelling of CO_2- and water vapour exchange: the FORUG-model

As already described in the previous part of this chapter H_2O- and CO_2-exchange between forest vegetations and the atmosphere is a very complicated process. However, it is important that these processes can be quantified and that their dynamic changes can be assessed. This, of course, can be done by performing measurements, but this approach implies a whole range of problems (experimental, financial and time problems). Therefore, measurements are in most cases conducted for only a limited period of time. Moreover, this experimental approach only yields information about a present situation and it does not allow to predict the future or describe the past. Particularly in the context of ″Global Change″ research, in which plant communities will be subjected to hitherto unusual combinations of environmental inputs, the existing databases are limited. As such the predictions of responses at whole-plant and ecosystem scales will increasingly rely on simulation models of the system in question (Harley & Baldocchi, 1995).

For modelling the canopy processes, a big-leaf approach or a multi-layer model can be used. The former considers the canopy as being one big leaf, placed at a certain height (see § 1.1.2.4) above the soil. This kind of model is rather simple and it requires only a limited number of input data. Because of this (over)simplification, errors are likely to occur. de Pury & Farquhar (1997), for example, report that such models overestimate rates of photosynthesis because, in reality, the vertical profiles of absorbed irradiation in canopies do not follow Beer's exponential extinction law. This is due to the occurrence of both sunspot penetration and of changing leaf angles. On the other hand, models that treat the canopy in terms of a number of horizontal layers (i.e. the multi-layer models) generally avoid these errors (de Pury & Farquhar, 1997). The input parameters of such models should be able to describe the physiological status of the canopy with more precision.

Therefore, a multi-layer model, called FORUG, was developed to describe the CO_2- and water vapour exchange between a deciduous forest vegetation and the atmosphere. The new model was meant to be user-friendly and it should be physiologically and physically based on sound theoretical principles (see § 1.1). Its structure should be flexible as that it can be used for a whole range of deciduous forest types (e.g. forest of different species composition, with or without understory).

In this model four canopy layers will be distinguished: (i) an upper canopy layer, a (ii) middle and (iii) lower canopy layer, and (iv) an understory layer. Moreover the soil layer is taken into account (Figure 1.10).

As mentioned before (see § 1.1.1.2) the CO_2-exchange at the leaf level can be described using two different approaches: (i) the classical Light Response Curve (LRC), and (ii) the CO_2 response curve (Farquhar et al., 1980). The Farquhar approach gives more possibilities concerning the calculation of photosynthetic CO_2-exchange under changing atmospheric conditions, whereas the LRC-parameters are much more easy to obtain, and, at this moment, more available to a wider public. The user of FORUG can select one or both methods to calculate CO_2-exchange at the leaf level.
All parameters which are used in the model simulations are obtained from measurements (e.g. extinction coefficients and photosynthesis parameters from Samson et al., 1997a) or from literature (e.g. seasonal variation and temperature dependence of maximal gross photosynthesis from Wang, 1996).

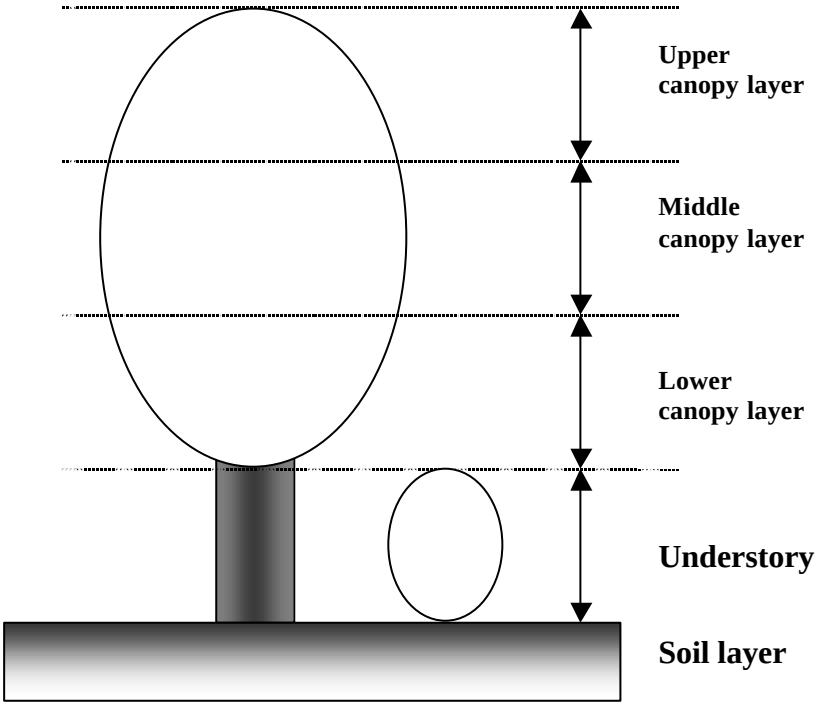

Figure 1.10 A schematic representation of the different layers considered in the multi-layer FORUG model.

1.2.1 Multi-layer CO_2-exchange

1.2.1.1 Submodel solar elevation

In this submodel the hourly position of the sun (solar elevation and hour angle) is calculated at any moment of the day. The solar elevation is calculated as:

$$\sin \beta_{se} = \sin \lambda_{lat} \sin \delta + \cos \lambda_{lat} \cos \delta \cos h \quad (1.116)$$

with β_{se} elevation angle of the sun (°), δ (°) the declination, λ_{lat} latitude (°) and h the hour angle (°). For Ghent (Belgium) λ_{lat} is 51°. The hour angle is given by:

$$h = 15(t - 0.5 - t_o) \quad (1.117)$$

with t the time of the day (h), and t_o the time of solar noon (h). The correction factor 0.5 in Equation 1.117 accounts for the fact that the meteorological data used in the model are hourly means. Data acquisition systems provide this mean value at the end of one hour measuring period (e.g. at 1500 h for the period between 1400 h and 1500 h). In this example the mean value should correspond to 1430 h and not to 1500 h, which explains the conversion of 0.5 h.

Solar noon is calculated as:

$$t_o = 12 + \left[4(L_s - L_e) - E_t\right]/60 + SW \quad (1.118)$$

with L_s the standard longitude of the time zone (°), L_e the local longitude (°), E_t the equation of time in minutes, and SW a factor which corrects for the “summer and winter hour”. During the 'summer hour' period, SW equals one and during 'winter hour period' SW equals zero. The standard longitude for Belgium is 15° E, and L_e is 4° for Ghent. Note that Equation 1.118 only holds for longitudes measured east of Greenwich (Iqbal, 1983).

Different empirical equations exist for describing the equation of time. The differences are negligible, so the most simple formula is chosen (Woolf, 1968):

$$E_t = 0.258\cos J - 7.416\sin J - 3.648\cos 2J - 9.228\sin 2J \quad (1.119)$$

where the variable J is given by:

$$J = \frac{360}{365.242}(D_n - 1) \quad (1.120)$$

with D_n the calendar day number since 1 January.
The declination δ (°) for a given day can be calculated using the formula given by

Cooper (1969):

$$\delta = 23.5 \sin\left[\frac{360(D_n + 284)}{365.25}\right] \quad (1.121)$$

According to Burman and Pochop (1994), Equation 1.121 yields accurate results (error less than 0.6 °) during the growing season. In October the error is more than 1 degree.

1.2.1.2 Submodel diffuse and direct incident short-wave radiation

In this submodel the incident short-wave radiation is divided into a direct and diffuse component. Inputs are the declination, the latitude, the day of the year D_n and the mean hourly solar elevation. The output is the variable P_d, describing the average portion of the diffuse and direct part in the short-wave radiation during the hourly period. The method used is described in Spitters et al. (1986).

The hourly value of the radiation on top of the atmosphere (extra-terrestrial radiation) R_a (W m^{-2}), at a plane parallel to the earth surface changes with the sine of the elevation angle of the sun, and is calculated according to Spitters et al. (1986):

$$R_a = S_o\left[1 + 0.033\cos\left(\frac{360 D_n}{365}\right)\right]\sin\beta_{se} \quad (1.122)$$

where S_o is the solar constant of 1370 W m^{-2} (Frolich, 1982) measured perpendicular to the sun's rays. The term between brackets corrects for the seasonal variation in the sun-earth distance (Burman & Pochop, 1994).

In a second phase the daily atmospheric transmittance of the solar radiation is calculated. Here, the atmospheric transmittance is defined as the ratio (R_s/R_a) of the incoming solar radiation at the earth's surface to the extra-terrestrial radiation, with R_s and R_a respectively the hourly total downward short-wave radiation flux density at the surface, and the hourly flux density of extra-terrestrial radiation, both expressed in W m^{-2}. The portion of diffuse radiation in R_s (W m^{-2}) can be represented as P_d, and, according to de Jong (1980), this parameter varies in relation to the atmospheric transmittance as follows:

$$
\begin{aligned}
&P_d = 1 && \text{when } R_s / R_a \leq 0.22 \\
&P_d = 1\text{-}6.4(R_s / R_a - 0.22)^2 && \text{when } 0.22 < R_s / R_a \leq 0.35 \\
&P_d = 1.47\text{-}1.66(R_s / R_a) && \text{when } 0.35 < R_s / R_a \leq W \\
&P_d = N && \text{when } W < R_s / R_a
\end{aligned}
\qquad (1.123)
$$

with,

$$N = 0.847 - 1.61\sin \beta_{se} + 1.04\sin^2 \beta_{se} \quad (1.124)$$

$$W = (1.47 - N)/1.66 \quad (1.125)$$

1.2.1.3 Submodel diffuse and direct incoming PAR

In this submodel the incoming PAR (Photosynthetic Active Radiation) is calculated from the incident short-wave radiation R_s, and the PAR is also divided into a diffuse and a direct component. The variable P_d is used again, together with the measured hourly total short-wave radiation R_s. The output of the submodel is the diffuse and direct PAR. The method of Ross (1976), also used by Baldocchi and Hutchison (1986), is applied to calculate the direct PAR intensity $I_{PAR,b}$. It is hereby accepted that the portion of PAR energy contained in the short wavelenght interval of direct-beam radiation is constant, namely 43 %. This gives:

$$I_{PAR,b} = 0.43 R_s (1 - P_d) \quad (1.126)$$

$$I_{PAR,d} = R_s (0.07 + 0.43 P_d) \quad (1.127)$$

with $I_{PAR,b}$ and $I_{PAR,d}$ (W m^{-2}) the direct-beam and diffuse PAR intensity respectively. The diffuse PAR intensity is calculated as the difference between the total downward PAR intensity and the downward direct PAR intensity. Therefore it is assumed that the fraction PAR in the total short-wave radiation amounts 0.5. This fraction is relative constant over different atmospheric conditions and solar elevations, provided that β_{se} > 10° (Szeicz, 1974). From here on the subscript PAR will be omitted. The conversion factor between energy units W (PAR in W m^{-2}) and photon units (PAR in µmol m^{-2} s^{-1}) used in the model is 4.61 µmol J^{-1}. This conversion factor is valid for the natural energy spectrum of the sun.

1.2.1.4 Submodel LAI of sunlit and shaded leaves

In this submodel the LAI fractions of sunlit and shaded leaves are calculated for each considered canopy layer. The extinction coefficients for direct PAR and the total LAI for each species are the input parameters.
The leaf area index L is divided in the sunlit L_{sun} and shaded L_{shade} fraction (m^2 m^{-2}).

Sunlit leaves are situated in sunflecks, thus intercept high PAR intensities (direct and diffuse) and consequently have high photosynthesis rates. On the contrary, shaded leaves are situated in the shade, thus only intercept diffuse radiation, and consequently have low photosynthesis rates. The upper canopy layer is numbered as layer one, the middle and lower layer as layer two and three respectively, and the understory layer as layer four. The LAI of the sunlit leaf area, for canopy layer *i*+1, is calculated as the difference of the downward cumulative sunlit leaf area between the canopy levels *i*+1 and *i*:

$$L_{sun,i+1} = \left[\exp\left(-k_b L_i\right) - \exp\left(-k_b L_{i+1}\right)\right] / k_b \qquad (1.128)$$

with L_i and L_{i+1} the downward cumulative LAI (measured from the top of the canopy), layer *i* respectively layer *i+1* included and k_b the extinction coefficient for direct (e.g. beam) radiation. This formula is derived from the exponential extinction law (Beer's law). The LAI of the shaded leaf area is then:

$$L_{shade} = L - L_{sun} \qquad (1.129)$$

where *L* is the downward cumulative LAI.

1.2.1.5 Submodel extinction coefficient

In this submodel the extinction coefficient for the direct PAR fraction k_b is specified as a function of the solar elevation, which is the only input parameter. Extinction coefficients were determined experimentally on a sunny day (July 21, 1996). Therefore, the PAR penetration was determined at the different layers and at the soil level of a forest canopy using a sunfleck ceptometer (Sunfleck Ceptometer, Delta-T Devices, Ltd, Cambridge, UK). LAI was measured at these levels as well (LAI-2000; Li-Cor, Lincoln, Nebraska). When ln(relative PAR penetration inside the canopy) is plotted against the downward cumulative LAI, a linear relation is obtained. The slope of this relation expresses the extinction coefficient as indicated by the following equations:

$$I_b(L) / I_b(0) = e^{-k_b . L} \qquad (1.130)$$

or

$$\ln\left[I_b(L) / I_b(0)\right] = -k_b . L \qquad (1.131)$$

where $I_b(L)$ and $I_b(0)$ are the direct beam PAR at downward cumulative LAI *L* and above the canopy respectively

The extinction coefficient for the diffuse PAR fraction was determined the same way, but on a cloudy day (August 12, 1996). The regression yielded now k_d = 0.70 (Samson et al., 1997a), and k_d is independent for variations in the solar elevation, and corresponds very well with the value found by Baldocchi et al. (1984). Also Spitters (1986) preferred an empirical value of k_d compared to a theoretical value.
The dependence of k_b in function of the solar elevation is given in Table 1.1 (Samson et al., 1997a). The observed trend of k_b in relation to solar elevation does not correspond with what can be expected from mathematical theory (e.g. for a spherical leaf angle distribution whereby $k_b = 1/(2\sin\beta_{se})$). According to Baldocchi et al. (1984) deviations from theory can be attributed to strong clumping of leaves and or large gaps in the canopy. In the model, the extinction coefficient for direct radiation is assumed to be a discrete value for a small range of solar elevations (10° range). It is also assumed that both relationships for diffuse and direct radiation, do not change during the growing season.

Table 1.1 Experimentally determined extinction coefficients for direct radiation (k_b) in function of the solar elevation (β_{se})(Samson et al., 1997a). The values are valid for the forest Aelmoeseneie, with a leaf area of around 5. Theoretical k_b-values for a spherical leaf angle distribution are given for comparison.

β_{se} (°)	0-20°	20-30°	30-40°	40-50°	>50°
k_b (-), measured	0.95	1.05	1.01	0.96	1.05
k_b (-), spherical	2.88	1.18	0.87	0.71	0.61

1.2.1.6 Submodel LAI-evolution

In this submodel the change of the LAI value for each of the considered tree and understory species is defined during the growing season. The driving variable for the LAI is the day number D_n. This seasonal LAI-evolution in function of the day number D_n is given in Figure 1.11, and can be described as three consecutive and linear relationships. The seasonal dynamics is assumed to be as follows: the growing season of the upperstory species is assumed to begin at May 1 and to end at November 30. From July 1 until September 15, the LAI has its maximal value. Before and after this period, the LAI increase as well as the decrease behaves linearly. The start of the growing season of the understory species is put at March 1 and its end at November 30. The maximal LAI is reached on April 20, and declines after September 15. The seasonal LAI evolution is comparable with the one used by Ogink-Hendriks (1995) for

an oak forest in The Netherlands. The relative LAI distribution of each tree species over the three canopy layers is assumed to remain constant during the growing season.

Total LAI of the different species in the oak-beech and ash forest site (see § 2.1.2) was estimated from the cumulative annual leaf litter collected in autumn of 1996, from August 15 until December 29. In each forest site 30 litter traps (1 m x 1 m) were used to collect litter fall at a height of 1 m above the soil level. The size and height of the litter traps was based upon the findings of McShane et al. (1983) and Morrison (1991). In the oak-beech site six spots where the leaf litter traps were installed were selected at random. At each spot five litter traps were installed, one in the centre, the others 5 m away from the central spot in the main wind directions. In the ash site these spots were chosen along a 100 m transect also used for the optical LAI determination using the LAI-2000 PCA (see Mussche, 1997). From October till December litter fall was collected every two weeks. Leaf area and leaf dry biomass was determined for each species separately. Determination of the leaf area of a weighed sub-sample (dry weight) was carried out with a Portable Area Meter (Li-3000, LI-COR, Lincoln, Nebraska), coupled at a Transparant Belt Conveyor (Li-3050A, LI-COR, Lincoln, Nebraska). Dry weight was obtained by weighing the leaves after drying them in an oven at 90 °C for 48 h. Total leaf area was then obtained by multiplying total dry weight of the collected leaves with the found relationship between area and dry weight of the leaves.
The forest Aelmoeseneie has a total upperstory LAI of 4.35, existing out of beech (43 %), oak (35%) and ash (22%)(Table 1.2). The total LAI of the understory is 0.75 from which 51% is attributed to sycamore and 49% to hazel. The total LAI of the forest Aelmoeseneie (5.10), is calculated from the LAI and the aerial contribution of the oak-beech and ash forest site in the fenced scientific zone (see § 2.1.2).

Table 1.2 Total leaf area per m^2 of soil surface (m^2 m^{-2}) and its vertical distribution in the canopy for the three main tree species in the Aelmoeseneie forest (Samson et al., 1997a). Values between brackets are corrected and used as input to the model.

			Vertical distribution (%)		
Species	Mixed stand	Uniform stand	Lower	Middle	Upper
Ash	22 % = 0.96	100 % = 2.49	6.8 (0.0)	44.2 (51.0)	49.0
Oak	35 % = 1.53	100 % = 4.37	1.8 (0.0)	70.3 (72.1)	27.9
Beech	43 % = 1.86	100 % = 5.87	17.9	18.2	63.9
Total LAI	100 % = 4.35				

1.2.1.7 Submodel PAR interception

In this submodel the PAR intensity intercepted by the sunlit and shaded leaves is calculated. The inputs to the model are extinction coefficients for direct and diffuse PAR radiation (k_b and k_d), the hourly incoming PAR intensity (above the canopy), the LAI of sunlit and shade leaves (L_{sun} and L_{shade}), and the PAR reflection coefficient for the tree crown canopy.

For the direct and diffuse component of the PAR radiation, the formula for the calculation of the penetrated intensity can be respectively written as (Goudriaan, 1982):

$$I_b(L) = (1 - \rho_b) I_{o,b.} \exp(-k_b.L) \quad (1.132)$$

$$I_d(L) = (1 - \rho_d) I_{o,d.} \exp(-k_d.L) \quad (1.133)$$

with $I_{o,b}$ and $I_{o,d}$ respectively the direct and diffuse PAR intensity above the canopy, $I_b(L)$ and $I_d(L)$ the direct and diffuse PAR intensity at downward cumulative LAI equal to L, k_b and k_d are the extinction coefficients for respectively the direct and diffuse radiation components, and ρ_b and ρ_d (-) the corresponding reflection coefficients.

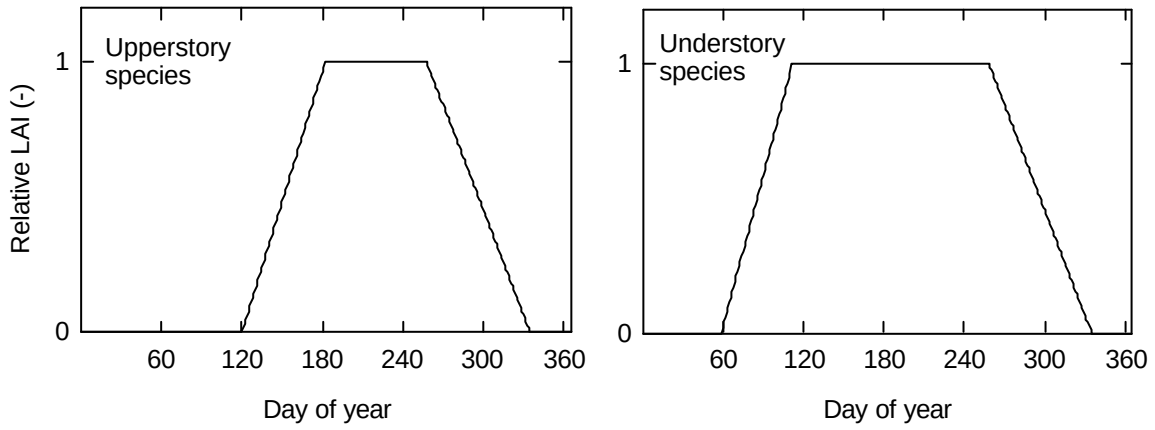

Figure 1.11 Assumed seasonal courses of the relative leaf area index (LAI) for the upperstory (left) and understory (right) plant species present in the heterogeneous forest Aelmoeseneie.

The relation between the canopy reflection coefficient of total PAR (ρ_c) and the reflection coefficients for direct and diffuse PAR, i.e. ρ_b and ρ_d, can be written as:

$$\rho_c = \rho_d . P_d + \rho_b . (1 - P_d) \qquad (1.134)$$

where P_d indicates the portion of diffuse radiation in R_s (Equation 1.123), and ρ_d is set equal to the value proposed by de Pury & Farquhar (1997), namely 0.036. The mean ρ_c measured above the mixed deciduous forest Aelmoeseneie during the growing season amounts to 0.039±0.001, which resulted in a mean ρ_b of 0.071±0.004 during the growing season.

As was mentioned in §1.2.1.4 every canopy layer can be divided in two parts: (i) the shaded leaf area which intercepts diffuse light only, and (ii) sunlit leaf area which intercepts both the diffuse and direct flux. Intercepted direct and diffuse PAR for respectively a sun fleck or a shade fleck (both expressed in µmol m^{-2} s^{-1}) can be written as:

$$I^i_{sun} = I^i_b + I^i_d \qquad (1.135)$$

$$I^i_{shade} = I^i_d \qquad (1.136)$$

with I^i_{sun} the intercepted PAR intensity in sunlit leaf area, and I^i_{shade} the intercepted PAR intensity in the shaded leaf area, both expressed in µmol m^{-2} s^{-1}.
The intercepted direct PAR is calculated by multiplying the incoming direct PAR intensity above the canopy $I_b(o)$ with the appropriate extinction coefficient k_b (Lemeur, 1973):

$$I^i_b = k_b . I_b(o) \qquad (1.137)$$

with $I_b(o)$ found from Equation 1.132 for L=0. The value I^i_b is constant for all sun flecks, found at all vertical levels in the canopy. The intercepted diffuse PAR at a particular level decreases exponentially with depth. The simplest calculation used here is similar to the approach according to Spitters (1986) and Johnson et al. (1995). This yields for a particular level with downward cumulative LAI equal to L:

$$I^i_d = k_d . I_d(L) \qquad (1.138)$$

with $I_d(L)$ found from Equation 1.133.

1.2.1.8 Submodel leaf photosynthesis: the CO_2 response curve

The theoretical background of the CO_2 response curve was already discussed in § 1.1.1.3. Once the intercepted PAR intensities for the sunlit and shaded leaf area (respectively I^i_{sun} and I^i_{shade}) are calculated, then these values can be used for calculation of the electron transport rate (see Equation 1.29) and the carboxylation rate (see Equation 1.20). In this submodel also the temperature dependence, as well as the seasonal variation of the photosynthesis parameters in the CO_2 response curve are described. The formulas used for the description of leaf photosynthesis for sun and shade leaves are given as well.

Temperature dependence

Many photosynthesis parameters used in these Farquhar equations (K_c, K_o, G^*, V_{cmax} and J_{max}) are temperature dependent. The functional temperature dependence were previously described and defined by the Equations 1.24-1.28.
The input in the mathematical relations is the air temperature expressed in °C.

Seasonal variation

It is assumed that the maximal carbon assimilation rate $V_{c\ max}$ and the maximal rate of electron transport J_{max} show a seasonal variation expressed by time dependent seasonal variation $f(D_n)$.

$$V_{c\max} = V^*_{c\max} \cdot f(D_n) \quad (1.139)$$

$$J_{\max} = J^*_{\max} \cdot f(D_n) \quad (1.140)$$

where $V^*_{c\ max}$ and J^*_{max} are the peak values of respectively $V_{c\ max}$ and J_{max} during the growing season.
An empirical function $f(D_n)$ is given by Wang (1996), and written as:

$$f(D_n) = \left(\frac{365 - D_n}{365 - b_1}\right)^{b_2} \exp\left\{\frac{b_2}{b_3}\left[1 - \left(\frac{365 - Dn}{365 - b_1}\right)^{b_3}\right]\right\} \quad (1.141)$$

where b_1, b_2 and b_3 are parameters. For the upperstory species the values of b_1, b_2 and b_3 are assumed to be 210, 2.84 and 5.62 respectively (Wang, 1996). From measured CO_2 response curves, of upperstory and understory species growing in the forest Aelmoeseneie, Vande Walle et al. (2000) suggested that the peak of maximal photosynthesis parameters for understory species occurred about one month earlier than that of the upperstory species. Therefore, for the understory species b_1 was assumed to be 180. The assumed seasonal variation (Equation 1.141) of the quantum efficiency and maximal photosynthesis rate for upperstory and understory species is shown in Figure 1.12.
The photosynthesis parameters which are used as input to the model, and which were assumed to vary during the season, were first divided by $f(D_n)$ to obtain their seasonal maximal value.

Leaf photosynthesis

In this submodel the hourly net photosynthesis rate of the sunlit and shaded leaf areas is calculated for each canopy layer. The input parameters are the hourly intercepted radiation intensities (I^i_{sun} and I^i_{shade}), the functional photosynthesis parameters of the Farquhar equations (at reference temperature), the hourly temperature functions as referred to above, and the seasonal variation functions for $V_{c\,max}$ and J_{max}.

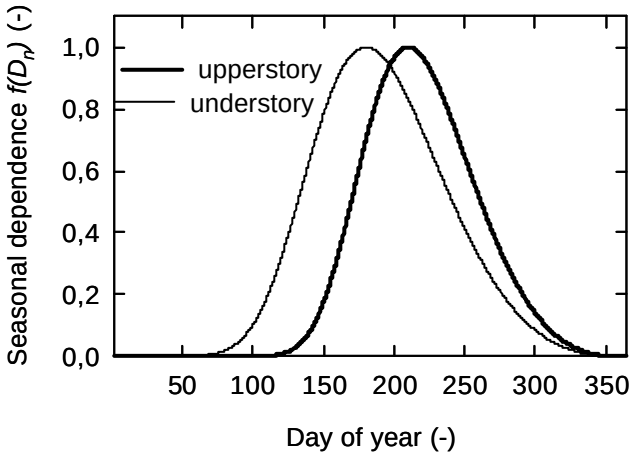

Figure 1.12 Graphic representation of the assumed seasonal variation (Equation 1.141) of the quantum efficiency and maximal photosynthesis rate for upperstory and understory species.

The light dependence of the electron transport rate *J* gives the following equations for the sunlit and shaded leaf area at depth *L* (see also Equation 1.29), respectively:

$$J_{sun}(L) = \frac{\alpha_{F,L} I^{i}_{sun}(L)}{\left\{1 + \frac{\alpha^{2}_{F,L}}{J\max_{L}} \left[I^{i}_{sun}(L)\right]^{2}\right\}^{0.5}} \tag{1.142}$$

$$J_{shade}(L) = \frac{\alpha_{F,L} I^{i}_{shade}(L)}{\left\{1 + \frac{\alpha^{2}_{F,L}}{J\max_{L}} \left[I^{i}_{shade}(L)\right]^{2}\right\}^{0.5}} \tag{1.143}$$

Based on Equation 1.142 and 1.143 for the sunlit and shaded leaf area respectively, the CO_2-limited and RuBP-saturated rate of photosynthesis $A_n(c)$, and the RuBP-limited rate of photosynthesis $A_n(j)$:

$$A_n(c) = \frac{V_{c\max}(p_i - \Gamma^*)}{p_i + K_m} - R_{day} \tag{1.21}$$

$$A_n(j) = \frac{J(p_i - \Gamma^*)}{4(p_i + 2\Gamma^*)} - R_{day} \tag{1.22}$$

can be calculated as explained in § 1.1.1.3. The minimum of the Equations 1.21 and 1.22 describes the full CO_2-response curve:

$$A_n = \min\{A_n(c), A_n(j)\} \tag{1.23}$$

For the final calculation of A_n, the intercellular partial pressure of CO_2 (p_i) has to be known. This partial pressure p_i can be calculated using the expression (see also Equation 1.30):

$$p_i = p_a - \left(\frac{1.6 A_n P_{atm}}{g_s}\right) \tag{1.144}$$

where g_s (mmol H_2O m^{-2} s^{-1}) is the stomatal conductance of the leaf to water vapour. As also A_n is included in Equation (1.144), a solution for A_n (Equation 1.23) can only be obtained through an iteration procedure. Therefore not the CO_2 response curves but light response curves will be used in this work to calculate leaf photosynthesis.

1.2.1.9 Submodel leaf photosynthesis: the light response curve

The theoretical background of the light response curve (LRC) was already discussed in § 1.1.1.3. Once the intercepted PAR intensities for the sunlit and shaded leaf area (respectively I^i_{sun} and I^i_{shade}) are calculated, then these values can be used for calculation of the leaf assimilation rate (see Equation 1.32). In this submodel also the temperature dependence of the maximal gross photosynthesis rate A_{max}, as well as the seasonal variation of A_{max} and the initial light efficiency α are described. The formulas used for the description of leaf photosynthesis for sun and shade leaves are given as well.

Measurements of photosynthetic gas exchange were executed in August and September 1996. A branch, from a particular level in the canopy, was excised. After cutting the branch was brought down the tower, and was re-cut under water (a shortening of 15 cm)(Wang, 1996), and transported to the laboratory. Rates of photosynthetic gas exchange were measured in the controlled environment (T_a 20 and 25 °C, and RH 78%) of the phytotron. CO_2 gas exchange rates of the leaves were analysed using an IRGA (225-MK3, ADC, UK) in differential mode. The measurements were begun at a high level of photon flux density, which was then decreased in steps, allowing sufficient time for the steady-state rates of gas-exchange to be attained (0.5-1 h)(Follens, 1997; Samson et al., 1997a).

Temperature dependence of A_{max}

The temperature dependence of the maximal gross photosynthesis rate A_{max} is described by Wang (1996):

$$F_A(T) = \frac{\exp\left(C_1 - \frac{\Delta H_{a,P}}{R_g T_a}\right)}{1 + \exp\left(\frac{\Delta S.T_a - \Delta H_{d,P}}{R_g T_a}\right)} \qquad (1.145)$$

where $F_A(T)$ is a temperature correction factor for A_{max} (dimensionless range from 0 to 1), C_1 is a constant, $\Delta H_{a,P}$ is the activation energy (J mol^{-1}) valid for A_{max}, ΔS is the entropy of the denaturation equilibrium of CO_2 (J K^{-1} mol^{-1}), and $\Delta H_{d,P}$ is the deactivation energy (J mol^{-1}) valid for A_{max}. R_g and T_a are the gas constant (8.31 J mol^{-1} K^{-1}) and air temperature (K) respectively.

The original parameter values reported by Wang (1996) were changed for the main species (beech, oak and ash) of the forest Aelmoeseneie, based on the before mentioned measurements of photosynthesis rate. For beech and oak measurements were conducted at 20 and 25 °C, for ash only measurements at 20 °C were available. The temperature at which the highest A_{max} was measured was considered to be the optimal temperature, and the maximal gross photosynthesis rate at this temperature is denoted as A'_{max}. For beech and oak this optimal temperature was respectively 20 and 25 °C. For ash the optimal temperature was assumed to be also 25 °C, as both oak and ash prefer light environments.
First C_1 was adapted so that $F_A(T)$ equals 1 at the optimal temperature. Next, while $DH_{a,P}$ was copied from Wang (1996), DS and $DH_{d,P}$ were changed so that the measurements of A_{max} agreed with the calculations [$A'_{max}.F_A(T)$]. This procedure was also used by Hollinger (1992). For beech measurements were conducted at three canopy levels, but only one temperature function $F_A(T)$ was considered. Therefore, DS was chosen as such that the difference between measured and calculated values of A_{max} for all canopy layers equalled zero. Values obtained for oak were assumed to be also valid for ash.
An overview of the parameters is given in Table 1.3.

Seasonal variation

Analogous to Wang (1996), the light efficiency α and A_{max} are also assumed to change during the growing season. The same time dependent function $f(D_n)$ as in § 1.2.1.8 was used for this purpose:

$$\alpha = \alpha^* . f(D_n) \qquad (1.146)$$

$$A'_{\max} = A^*_{\max} . f(D_n) \qquad (1.147)$$

where α^* and A^*_{max} are the maximum values of α and A_{max} respectively during the growing season for a certain tree species, and A'_{max} is the maximal gross photosynthesis rate at optimal air temperature.

Leaf photosynthesis

In this submodel the hourly net photosynthesis rate of the sunlit and shaded leaves is calculated for each canopy layer. The procedure is similar as the one explained in § 1.2.1.8 for the Farquhar equations. The input parameters are the hourly intercepted

radiation intensities, the functional parameters of the light response curve (at reference temperature), the hourly temperature functions for A'_{max} (see above) and R'_d (see § 1.2.1.10), and the seasonal variation functions for A_{max} and α. The light response curves based on Equation 1.32 are for the sunlit and shaded leaf area at depth L, respectively:

$$A_{n,sun}(L) = A_{\max}(L)\left[1 - \exp\left(\frac{-\alpha_L I^i_{sun}}{A_{\max}(L)}\right)\right] - R_d(L) \quad (1.148)$$

$$A_{n,shade}(L) = A_{\max}(L)\left[1 - \exp\left(\frac{-\alpha_L I^i_{shade}}{A_{\max}(L)}\right)\right] - R_d(L) \quad (1.149)$$

with $A_{n,sun}(L)$ and $A_{n,shade}(L)$ the net photosynthesis rate for sunlit and shaded leaf area respectively (µmol CO_2 m^{-2} s^{-1}), $A_{max}(L)$ the maximal gross photosynthesis (µmol CO_2 m^{-2} s^{-1}), α_i the quantum yield or initial light efficiency (µmol CO_2 µmol^{-1} PAR), $R_d(L)$ the respiration rate (µmol CO_2 m^{-2} s^{-1}) and I^i_{sun} and I^i_{shade} the PAR intensity respectively intercepted by the sunlit and shaded leaf area (µmol m^{-2} s^{-1}).
Values of the photosynthesis parameters used in this model are given in Table 1.4.

Table 1.3 The values of the parameters used in Equations 1.145 and 1.152 for the calculation of the temperature dependency of the maximal gross photosynthetic rate and the dark respiration rate (Light Response Curve (LRC)-approach), for the main tree species of the Aelsmoeseneie forest.

Parameters	Beech	Oak and Ash
$C_{1\,(-)}$	21.92	21.62
$C_{2\,(-)}$	13.54	13.54
ΔS (J mol^{-1} K^{-1})	709.95	700.00
$\Delta H_{a,P}$ (J mol^{-1})*	52750	52750
$\Delta H_{a,R}$ (J mol^{-1})*	33870	33870
$\Delta H_{d,P}$ (J mol^{-1})	211000	211000

*from Wang (1996)

As the photosynthesis process has a seasonal [i.e. $f(D_n)$] and a temperature dependence [$f(T)$], the corrected photosynthesis and respiration rate can be expressed as:

$$A_{\max} = A'_{\max}.F_A(T) \quad (1.150)$$

$$R_d = R'_d.F_R(T) \quad (1.151)$$

where A_{max} and R_d are respectively the values of A'_{max} and R'_d, at optimal respectively reference air temperature, corrected for actual air temperature T. From the gas exchange measurements mentioned above, it was found that the optimal temperature for A'_{max} is 20°C for beech and 25°C for oak and ash. In the case of R_d the reference air temperature is 20°C for all species.

Table 1.4 Mean experimental values (n = 3)(Samson et al., 1997a) for leaf photosynthesis parameters (see Equations 1.148 and 1.149) and their respective standard errors for the main tree species of the Aelmoeseneie forest, determined at different heights (m) in the crown layer. Measurements were executed at 350 ppm of atmospheric CO_2 concentration and 78% RH of the air. a^*, A^*_{max} and R_d are used as input to the model, and values in italics are corrected for their seasonal variation $f(D_n)$ based on the Equations 1.146 and 1.147. (a and a^*: respectively the initial quantum efficiency and the seasonal maximal value of a both in µmol CO_2 µmol^{-1} PAR, A_{max} and A^*_{max}: respectively the maximal gross photosynthesis rate and the seasonal maximal value of A_{max} both in µmol CO_2 m^{-2} s^{-1}, R_d: rate of dark respiration µmol CO_2 m^{-2} s^{-1})

Species	Height	α	α^*	A_{max}	A^*_{max}	R_d
Beech	21	0.088±0.004	*0.103*	5.47±0.17	*6.38*	0.31±0.06
	14	0.094±0.004	*0.110*	5.67±0.46	*6.61*	0.26±0.02
	7	0.071±0.008	*0.083*	5.79±0.49	*6.75*	0.40±0.04
Oak	21	0.070±0.010	*0.082*	12.57±0.63	*14.65*	0.98±0.08
Ash	21	0.110±0.007	*0.128*	11.88±1.03	*13.85*	1.38±0.16

1.2.1.10 Submodel leaf respiration

The temperature dependence of leaf respiration is calculated in this submodel. The respiration rate R_d (µmol CO_2 m^{-2} s^{-1}) is strongly dependent of temperature. Two relationships are given by Wang et al. (1995):

$$F_R(T)_{day} = \exp\left(C_2 - \frac{\Delta H_{a,R}}{R_g T_a}\right) \quad (1.152)$$

$$F_R(T)_{night} = 1.45 F_R(T)_{day} \quad (1.153)$$

where $F_R(T)$ is the temperature function for R_d (dimensionless), C_2 is a constant, T_a is the air temperature (K), R_g is the gas constant (8.31 J mol^{1} K^{-1}), and $\Delta H_{a,R}$ is the activation energy (J mol^{1}). The temperature-dependence of the respiration rate during the nighttime was assumed to have the same response pattern as the respiration rate in light. However a correction coefficient of 1.45, estimated from measurements of respiration during the day and during complete dark conditions, was used by Wang et

al. (1995). The parameter values used for the Equations 1.152 and 1.153 are presented in Table 1.3.

1.2.1.11 Canopy photosynthesis

The net canopy photosynthetic rate can be calculated for each time step, for each species considered, and for each canopy layer separately. This is done by integrating the net photosynthetic rate on the leaf level to the level of the different canopy layers. This is based on the LAI of the sun and shade leaf areas (see equations 1.128 and 1.129) and the corresponding CO_2 or light response curves (see equations 1.142-1.143 and 1.148-1.149 respectively). Hereafter the scaling to the level of the total canopy is done by addition of the photosynthesis rate of the different canopy layers. Cumulative values can then be obtained by summing up all the hourly values during the time period considered.

Total net canopy photosynthesis rate $A_c(t)$ (µmol CO_2 m^{-2} s^{-1}) for the time step (Dt) used and the cumulative net uptake of CO_2 over a time period (t) $A_{c,cum}$ (µmol CO_2 m^{-2}) can then be calculated as:

$$A_c(t) = \sum_{i=1}^{4} \left\{ \left[A_{n,sun}(L_i), L_{sun,i} \right] + \left[A_{n,shade}(L_i), L_{shade,i} \right] \right\} \quad (1.154)$$

and $$A_{c,\,cum} = \sum_{0}^{t} A_c(t)\Delta t \quad (1.155)$$

Using the relative occurrence in the forest of each considered species in the forest, the net photosynthetic CO_2-uptake of the forest can be calculated, assuming that the forest only consists of the upperstory and understory species which are considered and using an appropriated weighing procedure (upperstory species: beech 43 %, oak 35 % and ash 22 %; understory species: sycamore 61 % and hazel 39 %).

1.2.1.12 Submodel woody biomass respiration

In this submodel the respiration of the woody biomass of the upperstory and understory species is simulated separately. The woody biomass respiration contains both growth and maintenance respiration because the two components cannot be differentiated experimentally. The input parameters are the stem temperature and the stem and branch surface area (SBA) or sapwood volume (SV) of each species depending on which SBA or SV variable is available. Tables 1.5 and 1.6 list calculated values for stem respectively branch surface area of the main tree species in the Aelmoeseneie forest.

Table 1.5 Calculated stem areas (in m^2 m^{-2} soil) for the main upperstory and understory species of the Aelmoeseneie forest. The calculations are based on the mean radius, the mean tree height and the tree density (number of trees per ha). These data were obtained from Vande Walle et al. (1998).

	Stem area	
Species	Oak-beech forest	Ash forest
Beech	0.280	0.009
Oak	0.457	0.112
Ash	0.029	0.503
Sycamore	0.026	0.063
Hazel	0.012	0.043

The woody biomass (stem and branches) respiration can be calculated according to Ryan (1990):

$$R_{stem} = R_{stem,o} \exp\{[\ln(Q_{10})/10]T_{stem}\} \quad (1.156)$$

where R_{stem} and $R_{stem,o}$ are the total stem respiration rate at temperature of the stem, T_{stem} (°C), and at reference temperature of 0 °C respectively. Both expressed in µmol CO_2 per m^{-2} SBA and per s^{-1}, and Q_{10} is the temperature response factor (-). The parameter values are given in Table 1.7.

Table 1.6 Calculated branch areas (in m^2 m^{-2} soil) for the main upperstory species of the Aelmoeseneie forest. The calculations are based on the relationships between stem and branch biomass described by Janssens et al. (1998). These relationships are assumed to be also valid between stem and branch area. The branch area of the understory species is neglected.

	Branch area	
Species	Oak-Beech forest	Ash forest
Beech	0.145	0.005
Oak	0.133	0.033
Ash	0.009	0.163

If the stem temperature is not known, the air temperature T_a can be used as a substitute, or a linear relationship can be used to convert T_a to T_{stem}. Carey et al (1996) proposed a relationship between T_a and T_{stem}, both expressed in °C, based on measurements on 3-year old *Pinus ponderosa* trees:

$$T_{stem} = 0.66T_a + 4.22 \quad (1.157)$$

Table 1.7 Parameter values used for the calculation of the woody biomass respiration, according to Equation 1.156, of the main upperstory and one understory species of the Aelmoeseneie forest. The values for oak and sycamore are derived from Edwards and Hanson (1996) for a reference temperature of 0 °C. As no literature values for beech and ash were found, the parameter values for these species are assumed to be the mean of the values for oak and sycamore.

Species	$R_{stem,o}$ (µmol CO_2 m^{-2} s^{-1})	Q_{10} (-)
Beech	0.32	2.05
Oak	0.27	2.40
Ash	0.32	2.05
Sycamore	0.37	1.70

1.2.1.13 Submodel soil respiration

In this submodel the soil respiration is calculated from the soil temperature.
Soil respiration is also influenced by soil water and the content of organic material in the soil (Naganawa et al., 1989; Raich, 1998). In this model soil respiration R_{soil} (expressed as g CO_2 m^{-2} s^{-1}) is considered to depend solely on soil temperature, according to the formula (Nakane, 1995; Mallik & Hu, 1997; Rottiers, 1998):

$$R_{soil} = a\exp(bT_{soil}) \quad (1.158)$$

where T_{soil} is the soil temperature (°C), and a (g CO_2 m^{-2} s^{-1}) and b (-) are regression parameters. The regression parameters used here are the ones found by Rottiers (1998) and are listed in Table 1.8. The latter author found the best correlation when soil respiration was linked with air temperature measured at a height of 36 m.

Table 1.8 Regression parameters a and b and regression coefficient (R^2) for the exponential relation between soil respiration in the Aelmoeseneie forest and air temperature measured above the canopy at a height of 36 m (°C). Data from Rottiers (1998).

Parameter	Oak-beech forest	Ash forest
a (g CO_2 m^{-2} s^{-1})	$2.339\ 10^{-5}$	$1.749\ 10^{-5}$
b (-)	0.06245	0.06015
R^2	0.76	0.79

1.2.1.14 Net CO_2-exchange of the forest

The net CO_2-exchange of the total forest (A_{for}) can be calculated according to the following formula:

$$A_{for} = A_c - R_{stem} - R_{soil} \quad (1.159)$$

with A_c the total net canopy photosynthesis rate (Equation 1.154), R_{stem} the stem respiration rate (Equation 1.156) and R_{soil} the soil respiration rate (Equation 1.158); where all terms should be in the same units (M L^{-2} T^{-1}). Positive values of A_{for} indicate a net uptake of CO_2 by the forest, where negative values indicate a net release of CO_2 to the atmosphere.

1.2.2 Single-layer water vapour exchange

In this sub-model water vapour exchange between a forest canopy and the atmosphere is calculated according to the single-layer i.e. the big-leaf, or Penman-Monteith (Monteith, 1965) approach (see § 1.1.2.4). It is thereby assumed that evapotranspiration originates from a single hypothetical surface. This surface can be located at an effective height $z_e = d + z_0$ where the horizontal wind velocity theoretically becomes zero (see § 1.1.2.1).

The model allows to calculate potential (Equation 1.100) and actual evapotranspiration (Equation 1.103) with and without interception. Potential evapotranspiration lE_p can be defined in several ways:

(i) The potential evapotranspiration can be defined as the evapotranspiration of a grass or alfalfa crop, of respectively 15 or 30 to 50 cm height, totally covering the soil, without a shortage of soilwater and when transport of water in the crop is not limiting. Because there are no limitations this lE_p can be regarded as the maximal loss of water, solely dependent on climatological and stand conditions (Lemeur et al., 1984). This definition is used in land evaluation studies to determine land use management.

(ii) Another definition of lE_p is the evapotranspiration of the crop when $r_c = 0$.

(iii) Potential evapotranspiration can also be defined as the evapotranspiration of the

crop when soil water is not limiting, i.e. when the soil water submodel for the determination of r_c (or r_s) is optimal (i.e. has a value of one, see § 1.2.2.3).

In this single layer approach vegetation as well as soil is considered together. The potential (lE_p) and actual (lE_a) evapotranspiration are defined by the equations referred to above:

$$lE_p = \frac{\Delta}{\Delta + g}(R_n - S) + \frac{1}{\Delta + g}\frac{\rho_a c_p}{r_{ah}}[e_s(T_a) - e_a] \qquad (1.100)$$

$$lE_a = \frac{\Delta}{\Delta + g(1 + r_c/r_{ah})}(R_n - S) + \frac{1}{\Delta + g(1 + r_c/r_{ah})}\frac{\rho_a c_p}{r_{ah}}[e_s(T_a) - e_a] \qquad (1.103)$$

1.2.2.1 General input parameters

In this section the calculation method of all the necessary input parameters in Equation 1.100 and 1.103 is explained.

Virtual temperature, $T_{v,K}$

The virtual temperature $T_{v,K}$ (K) is the temperature that dry air must have to equal the density of moist air at the same pressure, and as mentioned before can be expressed as:

$$T_{v,K} = T_{a,K}(1 + 0.6q) \qquad (1.68)$$

This equation can be simplified to:

$$T_{v,K} = 1.01T_{a,K} \qquad (1.160)$$

where $T_{a,K}$ is the air temperature (K). Note that the subscript *K* refers to Kelvin.

Atmospheric pressure, P_{atm}

According to Burman & Pochop (1994) there is no need to take temporal (hourly, day to day) changes in atmospheric pressure P_{atm} (Pa) into account. A P_{atm} value depending on

height above sea level h (m), and $T_{a,K}$ can be found from:

$$P_{atm} = 101300\left(\frac{T_{a,K} - 0.0065h}{T_{a,K}}\right)^{5.256} \quad (1.161)$$

Density of the air, ρ_a

The atmospheric density ρ_a (kg m^{-3}) depends on the virtual temperature and atmospheric pressure:

$$\rho_a = \frac{P_{atm}}{T_{v,K} R} \quad (1.162)$$

where R is the gas constant of dry air (287 J kg^{-1} K^{-1}).

Actual vapour pressure, e_a

The actual vapour pressure of the air e_a (Pa) is the partial vapour pressure of the water vapour molecules in air, and depends on the relative humidity (RH) and the saturated vapour pressure of the air:

$$e_a = e_s \frac{RH}{100} \quad (1.163)$$

Saturated vapour pressure, e_s

The saturated vapour pressure e_s (Pa) is the maximal partial pressure of water vapour in air at a given temperature. For temperatures between 0 and 100 °C e_s is:

$$e_s(T_a) = 610.8\exp\left(\frac{17.27T_a}{T_a + 237.3}\right) \quad (1.164)$$

The difference between saturated and actual vapour pressure is the vapour pressure deficit De.

Slope of the saturation water vapour pressure curve, D

The slope D (Pa °C^{-1}) of the curve, expressed in Equation 1.164, at the point (T_a , $e_s(T_a)$) is given by:

$$\Delta = \frac{4098 e_s(T_a)}{(T_a + 237.3)^2} \qquad (1.165)$$

The latent heat of evaporation, l

Latent heat of evaporation l (J kg^{-1}) is the heat required to change a unit mass of water from a liquid to a water vapour at constant pressure and at constant temperature:

$$l = 2501000 - 2360.1 T_a \qquad (1.166)$$

1.2.2.2 Heat inputs

Net radiation

Net radiation R_n (W m^{-2}) is the algebraic sum of both the incoming and reflected short-wave and long-wave radiation components. If measurements of R_n are not available, this parameter can be calculated from other data. Therefore, the user of the model can choose between two possibilities:

(i) The net radiation R_n can be estimated from a linear relationship with short-wave radiation R_s:

$$R_n = a_R R_s - b_R \qquad (1.167)$$

where R_s (W m^{-2}) is the total downward (i.e. diffuse and/or direct) solar radiation, and a_R (-) and b_R (W m^{-2}) are regression parameters. For the Aelmoeseneie forest the following relationship based on hourly values, for the period June 1999, was found (n = 705, r^2 = 0.99):

$$R_n = 0.745R_s - 37 \quad (1.168)$$

Because R_n depends very much on the surface on which it is measured, the regression parameters in Equation 1.168 are very site specific. Therefore, the model user can fill in regression parameters which corresponds with the investigated ecosystem.

(ii) Net radiation R_n can also be calculated from other meteorological parameters. Net radiation R_n is the sum of net short-wave and net long-wave radiation:

$$R_n = R_{s,n} + R_{l,n} \tag{1.169}$$

where $R_{s,n}$ (W m^{-2}) is the net flux density of total solar radiation, and $R_{l,n}$ (W m^{-2}) is the net flux density of long-wave radiation. $R_{s,n}$ itself can be written as:

$$R_{s,n} = (1 - \alpha_R) R_s \tag{1.170}$$

where α_R is the albedo (-) for the total downward solar radiation. The mean albedo for the forest Aelmoeseneie was measured during the growing season and this yielded a value of 0.136±0.001. $R_{l,n}$ is the difference between the long-wave downward radiation $R_{l,d}$ and the long-wave upward radiation $R_{l,u}$, both expressed in W m^{-2}:

$$R_{l,n} = R_{l,d} - R_{l,u} \tag{1.171}$$

As measurements of $R_{l,d}$ and $R_{l,u}$ are usually not available, $R_{l,n}$ can be calculated as:

$$R_{l,n} = f_c (\varepsilon_a - \varepsilon_{vs}) \sigma T_{a,K}^4 \tag{1.172}$$

where f_c (-) is the correction factor for cloudiness or the atmospheric transmittance, σ is the Stefan-Boltzmann constant (5.67 10-8 W m^{-2} K^{-4}), ε_a is the emissivity of the atmosphere (-), and ε_{vs} is the emissivity of vegetation and soil (-). Brunt (1952) and Smith et al. (1991) defined the differences in emissivity from the actual vapour pressure of the air e_a:

$$\varepsilon_a - \varepsilon_{vs} = -\left(a_1 + b_1 \sqrt{\frac{e_a}{1000}} \right) \tag{1.173}$$

The regression parameters a_1 and b_1 are 0.34 and -0.14 respectively.

The atmospheric transmittance f_c is defined as:

$$f_c = a_c \frac{R_s}{R_{so}} + b_c \tag{1.174}$$

where R_s (W m^{-2}) is the hourly total short-wave radiation, R_{so} (W m^{-2}) is the maximal total

short-wave radiation flux at the earth's surface (for a particular location and hourly period during the year), and is defined as $R_{so}=0.75R_a$ (Allen et al., 1989) where R_a is the extra-terrestrial radiation (see Equation 1.122). For humid climates the constants a_c and b_c equals 1 and 0 respectively (Smith et al., 1991).

Soil heat flux

In comparison with the net heat supply, the net change in energy storage within the canopy S is often simplified to the losses by the soil heat flux G (W m^{-2}), being mainly dependent of the degree of soil coverage. For bare and dark coloured soils, G will be large; while it will be small for dense vegetations. Often the soil heat flux is considered as a fixed fraction of R_n. Some values are given in Table 1.9.

In this model measured G values can also be used as input. If measured values are not available a preset value for G of $0.03R_n$ is taken.

Table 1.9 Soil heat flux G for several vegetations as a mean fraction of the net radiation measured above the canopy R_n.

Vegetation	Fraction (-)	Author
Closed vegetation	0.10	Lemeur et al., 1984
Dense forest	0.01	Lemeur et al., 1984
Mixed coniferous/deciduous forest	0.03-0.05	McCaughey, 1985
Subarctic forest	0.09	Lafleur, 1992

1.2.2.3 Physiological inputs

Canopy resistance

As mentioned before (see Equation 1.106), the canopy or surface resistance r_c can be defined as:

$$r_c = \frac{r_s}{LAI} \tag{1.106}$$

where r_s is the stomatal resistance of leaves with stomatal pores located at one leaf

surface only, and r_s and r_c have units of s m^{-1}, and LAI (m^2 m^{-2}) is the total leaf area per unit ground surface.

Stomatal resistance r_s depends on the anatomical characteristics of the stomata and it varies throughout the day due to the response of the stomata to climatic conditions as (i) solar radiation, (ii) atmospheric CO_2 concentration, (iii) specific humidity deficit, (iv) leaf temperature, and (iv) leaf water potential (Jarvis, 1976). Based on Jarvis' work, Stewart (1988) developed a model in which the canopy conductance was related to solar radiation, air temperature, specific humidity deficit, soil moisture deficit and leaf area index. The so-called Jarvis-Stewart model was applied to data from a Scots pine forest in England (Stewart, 1988), and e.g. in an oak forest in The Netherlands (Ogink-Hendriks, 1995). It can be written as:

$$1/r_s = g_s = g_{c,\max}/L_{\max}\ f(R_s) f(\Delta q) f(T_a) f(\Delta \boldsymbol{q}) \tag{1.175}$$

where g_s is the stomatal conductance (m s^{-1}), being the inverse of the stomatal resistance r_s, $g_{c,max}$ is the maximum canopy conductance (m s^{-1}), L_{max} is the maximal LAI of the canopy during the growing season (m^2 m^{-2}), $f(R_s)$ is a global radiation function, $f(\Delta q)$ is a specific humidity deficit function, $f(T_a)$ is an air temperature function and $f(\Delta \boldsymbol{q})$ is a soil moisture deficit function. All functions yield a value between 0 and 1, as they express a reduction with respect to the maximum conductance, and are described by Ogink-Hendriks (1995) as follows:

$$f(R_s) = \frac{1254.1 R_s}{1000(R_s + 254.1)} \tag{1.176}$$

$$f(\Delta q) = 0.2305 + 0.7695 \cdot 0.7089^{\Delta q} \tag{1.177}$$

$$f(T_a) = \frac{T_a(40 - T_a)^{1.382}}{1295.43} \tag{1.178}$$

$$f(\Delta \boldsymbol{q}) = 1 - \exp[0.0876(\Delta \boldsymbol{q} - 141.9)] \tag{1.179}$$

where R_s, T_a, $\Delta \boldsymbol{q}$ and Δq are respectively expressed in W m^{-2}, °C, mm and g kg^{-1}.
Because stomata will mainly react on visible radiation, $f(R_s)$ is substituted by $f(PAR)$:

$$f(PAR) = \frac{4100 PAR}{4010(PAR + 46)} \tag{1.180}$$

where PAR is expressed in µmol m^{-2} s^{-1} and defined as the incoming PAR (both the diffuse and beam components) above the forest canopy.

The value of $g_{c,max}$ (0.05313 m s^{-1}) is calculated from the value found by Ogink-Hendriks for an oak forest in The Netherlands (1995). Therefore, the value of $g_{c,max}$ found by Ogink-Hendriks (1995) was, according to Equation 1.106, re-calculated to a value of $g_{s,max}$, using the LAI of this oak forest in The Netherlands (LAI = 4.9). This $g_{s,max}$ value was then again converted to $g_{c,max}$, based on Equation 1.106, and taking the LAI of the forest Aelmoeseneie into account (LAI = 5.1). During rain and when the leaves are wet, r_s is set to zero. During night r_s is given the value of 10000 s m^{-1}. This value is deducted from the maximal cuticular conductance of beech (8200 s m^{-1}, Hoad et al., 1997).

By combining Equation 1.175, Equation 1.180 and Equation 1.106, canopy resistance r_c (s m^{-1}) can be calculated from the following expression:

$$1/r_c = g_c = g_{c,\max}\left(L/L_{\max}\right) f\left(PAR\right) f\left(\Delta q\right) f\left(T_a\right) f\left(\Delta \boldsymbol{q}\right) \qquad (1.181)$$

where g_c is the canopy conductance (m s^{-1}), L the LAI of the forest at the considered moment in the growing season (m^2 m^{-2}), and the different reduction functions are defined above (Equations 1.177-180). During rain and when the leaves are wet, r_s is set to zero. During night r_s is given the value of 2000 s m^{-1}.

Leaf area index

As mentioned before (§ 1.2.1.6) the value of L_{max} (see Equation 1.175 and 1.181) for the main tree species in the forest Aelmoeseneie is shown in Table 1.2. The LAI at a certain moment during the growing season L (Equation 1.181), can be found from the seasonal LAI evolution which is described as three consecutive and linear relationships (see § 1.2.1.6) and is shown in Figure 1.11.

1.2.2.5 Interception of rain

Forest type, ground cover and climate determine the amount of precipitation that reaches the ground surface. Precipitation is partitioned into three fractions: (i) that which remains on the vegetation and is evaporated after or during rainfall (interception); (ii) that which flows to the ground via stems (stemflow); and (iii) that which may or may not contact the canopy and which falls to the ground between the various components of the vegetation (throughfall).

No distinction is made between rainfall intercepted by the leaves or by the stem and branches. The coverage of the vegetation *c* (-) is the vertical projection of leaves, branches and stem per unit soil surface. This parameter *c* has a minimal value in winter c_w, and a maximal value once the maximal LAI is achieved during the growing season in summer c_s. The rainfall intercepted by trees can be determined by a throughfall coefficient *p* (-). The seasonal dynamics of this parameter is reversed compared to the one by parameter *c*. When c_w and c_s are respectively the minimal and maximal value of *c*, and p_s and p_w are respectively the minimal and maximal value of *p*, then *c* and *p* on a certain moment can be calculated from:

$$c = c_w + \frac{L}{L_{\max}}(c_s - c_w) \tag{1.182}$$

$$p = p_w - \frac{L}{L_{\max}}(p_w - p_s) \tag{1.183}$$

where L_{max} is the maximal LAI during the growing season.

The interception capacity of the vegetation S_{cap} (expressed in mm of rain) at that moment is given by:

$$S_{cap} = \frac{c}{c_s} S_{cap,\max} \tag{1.184}$$

where $S_{cap,max}$ is the maximal interception capacity at full leaf development during the growing season (mm). S_{cap} indicates the theoretical total amount of rain (l per m^2 or mm) which can be intercepted after a sufficiently long period of precipitation while on the other hand, the actual amount of rain that is intercepted during a particular period of time Δt I_{int} (mm) can be found in the difference between incoming rain *R* measured above the canopy and throughfall *pR* measured at ground level during that time period, or:

$$I_{\text{int}} = (1 - p)R$$

(1.185)

It is clear that intercepted rain I_{int} will evaporate, and that the rate of evaporation E_{int} can be calculated from the Penman-Monteith equation where the canopy resistance r_c is set to zero as no stomatal control occurs this time (Equation 1.100).
From the moment rainfall starts, it is calculated for each time step Δt if the intercepted amount of rainfall I_{int} (Equation 1.185) exceeds the interception capacity S_{cap} (Equation 1.184), and also the evaporation rate E_{int} is calculated. In a first case, the amount of

intercepted rainfall I_{int} in the considered time step Δt is smaller than the interception capacity S_{cap}. On that moment there are two possibilities, or during the considered time step Δt all intercepted water is evaporated or it is not, this is expressed by the following equations:

if $(1\text{-}p)R<S_{cap}$, then $I_{int} = (1\text{-}p)R$ and

$$E_{\text{int}} \geq I_{\text{int}} \Rightarrow excess = 0 \quad (1.186)$$

$$E_{\text{int}} < I_{\text{int}} \Rightarrow excess = I_{\text{int}} - E_{\text{int}} \quad (1.187)$$

If not all the intercepted rain is evaporated during the considered time stem Δt (i.e. if the excess > 0, see Equation 1.187), the excess is transferred to the next time step t+1. If during this time step t+1 it rains than the intercepted amount of rain that has to be evaporated is not just $(1\text{-}p)R$ but $[(1\text{-}p)R + excess]$. Again it will be calculated if this amount of water can evaporate during the considered time step.
In a second case, the amount of intercepted rainfall I_{int} in the considered time step Δt is larger than the interception capacity S_{cap}, then $I_{int} = S_{cap}$. Again there are two possibilities, or during the considered time step Δt all intercepted water is evaporated or it is not, this is expressed by the following equations:

if $(1\text{-}p)R \geq S_{cap}$, then $I_{int}=S_{cap}$ and

$$E_{\text{int}} \geq I_{\text{int}} \Rightarrow excess = 0 \quad (1.186)$$

$$E_{\text{int}} < I_{\text{int}} \Rightarrow excess = I_{\text{int}} - E_{\text{int}} \quad (1.187)$$

Just as before when this amount of intercepted rain can not evaporate during the considered time step Δt (i.e. if the excess > 0, see Equation 1.187), then the excess is transferred to the next time step. When all intercepted rain is evaporated the evapotranspiration rate is again calculated with the Penman-Monteith formula (Equation 1.103).
The used values for the different parameters were taken from Herbst et al. (1999) who measured the interception parameters in a beech forest in northern Germany with a seasonal maximal LAI of 4.46 which is close to the seasonal maximal value measured in the forest Aelmoeseneie (5.1, see Table 1.2): $S_{cap,max}$ = 1.28 mm during summer and 0.80 mm during winter, p_w = 0.90 and p_s = 0.25. The coverage of the vegetation in the forest Aelmoeseneie is estimated from visual observations, as: during winter c_w = 0.3 and during summer c_s = 0.8.

1.2.3 Multi-layer water vapour exchange

In this part it will be explained how the FORUG-model is extended for a multi-layer approach applicable in forest canopies. More exactly the forest will be considered to be composed of three upper canopy layers, one understory layer, and a soil layer. The Penman-Monteith equation will be applied for each canopy layer which is considered to be a single big-leaf, instead of considering the total canopy as one big-leaf.

Before the Penman-Monteith equation (Equation 1.103) was applied on canopy level. At its simplest, the Penman-Monteith equation describes a single evporating element in the canopy, say a leaf. In this case the canopy resistance and the aerodynamic boundary layer resistance in Equation 1.103 are replaced by a stomatal resistance and a leaf boundary layer resistance respectively (Raupach and Finnigan, 1988). When the canopy is considered to be composed from several distinct horizontal layers (several big-leaves), then the stomatal resistance is replaced by a canopy resistance valid for that layer, and the leaf boundary resistance is replaced by a boundary resistance also valid for that layer (see later § 1.2.3.2). In such a horizontal canopy layer, all resistances as well stomatal as leaf boundary layer resistance are acting in parallel, and just as for the conversion between stomatal resistance and total canopy resistance (see Equation 1.106) the LAI of the considered horizontal layer is the scaling factor.

In this model climatic parameters vary only according to the depth inside the canopy and not according to the species. It should be remarked that the net change of heat storage *S* in the canopy is neglected (see later § 3.5)(Shuttleworth, 1994), and that it is replaced by the soil heat flux *G* for the soil layer.

1.2.3.1 Introduction of a net radiation profile

The vertical decrease of net radiation in the canopy is described in a way analogous to the extinction of short-wave radiation (see Equation 1.130):

$$R_n(L) = R_n(0)\exp(-k_{Rn}L) \tag{1.188}$$

where $R_n(L)$ (W m^{-2}) is the available net radiation at the level of downward cumulative leaf area index L, $R_n(0)$ is the net radiation at the top of the canopy, and k_{Rn} is the extinction coefficient for net radiation. Baldocchi et al. (1984) found a k_{Rn} value of 0.592 for the case of an oak-hickory forest. If net radiation is not measured above the canopy,

it then can be calculated according to the method as described above in § 1.2.2.2. As was also done before (§ 1.2.1.4) the upper canopy layer is numbered as layer one, the middle and lower layer as layer two and three respectively, and the understory layer as layer four. The net radiation $R_{n,i}$ (W m^{-2}) available to canopy layer situated between level i (L_i) and level i-1 (L_{i-1}) is:

$$R_{n,i} = R_n(0)\left[\exp(-k_{Rn}L_{i-1}) - \exp(-k_{Rn}L_i)\right] \quad (1.189)$$

The net radiation available to the soil layer $R_{n,soil}$ (W m^{-2}) is:

$$R_{n,soil} = R_n(0)\exp(-k_{Rn}L_{tot}) \quad (1.190)$$

where L_{tot} is the total downward cumulative LAI down to the soil level.

It is advisable to support the above-described theoretical extinction of net radiation in the canopy with measurements. These measurements should be executed during as well a foliated as a non-foliated period.

1.2.3.2 Resistances and conductances at different layers

Leaf boundary layer resistance

The leaf boundary layer resistance $r_{b,i}$ at the layer i is described according to Equation 1.4 (see § 1.1.1.1):

$$r_{b,i} = 307\sqrt{\frac{d_c}{u_i}} \quad (1.191)$$

The characteristic dimension d_c for the principal tree species of the forest Aelmoeseneie, namely beech, oak and ash and for the understory species are respectively 0.050, 0.045, 0.035 and 0.050 m. Besides d_c, also the wind speed u_i at the level i is necessary for the determination of r_b. As wind speed measured above the canopy is not representative for wind speed inside the canopy, the relative extinction of wind speed inside the canopy was measured with anemometers. Wind speeds were measured stepwise from the upper canopy level to the soil level and simultaneously compared to an anemometer which was fixed at the platform at 28 m (see § 2.2.2.2). The vertical wind speed profiles were measured on three days during the period August-

September 1998. Two classes of typical wind speed are considered i.e. ranges 0 to 3.5 m s^{-1} and 3.5 to 6.0 m s^{-1} (see Figure 1.13).

The boundary layer resistance $r_{bl,i}$ (s m^{-1}) of the big leaf representing canopy layer *i* is calculated as follows:

$$r_{bl,i} = r_{b,i} / \left(L_i - L_{i-1}\right) \quad (1.192)$$

where L_i and L_{i-1} are the downward cumulative leaf area index at the level *i* and *i*-1 respectively

Just as for net radiation it is advised to continuously measure wind speed at different heights in the canopy during a limited period. Again it is recommended to distinguish between foliated and non-foliated conditions.

Soil boundary layer resistance

The soil layer is characterised by a resistance describing the transition from soil to vegetation r_{sv} (s m^{-1}) and can be described in a way analogous to the laminar boundary layer resistance (Goudriaan, 1977):

$$r_{sv} = 180\sqrt{\frac{d_{cs}}{u_s}} \quad (1.193)$$

where d_{cs} (m) is the effective dimension of the soil which can be explained as the length of the roughness elements lying on the soil (personal communication, M. Aubinet, Gembloux, 1999), and u_s is the wind speed (m s^{-1}) above the soil (see Figure 1.13). The d_{cs} is assumed to have a value of 0.04 m and equals d_c of death leaves lying on the soil.

Stomatal conductance

As mentioned before (see § 1.2.2.3), stomatal conductance g_s (m s^{-1}) can be calculated according to Equation 1.175. The stomatal conductance $g_{s,i,j}$ taking into account a particular layer *i* and a tree species *j*, can be written as:

$$g_{s,i,j} = g_{s,\max,i,j}\, f\left(PAR_{i,j}\right) f\left(\Delta q_i\right) f\left(T_{a,i}\right) f\left(\Delta \boldsymbol{q}\right) \quad (1.194)$$

where $f(PAR_{i,j})$ is a visible radiation function for layer i and tree species j, $f(Dq)$ is a specific humidity deficit function for layer i and is calculated according to Equation 1.177 where Dq is measured at layer i, $f(T_{a,i})$ is an air temperature function for layer i and is calculated according to Equation 1.178 where T_a is measured at layer i and $f(Dq)$ is a soil moisture deficit function (Equation 1.179)(see also § 1.2.2.3). All functions yield a value between 0 and 1, as they express a reduction with respect to the maximum conductance.

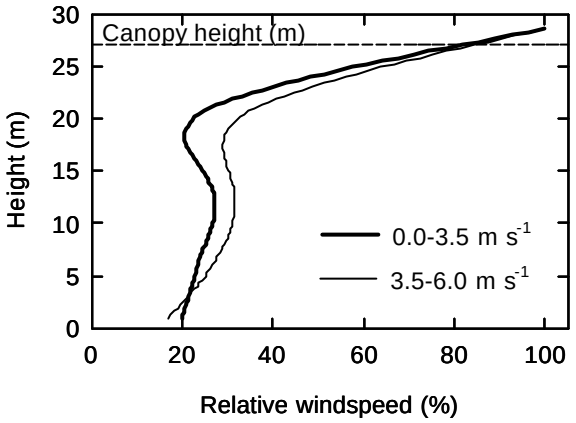

Figure 1.13 Relative extinction of wind speed inside the canopy of the Aelmoeseneie forest, during the fully-leaved period, for two wind speed classes (0-3.5 m s^{-1} and 3.5-6 m s^{-1}), and compared to the wind speed at a height of 28.6 m (platform 4). Canopy height is 27m.

It should be remarked that the maximal stomatal conductance $g_{s,max}$ and the radiation function $f(PAR)$ vary not only with the canopy layer but as well for the tree species. Values of $g_{s,max}$ used in the model are listed in Table 1.10. They are obtained from diurnal measurements with a porometer (AP4, Delta-T Devices, Ltd, Cambridge, UK) during the summer of 1997 (see also Vanhoutte, 1998). During this summer diurnal courses (from sunrise til sunset) of stomatal resistance of beech (at 21, 14, 7 m) and ash (21 m) was measured hourly. Before measuring the porometer was calibrated inside the canopy, at a height of 21 m. A measurement cycle started with measuring beech and ash (both at a height of 21 m), followed by beech at 14 m and beech at 7 m. If necessary, the porometer was, during the same measuring cycle recalibrated at each platform. During each measurement cycle, for each species at a respective level, 5 leaves were measured. Measurements were conducted on 6 days between July and

September.

The PAR function $f(PAR_{i,j})$ can now be written as (see also Equation 1.180):

$$f\left(PAR_{sun,i,j}\right) = \frac{4100 I^{i}_{sun,i,j}}{4010\left(I^{i}_{sun,i,j} + 46\right)} \quad (1.195)$$

$$f\left(PAR_{shade,i,j}\right) = \frac{4100 I^{i}_{shade,i,j}}{4010\left(I^{i}_{shade,i,j} + 46\right)} \quad (1.196)$$

where $I^{i}_{sun,i,j}$ and $I^{i}_{shade,i,j}$ are the intercepted PAR intensity in the sun and shade leaf area in layer *i* for species *j* (µmol m^{-2} s^{-1}). The intercepted PAR intensities are calculated as explained before (see Equations 1.135-136).

Table 1.10 Values of maximal stomatal conductance $g_{s,max}$ (m s^{-1}) for the main upperstory and understory species in the Aelmoeseneie forest. Values are obtained from porometer measurements (Vanhoutte, 1998), and from stomatal characteristics (Steppe, 2000) based on the methodology followed in Samson et al. (2000a). Values in bold are selected as model input parameters, and values in italics are calculated from the equation [(stomatal characteristics species X)/(stomatal characteristics beech 21m) = (porometer species X)/(porometer beech 21m)]. The stomatal pore depth is assumed to be 20 µm.(-: no measurements available)

Species	Porometer	Stomatal characteristics
Beech 21m	**0.0057**	0.0247
14m	**0.0036**	0.0168
7m	**0.0025**	0.0122
Oak	**0.0111***	-
Ash	**0.0093**	0.0473
Hazel	**0.0019**	0.0176
Sycamore	***0.0026***	0.0111
Rowan	***0.0018***	0.0078

* Ogink-Hendriks (1995)

The above equations (Equations 1.195-1.196) combined with Equation 1.194 allow stomatal conductance g_s to be calculated for as well sun and shaded leaf areas. If $g_{s,sun,i,j}$ and $g_{s,shade,i,j}$ are the stomatal conductance (m s^{-1}) of the sun and shade leaf areas in layer *i* and for species *j* respectively, and $L_{sun,i,j}$ and $L_{shade,i,j}$ are the leaf areas of both leaf classes in layer *i* and for species *j* respectively, then the canopy conductance $g_{c,i,j}$ (m s^{-1}) of the big-leaf representing canopy layer *i* can be calculated as

follows:

$$1/r_{c,i,j} = g_{c,i,j} = g_{s,sun,i,j} \cdot L_{sun,i,j} + g_{s,shade,i,j} \cdot L_{shade,i,j} \quad (1.197)$$

where $r_{c,i,j}$ is the corresponding canopy resistance (s m^{-1}).

Soil resistance

Water in the upper soil layer will, while diffusing to the air layers above the soil encounter a certain resistance (similar to stomatal resistance), namely the soil resistance r_{soil} (s m^{-1}). This resistance depends on the water content of the soil θ (m^3 m^{-3}) and on the composition of the soil. Both factors are combined in the next formula (Camillo & Gurney, 1986) which is preferred above other formulas (see De Dekker, 1999) because of its logical behaviour (the resistance increases when the soil dries out):

$$r_{soil} = 3.5\frac{\theta_s}{\theta} + 33.5 \quad (1.198)$$

where θ_s is the satuarated water content of the soil (m^3 m^{-3}). Values of θ_s at different depths in the Aelmoeseneie forest are determined by Willems (1998) and shown in Table 1.11. The water content of the soil θ can be calculated from tensiometer measurements, using the appropriate pF-curves for the different soil layers (see Willems, 1998). Measurements at a depth of -10 cm and -25 cm were used for the calculation of r_{soil}.

1.2.3.3 Interception of rain

Interception of rain is calculated as explained before (see § 1.2.2.4). The main difference between the single-layer and multi-layer approach is that the total interception capacity of the vegetation S_{cap} (see Equation 1.184) is divided over the different considered vegetation layers. The interception capacity $S_{cap,i}$ (mm) of canopy layer i, is calculated by the following equation:

$$S_{cap,i} = S_{cap}\frac{(L_i - L_{i-1})}{L_{tot}} \quad (1.199)$$

where L_i and L_{i-1} are the downward cumulative LAI L at level i and i-1 respectively, and L_{tot} is the total downward cumulative LAI of the total canopy.

When it starts raining, the above canopy layer starts to intercept the rain. When the interception capacity of the above canopy layer is exceeded the second canopy layer starts to intercept, and so on.

Table 1.11 The saturated water content of the soil q_s at different depths, for the two forest types in the Aelmoeseneie forest (Willems, 1998).-: no value available

Oak-Beech Forest		Ash forest	
depth (cm)	q_s ($m^3\ m^{-3}$)	depth (cm)	q_s ($m^3\ m^{-3}$)
-10	0.53	-10	0.56
-25	0.47	-25	0.63
-50	0.47	-50	0.51
-75	0.86	-75	0.45
-100	-	-100	0.71

1.2.3.4 Total multi-layer evapotranspiration

The evapotranspiration lE_i (W m^{-2}) for each canopy layer i, is calculated according to the Equations 1.100 and 1.103 for a wet and a dry canopy respectively. Total evapotranspiration (W m^{-2}) for a considered species is calculated as:

$$lE = \sum_{i}^{n} lE_i \qquad (1.200)$$

with n the number of layers for the considered species.

1.2.4 Overall structure of the FORUG model

As is clear from the above the FORUG model can as well be used to estimate the CO_2 (§ 1.2.1) and water vapour (§ 1.2.2 and 1.2.3) exchange between a forest and the atmosphere. The different submodels for calculating these fluxes are explained as well. The interaction between the different submodels is schematically represented in Figure 1.14 and Figure 1.15, respectively for the multi-layer CO_2-exchange model (§ 1.2.1) and for the water vapour exchange models (§ 1.2.2 and 1.2.3).

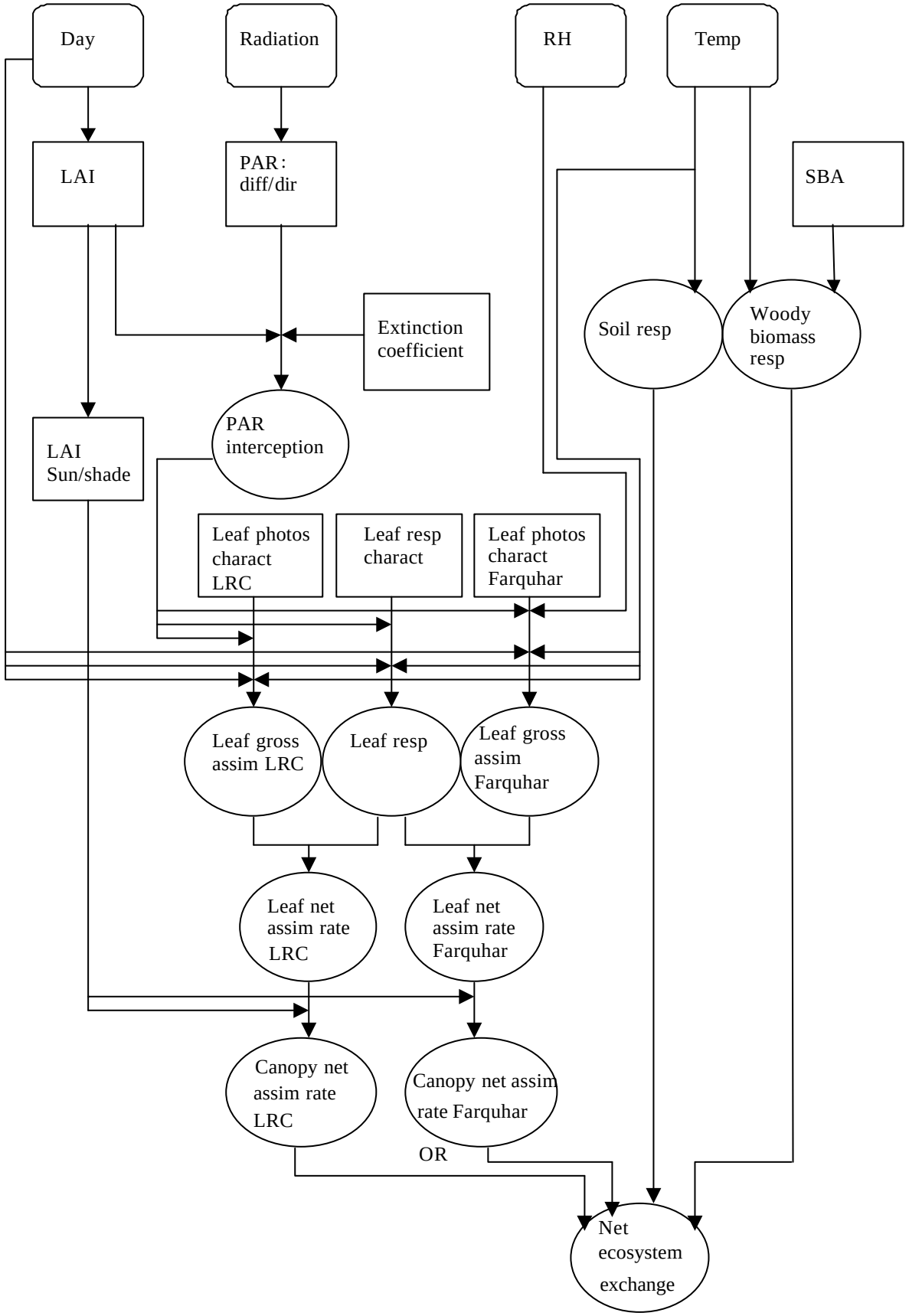

Figure 1.14 Flow chart of the CO_2-module of the FORUG-model. Symbols are ◯: input variable; □: state; ⬭: process. Symbols are: LAI: leaf area index; LRC: leaf response curve; resp: respiration; assim: assimilation; diff: diffuse; dir: direct; RH: relative humidity; SBA: stem and branch area.

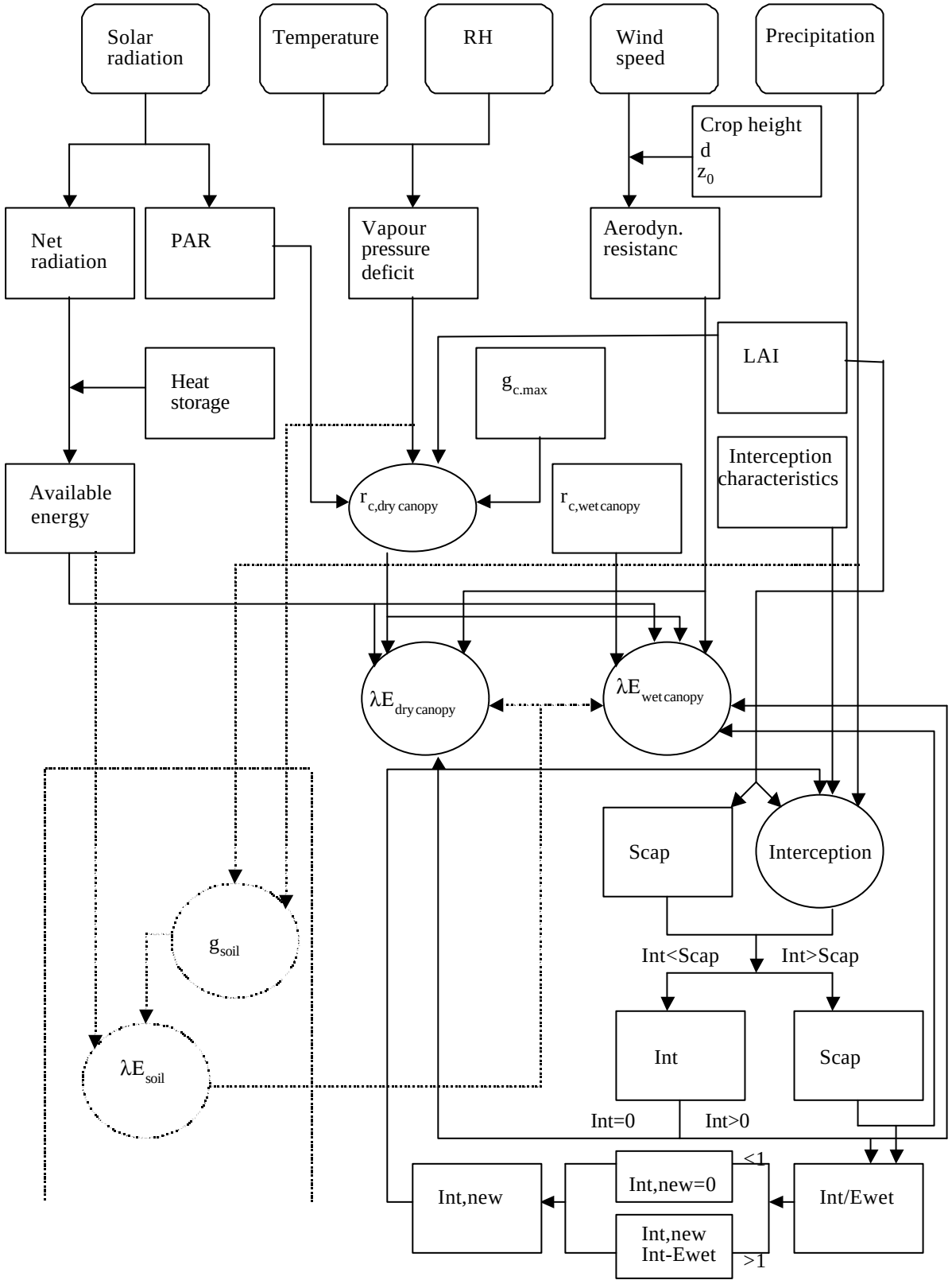

Figure 1.15 Flow chart of the evapotranspiration-module of the FORUG-model. Dashed lines indicate the soil evaporation sub-module which is only included in the multi-layer model. Symbols are ⬡: input variable; □: state; ⬭: process. Symbols are: RH: relative humidity; g_{soil}: soil conductance; d: zero plane displacement; z_0: roughness length; g_c: canopy conductance; r_c: canopy resistance; S_{cap}: interception capacity; Int: interception; Ewet: evaporation the wet canopy during the considered time stem.

Chapter 2
THE EXPERIMENTAL SET-UP IN THE FOREST AELMOESENEIE

In this chapter the experimental forest Aelmoeseneie will be portrayed. All experiments were conducted here. Besides its location, the history and the biotic and abiotic characteristics of this forest will be described in detail, including the measuring tower. Attention will also be given to the meteorological sensors and data-acquisition. Only the basic meteorological sensors will be described in this chapter, together with the registration on the data acquisition system. Special sensors used for specific experiments (e.g. sap flow sensors) will be described in the chapter related to the application. The text of the chapter here is partly based on the information given by Samson et al. (1996).

2.1 Characteristics of the experimental forest

2.1.1 Location and history

The forest Aelmoeseneie is a deciduous forest of 28 ha and it is located at Gontrode (50°58' N, 3°49' E) about 15 km in the South-East direction of Ghent, Belgium (see Figure 2.1). In a radius of 1 km the forest is mainly surrounded by agricultural land, in the West direction this radius is almost 2 km. The forest is situated between 11 and 21 m above sea level. It belongs to Ghent University and is managed by the Laboratory of Forestry. The main option of the forestry management is scientific research. Therefore a specific scientific zone of 1.83 ha was fenced in 1993, enclosing the area where the research activity is concentrated. Two plots and a measuring tower are installed in this zone. The interesting part of this scientific zone is the transition between two different populations, an ash population and an oak-beech population. The climatic conditions are typical for the Flanders region, as indicated by the standard climatic data from a nearby meteorological station operated by the Royal Meteorological Institute of Belgium (Table 2.1).

The part of Flanders where the forest Aelmoeseneie is located was covered with a large forest complex before the Early Middle Ages. The need for agricultural land caused several deforestations all over the region. The name of the village Gontrode, where the forest is located refers to these deforestations. The forest Aelmoeseneie was mentioned for the first time in 864, in a document belonging to Saint Baafs abbey. From the year 1200 on the forest belonged to the 'Aelmoesenei', which was a charity institution of the abbey. This situation lasted until the secularisation at the period of French occupations. From that moment the forest became property of the OCMW; which is the commission of public welfare of the city of Ghent. After World War I, a replantation was necessary because a lot of trees were cut by the local population and used for heating.

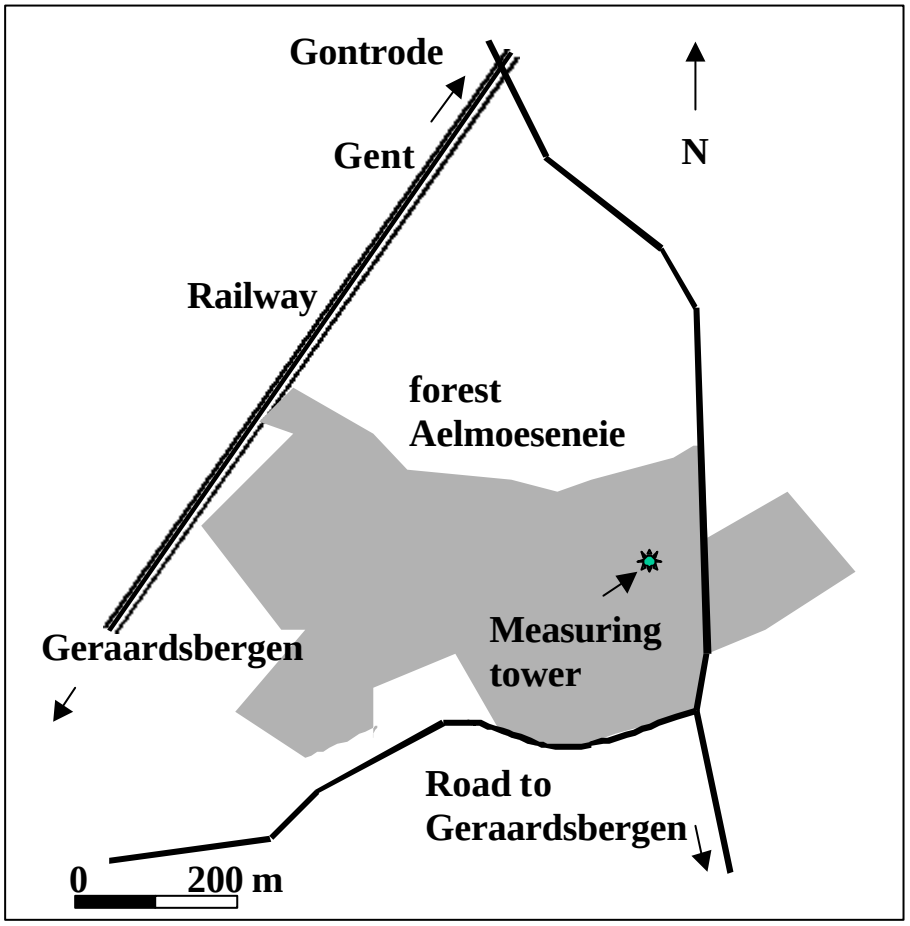

Figure 2.1 The location of the forest Aelmoeseneie at Gontrode (Belgium), with indication of the measuring tower.

Nowadays only 3 beeches remain that are older than 80 years. In the year 1968, the old forest of 20 ha and 10 ha wet pastures next to this forest were bought by the Ministry of National Education and this was granted to the Ghent University for scientific purposes. From 1968 to 1973 the pastures were forested, and in the year 1973 an arboretum with the main West European tree species was elaborated (Muys

& Van Eleghem, 1994). An appropriate forest management was worked out in 1988 by Lust et al. (1988).

Table 2.1 Annual means for standard climatic data measured during the period 1984-1993 at Kruishoutem, province of East-Flanders, Belgium.

Parameter	Mean value
Annual temperature	10.1°C
Temperature coldest month (February)	2.8°C
Temperature warmest month (July)	17.4°C
Date first frost	10 November (14 Oct. - 8 Dec.)
Date last frost	13 April (16 March - 29 April)
Days with frost	47 days
Annual precipitation	791 mm

2.1.2 Biotic and abiotic characteristics

The basic layer of the forest Aelmoeseneie exists out of tertiary clay-loam complexes of the Paniseliaan. In the Glacial Period of the Quartair, a loamy layer covered the tertiary layer. Loam was mixed with the local sand, which caused a sandloamy covering to 50 to 100 cm depth. Two brooks cross the forest. The Molenbeek flows in the young part of the forest, the Bloedbeek in the older part. The texture near these brooks is alluvial clay. All of the soils are more or less gleyic, what indicates the temporal wetness of the soil. The main part of the forest, about 25 hectares, is an individual mixture of mainly broad-leaved species. The mean stem number per ha is 380 and is divided over 26 tree and shrub species (Samson et al., 1996).

2.1.2.1 The scientific zone

In the Aelmoeseneie forest, a fenced zone of 1.83 ha was chosen for intensive scientific monitoring of the mixed deciduous forest ecosystem. This experimental zone is situated on the northern slope of a small elevation which includes the highest part of the forest (21 m above sea level) and the relative steep slope towards the Blood Brook, including the depression of this brook. Because of the presence of two different site types large differences in vegetation (see Figure 2.2 and Table 2.2) can be noted. This is due to differences in soil conditions, i.e. a thin quaternary layer of

sandy loam, and a ground water dependent alluvial part in the oak-beech and ash site respectively. This oak-beech and ash forest site are the two main forest types of the forest Aelmoeseneie. The dominating trees of both forest sites are all about 75 years old. Beech, oak and ash trees reach maturity around 130, 150 to 200 and 75 years respectively. This means that ash trees may be considered as mature, whereas oak trees have to be considered as young trees.

2.1.2.2 The oak-beech forest site

The oak-beech forest site or the sloped site (area: 1.06 ha) is a typical thin quaternary layer of sandy loam with a spotted texture B horizon on a shallow impermeable clay and sand complex of tertiary origin (uLdb-uLub). Shallow drains occur every ten meter showing litter accumulation. In this site, the upperstory is a mixture of different species (Table 2.2), with as main species Pendunculate oak (*Quercus robur* L.) and Common beech (*Fagus sylvatica* L.). In the shrub layer Sycamore (*Acer pseudoplatanus* L.), Hazel (*Corylus avellana* L.), and Rowan (*Sorbus aucuparia* L.) are the main species. The herb layer is dominated by Bramble (*Rubus sp.*) and Bracken (*Pteridium aquilinum* (L.) Kuhn) and to a lesser degree Yellow archangle (*Lamium galeobdolon* L.), Honeysuckle (*Lonicera periclymenum* (L.) L.) and Salomon's seal (*Polygonatum multiflorum* (L.) All.). The percentage of ground cover by the vegetation is between 60 and 90 %. The humus layer is of a moder type. The pH_{water} of the soil (upper horizon) is equal to 3.7.

Table 2.2 Stem number (number of trees per ha) and its distribution (%) over the tree species present in the two forest sites (oak-beech and ash) of the experimental zone in the forest Aelmoeseneie. The data are valid for 1997 (after Vande Walle et al., 1998).

	Oak-beech site		Ash site	
Species	Stem number	Distribution	Stem number	Distribution
Oak	139	40.2	38	9.4
Beech	81	23.5	4	1.0
Ash	8	2.2	162	40.1
Larch	18	5.2	8	1.9
Sycamore	56	16.1	119	29.4
Hazel	15	4.4	40	10.0
Other	29	8.4	33	8.2
Total	345	100.0	403	100.0

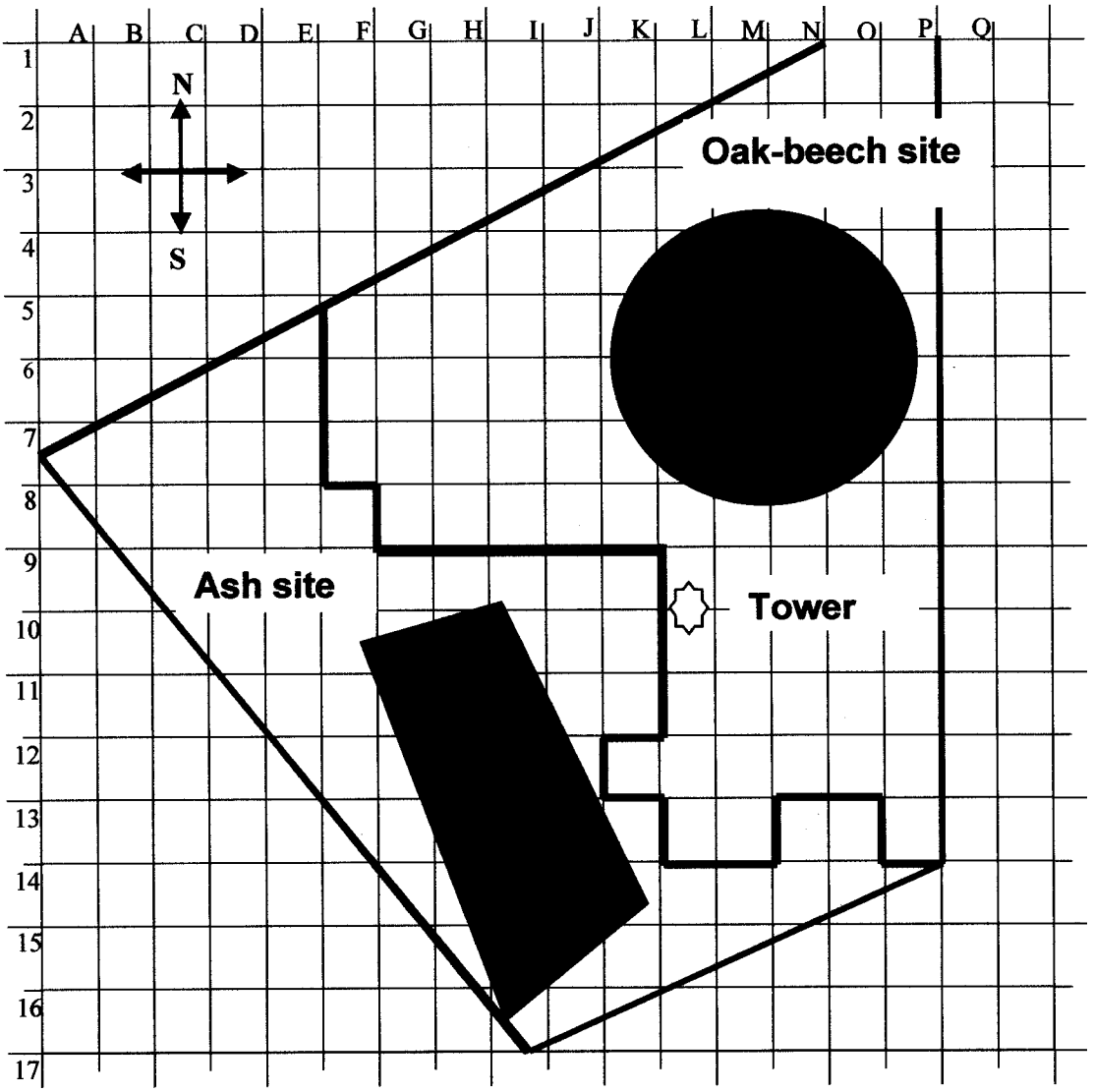

Figure 2.2 Detailed map of the scientific zone in the forest Aelmoeseneie, showing the oak-beech and ash sites, the areas (in black) for intensive ecosystem observations (Level II plots of the European project "Permanent monitoring of the forest ecosystem"), the measuring tower and the 10 x 10 m reference grid (after Mussche, 1997)

The basal area and the standing volume for this site amounts respectively to 26.56 m^2 ha^{-1} (Table 2.3) and 301.2 m^3 ha^{-1} (Table 2.4). The mean diameter of the tree species is given in Table 2.5. The maximal LAI of the oak-beech forest site was measured during a growing season and was found to be 5.52 (Mussche, 1997; Samson et al., 1997a)(see also § 1.2.1.6). This resulted from leaf litter measurements and a comparison with different optical methods to determine LAI was done as well.

2.1.2.3 The ash forest site

The ash forest type is located in the ground water dependent alluvial part (Ldp-Lhp) of the scientific zone where the impermeable layer ceases. Ash is the main species here (see Table 2.2) mixed with Pendunculate oak, Sycamore and a few Poplars. The shrub layer is very dense with mostly Hazel and regeneration of Sycamore. The herb layer is well developed in this site, especially the vernal vegetation: Primrose (*Primula elatior* (L.) L.), Yellow archangel, Moschatel (*Adoxa moshatellina* L.), Wavy hair-grass (Deschampsia cespitosa (L.) Beauv.), Greater stichwort (*Stellaria holostea* L.) and Lords-and-Ladies (*Arum maculatum* L.). The moss layer, being nearly absent (2% of cover) in the oak-beech site described above, is now well developed with a cover of 50 to 80%. Seedlings of Sycamore are also abundant. The humus layer is of a mull type with a litter layer that is mostly degraded before the start of the new growing season. The pH_{water} of the soil (upper horizon) amounts 4.0.

Table 2.3 Basal area at 1.3 m height (m^2 ha^{-1}) and its distribution (%) over the tree species in the two forest sites (oak-beech and ash) of the experimental zone in the forest Aelmoeseneie. The data are valid for 1997 (after Vande Walle et al., 1998).

	Oak-beech site		Ash site	
Species	Basal area	Distribution	Basal area	Distribution
Oak	12.93	48.7	3.25	10.6
Beech	7.06	26.6	0.40	1.3
Ash	1.07	4.0	18.32	59.5
Larch	3.32	12.5	1.39	4.5
Sycamore	0.81	3.0	4.87	15.8
Hazel	0.10	0.4	0.30	1.0
Other	1.28	4.8	2.24	7.3
Total	26.56	100.0	30.77	100.0

The basal area and the standing volume for this site amounts to respectively 30.77 m^2 ha^{-1} (Table 2.3) and 327.7 m^3 ha^{-1} (Table 2.4). The mean diameter of the tree species is given in Table 2.5. The maximal LAI of the ash canopy was measured during a growing season and found to be 4.53 (Mussche, 1997; Samson et al., 1997a)(see also § 1.2.1.6). This resulted from leaf litter measurements and a comparison with different optical methods to determine LAI was done as well.

Table 2.4 Standing volume (m^3 ha^{-1}) of tree species in the two forest sites (oak-beech and ash) of the experimental zone in the forest Aelmoeseneie. The data are valid for 1997 (after Vande Walle et al., 1998).

Site	Oak-beech site	Ash site
Oak	164.0	41.2
Beech young	10.1	1.4
Beech old	72.3	3.3
Ash	13.0	225.6
Larch	38.1	15.4
Sycamore	3.7	40.8
Total	301.2	327.7

Table 2.5 Mean diameter (cm) at 1.3 m height (standard error is given between brackets) of the tree species in the two forest types of the experimental zone in the forest Aelmoeseneie. The data are valid for 1997 (after Vande Walle et al., 1998).

Species	Oak-beech site	Ash site
Oak	33.3 (8.8)	31.2 (11.2)
Beech young	14.3 (6.6)	24.4 (12.0)
Beech old	65.5 (8.7)	50.9 (*)
Ash	40.7 (13.0)	36.3 (11.2)
Larch	46.9 (13.1)	46.3 (12.4)
Sycamore	10.8 (8.3)	18.7 (13.2)
Hazel	8.9 (1.3)	9.4 (2.1)

* Only one tree

2.2 The measuring tower, sensors and data acquisition

It is a fact that during the last decade forest research became more ecologically orientated. The forest is considered as a complex ecosystem in which the below- and above-ground compartments must be taken into account. The crown stratum of the above-ground compartment is thereby very important. The exchange of CO_2 and water vapour between forest and atmosphere occurs mainly in this crown canopy through the processes of photosynthesis and transpiration, as was already discussed in Chapter 1. Inversely related to the importance of this compartment is its accessibility, especially when *in situ* eco-physiological measurements like gas exchange have to be performed. Moreover, the study of such processes, be it on the level of the stand, the individual tree, a leaf or the soil, requires knowledge of the concomitant characteristics of the environment (e.g. climatic parameters).

This scientific strategy together with the fact that other international research groups had the disposal of a measuring tower, led to the decision to construct a measuring tower in the forest Aelmoeseneie as well.
Funds were granted by the Special Research Fund (BOF) of the Ghent University to install a measuring tower in 1993 (Lust and Lemeur, 1993) and to complete the basic meteorological sensors with data logging equipment and special physiological instrumentation in 1997 (Samson et al., 1997c).

2.2.1 The measuring tower

The measuring tower (Figure 2.3) is a metal frame construction of 36 m high. There are five working platforms 1, 2, 3, 4 and 5 spaced 7 m apart and respectively located at 7, 14, 21, 28 and 35 m above ground level. Each platform can be reached with a ladder from the lower platform. The height of the platforms was chosen as such that platform 1 corresponds with the base of the crowns of the surrounding trees. Platform 2 and 3 are situated in the middle and upper canopy. Platform 4 is constructed just above the top of the canopy and platform 5 is constructed more or less eight meters above it. The latter two platforms are situated in the turbulent boundary layer of the forest. The base of the tower is 16 m^2 (4 x 4 m). The metal frame is placed on a concrete foundation, and the whole construction is stabilised with stretch cables moored in concrete blocks. The surrounding trees are moored in order to avoid storm damage to the tower. At the base of the tower a cabin was constructed where datalogging and communication equipment is installed permanently.

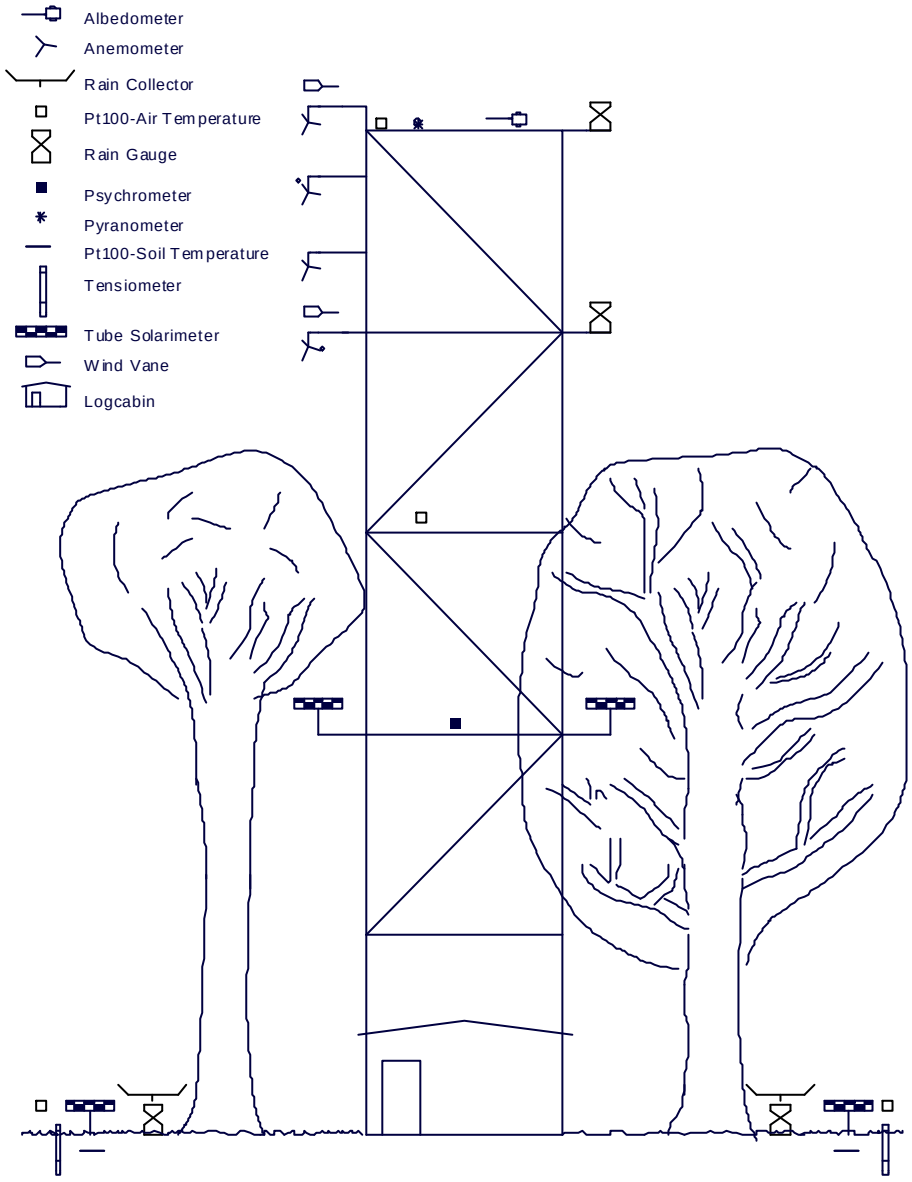

Figure 2.3 Schematic representation of the measuring tower in the forest Aelmoeseneie with indication of the meteorological sensors installed during the 1996 growing season.

The tower is situated at the boundary between the oak-beech and the ash forest site (Figure 2.2). Furthermore, the location of the tower has been chosen in such a way that the three major tree species of the Aelmoeseneie forest (beech, ash and oak) are growing in the nearby surroundings of the tower. From platform 1, 2 and 3 *in situ* measurements can be conducted on leaves and branches of the beech and ash tree

adjacent to the tower. Unfortunately, because of wind damage, the crown of the adjacent oak tree is just not within reach. Another criterion for the positioning of the tower in the scientific zone was the distance from the edge of the forest. This is necessary for establishing a satisfactory fetch in the Western direction. This is important for monitoring constant vertical fluxes for CO_2, water vapour and air pollutants using micro-meteorological methods, such as the Bowen-ratio, the flux-gradient or the eddy-covariance method.

2.2.2 Sensors

To be able to use power driven equipment a 220 V power line was installed on the ground level and on each platform. Besides specific instrumentation, basic climatic sensors were permanently installed, providing a basic micro-meteorological dataset. These basic sensors are described in this chapter, together with the data acquisition system. Experiment specific sensors (e.g. eco-physiological equipment) are described in the appropriate chapter.

The basic climatic sensors installed on the tower and in the forest are: sensors for measurement of radiation, temperature, wind speed, wind direction, rainfall, air humidity, and soil water. Sensors are mostly installed somewhat above the platform, so that measuring heights at platform 1, 2 ,3, 4 and 5 are respectively 7.5, 14.6, 21.6, 28.8 and 36.0 m. An overview of the basic meteorological and of the specific eco-physiological equipment installed on and around the measuring tower is given in the appendix (Appendix 2.1) at the end of this chapter (growing seasons 1995-2000).

2.2.2.1 Radiation and soil heat flux

Short-wave radiation (wavelength range 0.3-3.0 µm) was measured at three heights: above, in and below the crown canopy. Above the canopy, short-wave radiation was measured on platform five. Two sensors were installed at this level. The first one was a circular star-type pyranometer (358, Phillipp Schenk, Austria) measuring the incoming short-wave radiation. The second sensor (GS2, Delta-T Devices Ltd, Cambridge, UK) measured in addition to the incoming also the reflected short-wave radiation, and yielded the albedo of the tree stand. As mentioned above the mean albedo during the growing season was 0.136±0.001.

Picture 2.1 The oak-beech site.

Picture 2.2 The tower in the forest Aelmoeseneie.

The penetration of short-wave radiation in the crown canopy was measured on platform two. On this level, three tube solarimeters (TSL, Delta-T Devices Ltd, Cambridge, UK) were used to measure the short-wave radiation. Because of their linear shape, each sensor gave a spatial integration of the light intensity in the horizontal sun and shade flecks. Each tube solarimeter was fixed on a horizontal bar reaching out of the tower and was positioned under the crown of the beech, ash and oak tree next to the tower. Two tube solarimeters were also installed at ground level respectively in the oak-beech and ash site, in a north-south orientation. Data obtained from these radiation sensors allowed calculation of the absorbed short-wave radiation by the crown canopy. The pyranometers were yearly calibrated against a radiation standard (CM5, Kipp & Zonen, Delft, The Netherlands).

The incoming as the reflected Photosynthetic Active Radiation (PAR) was also measured on platform five, using two PAR quantum sensors (SKP 215, Skye Instruments Ltd, Powys, UK) looking respectively in the upward and downward direction. The mean reflection coefficient during the growing season was 0.039±0.001. The quantum sensors were yearly calibrated against a quantum sensor (Li-190, LI-COR, Lincoln, Nebraska) reserved for annual calibration purposes.

Net radiation (wavelength range 0.3-10.0 µm) was measured on platform five (Q*7.1, REBS, Seattle, USA). This net radiometer was yearly calibrated against a net radiometer used for calibration only (S-1, Swissteco Instruments).

All radiation sensors on platform five to measure incoming and reflected short-wave radiation, PAR and net radiation were mounted on 1.2 m arms extending from the south side of the tower to avoid shading effects.
The soil heat flux was measured at a depth of 8 cm below the surface in both forest sites using a self calibrating heat flux sensor (HFP01SC, Hukseflux, Delft, The Netherlands). Positive values indicate a heat flux into the soil and vice versa.
As an example diurnal courses of net incoming short-wave radiation, net radiation and net incoming PAR are shown in Figure 2.4, together with short-wave radiation measured above, in and under the ash canopy.

2.2.2.2 Temperature

Air temperature was measured using non-ventilated Pt100 sensors. The sensors were shielded by an aluminium housing, itself insulated at the inner side. This protection avoided the warming of the temperature sensor due to direct exposure to the sun, or avoided the cooling due to direct exposure to precipitation or to evaporation of rain or dew. Air temperature was measured on all platforms, and also

1 m above soil surface and at a depth of 4 cm (just above the soil heat flux sensors) in both the oak-beech and ash site.
Temperature sensors were calibrated once a year in a temperature controlled water bath and compared against an accurate (0.1 °C) mercury thermometer.

The diurnal change of the vertical profiles (air and soil temperatures) for a sunny day in summer and in winter are shown in Figure 2.5.

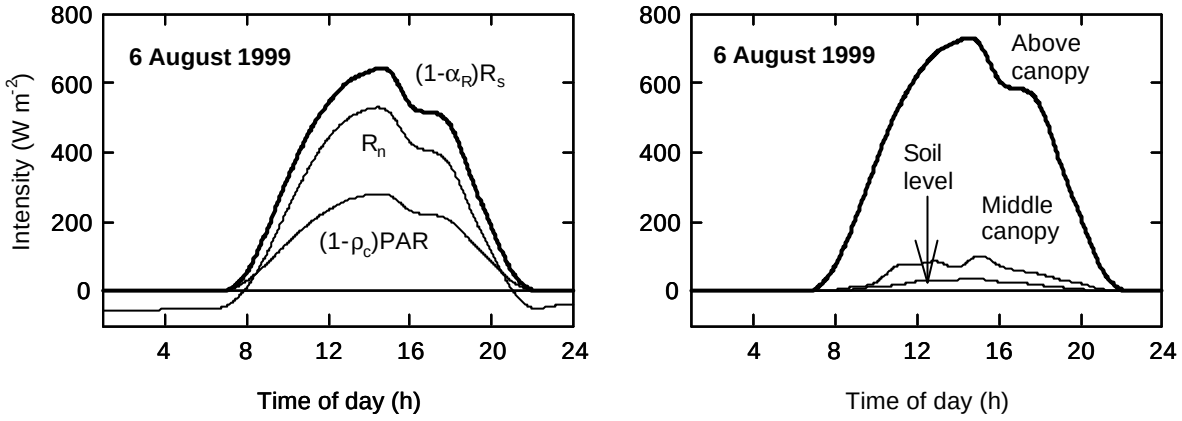

Figure 2.4 Smoothed diurnal courses of: (left) net short-wave radiation [$(1-\alpha_R)R_s$], net radiation (R_n) and net Photosynthetic Active Radiation [$(1-\rho_c)$PAR] measured above the crown canopy, and (right) short-wave radiation above, in the middle of the crown canopy (14 m height) and at the soil level. Measurements were conducted on 6 August 1999 at the ash site.

2.2.2.3 Wind speed and wind direction

Horizontal wind speed was measured at 4 heights above the crown canopy (i.e. at 28.6, 30.6, 32.7, 37.0 m between platform four and somewhat above platform five), using cup anemometers (AN1, Delta-T Devices Ltd, Cambridge, UK). This set-up allowed determination of the vertical wind profile above the forest, and also of the roughness of the forest (see Equations 1.40 and 1.41 in § 1.1.2.1). Wind speed below 0.2 m s^{-1} could not be measured accurately due to the stalling of the cups at low wind speed.

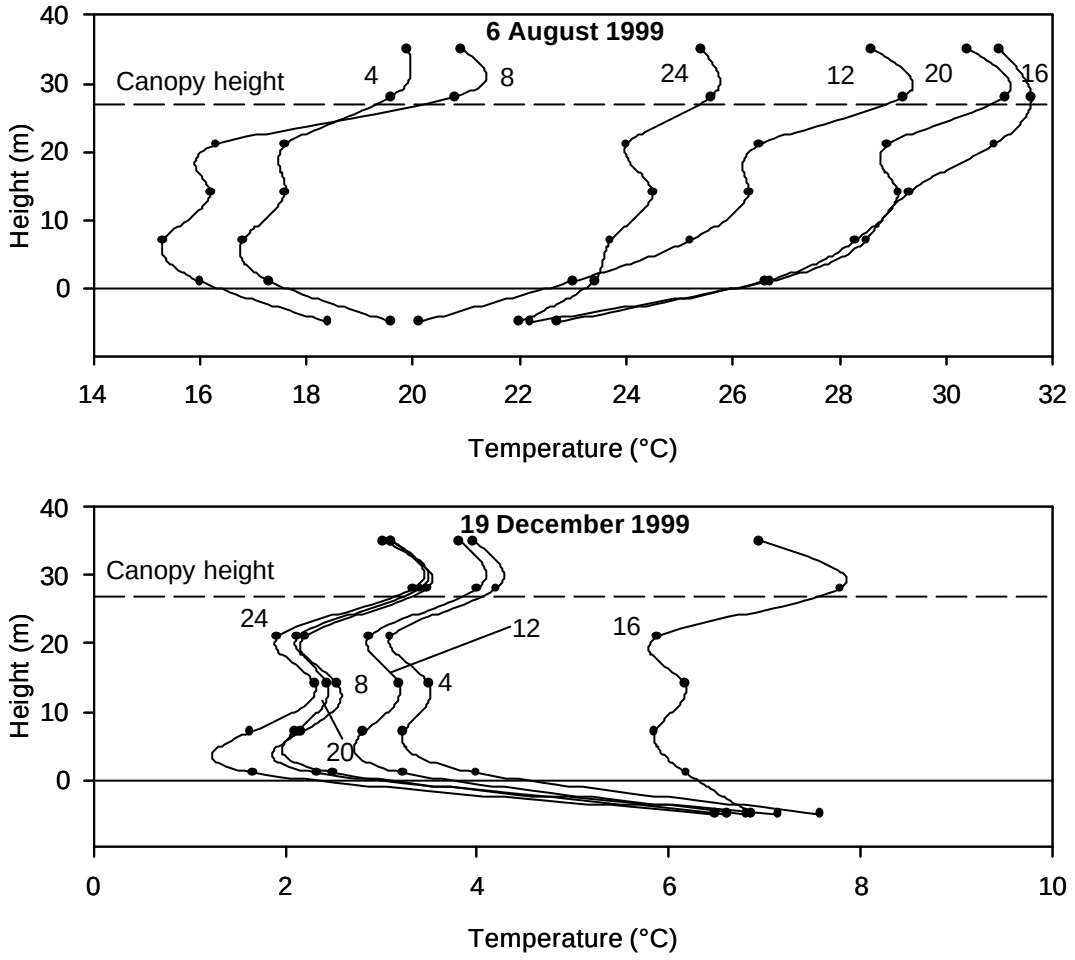

Figure 2.5 Diurnal changes of the vertical air temperature profiles measured at different heights above and inside the crown canopy, and in the soil. Heights indicate distance above the ground level. For clarity, soil depths are not shown at a correct scale, as soil temperature was measured at a depth of 4 cm. Data are shown for a sunny day in summer (6 August 1999) and winter (19 December 1999). Numbers on the profiles refer to the time of day and dots indicate measured values.

Wind direction was measured at two heights above the main canopy, on platform four and five, using wind vanes (WD1, Delta-T Devices Ltd, Cambridge, UK). Wind direction was expressed in degrees (°) between 0 and 360.

As an example, average wind speed (ten minute and hourly averages) measured at platform 5, as well as wind direction, are shown in Figure 2.6.

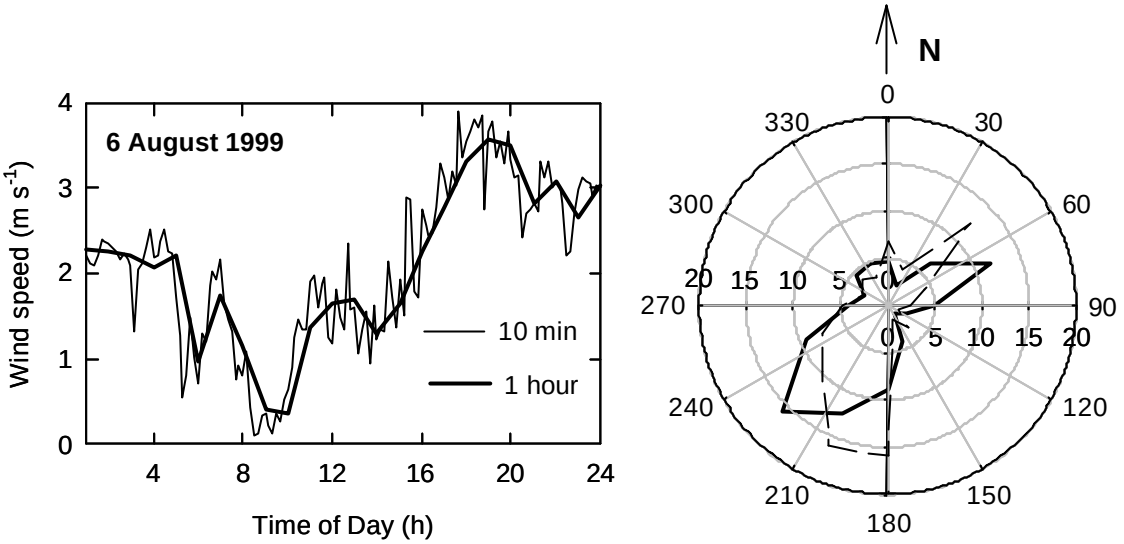

Figure 2.6 Left: comparison of mean wind speed values measured above the crown canopy at a height of 36 m, based on ten minute and hourly averages. Measurements were conducted on 6 August 1999. Right: comparison of the relative frequency (polar representation) of the wind direction measured at two heights above the crown canopy, respectively at 36 m (full line) and at 28,6 m (dashed line) during the month of August 1999.

2.2.2.4 Precipitation

In order to measure the precipitation, tipping bucket raingauges were installed. One raingauge (RG1, Delta-T Devices Ltd, Cambridge, UK) was installed on platform 5 above the crown canopy. With this gauge the free field or gross precipitation was measured.

Under the canopy and at soil level, both throughfall and stemflow was measured in both sites. Throughfall was collected in two gutters each with a length of 6 m and a width of 0.18 m and each gutter was connected with a raingauge. One gutter was placed at the east and one at the west side of the experimental tower, at a distance of approximately 20 to 30 m of this tower. This experimental set-up allowed to quantify throughfall in a spatially integrated manner. A typical problem for this experimental set-up was the large amount of dust, death leaves and branches collected by the gutter and blocking the drain to the raingauges. This problem was later partially avoided by putting a fine mesh over the drain of the gauge. Attention should be paid to the width of the meshes. Large meshes do not prevent dust to enter the drain, while fine meshes block the dust well, but finally prevent water to

enter the gauge. In this set-up meshes of 1 mm^2 were used. Very frequent, at least weekly, control of the gutters and gauges seemed to be necessary to obtain reliable results. During fall this frequency should be increased, and also after heavy showers and storms extra control is needed. Throughfall was expressed in mm of precipitation (l m^{-2}) per unit time.
Raingauges were calibrated yearly as described in the manual (Raingauge, 1992).

Stemflow water was collected in large recipients of 190 l by helicoidal gutters made of poly-urethane and silicone (both tested and found to be inert) which are glued around the tree stem. Collection of stemflow water was performed for the main tree species of the stand (beech, oak and ash). The sampling for each tree species is done on five trees representative for each of the five diameter classes of the stand (mean diameter, mean diameter plus and minus standard deviation and mean diameter plus and minus twice the standard deviation)(De Schrijver & Lust, 2000).

The relation between free field precipitation and throughfall measured respectively above and below the canopy during the months of August (foliated period) and December (non-foliated period) 1999 is shown in Figure 2.7.

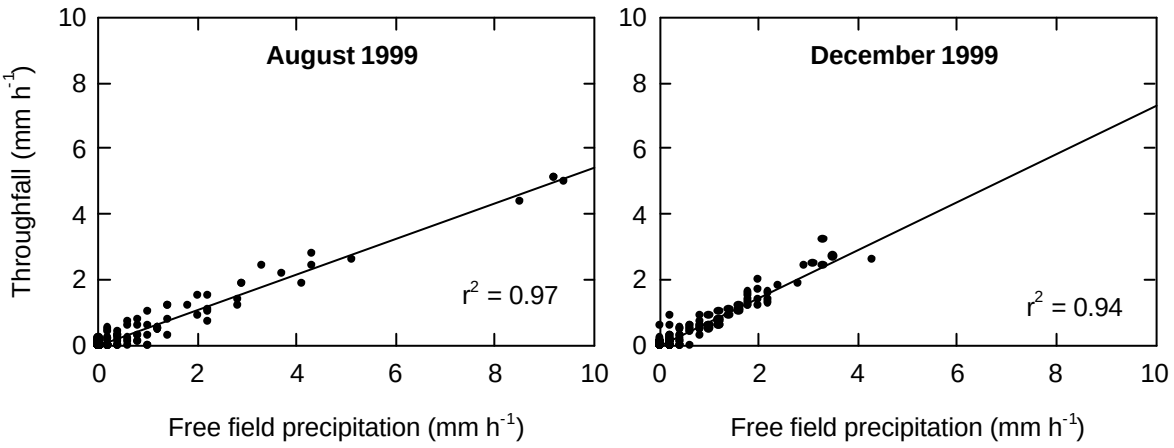

Figure 2.7 The relation between throughfall measured in the ash site and the free field precipitation measured above the canopy (36 m), during a foliated period (left) and a non-foliated period (right). Throughfall is respectively 54 and 73 % of free field precipitation for these periods.

2.2.2.5 Humidity

The humidity of the air above the stand was measured using two wet and dry bulb psychrometers (H301, Vector Instruments, Rhyl, UK) installed above the crown canopy on platforms four and five. Outputs were dry bulb and wet bulb temperature of the air, expressed in °C. These temperatures allowed to calculate the relative humidity (%) as well as the absolute humidity (vapour pressure in kPa) of the air.
Just as was done for the temperature sensors calibration occurred in a temperature controlled water bath.

Because of the high dust content of the air at the forest floor, a capacitive humidity sensor (HMP143A, Vaisala, Helsinki, Finland) was used at 1 m above ground level. The output of this sensor was air temperature (°C) and relative humidity (%).

The status of the leaves with respect to surface wetness was measured with leaf wetness sensors (EE 507-264/SW120D345, ELE) installed in the crown of the beech tree (levels of platform four and five and in the south direction). Leaf wetness is a discrete variable expressed as "dry" or "wet". This sensor was calibrated by manually wetting and drying the sensor's surface (De Dekker, 1999).

2.2.2.6 Soil water

Soil water (i.e. pF-value or soil water potential), and thus its availability to the forest canopy, was measured using two sets of six tensiometers (SWT6, Delta-T Devices Ltd, Cambridge, UK) positioned in the oak-beech and ash sites. They were installed at the depths of 10, 25, 50, 75, 100 and 150 cm. Soil water potential was expressed in hPa.

Each year, the sensors were calibrated at the Institute for Forestry and Game Management (Geraardsbergen, Belgium).

As an example seasonal courses of soil water potential in the oak-beech and ash site are shown in Figure 2.8.

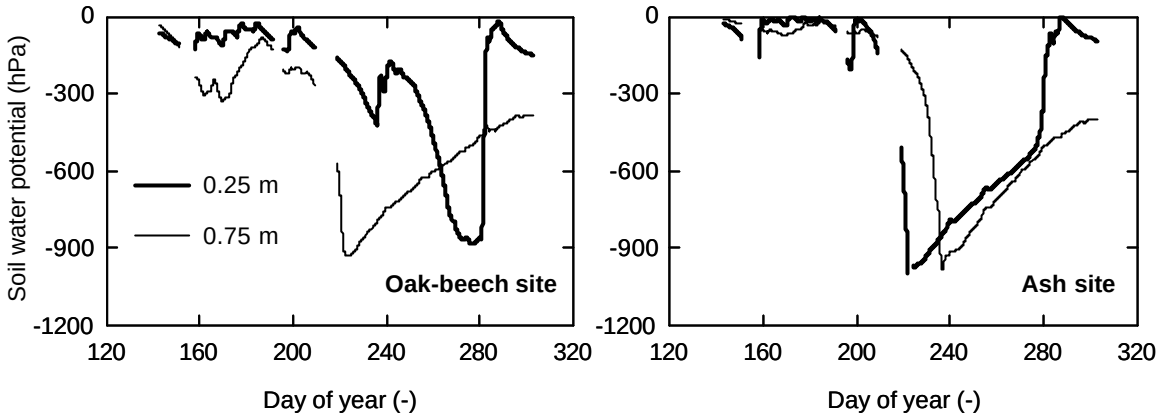

Figure 2.8 Seasonal courses of the soil water potential measured at two depths at the oak-beech forest site (left) and at the ash forest site (right), during the growing season 1997.

2.2.3 Data acquisition and data editing

All basic climatic variables mentioned above, and also some of the specific eco-physiological instruments, were measured every 10 s using a data acquisition system (HP 75000 series B and HP 34970A, Hewlet-Packard, Colorado, USA) connected to a PC. Every ten minutes, a mean value was written to the PC memory. Soil water was the only variable for which hourly mean values, based on measurements every 10 s, were stored.

The data acquisition scheme (number of channels, calibration factors, measuring frequency,…) was programmed in the HPVEE language with a graphical interface (HPVEE 5.0). This programme (torenuitbreiding.vee) also allowed the measurements to be recorded in separate ASCII-files for each basic variable (a radiation, a temperature, a wind, a precipitation and a soil water file).

Every day at midnight the files were transmitted from the computer installed in the tower cabin to a computer located in the Laboratory of Plant Ecology (Ghent) and one in the Laboratory of Forestry (Gontrode). This was done with modem connections operating at 56 kB per s^{-1} baud rate. A special communication protocol was written for one host PC (tower PC) and two or more guest PC's (software: NetOp Remote Control, version 6.00). The modem connections were first tested during the

growing season of 1999. In each laboratory, the data can be consulted with different computers connected to the Local Area Network (LAN-network). In a later phase the data were transferred weekly in order to reduce communication costs. However, polling for control purposes can be done at any moment of the day. A scheme of the data acquisition system and the modem network for data transmission is given in Figure 2.9.

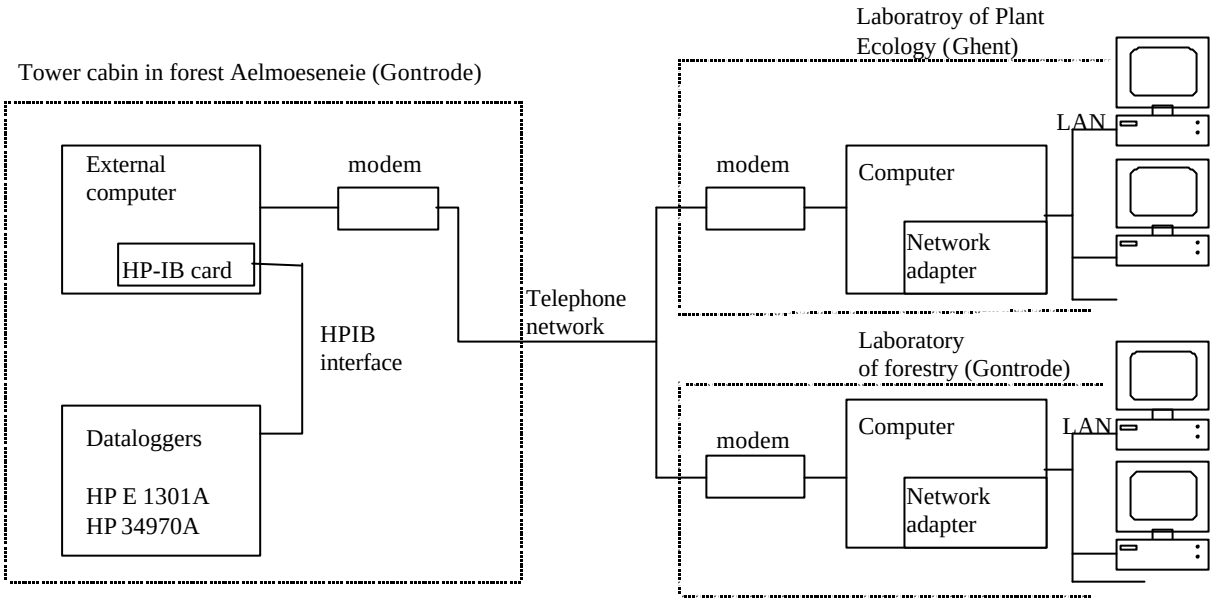

Figure 2.9 Flow chart for the data acquisition system (left) located in the cabin of the tower (Gontrode), and for the modem connection with the Local Area Networks (right) of the Laboratory of Plant Ecology (Ghent) and of the Laboratory of Forestry (Gontrode).

After collection of the data by the laboratory computers, the data were imported in Excel spreadsheets and were carefully controlled and filtered. This data control and filtering was done partly manual, partly automatic. Data control was done for ten minute values, and hourly and daily values were calculated from these ten minute values. The used restrictions for controlling the data are mentioned in the following section.

Short-wave radiation was supposed to be zero when measured values were below 5 W m^{-2}. Reflected short-wave radiation and short-wave radiation measured in or under the vegetation must be lower than incoming short-wave radiation measured above the crown canopy. PAR intensities must always be lower than short-wave radiation (both expressed in W m^{-2}) and also reflected PAR must be lower than incoming PAR. Net radiation must always be lower than net incoming short-wave radiation measured above the crown canopy.

For the soil heat flux the order of magnitude was checked, and the fluctuations with time in both forest sites were compared.

Air and soil temperature data were controlled by checking the order of magnitude, and by comparing the values measured at the different levels.
It was not allowed that wind speeds measured at a certain height above the crown canopy were higher than the wind speeds measured higher above the crown canopy.
The time courses of wind direction measured at both heights above the crown canopy were compared against each other.
Values of relative humidity must be lower than 100 %. When values of relative humidity were close to 100 % for a longer time period, then it was concluded that the wet bulb temperature of the psychrometer was not measured correctly (e.g. due to an empty water reservoir), and also these data were filtered out.

All data are finally presented with different time bases such as ten minute, hourly and daily values. The Excel spreadsheets are collected in annual overviews of the basic climatic data for the forest Aelmoeseneie (Samson et al., 2000b). Overviews are now available for the growing seasons 1996, 1997, 1998 and 1999.

Appendix to Chapter 2

Appendix 2.1 Overview of the meteorological and eco-physiological equipment installed at the measuring tower in the experimental forest Aelmoeseneie for the growing seasons from 1995 till 2000. Till 1997 time resolution of the measurements was 30 minutes, while the time resolution of the stored values is half hourly, hourly and daily. From 1998 till 2000 time resolution of the measurements was 10 minutes, while the time resolution of the stored values is ten minutes, hourly and daily. Abbreviations: I+R: incoming and reflected; SHB: stem heat balance; TDP: thermal dissipation probe

	1995	1996	1997	1998	1999	2000
Soil level						
Oak-Beech						
Short-wave radiation	X	X	X	X	X	X
Soil heat flux				X	X	X
Air temperature				X	X	X
Soil temperature	X	X	X	X	X	X
Throughfall	X	X	X	X	X	X
Soil water potential	X	X	X	X	X	
Ash forest						
Short-wave radiation	X	X	X	X	X	X
Soil heat flux				X	X	X
Air temperature				X	X	X
Soil temperature	X	X	X	X	X	X
Throughfall	X	X	X	X	X	X
Soil water potential	X	X	X	X	X	
Tower						
Relative humidity					X	X
Sap flow TDP				X	X	X
Sap flow SHB					X	
Platform 1						
Air temperature				X	X	X
Sap flow SHB				X	X	
Platform 2						
Short-wave radiation	X	X	X	X	X	
PAR	X	X				
Air temperature				X	X	X
Relative humidity	X	X	X			
Leaf wetness				X	X	X
Sap flow SHB				X	X	
Platform 3						
Air temperature	X	X	X	X	X	X
Leaf wetness				X	X	X
Sap flow SHB				X	X	

	1995	1996	1997	1998	1999	2000
Platform 4						
Air temperature				X	X	X
Wind speed	X	X	X	X	X	X
Wind direction	X	X	X	X	X	
Precipitation	X	X	X			
Relative humidity				X	X	X
Infrared radiation			X	X	X	
CO_2 flux			X	X		
Between Platform 4 and Platform 5						
Wind speed (2 heights)	X	X	X	X	X	
CO_2 flux (2 heights)			X	X		
Platform 5						
Short-wave radiation	X	X	X	X	X	X
Short-w. radiation (I+R)	X	X	X	X	X	X
PAR (I+R)			X	X	X	X
Net radiation				X	X	X
Air temperature	X	X	X	X	X	X
Wind speed	X	X	X	X	X	
Wind direction	X	X	X	X	X	X
Precipitation	X	X	X	X	X	X
Relative humidity				X	X	X
CO_2 flux			X	X		

Chapter 3
EXPERIMENTAL DETERMINATION OF THE ACTUAL EVAPOTRANSPIRATION IN THE FOREST AELMOESENEIE

The estimation of the actual evapotranspiration of forests is a difficult and complicated task. Most of the experimental techniques which can be used start from the determination of the water use of a single tree which is then scaled up to the level of the forest. Weighing lysimeters (e.g. Fritshen et al., 1973; Edwards, 1986), large-tree potometers (Roberts, 1977; Knight et al., 1981), tent enclosures or ventilated chambers (Greenwood & Beresford, 1979; Dunin & Greenwood, 1986), radio-isotopes like tritium (Kline et al., 1970; Waring & Roberts, 1979), stable isotopes like deuterium (Calder et al., 1986; Dye et al., 1992) and energy balance, heat dissipation and heat-pulse techniques (e.g. Swanson, 1994; Smith & Allen, 1996) have been used to obtain quantative estimates of the water lost by a single tree. Each of these techniques has its own merits and drawbacks.

Weighing lysimeters are indeed very sensitive to small water losses from the soil-plant system, but roots occupy only a limited soil volume. Lysimeters are also expensive to construct and to maintain. The use of large-tree potometers in the so-called ‘cut-tree’ experiments is intrusive. They often induce changes in leaf water potential and stomatal conductance that may otherwise preclude a clear physiological interpretation of data (Roberts, 1978). Ventilated chambers offer an interesting method to measure both water vapour and CO_2 exchange in trees (Denmead et al., 1993), but the micro-climate in the chambers is not representative for that outside the chambers. The use of radio-tracers like tritium and ^{32}P are increasingly subject to regulatory constraints and continuous seasonal patterns of water use are difficult to obtain with these chemical methods.

Estimates of water use derived from energy-balance, heat dissipation and heat-pulse sap flow techniques also suffer from uncertainties as a result of respectively calibration errors, thermal gradients in the stem and variation in water flux with sapwood depth (Granier et al., 1996). These systems are, however, inexpensive, easy to use and can be readily interfaced with data loggers for remote operation. For these reasons, sap flow techniques have become increasingly popular as means for estimating the actual transpiration in forest vegetations. Until now, most publications have dealt with one method for measuring sap flow separately. This chapter will

therefore address as well the energy-balance as the heat dissipation method for measuring sap flow simultaneously.

Although a lot of research has been conducted on sap flow measurements of forest tree species, little attention has been given to sap flow dynamics of understory species in temperate deciduous forests. Recently some authors report on medium-term sap flow monitoring in Scots pine (Oliveras & Lorens, 2001), however, limited information is available about seasonal sap flow dynamics of temperate upperstory tree species (e.g. Granier et al., 2000a; Herbst et al., 1999) but especially of understory species. The total hydraulic conductance can explain differences in sap flow dynamics between species, however, not many data are available about this parameter, and surely no data are reported where this hydraulic conductance is compared between upperstory and understory species in a temperate deciduous forest. Also very few is known about the role of water storage in the stems of temperate tree species in daily water losses.
Besides sap flow and transpiration of single trees, the knowledge of total forest transpiration is very important. Therefore sap flow measured in individual trees has to be scaled up, which implies several difficulties which depend on the method used for measuring sap flow and on the species composition and age distribution of the trees in the forest. To validate these upscaled sap flow measurements the values of forest transpiration can be compared against forest evapotranspiration measured using micro-meteorological techniques like the Bowen ratio energy balance (e.g. Aston, 1985b)(see § 1.1.2.3). The Bowen ratio technique requires a good estimation of the available energy for latent and sensible heat exchange (Aston, 1985a,b), which depends largely on the heat storage in the forest. One of the terms in the total heat storage of the forest, is the heat storage in the biomass, and Saxton and McCaughey (1988) suggested that this term could be estimated based on surface temperatures measured with an infrared radiometer.

As such, the purpose of this chapter is to deal with, and to provide experimental data for, transpiration and water use in forests, starting from sap flow and transpiration of single trees to eventually evapotranspiration of the total forest. In more detail the objectives of this chapter are to:
-measure and describe the seasonal sap flow dynamics of co-occurring upperstory and understory tree species in a heterogeneous deciduous forest;
-quantify the differences between day- and nighttime sap flow of upperstory and understory species;
-describe the effect of vapour pressure deficit on sap flow of upperstory and understory species;
-estimate the total hydraulic conductance of the soil-root-leaf pathway, based on sap flow measurements and measurements of leaf water potential for as well upperstory as understory species; and

-quantify water storage in beech and ash, and describe the seasonal dynamics of the contribution of water storage in total tree transpiration.
-scale-up sap flow data measured at the level of a single tree to the forest stand level;
-estimate the contribution of understory in total forest transpiration;
-estimate heat storage in the biomass based on surface temperatures of the canopy measured with an infrared radiometer;
-calculate the total heat storage in the biomass and describe the daily and seasonal dynamics of this heat storage;
-analyse the Bowen ratio data measured above the forest canopy;
-derive actual forest evapotranspiration from Bowen energy balance measurements combined with the total heat storage in the forest calculated before; and
-compare upscaled sap flow data with actual evapotranspiration calculated from Bowen ratio energy balance measurements.

To summarise, the data presented in this chapter will clarify the dynamics of the water losses at the level of the individual tree based on sap flow measurements. Moreover, water exchange between the forest and the atmosphere will be described based on upscaled sap flow data and based on a micro-meteorological approach, namely the Bowen ratio energy balance method.

3.1 Sap flow dynamics of upperstory and understory species

3.1.1 Introduction

Sap flow can now be continuously monitored for long periods of time with minimal maintenance using thermal techniques (Allen & Grime, 1995; Granier & Loustau, 1994). These techniques are based on heat transport in the stem due to sap flow and they can be used to measure the transpiration or water lost by a single tree or a single branch. Measurements can also be repeated on several branches so that the transpiration of the different layers in the crown canopy can be separated. The technique also makes it possible to measure transpiration from a particular species of a mixed tree stand (Allen & Grime, 1995). In case of a multi-species forest, the sap flow of the most important species can be measured separately. Moreover, sap flow behaviour of trees of different ages and diameter (Vertessy et al., 1997) can also be measured. In this way sap flow measurements can yield a continuous data set for testing single layer (evapo)transpiration models as well as detailed multi-layer models.

Sap flow methods, like the thermal dissipation method (Granier, 1985) or the constant power stem heat balance method (Sakuratani, 1984), have already successfully been used on pine trees (e.g. Granier et al., 1990), tropical trees (e.g. Goldstein et al., 1998) and deciduous trees (e.g. Zhang et al., 1997). Not so many authors, however, compared the sap flow measured at different levels in the canopy, and sap flow of different species growing at the same site. Also sap flow rates of understory tree species (e.g. Wullschleger et al., 1998a) are rather scarce and are hardly compared between understory and upperstory species.

The objectives of this part of the study (i.e. § 3.1) were multiple. Sap flows were measured for three upperstory species (beech, oak and ash) and two understory species (sycamore and hazel) during an entire growing season. This data should yield the seasonal differences of water use between different tree species. Secondly, the sap flow of three different layers in the crown canopy will be compared for two upperstory species (beech and ash). This might give information on the daily dynamics observed at different levels in the crown layer. Nighttime water use will also be checked for the selected species and crown layers. Finally, sap flow responses of upperstory, at stem and branch level, and understory species will be examined in relation to meteorological variables, especially vapour pressure deficit. The sap flow data described in this part of the chapter will be scaled up to the forest stand level (see later § 3.4).

To reach these objectives two different methods for measuring sap flow were used, as was also done by Ewers and Oren (2000). The thermal dissipation method was used on the lower part of the stem for the upperstory species, while the constant power stem heat balance method was used on branches in the crown canopy, and for the understory species. At branch level the stem heat balance method was applied instead of the thermal dissipation method, as for the former method the integrated sap flow through the whole branch is directly measured and no estimation of the sapwood is needed in contrast to the latter method (see § 3.1.2).
For each upperstory and understory species, and canopy level respectively, a single tree, shrub or branch was monitored, just as in Hogg et al. (2000).

3.1.2 Material and methods

Sap flow was continuously measured from the beginning of April until the end of October 1999, using two different methods, namely the Thermal Dissipation Probe (TDP) or Granier's continuous heating method (Granier, 1985; Granier, 1987b) and the constant power Stem Heat Balance (SHB) method (Baker & van Bavel, 1987; Sakuratani, 1981; Sakuratani, 1984; Steinberg et al., 1989; Steinberg et al., 1990b).

3.1.2.1 Sap flow measurements with the thermal dissipation technique

The thermal dissipation method is an empirical method for measuring sap flow in trees developed by Granier (1985). Two cylindrical probes are inserted radially into the stem, with one probe placed approximately 40-100 mm vertically above the other. The upper probe contains a heater element and a thermocouple junction that is referenced to another junction in the lower probe (Granier, 1985, 1987a)(Figure 3.1). Constant power is applied to the heater and the difference in temperature between the two probes (DT_p) is then dependent on the sap flux density around the probes; as sap flux density increases heat is dissipated more rapidly and so DT_p decreases (Smith & Allen, 1996).

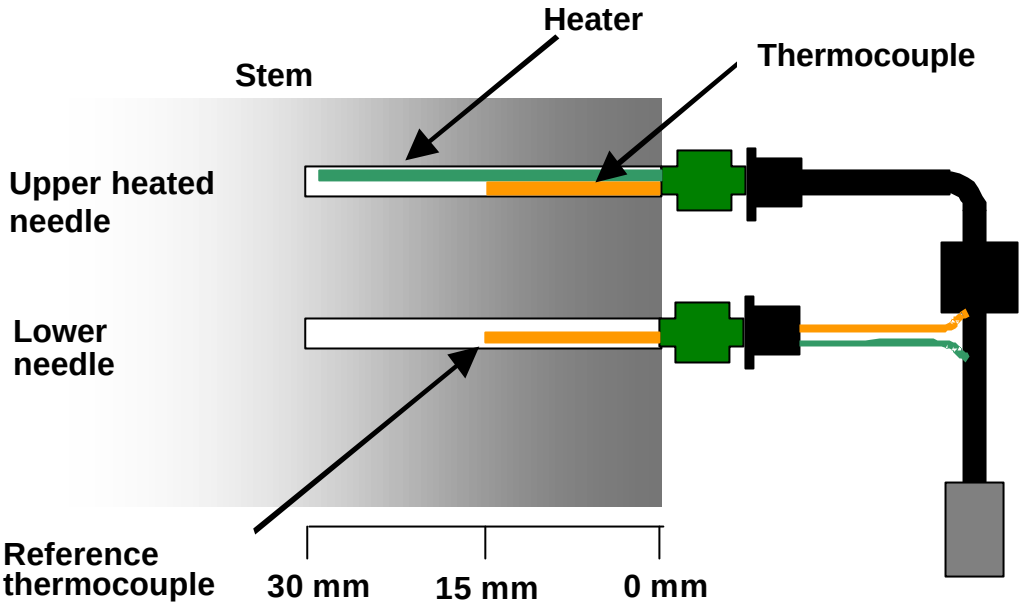

Figure 3.1 Schematic representation of a thermal dissipation probe (TDP30, Dynamax Inc., Houston, Texas, USA).

The TDP-method was applied to the stem of beech, oak and ash surrounding the measurement tower (Picture 3.1). The sensors (pairs of thermal probes)(type TDP30, Dynamax Inc., Houston, Texas, USA) were installed following the manufacturer's instructions in the sapwood at 1.30 m from ground level. To avoid direct heating by sunlight penetration the sensors were installed at the north-facing side of the trees, as done by Phillips et al. (1996). The lower unheated probe gave the reference temperature of the sapwood and was located 40 mm apart from the upper, continuously heated, probe. The 1.2-mm-diameter probes were inserted 30 mm into the sapwood. Bark was removed at the points of probe insertion to expose the outer surface of the sapwood.

Granier (1985) found experimentally that for *Pseudotsuga menziesii*, *Pinus nigra* and *Quercus pedunculata*, volumetric sap flux density (J_s, $m^3\ m^{-2}\ s^{-1}$) is related to DT_p by:

$$J_s = 0.000119 Z^{1.231} \qquad (3.1)$$

with Z defined as:

$$Z = \frac{\left(\Delta T_0 - \Delta T_p\right)}{\Delta T_p} \qquad (3.2)$$

where DT_0 is the value of DT_p when there is no sap flow.

Granier et al. (1990) suggested that the parameters in Equation 3.1 do not depend on characteristics of trees or wood anatomy and so it may be possible to utilise this method without calibration.

Picture 3.1 Installation of a TDP-sensor in the stem of oak in the forest Aelmoeseneie.

Sapwood area at breast height of the tree (Table 3.1) was determined by injecting dye, methyl-blue, into the bole through holes made by a 5-mm increment borer, and the holes were filled up once more after one hour. As done by Goldstein et al. (1998), after 1–2 h, a core was taken 4 cm above each dye injection point and the area of conducting tissue was determined from the thickness of the wood coloured by the dye as it moved up in the transpiration stream.

Table 3.1 The circumference, the stem cross-sectional area and the percentage sapwood of the cross-sectional area at breast height of the beech, oak and ash trees sampled for their sap flow in the experimental forest Aelmoeseneie.

Species	Circumference (cm)	Cross-sectional area (cm^2)	Sapwood (%)
Beech	193	2964	27
Oak	127	1284	20
Ash	137	1494	5

As sap flux density J_S is expressed per unit sapwood area ($m^3\ m^{-2}\ s^{-1}$ or $m\ s^{-1}$), the total mass flow rate of the sap in the stem F_s ($m^3\ s^{-1}$) is obtained by multiplying sap flux density by the sapwood cross-sectional area (m^2):

$$F_s = J_S \times \text{sapwood cross section} \qquad (3.3)$$

A typical diurnal course of J_s measured in beech is shown in Figure 3.2.

3.1.2.2 Sap flow measurements with the stem heat balance method

The energy balance method, know as the Stem Heat Balance (SHB) method, for measuring the sap flux density is an absolute measurement of the sap flux density in the stems of intact plants or the trunks of woody species. The principle is based on the continuous heating of a stem section over a short vertical distance. The partition of the radial and vertical conduction is found, as well as the convective transport by the sap stream. The flux density of heat transport is converted to the sap flux density from the measured rise in sap temperature.

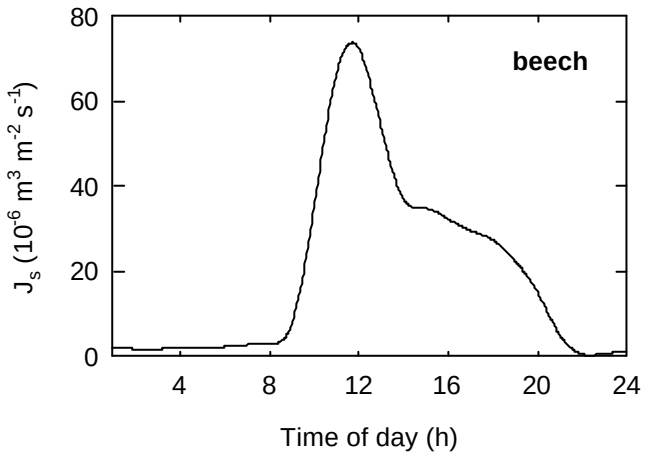

Figure 3.2 A typical diurnal course of sap flux density (J_s) at the stem level of beech, measured on July 31, 1999.

The SHB method requires a steady state and a constant energy input from the heater strip inside the gauge body to the stem. Therefore the stem section must be insulated from changes in the environment.
The heater surrounds the stem under test (Figure 3.3) and is powered by a DC supply with a fixed amount of heat Q_h, which is the equivalent to the power input to the stem from the heater, P_{in}. Q_r is the radial heat conducted through the gauge to the ambient. Q_v, the vertical or axial heat conduction through the stem has two components, Q_u (upward) and Q_d (downward). By measuring P_{in}, Q_u, Q_d and Q_r, the remainder, Q_f can be calculated. Q_f is the heat convection carried by the sap. After dividing by the heat capacity and the temperature increase, the heat flux is converted directly to mass flux density.

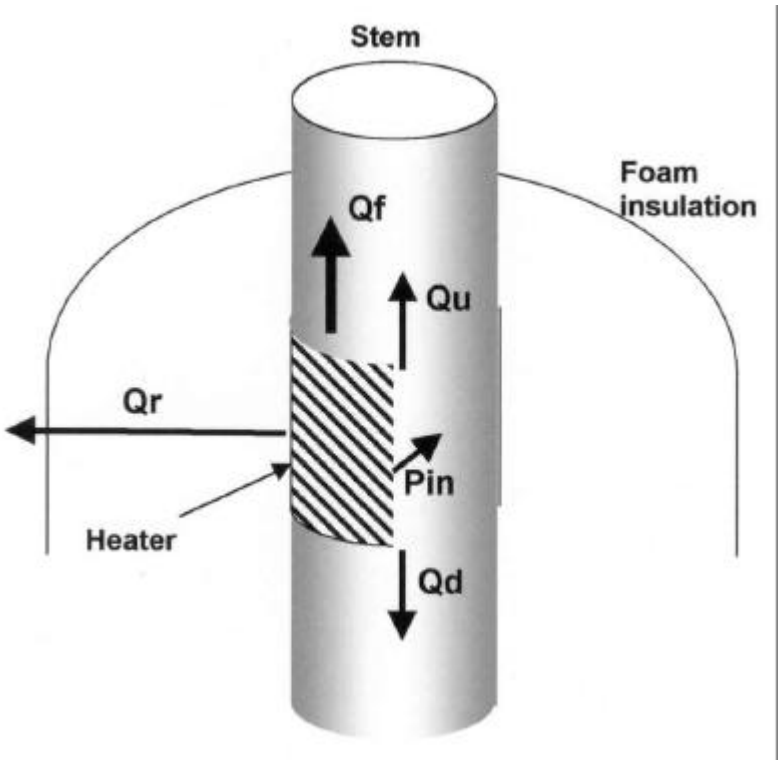

Figure 3.3 Schematic representation of a stem heat balance sensor with indication of the energy balance components. Symbols are: *Pin*: power input to the stem from the heater; *Qr*: radial heat conducted through the gauge to the ambient; *Qu*: upward conducted heat through the stem; *Qd*: downward conducted heat through the stem; *Qf*: heat convection carried by the sap.

The energy balance (W) equation is expressed as:

$$P_{in} = Q_r + Q_v + Q_f \qquad (3.4)$$

The vertical heat conduction (Q_v) has two components, Q_u (upward conducted heat) and Q_d (downward conducted heat):

$$Q_v = Q_u + Q_d \tag{3.5}$$

where

$$Q_u = K_{st}.A_s.\frac{\Delta T_u}{\Delta x} \tag{3.6}$$

$$Q_d = K_{st}.A_s.\frac{\Delta T_d}{\Delta x} \tag{3.7}$$

so that

$$Q_v = K_{st}.A_s.\frac{(\Delta T_u + \Delta T_d)}{\Delta x} \tag{3.8}$$

where K_{st} is the thermal conductivity of the stem (W m^{-1} K^{-1}), A_s is the stem cross sectional area (m^2), DT_u/Dx and DT_d/Dx are the temperature gradients (K m^{-1}), and Dx is the spacing between the thermocouple junctions. One pair of thermocouples is above the heater and one pair is below the heater as shown in Figure 3.4.

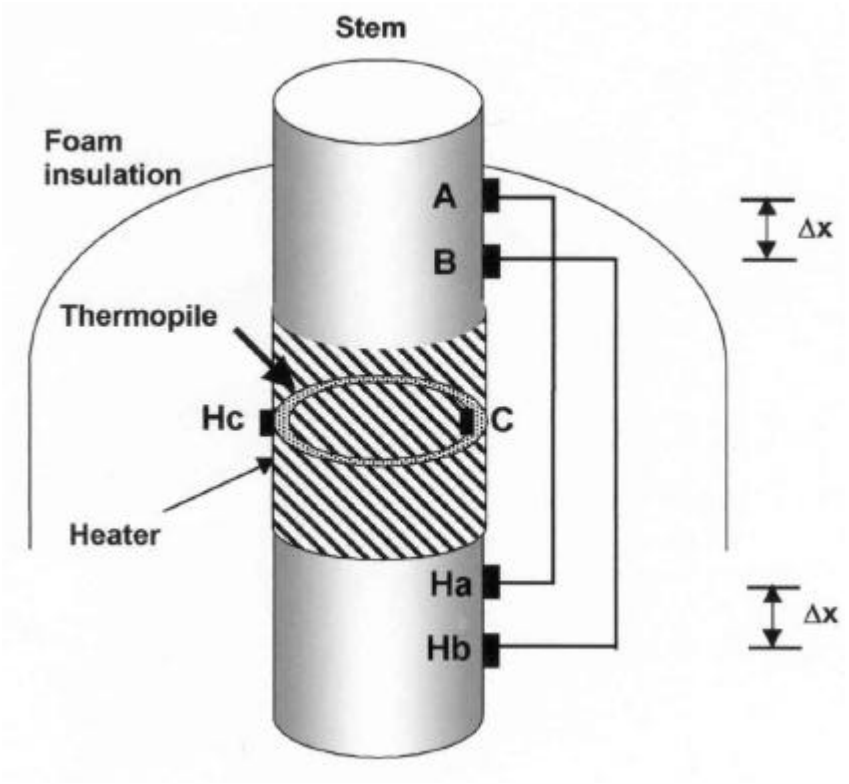

Figure 3.4 Schematic representation of a stem heat balance sensor.

There are two differentially wired thermocouples both measuring the rise in sap temperature (Figure 3.4). Channel AH measures the difference in temperature A-H_a (mV). Channel BH measures the difference in temperature B-H_b (mV). By subtraction of these two signals (mV):

$$BH - AH = (B - H_b) - (A - H_a) = (B - A) + (H_a - H_b) = \Delta T_u + \Delta T_d \qquad (3.9)$$

The result yields the two components of axial heat conduction out of the stem section Q_u and Q_d. Since the distances, Dx, separating the upper thermocouple pair and the lower thermocouple pair are fixed by design to the same value, the components of Q_v are combined with a common denominator, and Equation 3.8 can be written as:

$$Q_v = \frac{K_{st} A_s}{\Delta x}\left(\frac{BH - AH}{0.040}\right) \qquad (3.10)$$

The factor 0.040 mV K^{-1} converts the thermocouple (Cu-Constantan) differential signals (BH-AH, mV) to degrees (K).
After solving Equation 3.4 for Q_f, the sap flux is calculated as described by Sakuratani (1981) and Baker & van Bavel (1987):

$$F = \frac{P_{in} - Q_v - Q_r}{C_w . \Delta T_h} 10^{-6} \qquad (3.11)$$

where F is the sap flux expressed in m^3 s^{-1}, where C_w is the specific heat of water (J g^{-1} K^{-1}), DT the temperature increase of the sap (K), and the factor 10^{-6} is for the conversion from g of water to m^3 of water. The temperature increase of the sap DT_h is measured in mV by averaging the AH and BH signals, and is then converted to degrees (K) by dividing by the thermocouple temperature conversion constant as follows:

$$\Delta T_h = \frac{AH + BH}{2} . \frac{1}{0.040} \qquad (3.12)$$

In Equation 3.11 the radial heat loss is calculated as:

$$Q_r = K_{sh} . CH \qquad (3.13)$$

where K_{sh} is the thermal conductance for a particular gauge installation.

In the crowns of the beech (at 7, 14 and 21 m respectively bottom, middle and top layer) and the ash (at 21 m, thus only top layer) surrounding the tower, and on a single sycamore and hazel (respectively 1.3 and 2 m above ground level)(Table 3.2) sap flow was measured using the constant power SHB-method (model SGA10-ws and SGA13-ws, Dynamax Inc., Houston, Texas, USA). The branches in both tree canopies were carefully selected, because they had to be representative for the

investigated crown layer. Canopy branches were selected according to their architectural characteristics (Table 3.2). They were also surrounded by other branches, and we also tried to avoid direct illumination of large parts of the branches during certain moments of the day. However, the branch of beech at 7 m, was directly illuminated in the late afternoon, while this was not the case during the rest of the day. The understory species were selected because: (1) they grew in the vicinity of the tower, (2) they had a height between three and four meter, (3) leaf area downstream the measured branches was more than 1 m², and (4) leaf area development was easy to monitor during the growing season (e.g. their canopies were not mingled with other canopies).

Both the sensor and stem sections above and below the sensor were covered by insulation, and this was all wrapped in a white plastic to minimize the influence of fluctuations in solar radiation and air temperature and also to avoid rainfall wetting the sensor (Picture 3.2). Hall et al. (1998) stated that significant environmentally-induced temperature gradients over the stem surface at the measuring points are unlikely if the gauges are mounted well above the soil surface (at least 1 m) and are shaded by a closed, dense canopy of leaves above, just as was the case in this experiment. Measurements without applying heat to the sensors confirmed this. The power input to the sensor was monitored weekly and was changed if temperature differences during large parts of the days were too low (this means close to 0.5 °C). The experimental set-up allowed adapting the power input separately for sycamore, hazel, the bottom and middle layer of beech and the upper layer of ash and beech. The mean power input for all species and levels during the growing season was around 4.5V.

Table 3. 2 Architectural characteristics of the branches monitored with the constant power stem heat balance (SHB) method. The leaf area and branch length downstream from the SHB sensors is given for August 13, 1999.
(*) For the case sycamore the stem splits into two sub-branches, directly downstream from the sensor.

Species	Beech			Ash	Sycamore	Hazel
Sampling height (m)	21	14	7	21	1.5	2
Diameter (mm)	14.0	9.8	13.0	12.4	14.9	12.2
Length (m)	1.10	1.30	1.60	1.05	1.40/1.12*	1.54
Side branches (no)	4	5	4	4	6/3*	4
Leaf area (m^2)	0.543	0.733	0.683	0.544	1.011	1.230

Picture 3.2 Installation of a stem heat balance sensor on a branch in the upper crown level of beech in the forest Aelmoeseneie.

The thermodynamics equation of a heated fluid in an insulated cylindrical section at a constant temperature is included below to indicate the source of the K_{sh} computation and the effects of the radius of the cylinder's thermal conduction. The radial heat flux (Q_r) is defined as:

$$Q_r = 2\pi K_{co} L_c \frac{T_{in} - T_{out}}{\ln\left(r_{in}/r_{out}\right)} \qquad (3.14)$$

where K_{co} is the thermal conductivity of the cork substrate surrounding the heater (W m^{-1} K^{-1}), L_c is the length of the cylinder (m), T_{in} and T_{out} are respectively the inner and outer temperature of the insulating cylinder (K), and r_{in} and r_{out} are respectively the inner and outer radius (m).

For an installation of a fixed diameter, the K_{sh} represents all of the parameters and constants in Equation 3.14, and relates the radial heat flux to the thermopile output CH as follows:

$$Q_r = K_{sh}.CH = K_{sh}.E_r \quad (3.15)$$

since the signal CH, or E_r, is directly proportional to the temperature difference between inner and outer layers of the cork substrate.
The calculation for K_{sh} (W mV^{-1}) is determined by solving Equation 3.4 during no-flow conditions (Q_f = 0), and after combination with Equation 3.15 as follows:

$$K_{sh} = \frac{P_{in} - Qv}{E_r} \quad (3.16)$$

The minimum K_{sh} was determined daily (between 1500 h and 1500 h the next day) and was used to calculate F for the same period. The reason that the K_{sh}-value was changed in the afternoon was that the radial heat flow ($K_{sh}.E_r$) reaches a minimum at about 1500 h. When a new K_{sh}-value is calculated and taken into account at that moment, it will have only a limited effect on F.

So, by combining Equations 3.8, 3.11 and 3.15 sap flux (F, m^3 s^{-1}) was calculated as:

$$F = \frac{P_{in} - K_{sh}E_r - K_{st}A_s \dfrac{\Delta T_u + \Delta T_d}{\Delta x}}{C_w \Delta T_h} 10^{-6} \quad (3.17)$$

where P_{in} is input power to the heater (W); K_{st} is stem thermal conductivity (0.42 W m^{-1} K^{-1})(Steinberg et al.,1990b); A_s is the stem cross-sectional area (m^2); DT_u and DT_d are vertical temperature differences (K) over the distances Dx (m) above and below the heater, respectively; K_{sh} is the gauge or sheath conductance representing the radial power loss per millivolt (W mV^{-1}), through the gauge when F = 0; E_r is the output of a thermopile mounted outside the heater (mV); C_w is xylem sap (water) heat capacity (4.186 J g^{-1} K^{-1})(Steinberg et al., 1990b; Zhang et al., 1997); DT_h is the temperature difference across the heater (K).
When DT_h = 0, F is undefined and when $\div DT_h \hat{e}$ is close to 0, large errors occur in F. However, when DT_h = 0, theoretically F = 0; in this experiment, F was also assumed to be zero when $\div DT_h \hat{e} \leq$ 0.25°C. As sap flow could occur at night, F was interpolated between F-values calculated with DT_h = -1°C and 1°C, respectively, when $\div DT_h \hat{e}$ was < 1°C, because otherwise unrealistic high nighttime values were calculated.

The number of leaves on the branches, downstream of the stem heat balance sensor, was counted at about three weekly intervals during the growing season. At the end of the growing season, during fall, the number of leaves were counted weekly. Simultaneously, a representative number of leaves for each considered species and level were removed from neighbouring branches or shrubs, and the mean area per leaf was measured using a planimeter (Li-3000, LI-COR, Nebraska, USA). The total leaf area on the gauged branches was calculated by multiplying the number of leaves on each branch with the respective mean area per leaf. The leaf area downstream of the stem heat balance sensors permitted calculation of the sap flux density per m^2 of leaf area (F_{LA}, $m^3\ m^{-2}\ s^{-1}$).

A typical diurnal course of the sap flux density measured at different canopy levels for beech is illustrated in Figure 3.5.

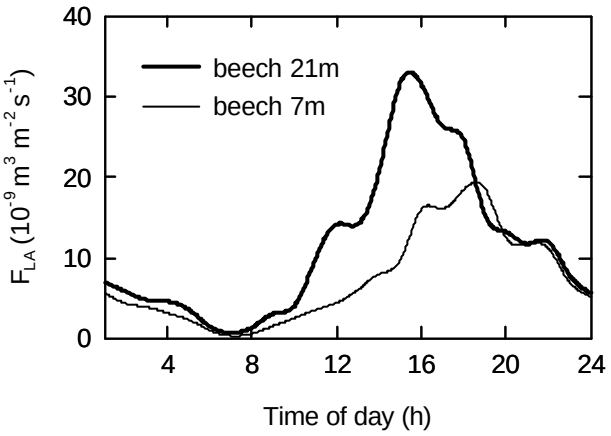

Figure 3.5 A typical diurnal course of sap flux density (F_{LA}) expressed per unit leaf area measured at the branch level of beech at two different heights, measured on July 31, 1999.

As mentioned before, sap flow was continuously measured from the beginning of April until the end of October 1999. Ten minute averages of input voltage (for the SHB-method) and sensor signals (TDP and SHB-method) were calculated from measurements every 10 s using a datalogger (HP 75000 series B and HP 34970A, Hewlet-Packard, Colorado, USA)(see § 2.2.3).

Until now, due to mainly financial restrictions, only one individual of each species was monitored using one sensor per individual. However, it is necessary to increase the number of of monitored individuals (both depending on species and distribution over diameter classes) to obtain a reliable mean basal sap flux density per species.

3.1.3 Results and discussion

3.1.3.1 Seasonal sap flow dynamics

The climatic variables and sap flow dynamics during the entire growing season of 1999 are represented in Figures 3.6 and 3.7-3.9 respectively. The longest period of sap flow was found for oak. For this species water use started at the end of April and ceased at the end of November (Figure 3.7). A clear seasonal trend was observed for this species. For ash, sap flow dynamics during the middle of the growing season showed a very high day to day variation, with high peak values. For beech, water use started later, at the beginning of May, as bud burst and consequently leaf growth started later as well.

In Figure 3.10 the seasonal course of the maximal daily temperature difference between the heated and unheated probe of the TDP-sensors (DT_0) is illustrated. Where initially beech, oak and ash followed the same pattern in the beginning of the growing season, a sudden drop in temperature difference was observed for ash after a pronounced warm and dry spell at the middle of July. This spell persisted until the beginning of August (day 217), and the drop in temperature became even more severe. The maximal daily temperature difference DT_0 (Figure 3.10) observed for ash slightly increased towards the end of the growing season.

The noisy pattern of J_S observed for ash from day 197 on (Figure 3.7), in contrast to beech and oak, can be explained by cavitation of some xylem vessels downstream the sensor, which can occur in ring-porous species like ash with wide xylem vessels (Zimmerman, 1983). Xylem vessels upstream of the point of cavitation remain water saturated, causing DT_0 to be low (Figure 3.10b), because of the high thermal conductivity of the wood. One could also attribute this observed behaviour (Figure 3.7, 3.10b) to root activation at a deeper depth, supplying different or extra xylem vessels with water, due to the drier soil conditions during this period (Figure 3.6). This phenomenon has been observed by Cermak (personal communication). However, it is not likely that root activation explains the observations in our research, because during the same period the SE of the mean DT_p also decreased (Figure 3.10b), indicating low daily sap flow variation, and thus cavitation. The observed cavitation was not permanent. Recent studies also suggest that a substantial fraction of the functional xylem conduits is dynamically emptied and refilled throughout the day (Zwieniecki & Holbrook, 1998).

The rapid variation of DT_0 observed in beech at the beginning of the growing season (Figure 3.10) is not usual, even under variable climatic conditions, and is probably

caused by technical problems. The consequence is wrong sap flow measurements during the period from day 159 to day 190 (see Figure 3.7).

From Figure 3.8 it can be seen that sap flow dynamics measured at different heights in the crown canopy of beech was very similar. Also sap flow dynamics measured at the same height in the crown of different species (i.e. beech and ash)(Figure 3.9) was rather comparable.

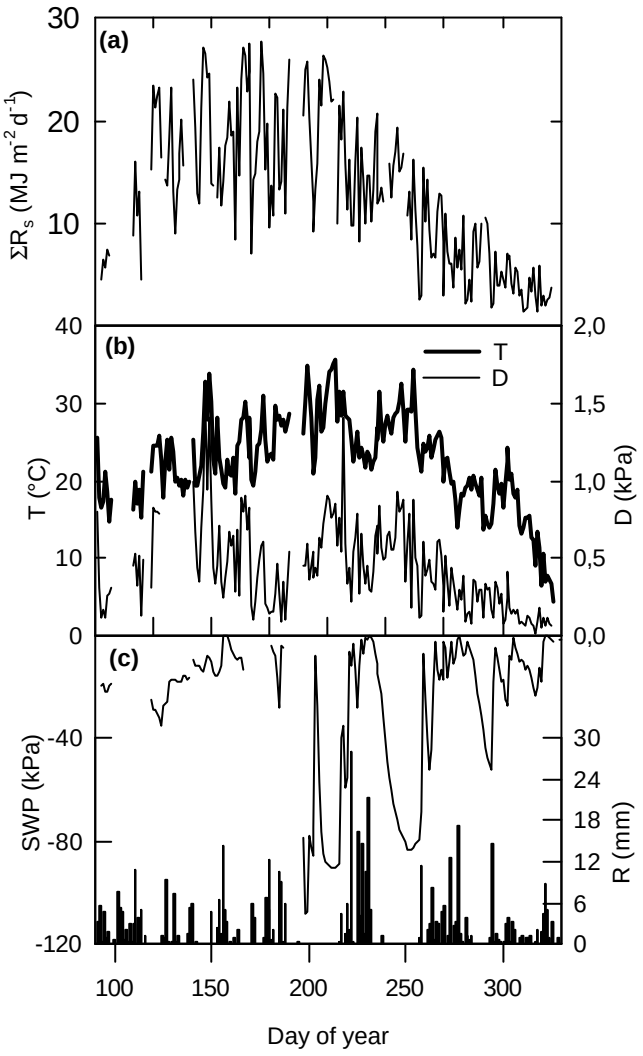

Figure 3.6 Seasonal dynamics of measured meteorological variables during the 1999 growing season: (a) daily radiation sum SR_s, (b) daily maximum temperature T and daytime mean vapour pressure deficit D (between 0800 and 1600 h), and (c) soil water potential (SWP) at a depth of 10 cm and precipitation (R).

Leaf growth, and thus water use of understory species (see Figure 3.9) started at least one month earlier (around half of March) as compared to the upperstory species. This might be a strategy to profit from the advantageous light regime that is reaching the forest floor at that moment. In early spring the understory contributes 100% to forest transpiration as the leaf area of the upperstory species is not yet developed at that moment.

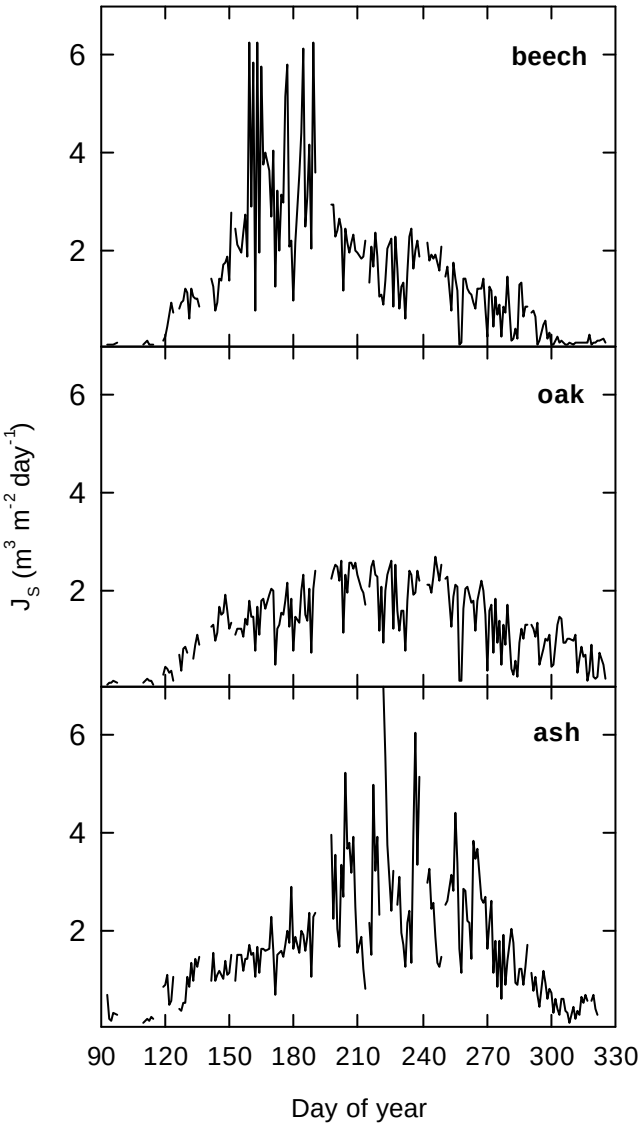

Figure 3.7 Seasonal sap flow dynamics (sap flux density J_s) at stem level for the three species.

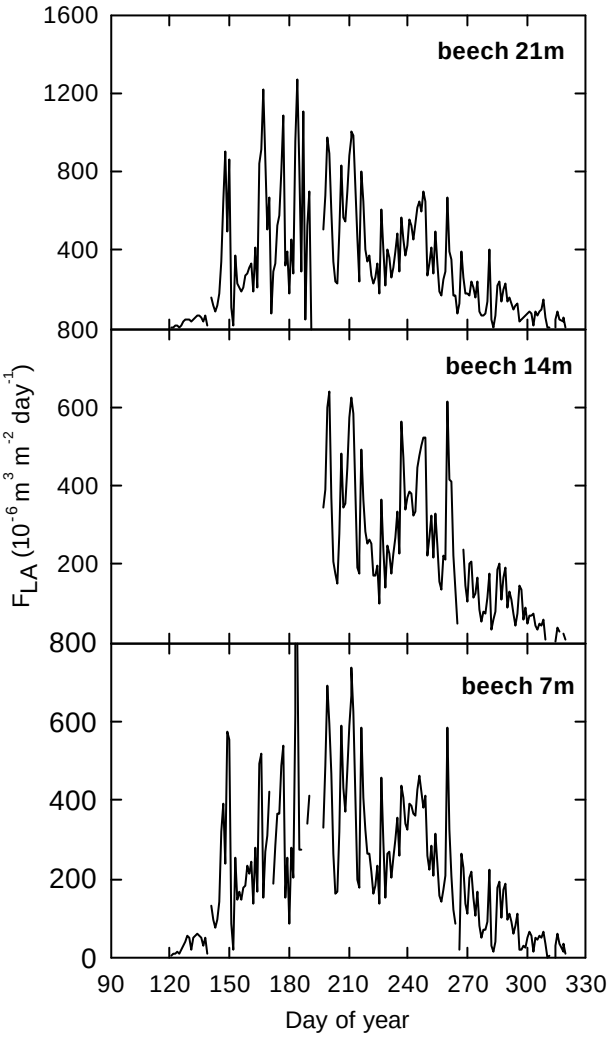

Figure 3.8 Seasonal sap flow dynamics (sap flux density per unit leaf area F_{LA}) at three branch heights for the case of beech. Note the differences in the scale of the vertical axis.

3.1.3.2 Daytime and nighttime sap flow

Average daytime sap flow densities at stem level (J_S) and maximum values were determined for the period from July 16 till August 31 (Table 3.3). The hourly averages for beech, oak and ash were 0.11, 0.12 and 0.16 m h^{-1} respectively, and the corresponding maxima were 0.38, 0.30 and 0.60 m h^{-1}.

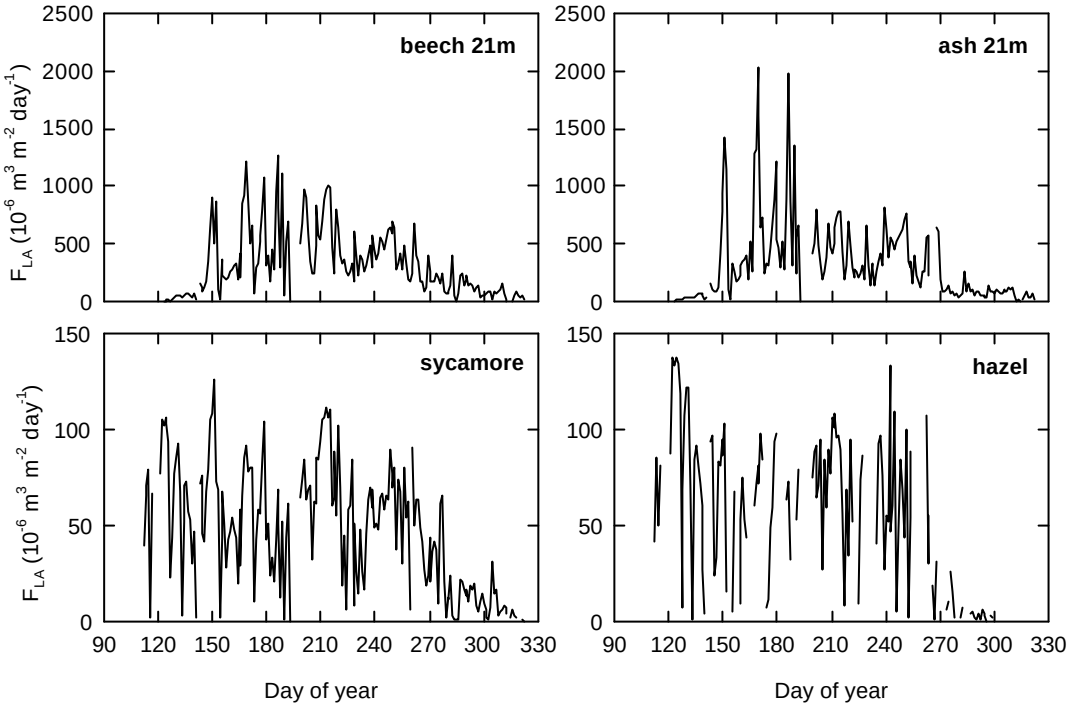

Figure 3.9 Seasonal sap flow dynamics (sap flow rate per unit leaf area F_{LA}) at the top crown level for upperstory species (beech 21 m and ash 21 m) and at branches of understory species (sycamore and hazel). Note the differences in the scale of the vertical axis.

A decreasing trend was observed in average sap flux densities (F_{LA}), at different levels in the crown canopy (Table 3.3). Sap flow (F_{LA}) seemed to be comparable for the middle and lower crown level of beech. Both understory species also show nearly equal F_{LA} values. Due to the low F_{LA} and low LAI of understory species (e.g. 0.3 in oak-beech forest and 1.4 in the ash forest), the understory vegetation will only modestly contribute (less than 20%) to daily and seasonal transpiration of the forest. Calculations for the period 16 July till 1 August revealed that mean understory transpiration was less than 1% and 16% of the beech and the ash transpiration respectively.

It is recommended to monitor sap flow of the understory species more intensively, and to carefully select the measured branches. This latter is important because, especially in the understory, the exposition of the sampled branches (sun exposed or not) seems to be of major importance. Moreover it should be tested whether stem heat storage influences the heat balance of the branches and thus has an effect on

the calculated sap flux density F_{LA}. This can be done according to the method of Grime et al. (1995).

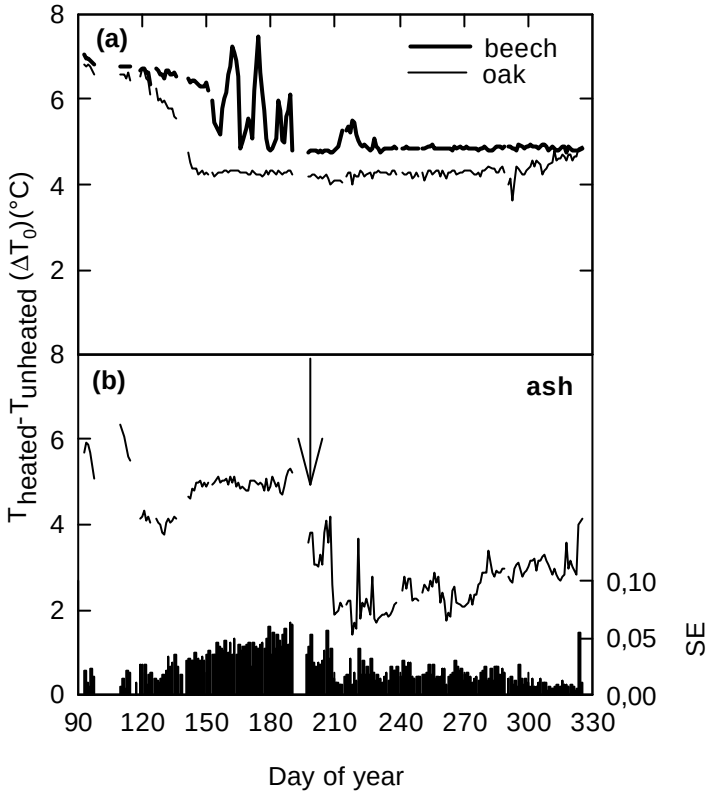

Figure 3.10 Seasonal course of the maximal daily temperature difference between the heated and the unheated probe of the TDP-sensors (DT_0), measured on: (a) beech and oak, and (b) ash. The arrow indicate the start of the hot and dry spell in July. The bars on the right hand side y-axis in (b) are 1 standard error (SE) of the mean daily temperature difference between the heated and the unheated probe of the TDP-sensor (DT_p). The mean values are obtained from recordings every 10 minutes, averaged over a day.

Nighttime sap flows were measured between 2200 and 0600 h (R_s = 0). The results are given in Table 3.3. Mean nighttime stem sap flux density J_S was small for beech and oak. Ash, on the contrary, yielded a high nighttime J_S that was up to 20 % of daytime flow. Also, Granier et al. (2000a) observed during most nights very small basal sap flow for beech trees. Green et al. (1989) measured nighttime sap flow rates as high as 15 % of daytime rates in an apple tree and 30% of daytime rates in two kiwifruit vines. Nighttime F_{LA} was also recorded for beech, ash and sycamore (Table

3.3), and mean nighttime F_{LA}, compared to daytime F_{LA}, was more important for beech (even up to 29% of daytime flow for the lowest canopy level) as for ash (up to 14%) and sycamore (up to18%). Becker (1998) observed nighttime sap flows almost as high as daytime flows in some understory trees in a lowland diptecocarp forest in Brunei. However, so high values were not measured for the understory species in this study.

Table 3.3 Average (±SE) and maximum values for sap flux densities at stem level (J_s) and for sap flux densities at branch level per unit leaf area (F_{LA}). Results are given for day (0600 till 2200 h) and night (2200 and 0600 h) periods, for different species and different branch heights. J_s is expressed per m^2 of sapwood area whereas F_{LA} is expressed per m^2 of leaf area. Measurement period is July 16 – August 1. Sycam = Sycamore

Period		Stem flow (J_s)			Branch flow (F_{LA})					
		Beech	Oak	Ash	B21	A21	B14	B7	Sycam	Hazel
		10^{-2} m^3 m^{-2} day^{-1}			10^{-6} m^3 m^{-2} day^{-1}					
Day	Mean	181	197	248	670	470	347	361	96	105
	SE	±8	±7	±16	±68	±40	±37	±33	±6	±5
	Max	289	252	491	1080	732	606	546	130	127
Night	Mean	4	8	57	154	66	54	105	17	-
	SE	±1	±1	±7	±15	±7	±7	±10	±2	-
	Max	17	21	211	242	113	114	168	30	-

A positive relationship between nighttime F_{LA} and vapour pressure deficit (D) was observed for as well beech as ash (Figure 3.11), just as found by some other authors (Benyon, 1999; Green et al., 1989; Hogg & Hurdle, 1997). In well coupled canopies, as is the case in this forest (see § 1.1.2.5, § 4.1.3.4, and Samson & Lemeur, 2001), and sufficiently large wind speeds (Jarvis & McNaughton, 1986), this slope equals the inverse of stomatal resistance ($1/r_s$) being equal to the stomatal conductance (g_s)(see § 1.1.1.1). This is true when leaf temperature is assumed to be equal to air temperature, which in this forest is a good assumption (Samson & Lemeur, 2000). The slopes of the relations illustrated in Figure 3.11 thus equal g_s, and thus indicate that stomata remained open at night (Figure 3.11). Maximal nighttime g_s was 0.0024, 0.0009 and 0.0017 m s^{-1} for the upper, middle and lower canopy layer respectively, and 0.0011 m s^{-1} for ash. Stomatal conductance for sycamore during night was below 0.0003 m s^{-1}. Minimal g_s for sycamore was reached at the end of the night, just as for ash and beech, and amounted to 0.0001 m s^{-1}. The calculated g_s (Figure 3.11) of all considered species and canopy layers was higher than the maximal cuticular conductance (below 0.0001 m s^{-1}) which has been reported for beech (Hoad et al.,

1997), indicating that nighttime transpiration occurred through open stomata (Benyon, 1999).

Because the relationship between *D* and nighttime F_{LA} showed the typical saturation response (Figure 3.11), it can be concluded that at the beginning of the night transpiration was controlled by stomata. In our study, F_{LA} steadily decreased until sunrise, which could also indicate refill of tissue water reserves to be completed. Therefore, nighttime sap flow can be ascribed to a combination of open stomata and refill of water storage reserves. Whereby nighttime sap flow through open stomata is believed to be the most important, because of the clear relationships between *D* and nighttime sap flow (see Figure 3.11).

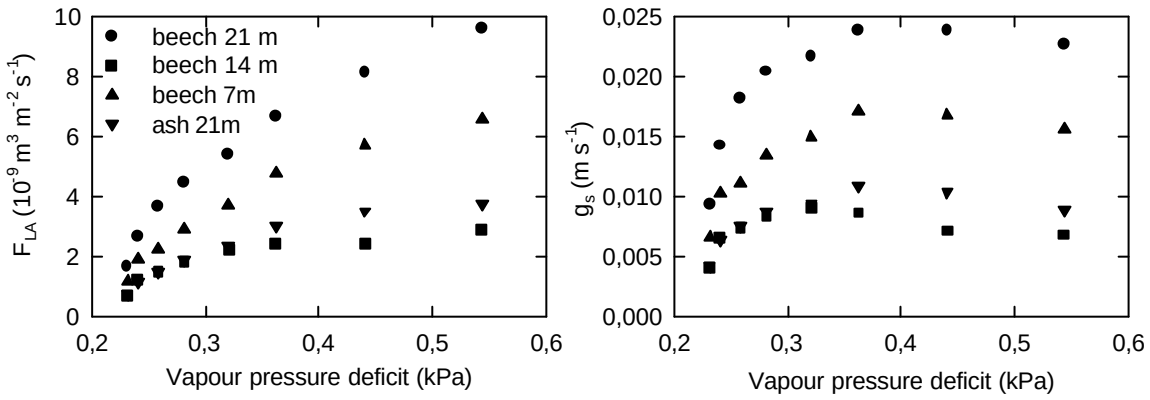

Figure 3.11 The relationship between mean hourly vapour pressure deficit for the period July 16-August 1, and: (left) branch sap flow rate per unit leaf area (F_{LA}) of beech at different canopy depths and ash, and (right) stomatal conductance (g_s) calculated from the sap flow measurements. Symbols indicate mean hourly nighttime values (between 2200 and 0600 h).

Because F_{LA} (Table 3.3) and the amount of leaf surface (see Samson et al., 1997a) is highest in the upper canopy layer, we advise that when only one canopy layer can be sampled for its sap flow, besides stem sap flow, the upper canopy layer should be chosen.

Nighttime sap flow should be checked with gas exchange apparatus applied on leaf or branch level. The leaf cuvettes, or even better branch bags, should preferentially be installed simultaneously, and on the same branches as monitored for their sap flow.

3.1.3.3 Effect of vapour pressure deficit on sap flow

The relationship between vapour pressure deficit (*D*) and sap flow is shown in the Figures 3.12-3.14, for two periods: a first period from July 24 till August 1 and a second one from August 14 till August 23, hereafter referred to as the dry and wet period respectively. Daily solar radiation sums, the maximum temperature, and the maximum *D* values were within the ranges 15.9 - 26.2 and 8.3 - 20.8 MJ m^{-2} day^{-1}, 24.5 - 32.4 and 19.5 - 24.2 °C, and 1.0 to 1.8 kPa and 0.2 to 0.7 kPa for the dry and wet period respectively. Soil water potential, measured at a depth of 10 cm, increased from minimal -0.1 MPa in the dry period to -0.01 MPa in the wet period.

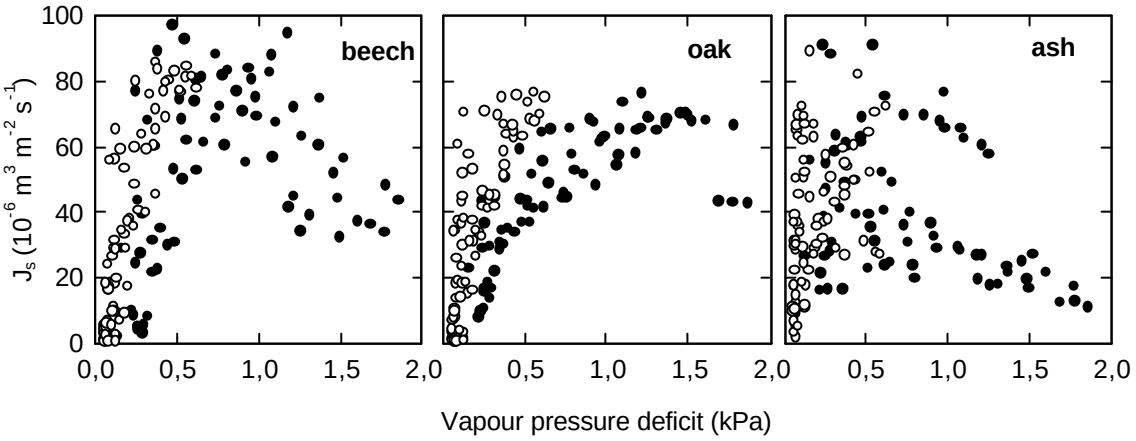

Figure 3.12 Sap flux densities (J_s) at stem level in relation to vapour pressure deficit measured at 13 m height. Open and closed circles refer respectively to a period with a higher soil water potential (August 14-23), and a dry period (July 24-August 1).

For all tree species measured, and for the upper and lower canopy levels, the relationship between the sap flow and *D* is nearly linear for low *D* values (*D*<0.5 kPa)(Figure 3.12-3.14). However, the saturation response of sap flow with increasing atmospheric demand is also observed in our experiment, especially for the sap flux density at stem level (Figure 3.12), and for the two understory species (Figure 3.14). For beech and ash the sap flux density in the stem (J_S) strongly decreased at high *D* than was the case for oak. For oak, the relation between J_S and *D* was clearly different for the wet and dry period, while this difference was less clear

for beech and ash, indicating that oak is sensitive to drought. Figure 3.14 also shows that hazel is more sensitive to higher *D* than sycamore, with the critical *D* around 0.8 kPa. On stem level this saturation response might be explained by the water storage capacity of the stem and the diurnal phase shift between *D* and R_S (maximal *D* during the day is reached long after R_S)(Zhang et al., 1999). As will be shown later (see Table 3.4) J_S was best related to R_S, so that in the later afternoon when R_S decreased, and *D* was still high, J_S also decreased. For the branch measurements (Figure 3.13), this indicates that stomata plays an important role in controlling water loss by transpiration (Zhang et al., 1999). It is remarkable that this saturation response between *D* and F_{LA} was only observed for ash and for the two understory species (Figure 3.14). For sap flux densities measured at branch level for beech the relationship was linear, indicating less stomatal control on transpirational water losses, which could be attributed, according to Goldstein et al. (1998) to a large storage capacity of the stem.

A decreasing slope of the relationship between sap flow and *D*, has also been found by Wullschleger et al. (1998a), when soils dries out, and between a “wet” and a “dry” treatment of red maple, indicating that although the small difference in soil water potential for the dry and wet period, the investigated species indeed were subjected to a light drought stress in the dry period.

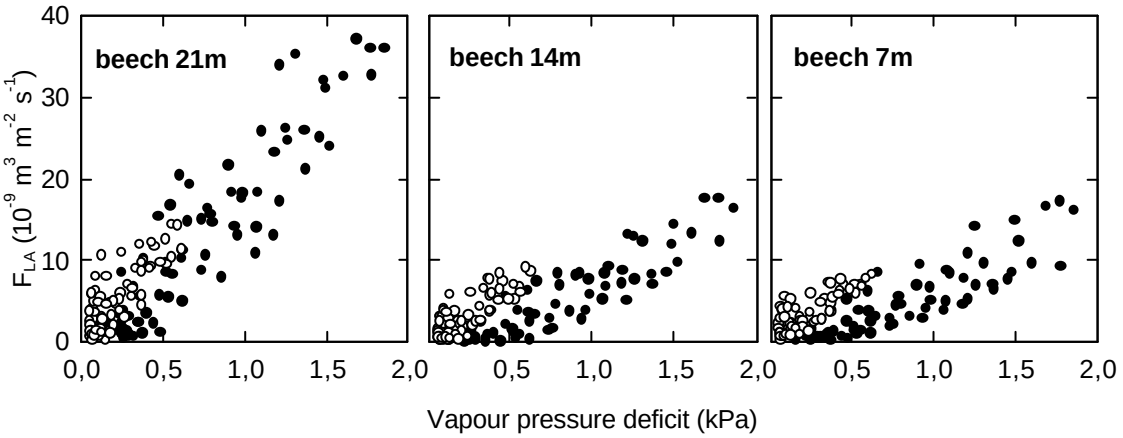

Figure 3.13 Effect of branch heights on the relationship between sap flux densities (F_{LA}) and vapour pressure deficit for the case of beech. Open and closed circles refer respectively to a period with a higher soil water potential (August 14-23), and a dry period (July 24-August 1).

Figure 3.13 also shows that the relationship between sap flux density per unit leaf area (F_{LA}) and D decreased with depth in the crown canopy. Based on these observations and on the assumptions formulated before, it was calculated that the stomatal conductance (g_s) decreased for the lower canopy layers and that g_s was higher during the wet period than during the dry period again indicating a stomatal control mechanism during the dry period. For the dry period g_s (±SE) amounted to 0.0027 (±0.0001), 0.0012 (±0.0001) and 0.0010 (±0.0001) m s^{-1} for the upper, middle and lower canopy layer respectively, and for the wet period this was respectively 0.0026 (±0.0002), 0.0017 (±0.00001) and 0.0015 (±0.0001) m s^{-1} (Figure 3.13). This dependency of g_s on depth was also confirmed by field measurements of g_s using a dynamic diffusion porometer (AP4, Delta-T Devices, Ltd, Cambridge, UK). The maximal g_s values measured during the summer of 1997 were 0.0055 (±0.0012), 0.0035 (±0.0005) and 0.0023 (±0.0004) m s^{-1} for the upper, middle and lower canopy layer respectively, in the upper canopy layer of ash g_s was 0.0089 (±0.0037) m s^{-1}.
In accordance with our results, Roberts and Rosier (1994) found maximum values of g_s at the top of ash and beech, while at the canopy base g_s also was about half of these values. So, just as F_{LA} (Table 3.3), g_s decreased with depth in the canopy, which can be explained by increased self-shading of the above leaves and shading from neighbouring trees, combined with a less demanding micro-climate for transpiration deeper in the canopy.

The higher g_s of ash can explain the higher sap flow, compared to beech (Figure 3.9), observed in the beginning of the growing season, in absence of any water stress. However, despite this high g_s, F_{LA} of ash was significantly lower of that of beech at the same canopy level (Table 3.3) during the dry period (July 16- August 1). This indicates that ash is more sensitive to drought than beech, which can be explained by differences in wood anatomy. North-temperature ring-porous tree species (like ash) have so large earlywood vessels that cavitation takes place at least by the end of the winter (Zimmermann, 1983). The result is that most water is conducted in the wide earlywood vessels of the most recently formed growth ring. Thus, for ash it is of the utmost importance to avoid cavitation, by reducing g_s, and thus F_{LA} (Table 3.3) during drought. Calculation of g_s (based on Figure 3.14) confirmed the above statements. During the dry period g_s (±SE) of ash was 0.0014 (±0.0001) m s^{-1}, while during the wet period g_s more than doubled to 0.0032 (±0.0003) m s^{-1}.
Based on the same figure (Figure 3.14) it can be concluded that the g_s of the understory species is lower (for the wet period 0.0007 (±0.0000) and 0.0011 (±0.0001) m s^{-1} for respectively sycamore and hazel) than those of the upperstory species, which is also found by other authors for herbs (Roberts & Rosier, 1994) and shrubs (Hogg et al., 2000).

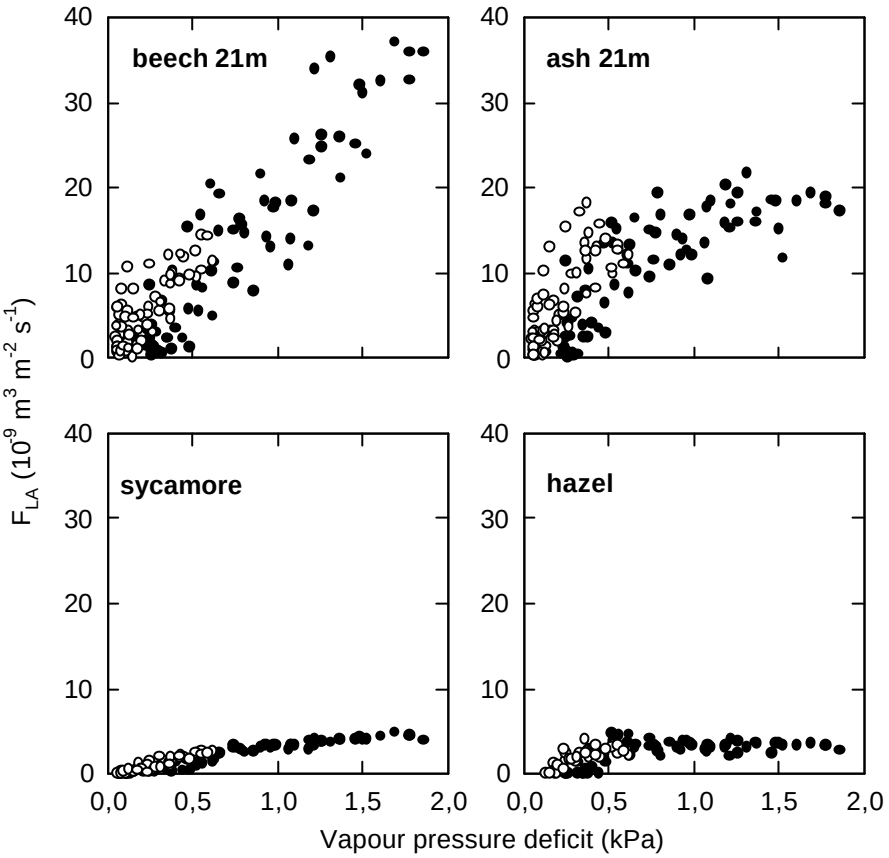

Figure 3.14 Sap flux densities expressed per unit leaf area (F_{LA}) measured on branches at the top crown level (beech 21 m and ash 21 m) and for branches of understory species (sycamore and hazel). The dependence of F_{LA} on vapour pressure deficit is shown. Open and closed circles refer respectively to a period with a higher soil water potential (August 14-23), and a dry period (July 24-August 1).

The cross-correlation and lag in time between a change in a given meteorological variable and a change in sap flow is given in Table 3.4. Both cross-correlation and time-lag analyses were performed using SPSS Release 10.0.5 (SPSS Inc., Chicago, Illinois, USA). From Table 3.4 it can be seen that on sunny days the upper canopy layers as well as the understory species mainly react to a change in solar radiation, while middle canopy layers are primarily reacting to a change in *D*. In the understory of the forest, solar radiation seems to be a more limiting parameter than *D* which, at that level close to the ground, has a much smaller diurnal variation compared to solar radiation. Also the sap flux density at stem level (J_S) seems to react primarily to variations of solar radiation.

Table 3.4 The most significant cross-correlation, and associated lag in time (min) between a change in a climatic variable and a change in basal sap flux density (J_s) for beech, oak and ash, and sap flux density at branc level (F_{LA}) for beech at 21 (B21), 14 (B14) and 7 m (B7) height, for ash at 21 m (A21), and for the understory species sycamore and hazel. A distinction is made between sunny (radiation sum > 16 MJ m^{-2} day^{-1} of solar radiation)(n = 1008) days, and cloudy (< 16 MJ m^{-2} day^{-1})(n = 864) days during the month of August 1999. Only days without precipitation were selected. Ten minute average values were used for the calculations. Abbreviations: Variables are: *S* = solar radiation; *T* = temperature; *D* = vapour pressure deficit; (-) means no significant correlation found. All climatic variables were measured above the canopy. Sycam = Sycamore.

		Stem flow (J_s)			Branch flow (F_{LA})					
		Beech	Oak	Ash	B21	A21	B14	B7	Sycam	Hazel
Sunny		S	S	-	T	S	D	D	S	S
	r^2	0.90	0.86	-	0.76	0.81	0.76	0.81	0.90	0.85
	lag	10	20	-	0	10	20	10	20	10
Cloudy		S	S	S	D	S	D	D	D	D
	r^2	0.90	0.86	0.53	0.82	0.73	0.78	0.85	0.88	0.67
	lag	20	60	10	0	10	0	10	0	0

Just as for the variation in g_s (Figures 3.13-3.14) and F_{LA} (Table 3.3), the different reaction of sap flow to meteorological parameters (Table 3.4) between the upper canopy layers and the understory can be explained by the specific micro-climate occurring in forests. Because turbulence is more important in the upper canopy layers compared to the lower layers, the air in this layer is better mixed with the above atmosphere. This causes the higher intra-canopy relative humidity due to evapotranspiration, to decrease quickly in the upper canopy, causing light to be the limiting factor for transpiration. For the middle canopy layers, sap flow seems to be more limited by *D*, as the more water vapour saturated air is more slowly exchanged with the above atmosphere due to the attenuation of wind speed in the tree crowns (see Figure 1.13).

3.2 Hydraulic conductance of the upperstory and understory species

3.2.1 Introduction

The hydraulic design of trees influences the transport of water from roots to leaves, and it can limit their water relations, gas exchange throughout the crown of trees, the distribution of trees over different habitats and, perhaps, even the maximum height a particular species can achieve (Tyree and Ewers, 1991). Differences in the total hydraulic conductance for the soil-root-leaf pathway of water movement has important implications for variations of transpiration rate and leaf water potential observed within forest canopies. These differences also permit assessment of the trade-off between conductance and vulnerability of woody stems to xylem cavitation, and for evaluating the importance of stored water to the survival of trees during periods of severe drought (Wullschleger et al., 1998b). Kowalik et al. (1997) found that plant conductance is still considered as a major uncertainty in modelling plant-water relations, especially considering the low accuracy with which it can be determined experimentally (Cienciala et al., 1994).

Estimates of whole-plant water use expressed per unit sapwood area or leaf area (Landsberg et al., 1976), or water flux through various parts of the soil-plant-atmosphere-continuum (Tyree and Ewers, 1991) can be related to the concept of leaf water potential. Sap flow measurements, together with simultaneous determinations of leaf water potential, make it possible to estimate the hydraulic conductance for water flow in single trees (Zhang et al., 1999).

Several methods have been devised in the past. Schulze et al. (1985) showed that, for *Picea abies* and *Larix* species, a regression approach could be used to calculate the hydraulic conductance of trees (G_t) from the inverse relationship between their transpiration rate of leaves and their leaf water potential (Wullschleger et al., 1998b). Stored water within the stem or branches of large trees may, however, introduce a time lag or hysteresis into the relationship between transpiration rate and leaf water potential. If these lags are large, they can make calculations of G_t by the regression method very difficult. This problem can be avoided by using measurements of the water flux at branch level to estimate the transpiration rate of the leaf area (Wullschleger et al., 1998b). Meinzer et al. (1995) applied a simpler single-point method to estimate G_t for several tropical forest gap species from branch measurements of water flux. As such, various studies have estimated G_t from water

flux data obtained for branches and for entire trees (e.g. Schulze et al., 1985; Bréda et al., 1993; Meinzer et al., 1995; Andrade et al., 1998).

Cochard et al. (1996) concluded that both stomatal conductance (g_s) and hydraulic conductance (G_t) play a major role in the control of xylem embolism by maintaining a minimum water potential which is less negative than the threshold value for xylem dysfunctioning. There is substantial evidence that g_s and transpiration rate are positively correlated with the hydraulic conductance of the soil-root-leaf pathway (Sperry and Pockman, 1993; Meinzer et al., 1995). Stomatal conductance and leaf transpiration often increase sharply with increasing G_t and then reaches an asymptotic value as G_t continues to increase (Meinzer et al., 1988; Sperry and Pockman, 1993). Meinzer et al. (1995) observed such an asymptotic relationship for five tree gap species in a tropical forest. The pattern suggests that the stomata of these species responded in a similar way to changes in hydraulic conductance, and that stomatal adjustments in response to changing G_t co-ordinated transpiration rate rather with water transport efficiency than with bulk leaf water status (i.e. leaf water potential). Wullschleger et al. (1998b) thereby suggested that when stomatal conductance or transpiration rate are plotted against the hydraulic conductance of the soil-leaf pathway, a common relationship may be observed for diverse species growing under similar conditions at the same site. This requires that G_t is normalised for the total leaf area of the tree. However, such relationships were, to our knowledge, not yet frequently reported for temperate deciduous tree and shrub species.
This part of the study will verify these relationships for two upperstory tree species (i.e. beech and ash), and two understory species (i.e. sycamore and hazel). The effect of branch height in the crown will be analysed as well (case of beech).

The first step of this research is to study the diurnal dynamics of leaf water potential (Ψ_l). Also the total hydraulic conductance of the soil-root-leaf pathway (G_t), based on branch level measurements of water flux will be determined. Finally, the interlinkage between the liquid phase conductance (G_t) and vapour phase conductance (g_s) will be checked and compared with similar relationships found by Meinzer et al. (1995) and Andrade et al. (1998) for tropical shrub and tree species.

3.2.2 Material and methods

3.2.2.1 Measurement of leaf water potential

Water potential measurements were conducted hourly on a partially cloudy (September 17, 1999) and a sunny (September 18, 1999) day (Figure 3.15). Solar radiation sums were for the cloudy and the sunny day 10.2 and 14.2 MJ m^{-2} day^{-1} and mean daily temperature was 19.8 and 19.1 °C respectively. Mean vapour pressure deficit was rather similar for both days, i.e. 0.35 and 0.37 kPa above the canopy, and 0.23 and 0.26 kPa at soil level, for the cloudy and sunny day respectively. During this period soil water potential at a depth of 10 cm was around -0.02 to -0.05 MPa indicating non-limiting soil water availability. On both days leaf sampling started two hours before dawn, and the last two samples were collected one and a half hour after sunset and at sunset, respectively for the cloudy and the sunny day. The water potential was determined using a Scholander-type pressure chamber (PMS, Instrument Corp., Corvallis, Oregon, USA) installed in the cabin at the base of the measuring tower.

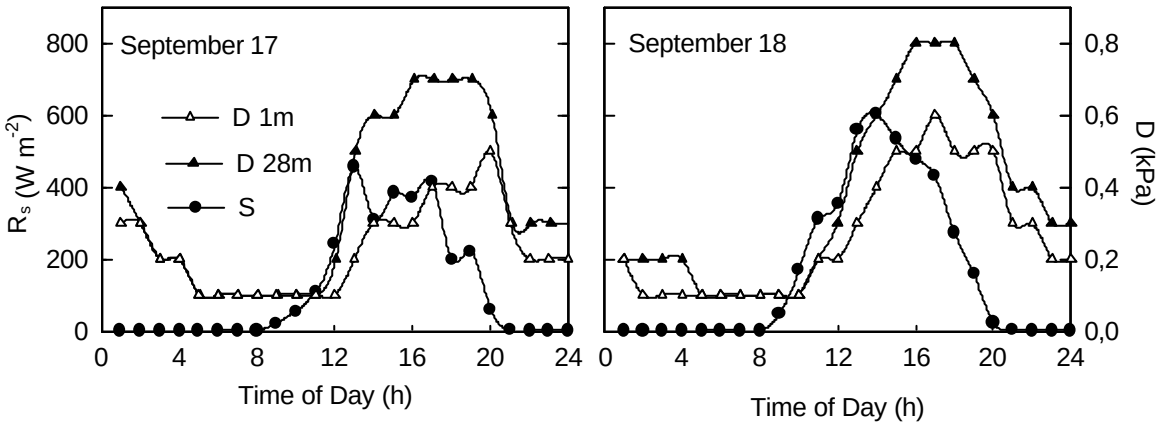

Figure 3.15 Incoming solar radiation (R_s) and vapour pressure deficit (D) measured 2 m above the canopy and 1 m above the forest floor on September 17 (partially cloudy) and 18 (sunny), 1999.

If a leaf is cut from a plant, the tension in the xylem causes the xylem sap to be withdrawn from the cut surface. This leaf may then be sealed into a pressure chamber (Figure 3.16), with the cut end exposed. The chamber is then pressurised until the sap just wets the cut surface, thus restoring the sap to its position *in vivo*. At the time of leaf collection the original average leaf water potential (Ψ_l) would be given by:

$$\Psi_l = \Psi_p + \Psi_p \qquad (3.18)$$

where Ψ_p and Ψ_P are leaf averages of turgor and intracellular osmotic potentials. As the chamber is pressurised the water potential is raised by the amount of pressure applied so that, at the balance pressure (P^*), the water potential is zero (there is free water at the cut surface) so

$$\Psi_l + P^* = 0 \qquad (3.19)$$

The negative of the balance pressure therefore equals the original Ψ_l. For precise work it is necessary to correct Equation 3.19 for the osmotic potential of the apoplast (the water-filled space outside the cell membranes and including the xylem sap).

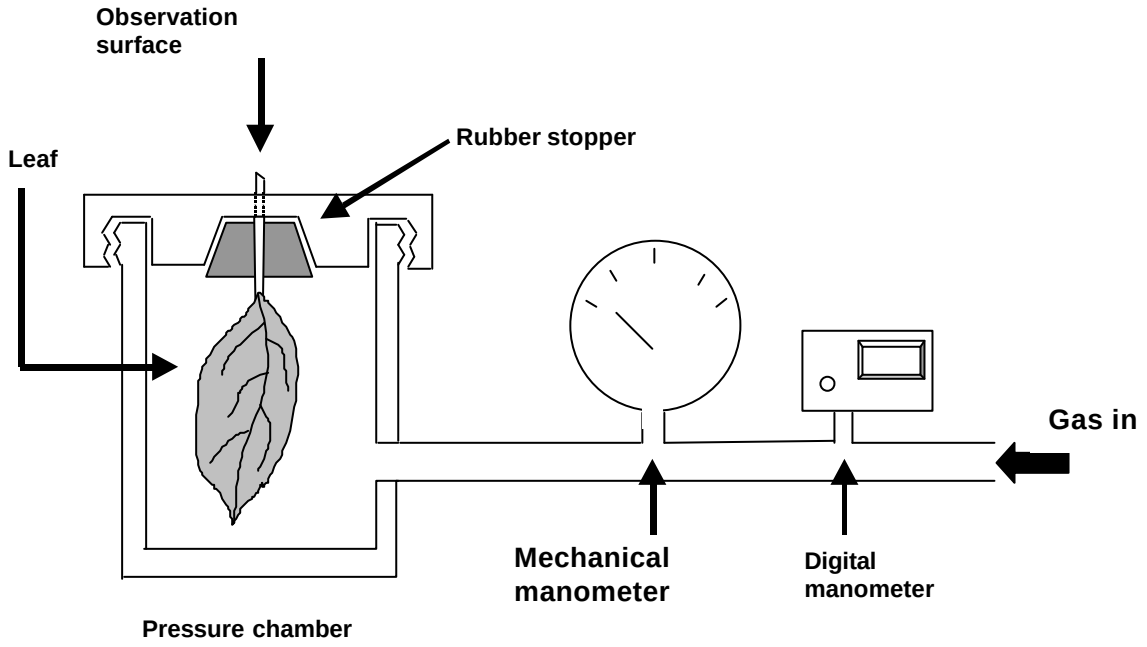

Figure 3.16 Schematic representation of the used pressure chamber to determine leaf water potential Ψ_l. Actual gas pressure is monitored on a mechanical manometer, and the pressure at the moment of the reading can be registered by a digital manometer.

The following species and canopy levels were sampled: beech (21, 14 and 7 m), ash (21 m), sycamore and hazel (both at 1.3 m). Leaf collection (n =3) started at the upper crown level, and the understory species were sampled last. Samples were not taken from the branches equipped with heat balance sensors, but from neighbouring branches. Sampling of all species and crown levels did not require 15 minutes. Three leaves were randomly sampled for each species and crown level. Immediately after sampling each leaf was wrapped in aluminium foil, and then enclosed in a separate plastic bag to avoid transpirational water loss prior to the measurement in the pressure chamber. During the time the water potential of a leaf was measured, the other leaves were kept in a cooled box.

3.2.2.2 Calculation of hydraulic and stomatal conductance

The total hydraulic conductance of the soil-root-leaf pathway G_t (m^3 m^{-2} s^{-1} MPa^{-1} or m s^{-1} MPa^{-1}) can be calculated from a simple hydraulic flow equation (electric analogon model), called by Meinzer et al. (1995) the single-point method:

$$E = G_t . \Delta\Psi \qquad (3.20)$$

or

$$G_t = E / \Delta\Psi \qquad (3.21)$$

where E (g m^{-2}_{leaf} s^{-1} or m^3 m^{-2} s^{-1}) is the actual transpiration rate, and $\Delta\Psi$ (MPa) is the difference between pre-dawn and actual water potential. Pre-dawn leaf water potential can be used as an approximation of soil water potential. At pre-dawn $\Delta\Psi$ = 0 as stomata are closed and no flow occurs.
Our forest is highly coupled to the atmosphere, Ω (Jarvis and McNaughton, 1986) was 0.1 for the period 15 to 20 August 1998 (see § 1.1.2.5, § 4.1.3.4, and Samson and Lemeur, 2001). Because of this high degree of coupling, stomatal conductance g_s (m s^{-1}) was calculated according to (Equation 1. 8, see § 1.1.1.1):

$$E = g_s \left[\rho^{\circ}(T_l) - \rho_v \right] \qquad (3.22)$$

or

$$g_s = \frac{E}{\rho^{\circ}(T_l) - \rho_v} \qquad (3.23)$$

with $\rho^{\circ}(T_l)$ the saturated density of water vapour inside the leaf at leaf temperature, and ρ_v is density of water vapour in the air, both expressed in g m^{-3}. Leaf temperature is considered to equal air temperature, which is a good assumption for our forest (Samson and Lemeur, 2000).

The actual transpiration rate of the leaf E is set equal to the sap flux density per unit leaf area F_{LA} obtained from branch measurements, corrected for the time lag between leaf water potential and F_{LA} (see Figure 3.17). As leaf temperature is assumed to equal air temperature, the vapour density measurements above the canopy and at soil level are used to determine [$r°(T_l)$ - r_v] representative for the upperstory and understory species respectively (see Figure 3.15).

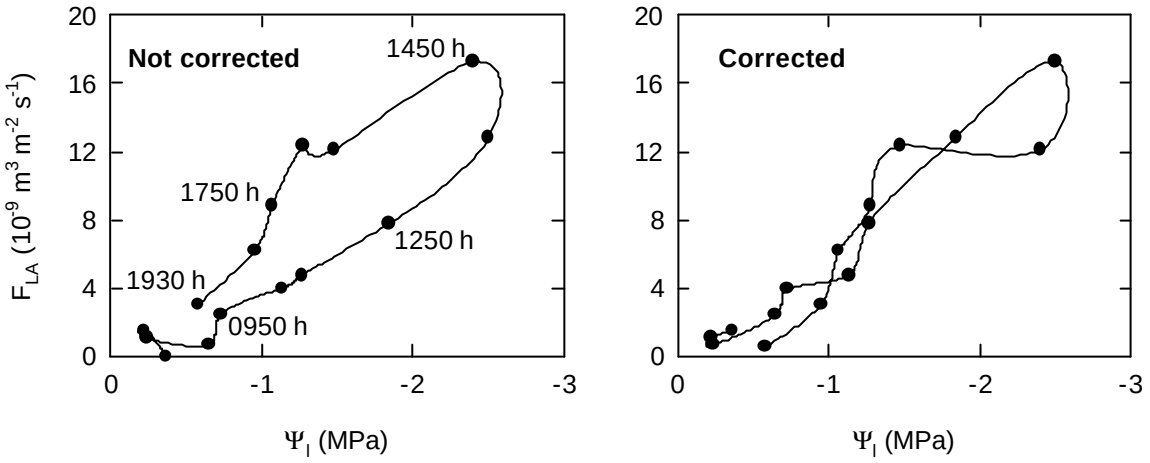

Figure 3.17 Relationship between sap flux density per unit leaf area F_{LA} and leaf water potential (Y_l) for beech both measured at 21 m height and for September 18 (sunny day). Data of F_{LA}, as well not corrected (left) as corrected (right) for the time lag between Y_l and F_{LA}, are shown. Measuring time is indicated for some points (case of not corrected sap flow).

3.2.3 Results and discussion

3.2.3.1 Diurnal pattern of leaf water potential and sap flow

The diurnal pattern of Y_l and corresponding sap flux density per unit leaf area F_{LA} is shown in Figure 3.18 for all the investigated species and canopy layers. At the highest crown layer the most negative leaf water potentials were observed, while they were much less negative for the understory species, especially for sycamore. This indicated that root water uptake by sycamore almost balanced the instantaneous water loss through the leaves. Moreover this small diurnal variation in

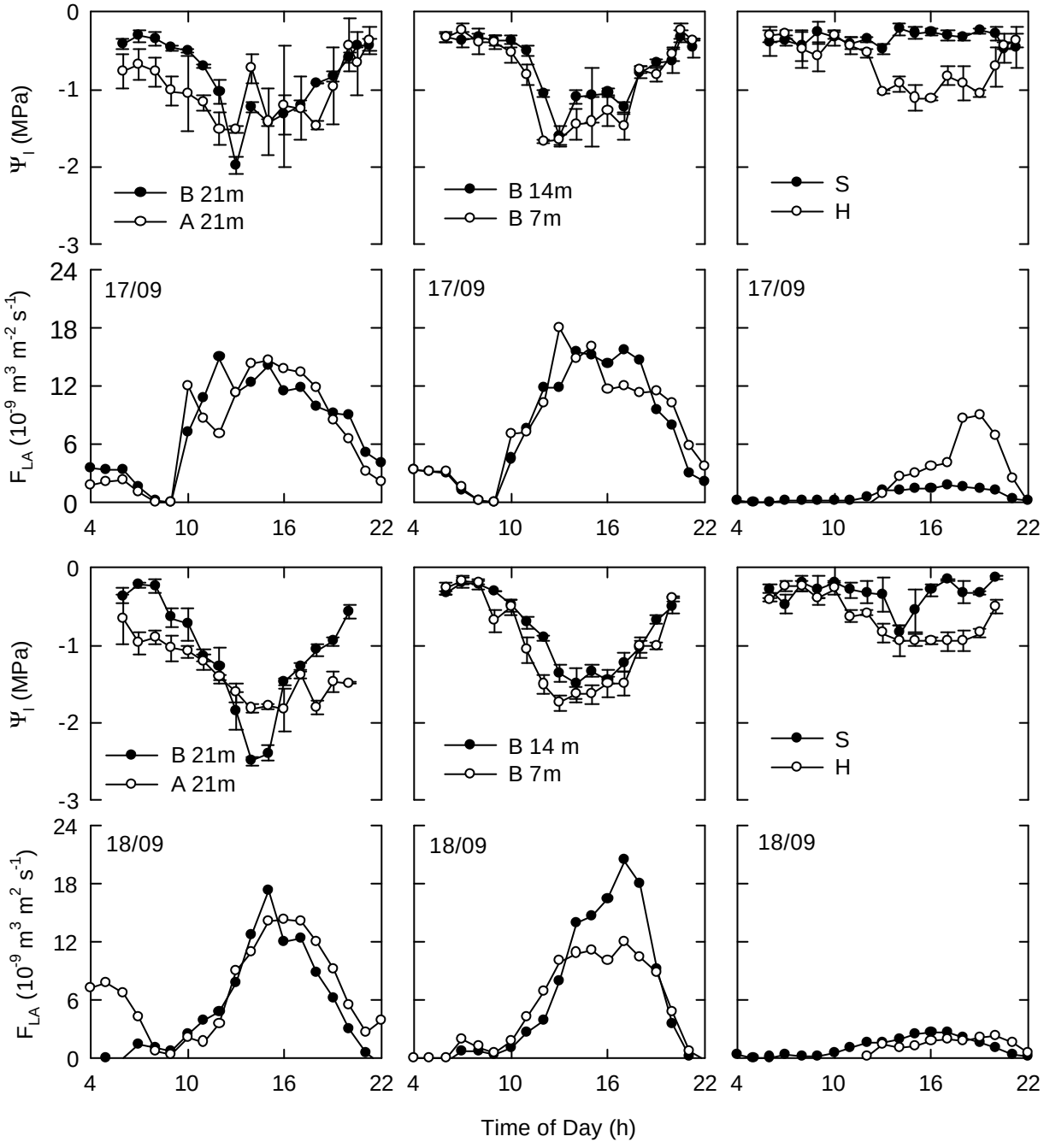

Figure 3.18 Diurnal course of mean leaf water potential (Y_l) and sap flux density per unit leaf area (F_{LA}), for beech at 21 (B 21m), 14 (B 14m) and 7m (B 7m), ash at 21 m (A 21m), and understory species sycamore (S) and hazel (H). Measurements recorded on September 17 (partially cloudy day) and September 18 (sunny day). Error bars on Y_l are ± SE (n=3).

Y_l can also be explained by the rather stable and less water demanding (see low vapour pressure deficit, Figure 3.15) micro-climate in the understory layer of the forest. As expected, the diurnal amplitude of Y_l was most pronounced in the upper crown layer. In the middle and lower crown levels of beech the diurnal course of Y_l was very similar. During the sunnier day a more negative Y_l was observed compared to the cloudy day.

Pre-dawn leaf water potentials are almost the same for all species and crown layers except for ash.

Zhang et al. (1999) stated that pre-dawn leaf water potential is very representative for soil water potential. Hence, the mean soil water potential of the root extraction zone can be estimated as -0.4 MPa. which is lower than the values measured at a single depth of 10 cm. A reason for this difference between soil water potential deducted from leaf water potential and tensiometer measurements, besides the fact that the former is an average value over the total rooting depth, could be nighttime transpiration due to open stomata, which was indeed observed for all species (see § 3.1.3). Nighttime transpiration of ash (Figure 3.18) is also thought to be responsible for the low predawn Y_l of this species compared to the other species.

Leaf water potential measured in the mid-crown level of beech (Figure 3.18) is characterised on the sunnier day by a slight increase at 1500 h. This could be attributed to the "midday-closure" of the leaf stomata. When the leaf dehydrates, stomatal guard cells will close temporarily, minimising water losses, and allowing water reserves to be refilled again (Lambers et al., 1998). Andrade et al. (1998) suggested that this frequently observed "midday-closure" of the stomata, followed by a partial repair in the afternoon, could be a reflection of the hydraulic consequences of the daily use and refilling of internal water reserves. This hypothesis is supported by the observation of the time delay between fluctuations of leaf water potential and sap flow (see Figure 3.17 and 3.18).

Changes of sap flow lagged behind changes in Y_l by one hour on the sunny day (2 hours for the understory)(Figure 3.17 and 3.18). Leaf water potential dynamics are closely linked to the diurnal change of solar radiation, which regulates stomatal movement and, as such, stomatal control of sap flow.

3.2.3.2 Diurnal patterns of hydraulic conductance

Leaf water potential of ash was less negative during the day compared to Y_l of the corresponding beech layer, but sap flow for both species was comparable (Figure 3.18). This observation can be explained by the differences in wood anatomy. The vessel diameter of the ring-porous ash and the diffuse porous beech is estimated 300 and 75 µm, respectively (Zimmermann, 1983). The wider xylem vessels of ash are more vulnerable for cavitation, so Y_l is kept above a minimal threshold value associated with leaf desiccation and cavitation, which is higher than that for beech with smaller and less vulnerable xylem vessels for cavitation. The wider xylem vessels of ash make the water transport system more efficient, which is also reflected in the higher hydraulic conductance for ash (see Table 3.5). From the results obtained for sycamore, it was concluded that the applied method (Equation 3.21) does not yield good results when diurnal fluctuations in Y_l are small (Figure 3.19).

The small fluctuations observed for G_t (Figure 3.19) during the sunny day can be attributed to measurement errors. The more pronounced fluctuations, observed on the cloudy day were in addition due to the different time responses and averaging periods for Y_l, F_{LA} and meteorological variables.

Table 3.5 Mean (±SE) hydraulic conductance per unit leaf area of the soil-root-leaf pathway (G_t), for a sunny day (18 September 1999), between 1100 and 1600 h (n=5), for: beech at 21 (B21), 14 (B14) and 7m (B7), ash at 21 m (A21), sycamore (S) and hazel (H). The water potential gradient (DY/Dd) was defined as ($DY_{predawn}$- $Y_{l\ minimal}$)/soil-to-leaf-distance. -: means that no value could be calculated.

	B21	A21	B14	B7	S	H
Hydraulic conductance	9	12	15	8	-	4
(10^{-9} m^3 m^{-2} s^{-1} MPa^{-1})	±2	±1	±2	±1	-	±1
$\Delta\Psi/\Delta d$ (MPa m^{-1})	0.10	0.06	0.08	0.21	0.38	0.41

The diurnal pattern of the total hydraulic conductance (G_t) of the soil-root-leaf pathway is shown in Figure 3.19. This figure (Figure 3.19) illustrates that G_t was highly variable during the partly cloudy day, while being relatively constant during the sunny day, except for sycamore. A mean G_t value for the sunny day could be calculated for all species except for sycamore (Table 3.5). G_t for all species and canopy layers was not significantly different (ANOVA, P=0.05), but for hazel a much lower value was observed compared to the other species. When F_{LA} was not corrected for lagging behind Y_l (Figure 3.17), and thus transpiration, a steady increase in G_t throughout the day was observed (data not shown).

The G_t values reported in Table 3.5 agree with the values observed by Meinzer et al. (1995) and Andrade et al. (1998). Both authors found for tropical forest gap and canopy tree species values for soil-root-leaf hydraulic conductance within the range of 18-178 10^{-9} m^3 m^{-2} s^{-1} MPa^{-1} and 4-104 10^{-9} m^3 m^{-2} s^{-1} MPa^{-1} respectively. Schulze et al. (1985) found for a *Larix* species a conductance of 8 10^{-9} m^3 m^{-2} s^{-1} MPa^{-1} and Kowalik et al. (1997) reported a plant conductance in beech of 17 10^{-9} m^3 m^{-2} s^{-1} MPa^{-1} which they considered to be very low. These authors observed no hysteresis between twig water potential and sap flow, however recognised in many other trees, which they explained by the low hydraulic conductance. Magnani and Borghetti (1995) attributed lack of hysteresis to the lack of internal water storage. Wullschleger et al. (1998b) noticed that G_t values can vary by more than 30-fold (6-fold in our study), and they also believe that one explanation (among many) for this variation involves species-related differences in leaf area per unit cross-sectional sapwood area.

To transport sufficient water to the leaves, a lower G_t must correspond with a higher water potential gradient (Tyree and Ewers, 1991). This water potential gradient was defined as the ratio of the potential difference ($\Psi_{predawn} - \Psi_{l\ minimal}$) to the soil-to-leaf-distance or $\Delta\Psi/\Delta d$. This gradient appeared to be the highest for the understory species, followed by beech and finally ash (Table 3.5). The lower $\Delta\Psi/\Delta d$ for the upperstory trees compared to hazel indicates that a substantial compensation has taken place to avoid too low xylem water potentials, which can cause cavitation. In shrubs the transport distances are not normally as large as in trees, but the branching system can be quite complex. As mentioned by Tyree and Ewers (1991), the smallest stem segments have potential gradients that are 30-300 times steeper than in the base of the boles of trees. This might explain the high $\Delta\psi/\Delta d$ observed for the understory species. The comparable $\Delta\Psi/\Delta d$ for beech at 14 and 21 m height indicates that these branches behave like independent plants rooted in a common, highly conductive bole (Tyree and Ewers, 1991).

3.2.3.3 Relation between hydraulic and stomatal conductance

The relationship between stomatal (g_s) and hydraulic conductance (G_t) is illustrated in Figure 3.20. A unique relationship appeared to describe the response of all species. An asymptotic curve between G_t and g_s was also found by Meinzer et al. (1995) and by Andrade et al. (1998) for tropical tree species. These last authors also mentioned that comparable relationships between vapour and liquid phase conductance have been observed in sugarcane (Saliendra and Meinzer, 1989) and the riparian tree *Betula occidentalis* (Sperry and Pockman, 1993).

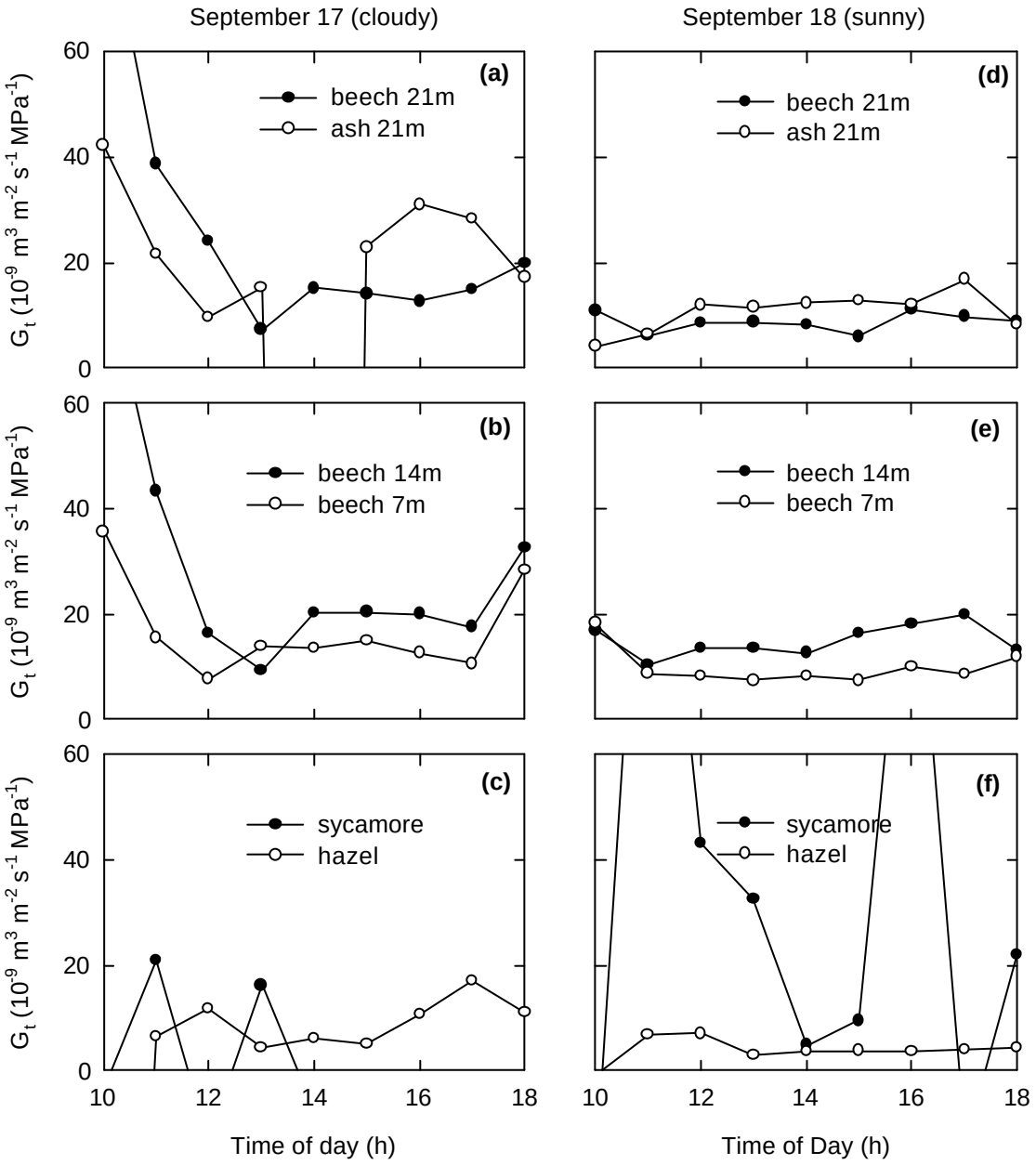

Figure 3.19 Diurnal patterns of hydraulic conductance (G_t) for the uppertory species beech (measured at three heights in the crown) and ash, and for the understory species sycamore and hazel. The patterns are for the partly cloudy day September 17 (a-c), and sunny day September 18 (d-f).

This unique relationship suggests that differences in stomatal regulation of transpiration appeared to be governed largely by tree size and architectural features rather than intrinsic physiological differences in the responsiveness of stomata to variables affecting their aperture. Both Meinzer et al. (1995) and Andrade et al. (1998) suggest that this relationship could indicate that stomatal adjustments occur to

balance transpiration with water transport efficiency (i.e. hydraulic conductance) rather than with the bulk leaf water status (i.e. water potential). As in this study, this relationship is now established for temperate deciduous tree species as well, this could mean that all (woody) species respond similarly with respect to stomatal conductance, in relation to water transport efficiency. This was also suggested by Wullschleger et al. (1998b).

However, this last hypothesis should best be tested by independent measurements of G_t and g_s. Stomatal conductance should thus be measured with a porometer, or even better by measuring the water vapour exchange from a part of a branch, downstream of the sensor, enclosed in a branch bag.

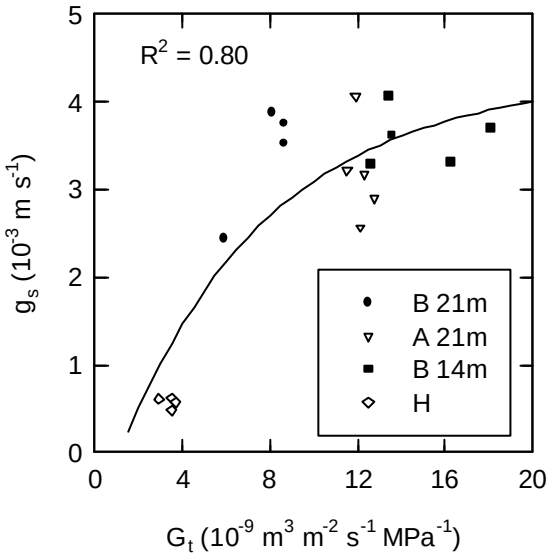

Figure 3.20 Stomatal conductance (g_s) in relation to total hydraulic conductance of the soil-root-leaf pathway (G_t) for beech at 21 (B 21m) and 14 m (B 14m), ash at 21 m (A 21m) and hazel (H). Data for September 18 (sunny day), 1999. The relationship can be expressed as $g_s = -0.75 + 5.02[1-\exp(-0.145G_t)]$.

The mechanism that correlates g_s to G_t is not known (Meinzer et al., 1995; Andrade et al., 1998). According to Meinzer et al. (1995) it is possible that not the intrinsic reaction of species to a variable differs, but that a difference in morphology and external factors (like a different root system or the distribution of the available soil water), can lead to different physiological operating ranges. This could mean that hazel, having a smaller G_t and g_s than the other tree species (Figure 3.19 and 3.20,

Table 3.5), acts in another physiological range than the other tree species. This might be because its root system is probably restricted to the unsaturated zone, while tree species could also make use of deeper layers close to and below the water table.

Cochard et al. (1996) presumed that the mechanism of stomatal behaviour to changes in G_t can be explained by integration of both hydraulic and chemical root generated signals. So, stomata could react on hydraulic signals caused by a decrease in leaf water potential, and also on absiscic acid (ABA) which would be the agent for root-leaf signalling, when the soil dries.

The sap flux density, measured at the base of the stem, is often smaller than 0.5 $m^3\,m^{-2}\,h^{-1}$ or 0.5 $m\,h^{-1}$ (Zhang et al., 1996; Granier et al., 2000a). This implies that it may take several hours or even days before soil water, and consequently the dissolved substances, reaches the upper crown leaves. Furthermore, Andrade et al. (1998) mention that the rapidity and reversibility of responses of g_s to perturbation of the hydraulic pathway in some woody species or to soil drying, seems to be inconsistent with regulation of g_s by chemical signals generated in the roots. Therefore it has been suggested that rapidly propagated hydraulic perturbations could trigger the release of chemical regulators of g_s directly within the leaves (Whitehead et al., 1996). Because low basal sap flux densities are also measured in this study (§ 3.1.3), it can also be stated that in temperate forests the hydraulic conductance is an important regulator of tree water use.

3.3 Water storage in stems and branches

3.3.1 Introduction

When water is lost from leaves, it has to be replaced by water from the soil or from the branch, stem or root tissue. Although the soil is the main and often largest source of water, stored water in plant tissues is also contributing to transpiration. Depending on sap flow velocity it usually takes several hours (probably even days) before the water reaches the top of a tall tree. In addition, the hydraulic structure of the tree can have large impact on the characteristics of the water movement from roots to leaves. The low hydraulic conductance of soil-root-leaf pathway may impose water deficits at the leaf level of tall trees during periods of high evaporative demand, even when the soil water availability is high. This temporal imbalance between water supply and demand can be minimised by using the internal water reserves, especially the ones that are closely located with respect to the sites of water loss.

The significance of water storage in stems and branches may be in buffering of variations in stem xylem potential during periods of high transpiration (Holbrook & Sinclair, 1992). Hence, xylem cavitation by air bubbles, being an effective hydraulic signal for stomatal closure (Salleo et al., 2000), may occur less fast so that photosynthesis can be prolonged. Water storage may partially compensate for a decrease in hydraulic conductance, because water reaching the transpiring leaves might have bypassed a major fraction of the total hydraulic resistance of the soil-root-leaf pathway (Stratton et al., 2000). Thus, water storage plays an important role in regulating the water status of leaves exposed to the large diurnal variation in evaporative demand (Goldstein et al., 1998).

Water storage capacity has already been reported for several tree species, such as tropical trees (Goldstein et al., 1998; Stratton et al., 2000), a palm tree (Holbrook & Sinclair, 1992), coniferous trees (e.g. Waring et al., 1979) and deciduous trees (e.g. Kowalik et al., 1997). However, the dynamic aspects concerning diurnal and seasonal change of stored water from stems and branches are rather scarce, especially for deciduous tree species.

Because sap flow was simultaneously measured at stem and branch level, respectively by using the thermal dissipation technique and the stem heat balance approach (see § 3.1.2), this experimental set-up gave a unique opportunity to determine water storage in stem and branches of upperstory species. The objectives of this part of the study are to describe and quantify the diurnal and seasonal use of

water stored in trees with a diffuse-porous (beech) and a ring-porous (ash) xylem morphology.

3.3.2 Material and methods

Tree water storage can be determined by balancing water uptake (i.e. basal sap flow) and leaf water loss (i.e. branch sap flow) over a particular time period (24 hours, several days,…). The sap flux density is expressed per unit leaf area downstream of the sensor (F_{LA})(see § 3.1.2). It then can be scaled up to the total crown level using the total leaf area of the crown. When sap flow is measured on branches of different crown layers, the contribution of the leaf area in that layer can be taken into account. The total crown water use obtained this way can then be compared to the water flow in the stem. Differences between both fluxes are due to loss or refill of stored water.

The water budget can be closed on a daily basis or for a longer period of time. Here the budget was closed for the period from July 16 till August 31, 1999, as it is not sure that basal flow equals the crown sap flow on a daily basis. This period was chosen because the transpiring leaf area during this period can be assumed to be maximal and constant, and because it also comprised a dry spell. Eventually water storage was calculated as the difference between crown sap flow and basal sap flow:

$$\Delta F_{SB} = \sum_{i=1}^{3} F_{LA}(i).LA(i) - J_S.SA \qquad (3.24)$$

with ΔF_{SB} the water storage in stem and branches expressed in m^3 per unit time, $F_{LA}(i)$ the sap flux density expressed per unit leaf area (see § 3.1.2) at crown layer i, $LA(i)$ the leaf area of crown layer i, J_S the basal sap flow given by Equation 3.1 and 3.2 and SA the sapwood area at the height of the basal sap flow measurements (see Table 3.1). The leaf area of crown layer i [$LA(i)$] is obtained by multiplying the LAI of crown layer i (see Table 1.2) with the vertical crown projection of the considered tree.

Tree water storage (ΔF_{SB}) is described in more detail for two contrasting periods in the 1999 growing season (Figure 3.21). The first period (July 27-August 1) was characterised by high solar radiation, high air temperature and high vapour pressure deficit without any precipitation (Figure 3.21). Lower values were measured during the second period (August 3-8) but precipitation now amounted to 12.0 mm (Figure 3.21). This first and second period will hereafter be referred to as the "dry" and "wet" period respectively.

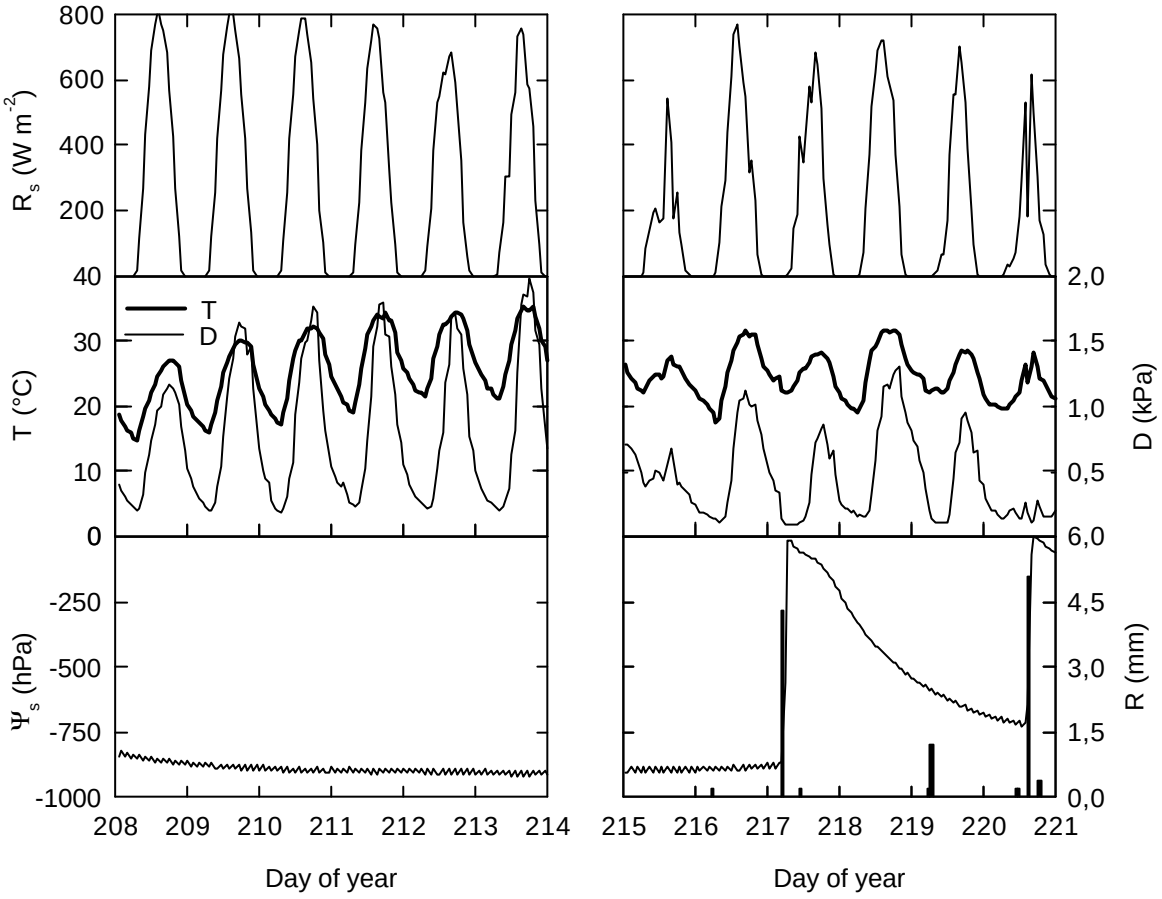

Figure 3.21 Diurnal variation of solar radiation (R_s), air temperature (T_a), vapour pressure deficit (D), soil water potential (Y_s) and precipitation (R) during a "dry" (left: July 27-August 1) and a "wet" period (right: August 3-8) during the 1999 growing season. Ticks on the horizontal axis indicate the beginning of each day (at 0000 h). July 27 is day 208; August 8 is day 220.

3.3.3 Results and discussion

Crown sap flow can be calculated taking sap flow measurements from just one canopy layer into account or from different canopy layers. Comparison for beech revealed that crown sap flow calculated based on sap flow measured in the three considered crown layers in combination with their respective leaf areas yielded the same result as when only upper crown sap flow was used for calculating total crown sap flow (Figure 3.22). Results deviated when whole crown sap flow was calculated

based on only middle or lower crown layer measurements. This is because the highest leaf area is present in the upper canopy layer (see Table 1.2) and also the highest sap flow rates per unit leaf area were measured in this layer (§ 3.1.3). These findings indicate that calculating total crown sap flow, and consequently water storage, from sap flow measured only in the upper crown will not produce unreliable results.

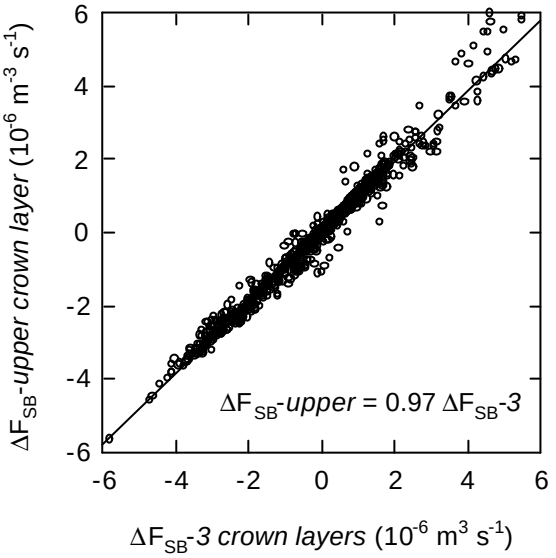

Figure 3.22 Comparison of hourly water storage use, during the period July 16-August 31, based on integration of sap flux density per unit leaf area for three different crown levels (*DF_{SB}-3 crown layers*), and only for the upper crown level (*DF_{SB}-upper crown layer*) to total crown sap flow. The solid line represents the regression line (r=0.99; n=1128).

Part of the water flowing through the terminal branches of the crown layer was considered to be supplied from internal storage when the total sap flow in the crown was larger than basal sap flow (Goldstein et al., 1998). In this case the water storage term (DF_{SB}) is positive (see Figure 3.23). When the opposite pattern was observed, that is when basal sap flow was larger than crown sap flow, the internal water stores were presumably being recharged ($DF_{SB} < 0$ in Figure 3.23). The hypothesis was imposed that the total storage over the period from July 16 till August 31 was zero. This hypothesis in fact states that no more water could be transpired during the considered time period than the amount that was flowing through the stem. Moreover it includes that the amount of water used for other processes than transpiration (e.g. photosynthesis) was negligible. The hypothesis also considers that the uptake and

loss of water should not necessarily be balanced over a short period of time (e.g. a single day). However, it should be balanced over a longer time period as water storage compartments can not be filled or emptied constantly because these storage capacities are limited. During the considered period, July 16 till August 31, LAI was assumed to be constant and maximal. From intensive LAI measurements (leaf litter collection and optical methods) during the 1996 growing season, it was concluded that this assumption of constant LAI is reasonable.

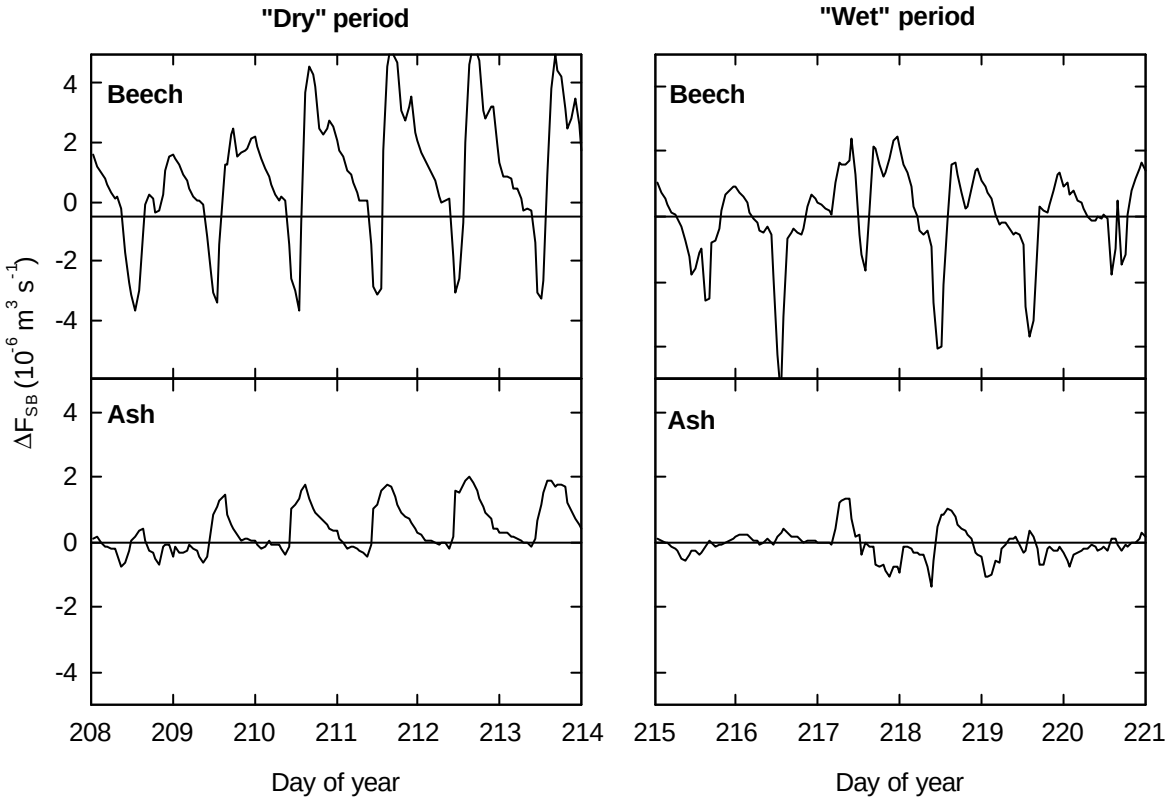

Figure 3.23 Diurnal variation of the water storage in stem and branches (DF_{SB}) of beech and ash during a “dry” (left) and a “wet” (right) period (see Figure 3.21). Positive values indicate time periods when transpired water was preferentially withdrawn from the water storage, and negative values indicate time periods when water from the soil was refilling storage. Ticks on the horizontal axis indicate the beginning of each day (at 0000 h). July 27 is day 208; August 8 is day 220.

For beech, recharge of the internal water storage occurred primarily around noon, while during the afternoon and night internal water was consumed (Figure 3.23). For ash, recharge mainly occurred during late afternoon and night, while during noon internal water was utilised (Figure 3.23). Goldstein et al. (1998) has also observed

different patterns of water storage for different species. Internal water consumption during night, for as well beech as ash, indicated nighttime transpiration (see also § 3.1.3). Nighttime water consumption is observed for many species (e.g. Becker, 1998; Green et al., 1989).

Tyree and Ewers (1991) stated that most water extraction from stems and branches will occur when the soil water potential becomes progressively more negative during a drought. This was confirmed by Holbrook and Sinclair (1992) and by Loustau et al. (1996). Although, during the period from July 27 till August 1, the atmospheric demand for water vapour was high, there was no soil drought stress as soil water potentials became not very negative (Figure 3.21). Nevertheless Figure 3.23 (left) illustrates that the consumption of water storage steadily increased, while refill remained more or less equal. This indicated that during periods of high evaporative demand there was a temporal imbalance between loss and uptake of water.

For ash, internal water use and consequently its recharge seemed to be much lower compared to beech, and was on some days almost negligible (e.g. days 215, 216, 219 and 220 in Figure 3.23). This points to a limited capacity of stem water storage. Tyree and Ewers (1991) state that large leaf and stem water capacitances could substantially reduce the maximum rate of water uptake from the roots being less than the transpiration rate at noon. This phenomenon will spread the period of water uptake by the roots over more hours in the diurnal uptake cycle.

Seasonal dynamics (July 16-August 31) of daily water storage use (WSU: integration of positive DF_{SB} values) is shown in Figure 3.24. During August daily WSU of beech was rather constant and low compared to daily water storage use in July. The total diurnal WSU differed between the two species, ranging from a mean seasonal value of 50 $\pm$ 6 kg for the diffuse porous beech and 15 $\pm$ 3 kg for the ring-porous ash, the latter species having a small conducting sapwood area (Clearwater et al., 1999). Taking the crown projection into account, total diurnal WSU was 1.0 $\pm$ 0.1 mm for beech and 0.4 $\pm$ 0.1 mm for ash. Maximum values reached 161 kg for beech and 69 kg for ash. The mean daily use of stored water fell within the range found by Goldstein et al. (1998) for five tropical forest canopy trees, namely from 4 to 54 kg. For beech the maximum storage of easily exchangeable water when no water stress is present was estimated to be 0.5 mm (Kowalik et al., 1997). The size of the pool of easily extractable water was estimated by Cienciala et al. (1994) to be 0.5 mm for spruce (*Picea abies*), and Carlson and Lynn (1991) calculated the magnitude of the capacitance effect in large trees to be about 0.5 mm as well. But Kowalik et al. (1988) estimated the amount of easily extractable water to be about 1 mm for Douglas fir (*Pseudotsuga menziesii*), which is identical to the value found for beech in this study. The capacitance effect of ash on the other hand is somewhat lower than the values found in literature.

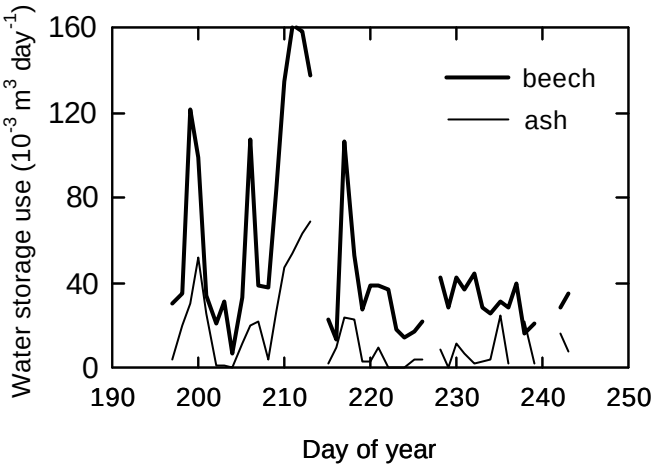

Figure 3.24 Seasonal course (July 16-August 31) of water storage use for beech and ash.

The daily average transpiration of beech calculated from sap flux density per unit leaf area measured at different crown layers and multiplied with the leaf area distribution for the respective layers (see Table 1.2), was 2.6 ± 0.2 mm for the period July 16 till August 31. For the same period maximum and minimum transpiration were respectively 5.1 and 0.9 mm. For ash daily transpiration was 1.1 ± 0.1 mm, and maximum and minimum transpiration were respectively 2.2 and 0.4 mm. Daily transpiration rates found in this study for beech are higher than the figures found by Kowalik et al. (1997) and Ladefoged (1963), namely 1.3 mm. However it should be mentioned that the transpiration rates in these studies were obtained for smaller trees (15-20m) and a lower LAI (3.85) compared to our forest.

Daily WSU amounted, for the period July 16 till August 31, 35 ± 2 % of daily transpiration for beech and 28 ± 4 % for ash. However, the day to day variation of the contribution of WSU to transpiration was high (Figure 3.25). In Scotland, where soils are wet and evaporative demand is low, stored water may account for 30-50% of the seasonal water use (Waring et al., 1979). Cienciala et al. (1994) indicated that the quantity of 0.5 mm represents roughly one quarter of the average daily water uptake, while Schulze et al. (1985) found the amount of available water storage to be 24% and 14% of the daily transpiration rate in *Larix* and *Picea* trees, respectively. Loustau et al. (1996) found that stored water in the stem (between a height of 6 to 18 m) amounted 12% of daily transpiration (10 kg), and that storage capacity in the crown was of the same magnitude.

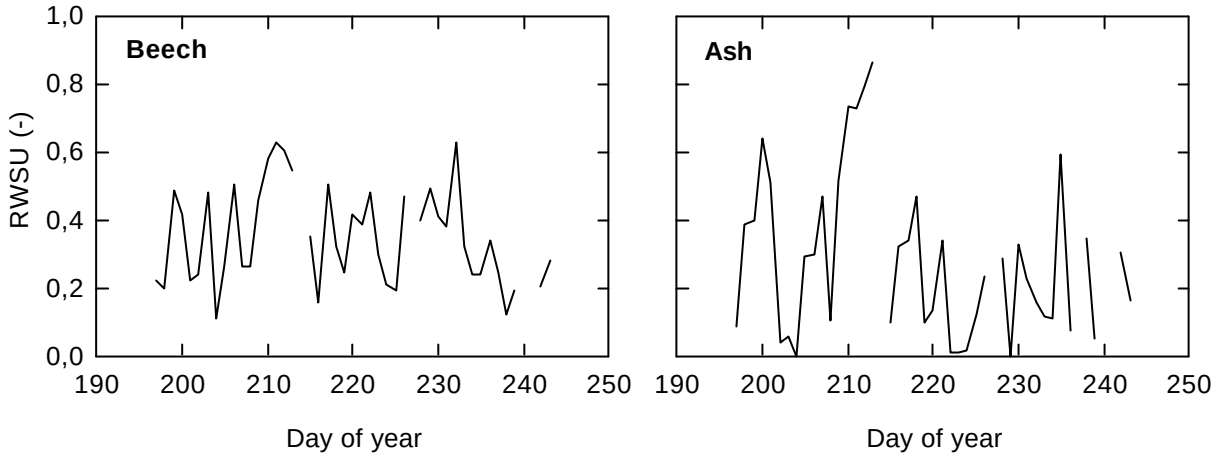

Figure 3.25 Contribution of daily water storage use to daily transpiration (relative storage water use: RWSU), during the period July 16-August 31, for beech (left) and ash (right).

Our results of water storage capacity do not agree with results found by Magnani and Borghetti (1995), for a 35-year-old European beech stand (LAI: 3.8, dominant height 19 m). These authors concluded there was a lack of internal storage for beech because no hysteresis was observed between sap flow and xylem water potential in apical twigs. Kowalik et al. (1997) suggested that the very high xylematic resistance of beech could explain the lack of such hysteresis. Despite total hydraulic conductance of the soil-root-leaf pathway was indeed rather low (§ 3.2.3), we observed, however, hysteresis between sap flow and leaf water potential (§ 3.2.3), and we observed considerable water storage in stem and branches of beech.

Just as Kowalik et al. (1997) we could not answer the question where (leaves or wood) the water was stored and which tissues (elastic or inelastic) were involved as internal storage for water. Monitoring stem diameter fluctuations could reveal whether internal water is stored in elastic tissues of the stem.

It should be remarked that the validity of the calculation of WSU depends on the reliability of the applied sap flow methods. Therefore, WSU is best calculated when sap flow in the crown and stem is measured using the same sap flow technique, because it is not impossible that the totally different techniques used in this study respond differently to environmental changes, and therefore yield different diurnal responses of sap flow.

3.4 Upscaling from single tree to stand level

3.4.1 Introduction

Forest transpiration is thought to have a significant impact on regional and global climates (Ogink-Hendriks, 1995). However, total forest evapotranspiration is difficult to determine. Therefore several authors tried to estimate forest evapotranspiration from measurements at the tree level (e.g. Granier et al., 2000a) or even from measurements at the leaf level (e.g. Roberts & Rosier, 1994; Herbst et al., 1999).

A common technique to estimate forest transpiration is to measure sap flow in trunks (e.g. Vertessy et al., 1997) or branches (e.g. Zhang et al., 1999). Measurements at these lower level of organisation (tree, branch, leaf) should at the end be extrapolated and scaled-up to the stand level in order to obtain an idea about the global forest behaviour. Several scaling factors exist to translate these lower level measurements to the stand level. Scaling factors can be: (i) leaf area (e.g. Vertessy et al., 1997), (ii) stem diameter (e.g. Vertessy et al., 1997) and (iii) sapwood area (e.g. Cermak & Nadezhdina, 1998). The sapwood cross-sectional area is a simple biometric parameter widely used for scaling the transpiration data between trees and forest stands (Cermak & Nadezhdina, 1998). However, it is not clear yet how the sapwood can be accurately estimated and this may cause large scaling errors. The classical way to distinguish the sapwood (which is the hydroactive xylem) from heartwood (which is the inactive xylem) is to determining the xylem water content (e.g. Cermak & Nadezhdina, 1998; Granier et al., 2000a). Sapwood and heartwood are then distinguished as woody tissues containing higher and lower amounts of water respectively, but unfortunately this difference is not always clear or is even reversed (Cermak & Nadezhdina, 1998). Some authors determined sapwood by injecting dye into the bole through holes above which a stem core is taken. The area of conducting tissue is then determined from the thickness of the wood coloured by the dye as it moves upwards with the transpiration stream (e.g. Goldstein et al., 1998). Another way for determining sapwood is thought to be more reliable. This method estimates the depth of conducting wood and its corresponding area from the radial profiles of sap flow. The boundary between sapwood and heartwood is then estimated from the point where the sap flow approaches zero (Cermak & Nadezhdina, 1998).

Besides from scaling over space, data can also be scaled over time. In this case, e.g. measurements conducted on small diameter trees will be used to predict behaviour of mature, large diameter trees of a different age. Or, measurements conducted at a

certain moment during the growing season are used to predict water consumption during a whole growing season or even during several growing seasons. Related problems are e.g. that the radial pattern of sap flow changes with tree size and age or under drought (Cermak & Nadezhdina, 1998). According to Wilson et al. (2001) scaling can be particularly difficult in forests with age and species diversity.

This part of the study focuses on the determination of transpiration from a forest stand by scaling up sap flow measurements of upperstory species (beech, oak and ash) measured during the year 1999. Also the contribution of understory species (sycamore and hazel) to the total forest transpiration will be applied. To obtain forest transpiration two upscaling procedures will be followed. The first upscaling procedure will be based on sapwood area, and the second one will be based on leaf area. Upscaled sap flow values will be integrated over monthly time periods, and for the whole growing season. The upscaled sap flow to total forest transpiration will yield a reference data set for comparison with the micro-meteorological Bowen ratio method.

3.4.2 Material and methods

3.4.2.1 Determination of the sapwood cross-sectional area of single trees

Sap flux densities measured with TDP sensors have to be multiplied by the sapwood cross-sectional area for scaling up purposes (Granier, 1985). As it is impossible to determine sapwood cross-sectional area on the trees where the sap flow sensors were installed, the sapwood cross-sectional area had to be determined on trees of similar diameter outside the experimental plot. As was done by Goldstein et al. (1998), the sapwood area at breast height of the trees was determined by injecting dye into the bole through holes made by a 5 mm increment borer, and the holes were filled up once more after one hour. After one to two hours, a core was taken 4 cm above each dye injection point and the area of conducting tissue was determined from the thickness of the wood coloured by the dye. Methyl blue was chosen for dye as it is water soluble, and because Bortier (1999) mentioned that it is quickly transported (case of poplars). Dye was injected for the tree species beech and ash.

For the case of oak it was sufficient to take stem cores without injecting dye before because heartwood and sapwood could be distinguished visually. Determination of sapwood area in oak allowed defining a linear relationship between sapwood cross-sectional area and stem cross-sectional area at breast height (Figure 3.26). By analogy with oak, and also because in literature linear relationships were reported

(e.g. Allen and Grime, 1995), such a linear relationship between sapwood cross-sectional area and stem cross-sectional area at breast height was also supposed for ash and beech. For oak sapwood area amounted 20 % (i.e. the slope of the relationship)(Figure 3.26) of the stem cross-sectional area at breast height. Only a small sapwood area was detected from the dye method for ash. For beech a strongly coloured outer ring was observed, and a less coloured area more to the centre of the stem. As such, the total sapwood area for beech was, in relative terms, several times the one of ash. More specifically sapwood area amounted 27 and 5 % of stem cross-sectional area at breast height for beech and ash respectively (Table 3.1). These findings were consistent with literature. Anfodillo et al. (1993) showed with a thermal imaging technique that sap flow of ash was strictly limited to the last annual ring, and that beech indeed had an irregular water transport distributed over the sapwood area. Also Hacke & Sauter (1996) showed, by means of the dye method, that the functional xylem of ash was restricted to the most recent annual ring.

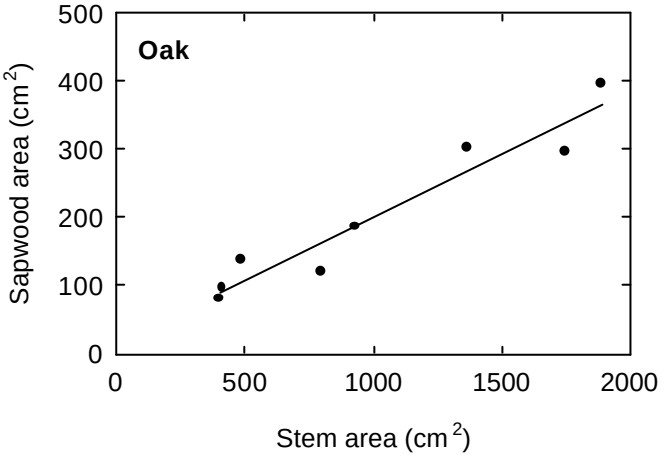

Figure 3.26 The linear relationship between sapwood area (A_{sap}) and stem area (A_s) for cross-sections of oak stems at breast height (A_{sap} = 0.187A_s + 15.3; R^2=0.93).

The sampled oak trees were selected according to the diameter distribution of this species in the oak-beech forest (Vande Walle et al., 1998). Trees from the most frequent diameter class (30-40 cm)(Table 2.5) and from the class below (20-30 cm) and above (40-50 cm) were sampled. It has to be remarked that the linear relationship (Figure 3.26) established on young oak trees (see § 2.1.2) is only valid for the considered diameter classes. As for oak sapwood depth is rather independent of diameter (pers. Communication F. Devillez, UCL, Belgium), it can be expected

that, extrapollating to larger diameters, the relationship between stem area and sapwood area becomes hyperbolic. Ash and beech trees were not sampled in the experimental zone of the forest Aelmoeseneie to prevent possible infections of trees, nor in the rest of the forest Aelmoeseneie, because the wood of the trees had a commercial purpose and thus dye could not be used. Therefore, for as well beech as ash, two trees of comparable diameter as the monitored trees (see Table 3.1) outside the forest Aelmsoeseneie were injected with dye to estimate their sapwood area.

3.4.2.2 Sapwood area as a scaling factor

Multiplying sap flux density at stem level with the sapwood area of the specific tree yields transpiration of the individual tree. Scaling sap flux densities measured for the individual trees to stand level was here done by multiplying sap flux density with total sapwood area of the forest. By doing so, we assumed a constant linear relationship between stem cross-sectional area at breast height and sapwood cross-sectional area at the same height, for all diameters. Total sapwood area of the forest, for a respective species, was calculated from the basal area of the forest (Table 3.6) multiplied with the percentage of sapwood of that species (Table 3.1 and 3.7).
The above mentioned procedure can be translated into equations as follows:

$$E_{F,S} = \sum_i J_s(i).SAI(i) \qquad (3.25)$$

where $E_{F,S}$ is the total forest transpiration (m^3 m^{-2} soil $time^{-1}$ or 10^3 mm $time^{-1}$), $J_s(i)$ is the basal sap flux density for species *i* (m^3 m^{-2} sapwood $time^{-1}$)(see for typical values e.g. Table 3.3 and Figure 3.7) and *SAI(i)* sapwood area index of the considered species *i* (m^2 sapwood m^{-2} soil). The sapwood area index is calculated as follows:

$$SAI(i) = BA(i).RSA(i) \qquad (3.26)$$

where *BA(i)* is the basal area of species *i* (m^2 stem m^{-2} soil) and *RSA(i)* is the relative sapwood area of species *i* (m^2 sapwood m^{-2} stem). Values for *BA(i)* and *SAI(i)* used for the calculations are given in Table 3.6 and 3.7 respectively.
Transpiration of a uniform stand of species *i* is calculated by considering that the basal area of species *i* [*BA(i)*] equals the total basal area of the forest Aelmoeseneie (Table 3.6) from which *SAI(i)* is then calculated (Table 3.7).

3.4.2.3 Leaf area index as a scaling factor

Sap flux density of branches has been defined as a volume of water per unit of time and per unit of downstream leaf area (see § 3.1.2). For a species of type *i*, and with leaves distributed over *j* crown layers, total forest transpiration ($E_{F,L}$)(m^3 m^{-2} soil $time^{-1}$ or 10^3 mm $time^{-1}$) can also be expressed as:

$$E_{F,L} = \sum_{i,j} F_{LA}(i,j).LAI(i,j) \qquad (3.27)$$

where $F_{LA}(i,j)$ is the sap flux density measured at branch level (m^3 m^{-2} leaf $time^{-1}$) for species *i* at crown level *j* (see for typical values e.g. Table 3.3 and Figure 3.8 and 3.9) and $LAI(i,j)$ is the leaf area index (m^2 leaf m^{-2} soil) of species *i* at crown level *j* (see Table 1.2 and Figure 1.11).
Values for $LAI(i,j)$ used for the calculations are given in Table 3.8.

Table 3.6 Values for basal area (in m^2 ha^{-1} and in percentage of total basal area) of the main upperstory species in the oak-beech and ash site and in the forest Aelmoeseneie. Values are recalculated from Table 2.3, with the basal area of other upperstory species equally distributed over the three main species, and added to the basal area of these main species. Values given for the forest Aelmoeseneie are obtained by considering the relative contribution of the oak-beech (1.06 ha) and ash (0.77 ha) site in the experimental zone (1.83 ha).

	Oak-beech site		Ash site		Forest Aelmoeseneie	
Species	m^2 ha^{-1}	%	m^2 ha^{-1}	%	m^2 ha^{-1}	%
Oak	14.25	57	4.90	18	10.31	40
Beech	8.38	33	2.05	8	5.72	22
Ash	2.39	10	19.97	74	9.79	38
Total	25.02	100	26.92	100	25.82	100

Table 3.7 Values of the percentage of sapwood of the cross-sectional area at breast height (% sapwood)(see also Table 3.1) and of the sapwood area index (10^{-3} m^2 m^{-2}) for the three main upperstory species in the forest Aelmoeseneie. Values of sapwood area index are obtained from multiplying values of basal area (Table 3.6) with the percentage of sapwood. For the uniform stands, the basal area of the forest Aelmoeseneie is multiplied with the percentage of sapwood of the considered species.

		Sapwood area index			
Species	% sapwood	Oak-beech	Ash	Aelmoeseneie	Uniform
Oak	20	0.285	0.098	0.206	0.516
Beech	27	0.226	0.055	0.154	0.697
Ash	5	0.012	0.100	0.049	0.129

Table 3.8 Leaf area index of the considered upperstory and understory species in the oak-beech and ash site and in the forest Aelmoeseneie. Values given for the forest Aelmoeseneie are obtained by considering the relative contribution of the oak-beech (1.06 ha) and ash (0.77 ha) site in the experimental zone (1.83 ha). A dash denotes that the LAI of the species in the site is neglible.

Species	Oak-beech site	Ash site	Forest Aelmoeseneie
Oak	2.21	0.60	1.53
Beech	3.03	0.24	1.86
Ash	-	2.29	0.96
Sycamore	0.14	0.72	0.38
Hazel	0.14	0.68	0.37
Total	5.52	4.53	5.10

3.4.2.4 Time integration

For the time integration, daily sap flow data were used as presented in Figure 3.7 for basal sap flux measurements and in Figures 3.8 and 3.9 for sap flow measured in the branches.

As sap flow data, especially when using the stem heat balance method, are sensitive to errors, it is very difficult to obtain a continuous data set for a long period of time. However, to estimate seasonal transpiration a continuous data set is needed. To obtain such a continuous data set a mean daily transpiration rate was calculated for each separate month from the data presented in Figures 3.7 till 3.9. Thereafter this mean value was multiplied with the number of days in that respective month. Yearly transpiration is then obtained by summing all monthly values.

The reported errors on monthly transpiration values are calculated from the standard error on the monthly mean calculated for the days for which sap flow data were available, and then corrected for the number of days in the respective month.
During the months of May and June sap flow could not be measured in the middle crown layer of beech. Therefore, in order to be able to estimate seasonal $E_{F,L}$ for beech, transpiration for May and June was estimated from the relation between daily radiation sums and daily $E_{F,L}$ observed during the rest of the season (Figure 3.27). No difference was found in the relationship between radiation sums and transpiration (Figure 3.27) for dry and wet periods.

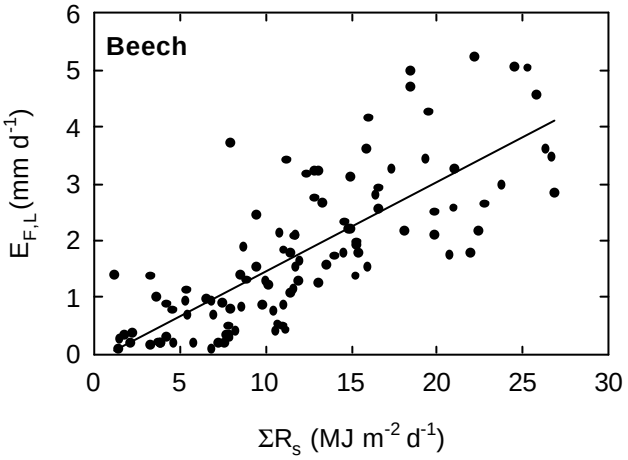

Figure 3.27 Relationship between the daily transpiration ($E_{F,L}$) and the daily radiation sum (SRs) for a uniform beech stand with a leaf area index of 5.48 (see Table 1.2). The linear relationship between both parameters is $E_{F,L}$ = 0.16 SR_s – 0.15 (R^2=0.60; n = 105).

3.4.3 Results and discussion

3.4.3.1 Comparison of both upscaling methods

Transpiration values are provided for as well the forest Aelmoeseneie, the oak-beech and ash site, the understory species of both sites, as for uniform beech, oak and ash stands. A uniform stand is considered to be composed out of only one upperstory

species, and the necessary upscaling parameters are given in Tables 1.2 and 3.6 till 3.8. The aim of these calculations for uniform forest stands, although not representative for the forest Aelmoeseneie, is that the obtained values can be more easily compared with literature data (which often report data for uniform stands), and that the water use of different forests can easily be compared. This latter can be very important for decision-makers.

The monthly transpiration totals, derived from sap flux density measurements at stem level ($E_{F,S}$) for beech, oak and ash, and derived from measurements of sap flux density at branch level ($E_{F,L}$) for beech and ash are shown in Figure 3.28. Highest water consumption ($E_{F,S}$) was observed during June-July for beech, and during July-August for oak and ash. Monthly water use ($E_{F,L}$) was again highest during June-July for beech but now also for ash.
Both methods, $E_{F,S}$ and $E_{F,L}$, did not yield the same results (Figures 3.28 and 3.29). Where for beech results were still more or less comparable they were not for ash. Differences between both methods are attributed to as well the upscaling parameters (sapwood versus leaf area index) as to the technique for measuring water use (thermal dissipation probe versus stem heat balance method).

Sapwood has to be determined for individual trees, and in a non-uniform uneven-aged stand one sampling point per stem is not satisfactory (Cermak & Nadezhdina, 1998) because sapwood depth can change with azimuth. Moreover, in such a non-uniform uneven-aged stand a large number of trees should be sampled, and if the stand is mixed this number still increases. Sapwood also varies with height, with a more uniform sap flux density closer to the crown (Loustau et al., 1998). As mentioned before, also the determination of sapwood is not straightforward, e.g. Wullschleger & King (2000) reported that the significant decline in sapwood water content between different probe positions was not sufficient to account for the observed radial variation in sap velocity. Cermak and Nadezhdina (1998) mentioned that sapwood should best be determined by radial profiles of sap flux density. Another weak point in using sapwood as a scaling factor is the seasonal dependency of sapwood area, e.g. Cermak & Nadezhdina (1998, 2000) assumed a dramatic change in the radial sap flow pattern of spruce under drought. Little information is available about seasonal variation in sapwood, and future research should focus on this topic. Wullschleger & King (2000) also mentioned that future studies should devise sampling strategies for assessing radial variation in sap flow and such strategies should be used to identify the magnitude of this variation in a range of non-, diffuse- and ring-porous trees.

In contrast to sapwood, leaf area index is in many research projects routinely measured using many different methods (McIntyre et al., 1991), and can e.g. be determined using optical methods (e.g. Granier et al., 2000a) which yield area

averaged values. This optical approach is non-destructive and a seasonal dynamics can be obtained (e.g. Herbst et al., 1999; Samson & Lemeur, 2001). Steinberg et al. (1990a) mentioned that normalisation of sap flow by leaf area is preferred compared to other normalisation methods, e.g. projected crown area and sapwood area. Vertessy et al. (1997) scaled individual tree sap flow estimates to the stand level based on stem diameter and LAI measurements. The two procedures yielded similar results; however the authors concluded that the first procedure was more robust but it required more sampling effort than the second procedure. A disadvantage of working with $E_{F,L}$ is that measurements at the branch level are required, and in most forest where no (expensive) experimental tower is available, the canopy is not easily accessible.

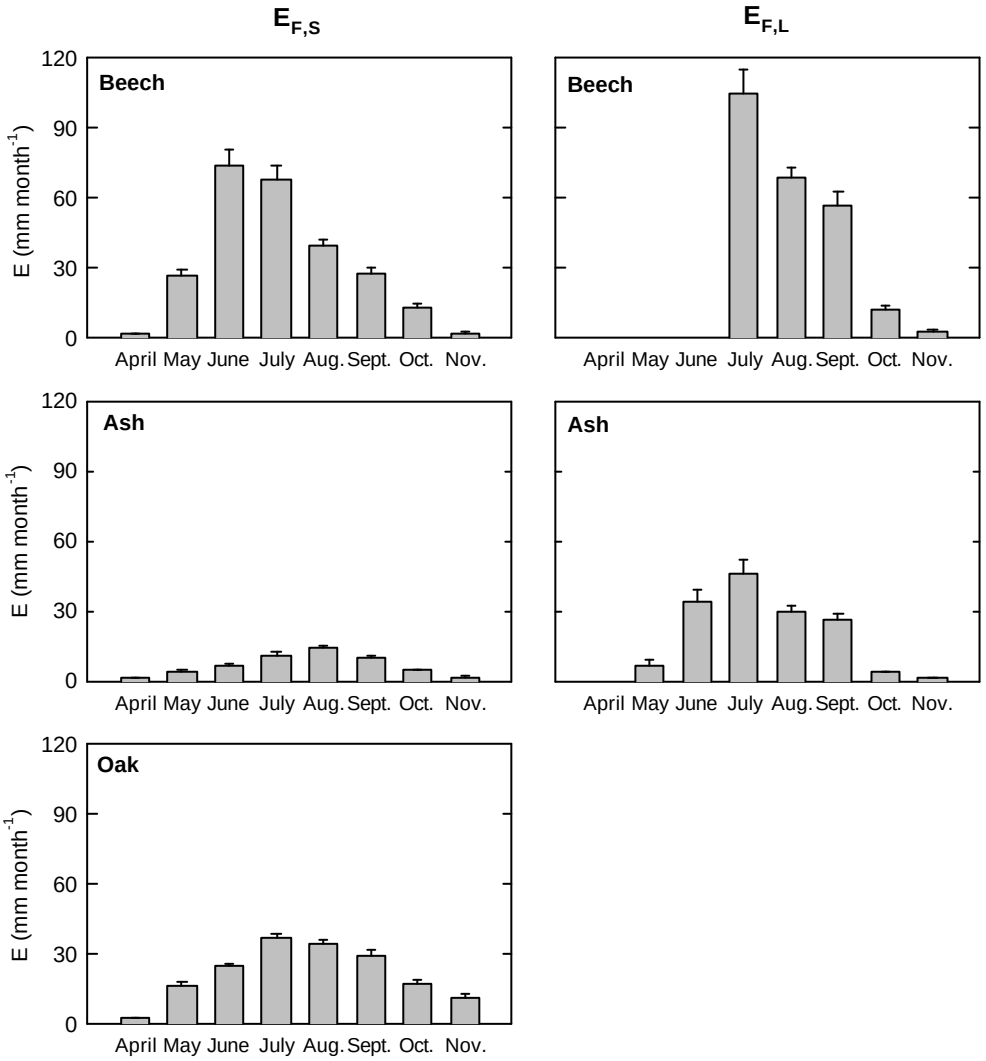

Figure 3.28 Monthly water loss by transpiration estimated from the upscaling of sap flow at stem level $E_{F,S}$ (left) and at crown level $E_{F,L}$ (right). Results are represented for uniform beech, oak, and ash stands with leaf area index of respectively 5.48, 4.07 and 2.32 (see Table 1.2).

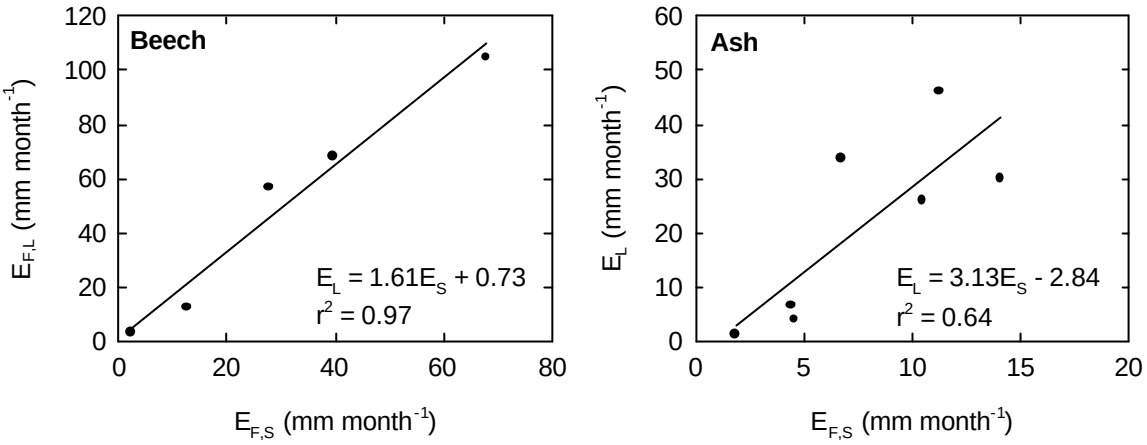

Figure 3.29 Comparison of the monthly water loss by transpiration estimated by the two scaling up procedures, i.e. basal sap flow scaled up using sapwood as the scaling factor ($E_{F,S}$) and sap flow at branch level using leaf area index as the scaling factor ($E_{F,L}$) for beech (left) and ash (right). Note the differences in scale.

Transpiration values deducted from stem sap flux density measurements ($E_{F,S}$) were 62 and 37 % of $E_{F,L}$ values for beech and ash respectively. These large differences in $E_{F,S}$ and $E_{F,L}$ (Figure 3.28 and 3.29) for ash were ascribed, besides the different upscaling parameters used (i.e. sapwood and leaf area index), to measurement errors mainly for basal sap flux density. Errors can be associated with radial gradients in sap flow and the perceived inability of sap flow probes to adequately integrate observed rates of sap flow along their length (Phillips et al., 1996; Clearwater et al., 1999). The largest errors are expected to occur in ring-porous trees, like ash (Cochard et al.,1997), and oak (Cochard & Tyree, 1990), because these species have a pronounced radial sap flow profile (Cermak et al. 1992; Granier et al. 1994) in contrast to diffuse-porous species like beech (Phillips et al., 1996; Cochard et al., 2001). Therefore, in ring-porous tree species underestimates of sap flow up to 45 % are theoretically possible (Clearwater et al., 1999). However, Granier et al. (2000a) and Köstner et al. (1998) found a radial profile of sap flux density in beeches, which means that also for this species errors can be expected. Wilson et al. (2001), who used the same sensors as in this study, mentioned that technical differences between the original probe design (Granier, 1987a) and the commercially-available thermal dissipation probes used in their, and thus also our study, should also be evaluated as a possible source of uncertainty. The TDP-probes are 30 mm in length and have the heating element contained within a cylindrical stainless-steel housing. This contrast with the original design of Granier (1987a)

where the probes were only 20 mm in length and had the heating wrapped around probe's external surface. The possibility that such differences in construction could lead to an underestimation of stand transpiration is unresolved (Wilson et al., 2001), but an underestimation is also found in our study for ash (Figure 3.28 and 3.29 and see also later). Moreover, not the whole TDP-sensor was in contact with conducting sapwood for oak and ash having a sapwood depth of 21 and 6 mm respectively, and this will, besides the radial sap flow profile, also introduce errors in the measurements (Clearwater et al., 1999).

Thus, for scaling up to the stand level an accurate knowledge of sapwood area is required, as well in a radial, azimuthal and longitudinal direction. Determination of the active sapwood can best be done by measuring the radial sap flow profile, and this should be done throughout the growing season because of the possible seasonal dynamics of sapwood area (Cermak & Nadezhdina, 1998, 2000). When applying the TDP technique care should be given to an appropriate needle length so that the needles are in full contact with the conducting sapwood, to avoid over- or underestimation of sap flow. To optimise the basal sap flow measurements, i.e. to obtain high quality data with a minimal equipment per tree, it is recommended to analyse the radial, azimuthal and longitudinal variation in basal sap flux density. Especially, the radial position and, as mentioned above, the length of the used TDP is of major importance to obtain reliable sap flux densities.

3.4.3.2 Monthly water loss

Monthly transpiration ($E_{F,L}$) for the understory in the oak-beech and ash site was rather constant during the growing season (Figure 3.30). Transpiration of understory species started earlier in the growing season, but also ceased one month earlier compared to the upperstory species (Figure 3.30). Contribution of understory to monthly forest transpiration was very low in the oak-beech site during the growing season (June till September), namely 1.0 ± 0.1 %. In the ash site the contribution was 8.6 ± 0.5 %. During March (no measurements available) and the beginning of April, when upperstory leaves were not yet unfolded, transpiration was solely due to the understory, during May understory contribution was 1.5 and 22.3 % for the oak-beech and ash site respectively. Roberts and Rosier (1994) estimated that the contribution of the understory, composed out of bramble and hazel, to transpiration in an ash forest was 30 % of total forest transpiration, and this contribution decreased to 15 – 20 % at the end of the growing season. These higher values were due to the higher LAI (3 ± 0.5) of the understory compared to the understory LAI in our ash site. From Figure 3.30 it can also be observed that the transpiration of the upperstory

species in the oak-beech site during all months clearly exceeded transpiration of the upperstory species in the ash site.

Monthly transpiration dynamics of the forest Aelmoeseneie is illustrated in Figure 3.31, and peaked for both methods ($E_{F,S}$ and $E_{F,L}$) in July. Whereas during September transpiration was still high, it severely dropped in October. The contribution of the understory to total monthly transpiration of the forest Aelmoeseneie was 4.8 % during the month of May and 3.3 ± 0.3 % during the period June till September.

The high LAI of the upperstory (Table 1.2) can explain the low understory transpiration, in the oak-beech and ash site and in the forest Aelmoeseneie. This high LAI limited solar radiation, as a driving force for photosynthesis and transpiration, to reach the understory. The understory contribution in the ash site was somewhat higher due to the lower upperstory and higher understory LAI in this site compared to the oak-beech site (Table 1.2 and 3.8). While a high upperstory transpiration and a low understory transpiration was observed in the oak-beech site (Figure 3.30), a lower upperstory and higher understory transpiration was observed in the ash site (Figure 3.30). These results agree with the idea that total forest transpiration remains equal, even when forest structure differs (Roberts et al., 1980; Whitehead et al., 1994; Lüttschwager et al., 1999). Thus understories can be regarded as effective buffers to the canopy differences (Roberts, 1983).

3.4.3.3 Annual water loss

Total seasonal transpiration for a uniform beech, oak and ash stand, for the oak-beech and ash site, and for the forest Aelmoeseneie is given in Table 3.9. Seasonal transpiration ($E_{F,S}$ and $E_{F,L}$) was higher for a uniform beech stand compared to a uniform oak and ash stand. This can be mainly explained by the high sapwood area and LAI of beech (see respectively Table 3.7 and Table 1.2) as sap flux density (J_S and F_{LA}) for the different species is rather comparable (see e.g. Figure 3.7 and 3.9). Transpiration in the oak-beech site is higher than that in the ash site, which is a direct consequence of the species distribution in both sites (Table 2.2). Total seasonal understory transpiration for the oak-beech and ash forest site is respectively 5 and 25 mm year^{-1}. As also shown before (Figure 3.28 and 3.29), a comparison of seasonal $E_{F,S}$ and $E_{F,L}$ for beech and ash again revealed that the former method resulted in the lowest estimates (Table 3.9). Comparing our results (Table 3.9) to the mean seasonal transpiration for NW European forests, namely 333 ± 36 mm yr^{-1} (Roberts, 1983), we may conclude that $E_{F,L}$ is more reliable than $E_{F,S}$. However, it is important to mention that the conservative value of forest transpiration as reported by

Roberts (1983) is not always valid. Herbst et al. (1999) showed for a black alder forest situated nearby a lake that transpiration exceeded the value of Roberts (1983) by on average 200 mm $year^{-1}$. The authors supposed that advection to the alder belt or downward fluxes of sensible heat caused the high transpiration rates.

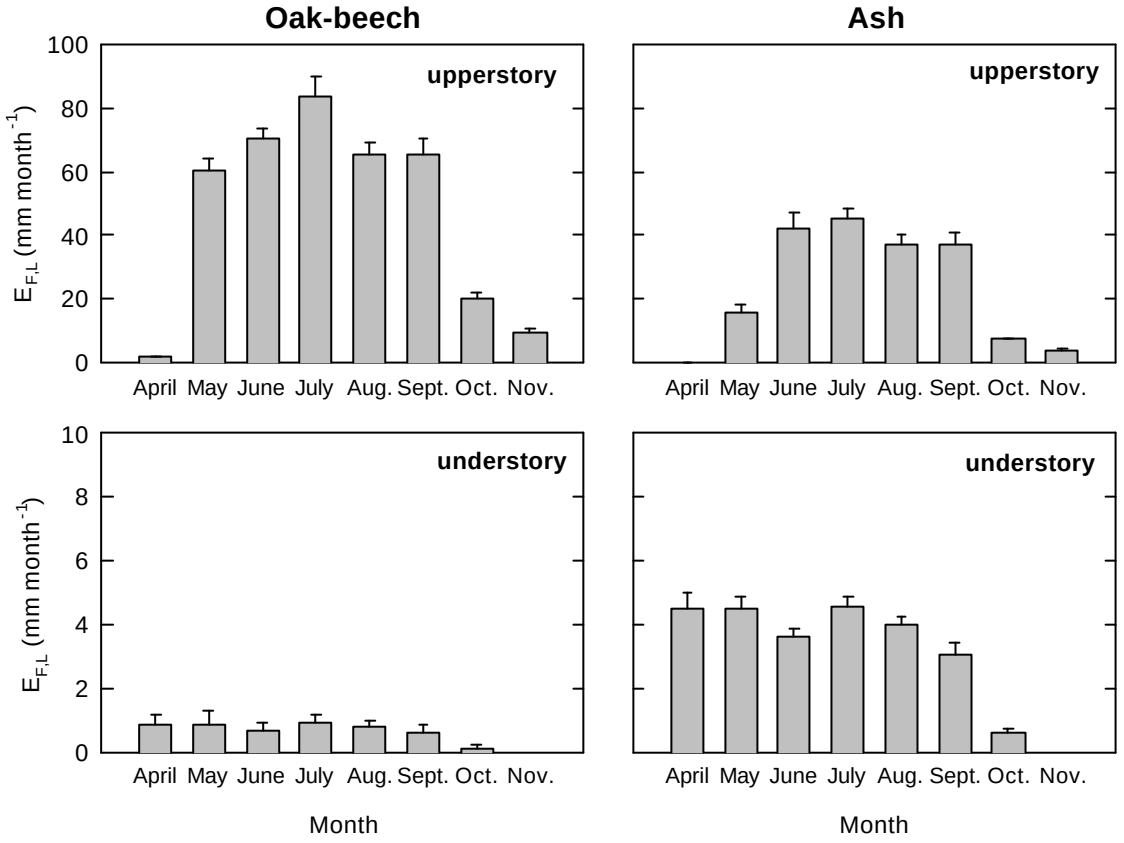

Figure 3.30 Comparison of the monthly water loss by transpiration in the oak-beech and ash site of the forest Aelmoeseneie. Results are obtained from the upscaling procedure based on leaf area and are given for both the upperstory and the understory. Note the differences in vertical scale between upperstory and understory.

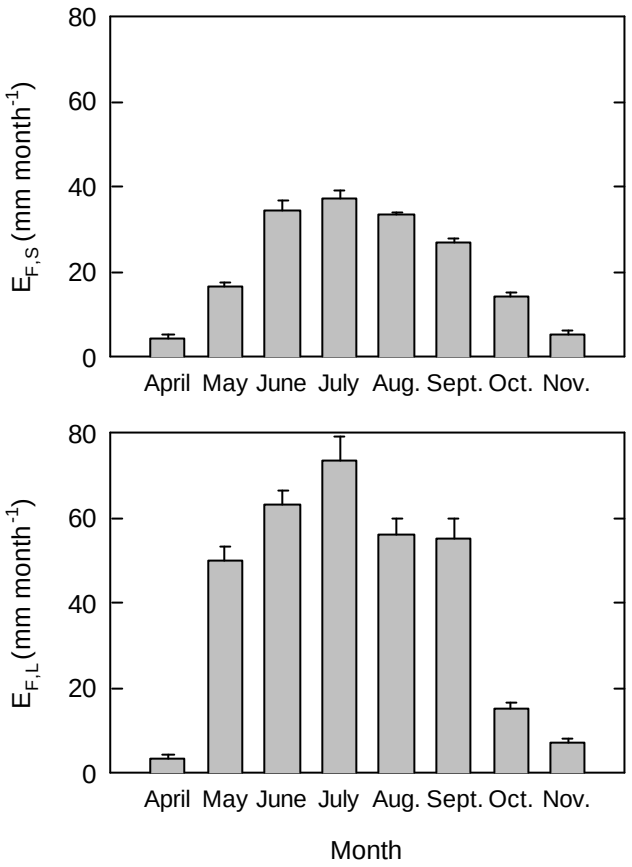

Figure 3.31 Monthly total transpiration (upperstory and understory) of the forest Aelmoeseneie estimated from (above) basal sap flux density measurements using sapwood as the scaling factor ($E_{F,S}$), and (below) sap flux density measured at the branch level using leaf area index as the scaling factor ($E_{F,L}$).

Seasonal transpiration calculated from basal sap flux density measurements and using sapwood as the scaling factor, $E_{F,S}$, was for all species, even when understory transpiration was included, lower than the value of 333 ± 36 mm yr^{-1} as reported by Roberts (1983). Especially values for oak and ash, both ring-porous species characterised by a steep radial profile, are rather low. From the low seasonal value reported in Table 3.9 it can be concluded that the used TDP-sensors were totally inappropriate for use on ash, due to the very small sapwood area of this species. Nizinski & Saugier (1989) calculated for an oak forest (Fontainebleau), using the water balance method, a yearly transpiration of 288 mm. Comparison with this latter value indicate that, although the very smooth seasonal pattern observed (Figure 3.7 and 3.28), that the $E_{F,S}$ value of 173 mm (Table 3.9) is an underestimation. For beech, a diffuse porous species with a larger sapwood area and less steep radial sap

flow gradient (e.g. Granier et al., 2000a) compared to ring-porous tree species, $E_{F,S}$ was closer to the value of Roberts (1983) and between the $E_{F,S}$ values of 230 and 269 mm as reported by Wilson et al. (2001) for two consecutive years for an uneven-aged mixed deciduous forest in the South-eastern United States. So the fact that a radial sap flow profile is present, and that the sensors are not totally in contact with conducting sapwood (ring-porous species) is responsible for the supposed underestimation of transpiration when using the here installed TDP-sensors.

Table 3.9 Seasonal upperstory transpiration (mm year^{-1}) for different uniform forests, the oak-beech and ash forest site and the forest Aelmoeseneie, calculated from basal sap flux density measurements, using sapwood as the scaling factor ($E_{F,S}$) and from sap flux density measurements at the branch level, using leaf area index as the scaling factor ($E_{F,L}$). As $E_{F,L}$ for beech during the months May and June was not available, $E_{F,L}$ for these months was estimated from the relationship between radiation sum (SR_s) and $E_{F,L}$. A dash denotes that measurements were not available.

	Seasonal transpiration	
Forest	$E_{F,S}$	$E_{F,L}$
Beech	253	406
Oak	173	-
Ash	55	147
Oak-beech site	208	376
Ash site	99	188
Forest Aelmoeseneie	160	311

For beech seasonal $E_{F,L}$ was between the values estimated from a two-layer evaporation-model (type Shuttleworth-Wallace (1985)) by Herbst et al. (1999) for a 105-year old beech forest, namely 326 and 421 mm. These authors cite a review of Peck & Mayer (1996) who collected data of nine studies of evaporation components of European beech forests, and found a mean transpiration value of 363 mm yr^{-1}. Based on the Penman-Monteith approach Roberts & Rosier (1994) estimated yearly transpiration of a beech forest to be 393 mm. For ash these authors mentioned a value of 407 mm, while Ladefoged (1963) mentioned a lower transpiration value of ash compared to oak and beech what they explained by the low LAI of this species. Because of the large differences between $E_{F,S}$ and $E_{F,L}$ (Table 3.9) and the uncertainties in the measurement of basal sap flux densities, the main reason of potential errors in the estimation of stand transpiration is rather attributed to errors in the measurement of basal sap flux densities, than to errors in the upscaling procedure (see also Hatton et al., 1995).

As mentioned before, the low contribution of understory transpiration to total seasonal transpiration in the oak-beech site is attributed to the high upperstory LAI.

Beeches are known to be very competitive (Herbst et al., 1999), limiting growth and thus also transpiration of understory species. In contrast, Wullschleger et al. (1998a) mentioned a contribution of *Acer rubur* trees in the understory of an oak forest to be 20 % of total stand transpiration. Due to the higher LAI of the understory in the ash forest (five times the understory LAI in the oak-beech forest)(Table 3.8) the contribution of this layer to overall stand transpiration is higher. Roberts (1983) mentioned that lower transpiration of tree species is a consequence of having less dense foliage permitting greater levels of radiation to reach the forest floor below it, and this could lead to higher understory transpiration. Understory transpiration was scaled up from measurements conducted in the oak-beech site. Because of the lower upperstory LAI in the ash site, the available energy for understory transpiration will be higher in this site. This factor was not taken into account when scaling up sap flow, making that the understory transpiration in the ash forest was probably higher than 25 mm year^{-1}.

3.5 Energy balance storage terms and big-leaf evapotranspiration in a mixed deciduous forest

(Published in Annals of Forest Science, 58, 529–541; 2001)

3.5.1 Introduction

The evapotranspiration of vegetated surfaces can be estimated using the well-known Penman-Monteith equation (Monteith, 1965). By using this formula it can be seen that the evapotranspiration can be divided into two terms: (i) an equilibrium evapotranspiration term, and (ii) an imposed evapotranspiration rate (McNaughton & Jarvis, 1983). While the latter term depends on the water vapour deficit of the air and the aerodynamic conditions, the former term is driven by the amount of available energy (A) for latent (lE) and sensible heat (H) processes.

The available energy is defined as the net radiation (R_n), from which the net change in energy storage within the canopy (S) is subtracted. Canopy storage S can be further subdivide into five terms (McCaughey, 1985): soil heat storage (S_g), sensible heat storage in the canopy air (S_a), latent heat storage in the canopy air (S_w), biomass heat storage (S_v) and photosynthetic energy storage (S_p). Soil heat storage S_g can be further subdivided in the measured soil heat flux at depth z (G), and the soil heat storage to that depth ($S_g(z)$). In most studies S is simplified to G, while the other terms are considered to be negligible (Shuttleworth, 1994). For ecosystems with a limited height and LAI this latter simplification is believed to be valid. However for densely vegetated ecosystems, especially forests, several authors have already shown that storage terms may not be neglected in the energy balances (McCaughey, 1985; McCaughey & Saxton, 1988; Stewart & Thom, 1973). Sometimes S is also considered to be a fixed fraction of net radiation, or one or more components of S are thought to be negligible. One of the most commonly eliminated heat storage terms, due to its difficulty of determination, is the photosynthetic energy storage S_p (McCaughey & Saxton, 1988).

Taking into consideration the different simplifications which are used when determining S the question arises what the influence of these simplifications is on the determination of big leaf forest evaporation. Aston (1985a,b) pointed out that an accurate determination of the overall heat storage is of the utmost importance when determining forest evaporation using the Bowen ratio technique.

Energy balance studies have been conducted for several forest ecosystems. Examples of such work are available for temperate coniferous forest

(e.g. McNaughton & Black, 1973; Stewart & Thom, 1973; Tajchman, 1971; Tan & Black, 1976), for deciduous broadleaf and mixed forest (e.g. McCaughey, 1985; Verma et al., 1986), for tropical forest (e.g. de Abreu Sa et al., 1988; Pinkster et al., 1980; Shuttleworth et al., 1984) and subarctic forest (Lafleur, 1992).

This paper will first analyse the behaviour and magnitude of the different canopy storage terms (photosynthetic heat storage included) of a small mixed deciduous forest on an hourly, daily and seasonal basis, and examine their importance in respect to the net radiation. As suggested by Saxton and McCaughey (Saxton & McCaughey, 1988) the biomass heat storage will be determined using surface temperatures measured with an infrared radiometer, instead of the commonly used thermocouples (Aston, 1985a; Saxton & McCaughey, 1988). Finally the influence of storage terms on the determination of forest evapotranspiration using the big-leaf approach will be determined.

3.5.2 Materials and Methods

3.5.2.1 Heat storage calculation

The unit for all heat storage terms (Equations 3.28-3.32) is W m^{-2}. A positive value for these terms indicates the transfer of energy to storage.

Latent and sensible heat storage

According to McCaughey & Saxton (1988) the sensible S_a and latent S_w heat storage terms can be defined as

$$S_a = \int_0^{z_r} \rho C_p \left(\frac{dT_a}{dt} \right) dz \qquad (3.28)$$

$$S_w = \int_0^{z_r} \frac{\rho C_p}{g} \left(\frac{de}{dt} \right) dz \qquad (3.29)$$

where ρ is the air density (kg m^{-3}), C_p is the specific heat of air (1012 J kg^{-1} °C^{-1}), g is the psychrometric constant (Pa °C^{-1}), e is the vapour pressure (Pa), T_a is the air temperature (°C), z_r is the height of net radiation measurement (m) and t is time (s).

Equations 3.28 and 3.6.2 are solved using the approximation suggested by Thom (1975) and McCaughey & Saxton (1988) which assumes that ρ and C_p are constant through the canopy layer. As representative air temperature the mean temperature measured at 4 heights in the canopy (1, 7.5, 14.6 and 21.6 m) is used, while e is a mean value determined from humidity measurements inside (at 1m) and above (at 28m) the canopy.

Soil heat storage

Soil heat storage S_g can be formulated, also according to McCaughey & Saxton (1988), as

$$S_g = G + \int_0^z \rho_s C_s \left(\frac{dT_{soil}}{dt} \right) dz \qquad (3.30)$$

where $\rho_s C_s$ is the specific heat for average moist soil (2.1 MJ m^{-3} °C^{-1})(Shuttleworth, 1994), and T_{soil} is the soil temperature (°C), z is the depth of the soil heat flux measurements. For G a mean value of both forest types (see § 1.2.2.2 and § 3.5.3) is taken.

Heat storage in the vegetation

According to Thom (1975) and McCaughey & Saxton (1988) S_v can be written as

$$S_v = \int_0^{h_c} \rho_{veg} C_{veg} \left(\frac{dT_v}{dt} \right) dz \qquad (3.31)$$

where ρ_{veg} is the density of the vegetation (kg m^{-3} of column), C_{veg} is the specific heat of the vegetation (J kg^{-1} °C^{-1}), T_v is the temperature of the biomass and h_c is the canopy height. The solution of Equation 3.31 assumes that a representative biomass temperature is measured, and in this research this was done using an infrared radiometer measuring the surface temperature of the canopy (Samson & Lemeur, 2000). It can be assumed that C_{veg} is roughly 70% of the value of the specific heat of water (thus 2930 J kg^{-1} °C^{-1}), it can be deduced from Equation 3.31 that (Thom, 1975)

$$S_v = 0.8 m_{veg} dT_v \tag{3.32}$$

where m_{veg}, the integral of $r_{veg}dz$ from z=0 to z=h_c, is the mass of vegetation over unit horizontal area (kg m^{-2}) and dT_v is the representative canopy temperature change in °C per hour.

Photosynthetic heat capacity

The energy absorbed by biochemical processes S_p can be determined using the FORUG model (Samson et al., 1997a,b). This model was used to estimate net photosynthesis for different upperstory and understory species in the mixed deciduous forest, hetero- and autotrophic soil respiration, and above-ground woody biomass respiration. The net amount of carbon fixed by the forest is converted to energy based on the conversion that 1 g of CO_2 fixed yields 0.68 g of dry weight (DW)(Jones, 1992), and that on average energy content for dry matter of woody plants is about 20 kJ g^{-1} DW (Lieth, 1968).

3.5.2.2 Forest evapotranspiration

As mentioned before, the evapotranspiration of vegetated surfaces can be estimated using the well-known Penman-Monteith combination equation (Monteith, 1965)

$$lE = \frac{\Delta}{\Delta + g(1 + r_c/r_{ah})}(R_n - S) + \frac{1}{\Delta + g(1 + r_c/r_{ah})}\frac{r_a c_p}{r_{ah}}[e_s(T_a) - e_a] \tag{1.103}$$

where E is evapotranspiration (kg m^{-2} s^{-1}) and l the latent heat of evaporation (J kg^{-1}), D is the slope of the saturation vapour pressure curve at the air temperature (hPa °C^{-1}), g is the psychrometric constant (hPa °C^{-1}), $[e_s(T_a)-e_a]$ is the vapour pressure deficit of the air (hPa) and r_{ah} and r_c respectively the aerodynamic resistance and the canopy resistance, both expressed in s m^{-1}. If stability factors are neglected, and when the roughness length of sensible heat and momentum are assumed to be equal as is often done (e.g. Herbst, 1995), the aerodynamic resistance can be expressed as

$$r_a = \frac{\left[\ln\left(\frac{z-d}{z_0}\right)\right]^2}{k^2 u} \tag{1.90}$$

with z_0 the surface roughness length (m), d the zero place displacement (m), k the von Karman constant (0.41) and u the wind speed (m s^{-1}) at the reference height z (m). Deducted values for d and z_0 from measurements above the canopy are respectively 0.81 h_c (own, unpublished results) and 0.1 h_c (Dolman, 1986).

The surface resistance r_c can be determined using the approach of Stewart (1988), based on work of Jarvis (1976) for stomatal resistance, and further adapted by Ogink-Hendriks (1995) for an oak forest in The Netherlands (see § 1.2.2.3).

From intensive measurements during the 1996 growing season (leaf litter collection and optical LAI-sensors), the following LAI evolution during the growing season is used: (i) budburst occurs at May 1, and from then on there is a linear increase in LAI until July 1 (this is comparable to what is observed by (Ogink-Hendriks, 1995), but is somewhat later than what is observed by (Herbst et al., 1999)), (ii) from this date on the LAI remains constant until September 15, (iii) LAI decreases linearly and becomes 0 at December 1 (see also § 1.2.1.6).

3.5.2.3 Measurement period

Energy balance storage terms and forest evapotranspiration were intensively analysed during a period in August 1998 (15-23). This period was chosen because there were no technical problems measuring all the necessary parameters, and also because during this period LAI of the forest is maximal, thus representing good average conditions during the growing season. This period was characterised by some warm, dry summer days (August 15 till 20), and some cloudy, rainy days (August 21 till 23).

The seasonal evolution of the daily storage terms is analysed for the period August 15 - October 31. This period was characterised by intensive rain periods from August 21 - September 16 (143.5 mm), from October 6 till 14 (30.3 mm) and from October 22 until the end of the month (75.2 mm).

3.5.2.4 Measurement of surface temperature

The surface temperature was measured using an infrared radiometer (KT15, Heimann, wavelength sensitivity 8-14µm) with a field of view (FOV) of 34°. The instrument was installed 2 m above the canopy, and was orientated East with a

zenith angle of 65°. The radiometer was fixed in a green-painted zinc housing. This experimental set-up is comparable with the one described by Kalma & Jupp (1990). The infrared radiometer was calibrated in the laboratory against a blackbody submerged in a thermostatic bath. Comparable FOV geometry was also used by other authors (30° by Fuchs et al., 1967; 38° by Huband & Monteith, 1986; and 35° by Lagouarde et al., 1995). The advantage of this FOV is that the target observed by the infrared radiometer is much larger than the area of the shaded spots of the foliage. A drawback is the fact that the response of the radiometers results from the contribution of several viewing angles, and that the size of the target varies with the inclination (Lagouarde et al., 1995). Surface temperatures were measured every 10 s and averaged over 10 min periods using a datalogger (HP 75000 series B and HP 34970A, Hewlet-Packard, Colorado, USA)(see § 2.2.3).

Surface temperature cannot be directly derived from thermal measurements (Olioso, 1995). Measured radiation includes not only the radiation emitted by the surface itself, but also the radiation which is reflected by the surface towards the sensor and which originates from the environment (usually the atmosphere). The calculations presented by Olioso (1995), which account for surface emissivity, atmospheric emission and surface reflection in the thermal infrared, are used to correct the measured brightness temperatures for the case of clear sky conditions. In cloudy conditions, a cloudiness factor is taken into account (Bolz,1949; De Vries, 1955) as described in Brutsaert (1982). This cloudiness factor can be calculated following Wright & Jensen (1972). The canopy emissivity was set to 0.980, which is very close to values of 0.976 and 0.971 reported for canopy emissivity by respectively Fuchs & Tanner (1966) and Blad & Rosenberg (1976). The higher value of the canopy emissivity in this study compared to the above mentioned values, is selected because the canopy of a mixed deciuous forest is rather complex (see also Hutchison et al., 1986), and because a forest canopy has a higher LAI value than most agricultural crops.

3.5.3 Results and discussion

3.5.3.1 Diurnal behaviour of storage components

In conformity with McCaughey and Saxton (1988) three distinct weather conditions were chosen to characterise the diurnal behaviour of storage components. The selected conditions were: i) clear sky and dry canopy (August 16); ii) variable cloud and dry canopy (August 18); and iii) variable cloud and wet canopy (August 22).

During this last day rainfall was 6.7 mm (between 1500 and 1700 h). The hourly patterns of net radiation and of the different storage components for the three sample days are illustrated in Figures 3.32 and 3.33 respectively.

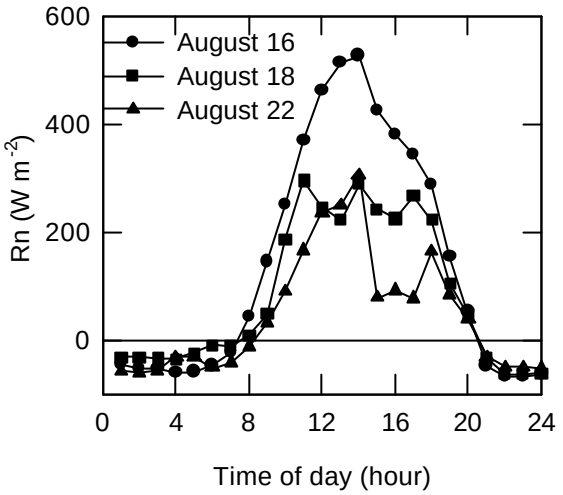

Figure 3.32 Diurnal pattern of net radiation (R_n) for August 16 (clear-sky conditions), August 18 (overcast conditions) and August 22 (variable cloud and rain).

Sensible heat storage (Figure 3.33a) in the canopy air followed patterns similar to those found by other authors (McCaughey, 1985; McCaughey & Saxton, 1988; Munro, 1979). Also our values corresponded extremely well with the findings of these authors. For August 16 and August 18 the increase in S_a was initiated at sunrise. Peak values occurred at 1000, 1100 and 1200 h for respectively the sunny, cloudy and rainy day. Throughout the rest of the day S_a decreased, until sensible heat was released to the atmosphere around 1600 h. Nighttime values of S_a were negative. The amplitude of the sensible heat storage was highest for the sunny day, due to important solar radiation during daytime, and significant long-wave radiation losses to the atmosphere during night. The rate of temperature change of the air was very similar as well above the canopy as for the four distinct levels in the canopy (figure not shown). However, the amplitude of the change in air temperature was most pronounced for the highest canopy level and the slightest change was observed at ground level, which partially illustrates the specific micro-climate occurring in forest ecosystems.

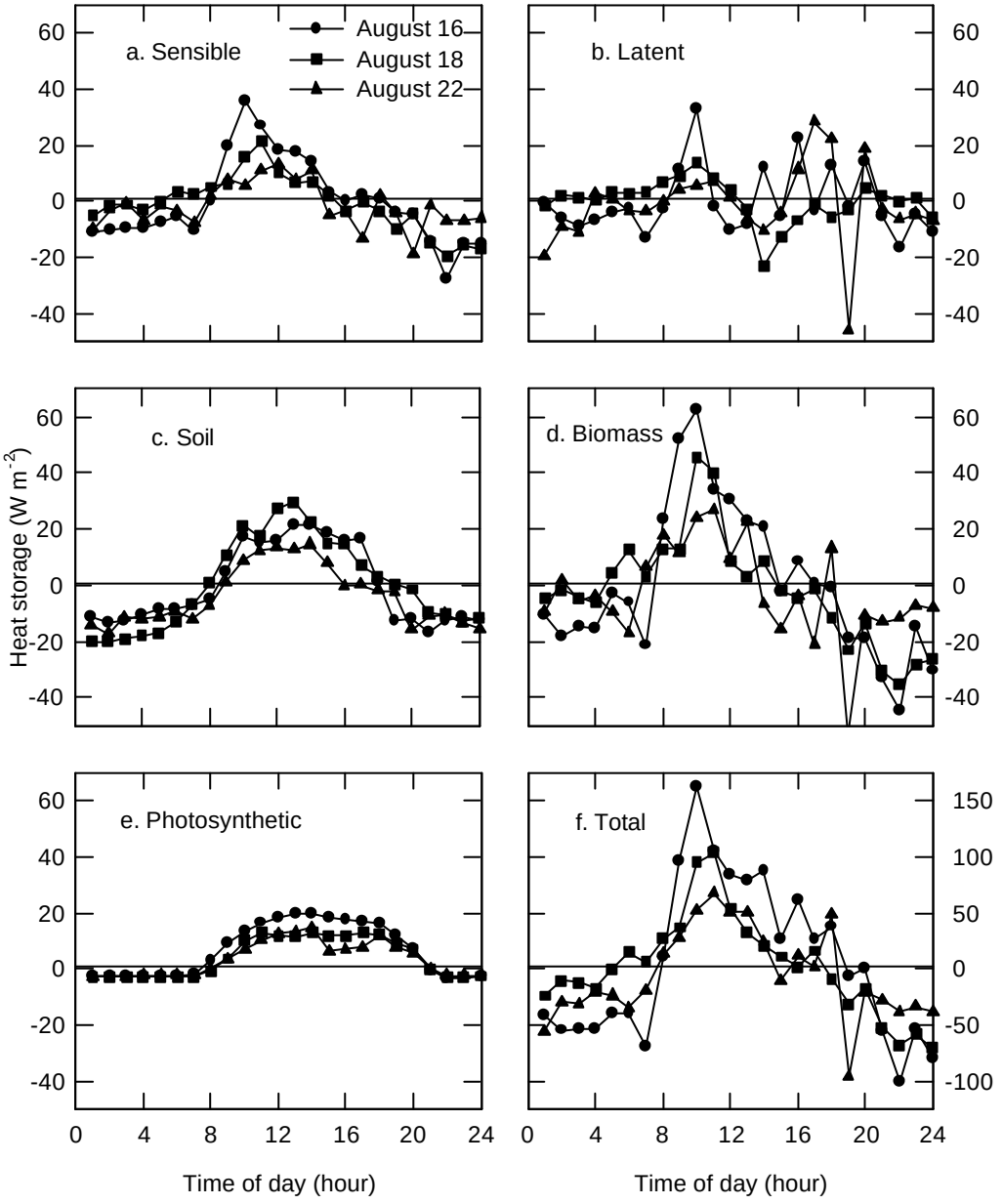

Figure 3.33 Diurnal pattern of: (a) sensible heat storage in the canopy layer; (b) latent heat storage in the canopy layer; (c) soil heat flux; (d) heat storage in the biomass; (e) heat stored by net photosynthesis; and (f) the overall heat storage. The sample days are August 16 (clear-sky conditions), August 18 (overcast conditions) and August 22 (variable cloud and rain).

In contrast to the other storage components, S_w (Figure 3.33b) was characterised by irregular patterns also reported by other authors (Lafleur et al., 1998; McCaughey & Saxton, 1988). For all weather conditions the sign of the flux varied around the zero line. The highest amplitude was found on the rainy day, due to evaporation of intercepted rain. Rain on August 22 was followed by an increase in wind speed which replaced the almost saturated air with dry air, and caused a sharp decrease in S_w. The hourly change in water vapour pressure in and above the canopy (data not shown) was highly variable and different for both heights, illustrating the specific micro-climate occurring in forest ecosystems, and thus the necessity of measuring the relative humidity as well above as in the canopy.

A clear diurnal course was observed for the soil heat storage (Figure 3.33c). The onset of S_g was a little delayed compared to sunrise. Heat storage increased till a plateau was reached, which existed throughout most of the day. Negative S_g values were reached somewhat later than for S_a. The observation of McCaughey and Saxton (1988) that the S_g is usually the largest flux on an hourly basis, was not valid in this forest.

In the two forest types a different diurnal pattern of S_g was observed (Figure 3.34). In the ash forest a pattern similar to that described by McCaughey and Saxton (1988) was found back for the sunny day (August 16). The hourly values of S_g in this ash forest easily reached 100 W m^{-2}, which can be explained by the absence of an important humus layer and the lower LAI in the ash stand, inducing more sun flecks at the soil surface. Due to a significant humus layer in the oak-beech forest (several centimeters) the amplitude of S_g is very small, and more independent of the weather type. On August 22 (low radiation and rain) the amplitude in the ash forest was similar to the pattern observed in the oak-beech forest. The presence of a humus layer and the LAI seems thus to be very important factors affecting the soil heat storage in forest ecosystems.

Heat storage in the biomass (Figure 3.33d) was characterised by a comparable pattern as observed for S_a. S_v became positive around sunrise, reached a peak around 1000 h for the dry days and around 1100 h for the wet day. Afterwards, S_v dropped considerably, became negative at 1500 h and then fluctuated between low positive or negative values. The increase and decrease in S_v was slightly in advance of S_a, indicating a quick heating up and cooling down of the canopy. The pattern observed here is different from S_v estimated by McCaughey and Saxton (1988), and discussed in detail by Saxton and McCaughey (1988). This difference can be explained by the different methods used. The above mentioned authors used thermocouples to measure the temperature of representative trees (different species, different heights and different depths in the stem) and shrubs. These authors found that the temperature change of stems was characterised by its lag in time of

response in comparison to that of the air. Aston (1985a) measured, besides the temperature of twigs, branches and stems, also leaf temperature by use of thermocouples and noticed a different thermal response of leaves (i.e. absence of the lag in thermal response) compared to trunks. The different pattern of S_v observed in this research can be explained by the fact that the measured re-emitted long-wave radiation by the canopy is besides the contribution of stems and branches mainly due to the thermal behaviour of the leaves, which explains why the lag in time is not observed. Stockfors (2000) mentions that there is a larger temperature amplitude in the upper parts of the stem, and thus also the branches, compared to the lower, more shaded parts of the stems. So, assuming that only the temperature of the upper part of the biomass was represented by the measured surface temperature, and the temperature of the lower stems equalled air temperature, taking a lag of two hours (Saxton & McCaughey, 1988) into account, S_v was recalculated (Figure 3.35). This assumption only had an impact on S_v on the sunny day (lower amplitude and a small phase shift), but on the cloudy and rainy day the impact was much less. Moreover, the obtained diurnal pattern for both days (Figure 3.35) resembled largely the diurnal course calculated when S_v was only based on surface temperature. So, the suggestion made by Saxton and McCaughey (1988) that the temperature change of tree tops and the upper canopy might be measured by an infrared radiometer, and used to calculate S_v seems to be valid. Because the upper part of the canopy is the major contributor to H_2O and CO_2 exchange processes (non-published FORUG-simulation results), and because the measurement of biomass storage is logistically difficult (McCaughey & Saxton, 1988), especially in mixed forests, assuming that surface temperature represents canopy temperature might yield a good estimation of heat storage in the vegetation, although more research is needed to confirm this statement. More precisely, it would be interesting to investigate the relationship between surface temperature and stem temperature. Stem temperature should hereby be measured for as well upperstory and understory species, at different depths in the stem, and at different heights. A distinction should also be made between branches and stems. Besides for the calculation of heat storage in the vegetation, this information will also be very useful for modelling respiration of the woody biomass (see § 1.2.1.12).

The heat stored by net carbon assimilation is illustrated in Figure 3.33e, and corresponds well with values found by other authors (Baldocchi, 1997; Baldocchi & Harley, 1995). A clear diurnal course was observed. Differences in pattern and magnitude for the considered days were attributed to differences in radiation and temperature. During night there is a small constant release of energy to the ecosystem due to respiration. To estimate the photosynthetic heat storage also micro-meteorological CO_2 flux measurements can be used to estimate S_p on the condition that also the storage of CO_2 in the canopy is measured. The photosynthetic heat storage is mostly denied in energy balance studies (McCaughey & Saxton,

1988) or is often found to be negligible in size in comparison to R_n (Thom, 1975). Jarvis et al. (1976) suggested that the average photosynthetic flux during the day for coniferous forests is about 3 % of R_n, but that it may reach much higher fractions in the early morning and evening. However, for the three selected days a mean daytime value of 6.1 % of R_n was calculated in this study. Maximum and minimum values were respectively 14.8 % (cloudy day) and 3.7 % (sunny day) of R_n. Daytime values were in the same order of magnitude as for S_a, S_g and S_w. Also, during nighttime values were not negligible (mean nighttime value of 6.3 % of R_n).

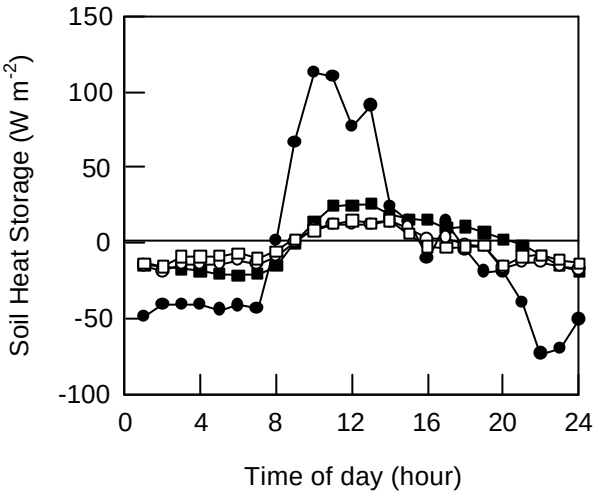

Figure 3.34 The diurnal pattern of the soil heat storage for the ash (circles) and oak-beech (squares) forest type. The sample days are August 16 (clear sky conditions)(closed symbols) and August 22 (variable cloud and rain)(open symbols).

The diurnal pattern for the total heat storage (Figure 3.33f) was comparable to those of S_a and S_v. Values also agree well with results found by McCaughey (1985) and McCaughey and Saxton (1988), somewhat smaller values were observed by Stewart and Thom (1973) for a pine forest. The highest amplitude was noticed on the sunny day, the lowest on the cloudy/rainy day. During daytime values can be as high as 160 W m^{-2} and during night as low as -100 W m^{-2}. If only S_g would be taken into account, as is sometimes done, than errors up to 150 W m^{-2} can occur, which clearly illustrates that the different components of the overall heat storage should be taken into account. Also McCaughey and Saxton (1988) concluded that using S_g as the sole indicator of canopy storage is not recommended.

The relative size of *S* with respect to R_n showed a high variability on an hourly basis. Early after sunset *S* sometimes exceeded R_n, resulting in a positive energy term available for sensible and latent heat exchange. Later during night *S* dropped to 40-50 % of R_n, but under certain conditions it compensated R_n throughout almost the entire night. At sunset and sunrise, when R_n was small and changed from negative to positive values, or vice versa, *S* varied between more than -200 % to more than 100 % of R_n. During the morning *S* was at least around 30 % of R_n but *S* decreased to less than 10 % as R_n increased.

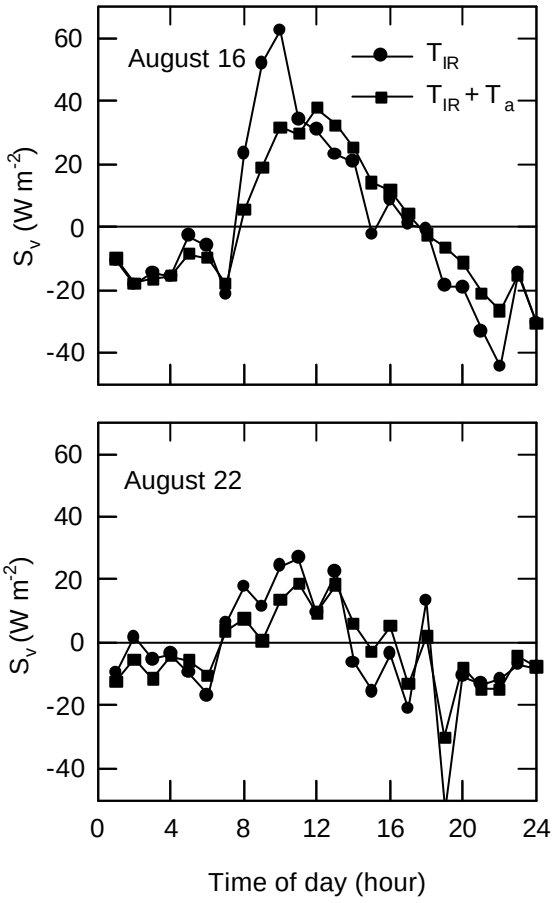

Figure 3.35 The diurnal pattern of heat storage in the biomass (S_v), calculated based on Equation 5 where: (i) T_v is measured using an infrared radiometer (T_{IR}), or (ii) assuming that only the temperature of the upper part of the biomass is represented by the measured surface temperature, and the temperature of the lower stems equals air temperature, taking a lag of 2 hours into account ($T_{IR} + T_a$).

3.5.3.2 Daily and daytime pattern of heat storage

The daily and daytime totals of the five considered storage terms and the total storage are shown in Table 3.10 and 3.11, for the considered measurement period (August 15 - 23). Daytime is defined as the period with positive R_n values. It is important to remark that during the measurement period no obvious air mass change occurred (demonstrated by a significant change in mean air temperature (McCaughey & Saxton, 1988))(Table 3.10), which affects different storage components, particularly S_w (McCaughey & Saxton, 1988).

Table 3.10 illustrates that on a daily basis the largest net amount of heat was stored by the photosynthetic process, and thus that S_p should always be taken into account. Other storage terms were close to zero, indicating there was no net gain or loss of energy to the system. The net loss of energy out of the soil compartment is not directly expected, but can be explained by the fact that the preceding period was rather warm, resulting in a gain of energy, a part of which was again released when air temperature decreased. During the wet period (August 21-23) energy storage in water vapour became important.

Table 3.10 Summary of daily totals of the different storage terms (S_a the sensible heat storage, S_w the latent heat storage, S_g the soil heat storage, S_v the biomass heat storage, S_p the photosynthetic heat storage), the overall storage (S) and net radiation (R_n)(all expressed in MJ m^{-2} day^{-1}), together with values of daily mean air temperature (T_a)(°C) and precipitation (R)(mm) for the period August 15 – 23, 1998.

	S_a	S_w	S_g	S_v	S_p	S	R_n	T_a	R
Aug. 15	-0.125	-0.188	-0.018	-0.225	0.532	-0.024	11.617	22.6	0.0
Aug. 16	-0.017	-0.027	-0.131	0.005	0.588	0.419	12.108	22.1	0.0
Aug. 17	0.023	0.018	0.035	0.046	0.482	0.604	10.685	21.7	0.0
Aug. 18	-0.071	-0.001	-0.011	-0.152	0.365	0.130	7.218	21.9	0.0
Aug. 19	0.014	-0.107	-0.142	0.032	0.446	0.243	9.735	21.2	0.0
Aug. 20	0.074	-0.063	-0.027	0.194	0.414	0.592	10.305	20.8	0.0
Aug. 21	-0.070	0.094	-0.042	-0.177	0.211	0.015	4.199	19.9	5.6
Aug. 22	-0.141	-0.117	-0.342	-0.222	0.305	-0.516	3.899	18.1	6.7
Aug. 23	0.210	0.289	0.201	0.440	0.178	1.318	3.258	17.5	21.7

McCaughey (1985) stated that when canopy is dry and net radiation is high, the daily total storage seldom exceeds 2-3 % of R_n, and that storage can be safely ignored. Our research yielded more or less comparable results, for moderate R_n total storage ranged from -0.2 to 5.7 % of R_n, with a mean value around 3.2 %. However for cloudy

days with rain or a drying canopy, the comparative size of S can be much larger (40.5 % on August 23) and also negative (-13.2 % on August 22). So, it is safer to calculate the total energy storage for each day instead of ignoring it beforehand.

Table 3.11 Summary of daytime totals of the different storage terms (S_a the sensible heat storage, S_w the latent heat storage, S_g the soil heat storage, S_v the biomass heat storage, S_p the photosynthetic heat storage), the overall storage (S) and net radiation (R_n), all expressed in MJ m^{-2} day^{-1}, for the period August 15 - 23. Daytime is defined as the period with positive R_n values.

	S_a	S_w	S_g	S_v	S_p	S	R_n
August 15	0.098	0.070	0.346	0.168	0.628	1.309	13.097
August 16	0.381	0.192	0.474	0.574	0.676	2.296	14.241
August 17	0.282	0.118	0.547	0.444	0.570	1.963	12.684
August 18	0.135	-0.025	0.278	0.160	0.464	1.012	8.664
August 19	0.389	0.064	0.628	0.393	0.528	2.002	11.735
August 20	0.277	0.058	0.444	0.466	0.502	1.747	12.146
August 21	0.164	-0.057	0.257	0.148	0.259	0.772	5.012
August 22	0.118	0.036	0.172	0.049	0.371	0.747	5.818
August 23	0.147	0.215	0.380	0.315	0.259	1.316	4.717

The contribution of the different storage terms to the overall storage during the daytime when $R_n > 0$ is shown in Table 3.11. During the entire period, all terms, and consequently the total storage, were positive. The only exception, in accordance with findings of McCaughey and Saxton (1988), was S_w, which also on hourly basis was the most variable term. The largest heat storage was due to the photosynthesis process, followed by heat storage in the soil and vegetation. The smallest values were observed for S_w. S was between 10.0 and 17.1 % of R_n for the dry period , and varied between 12.8 and 27.9 % for the wet period. Again it is clear that the day to day variability of S compared to R_n can be high.

3.5.3.3 Seasonal pattern of storage

The seasonal evolution of the daily heat storage from August 15 till October 31 is illustrated in Figure 3.36. Only data from one psychrometer, installed above the canopy, could be used for calculating daily S_w values. Missing data of other parameters are due to technical, mainly datalogging, problems.

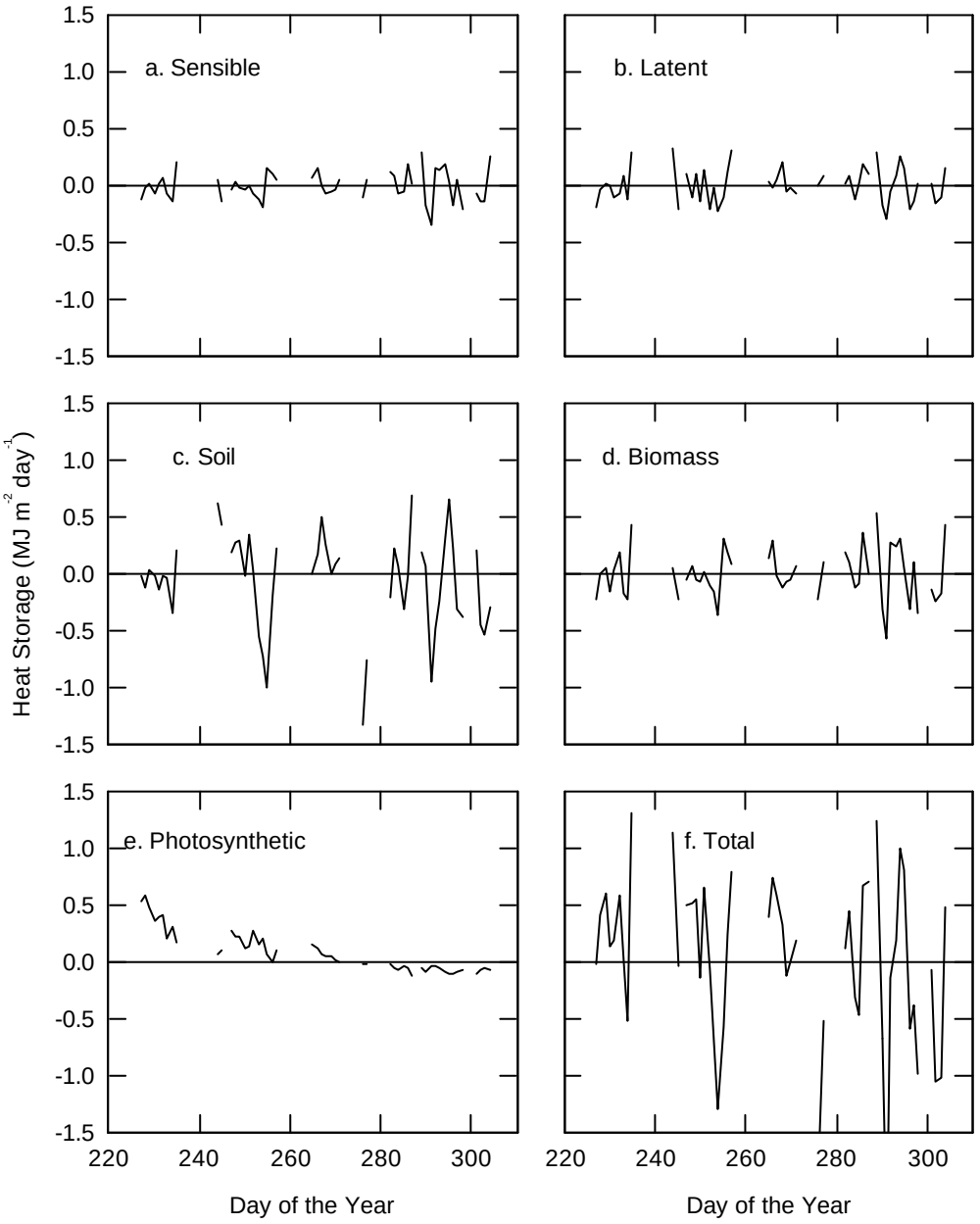

Figure 3.36 Seasonal patterns of daily totals of: (a) sensible heat storage in the canopy layer; (b) latent heat storage in the canopy layer; (c) soil heat flux; (d) biomass heat storage; (e) heat storage by net photosynthesis; and (f) overall heat storage. Day 220 is August 8 and Day 310 is November 6, 1998.

The daily sensible and latent heat storage (respectively Figure 3.36a and 3.36b) were, as found earlier, rather small, and there was no seasonal evolution for both storage terms. Just as found by McCaughey and Saxton (1988), the soil heat storage

term (Figure 3.36c) was significantly larger than the other storage terms. Summing the daily values S_g was strongly negative during the considered period, indicating a net release of heat from the soil. The only term indicating a clear seasonal trend was the heat fixed by the photosynthesis process (Figure 3.36e). This behaviour is not surprising as net photosynthesis decreases towards the end of the growing season (Samson et al., 1997a). Hence, during the growing season the positive contribution of S_p to the overall heat storage seems to be important, while at the beginning, at the end and periods out of the growing season its contribution becomes negligible. The total daily heat storage (Figure 3.36f) fluctuated between 1.32 (day 235) and -2.20 (day 291) MJ m^{-2} day^{-1}. During fall the ecosystem released heat to the environment, which was earlier accumulated during the growing season (Figure 3.36f).

Large fluctuations in overall heat storage (Figure 3.36f) can sometimes, but not always, be attributed to obvious changes in air mass. Examples of this phenomenon are the drops in air temperature (-3.7 °C) and wind speed (-2.5 m s^{-1}) between day 253 and 254 accompanied with a decrease in overall heat storage. A larger decrease in temperature (-5.4 °C) and wind speed (-4.7 m s^{-1}) is registered between day 290 and day 291, now with an even more pronounced release of energy as the result. On the other hand, air temperature (+3.5 °C) and wind speed (+4.2 m s^{-1}) suddenly increased between day 293 and day 294, with a rise in heat storage as the result. However, an obvious change in air mass is not always reflected in the overall heat storage, e.g. between day 286 and day 287 a clear increase in air temperature did not cause the expected increase in overall heat storage, which is explained by rain and cloudy weather conditions occurring during daytime period. Fluctuations in overall heat storage are thus a result of complex changes in different climatic parameters as air temperature, wind speed, radiation and the occurrence of rain.

3.5.3.4 Storage and big leaf evapotranspiration

Forest evapotranspiration was only calculated for the dry period (August 15-20). Two different approaches were used for taking the available energy to the ecosystem into account. First, the storage term was considered to be a constant fraction (3 %) of R_n, which is a typical value when canopy is dry (McCaughey, 1985). In the second case, the measured total heat storage was used. For August 16 and 18 the effect of the difference in storage approximation is given in Figure 3.37. For these days the difference between both storage terms (with a peak value around 1000-1100 h of up to 150 W m^{-2}), followed mainly the diurnal course of the measured *S*. This was because of the small values calculated from 0.03*R_n. The amplitude of the estimated difference between both storage terms was more pronounced for the sunny day (August 16).

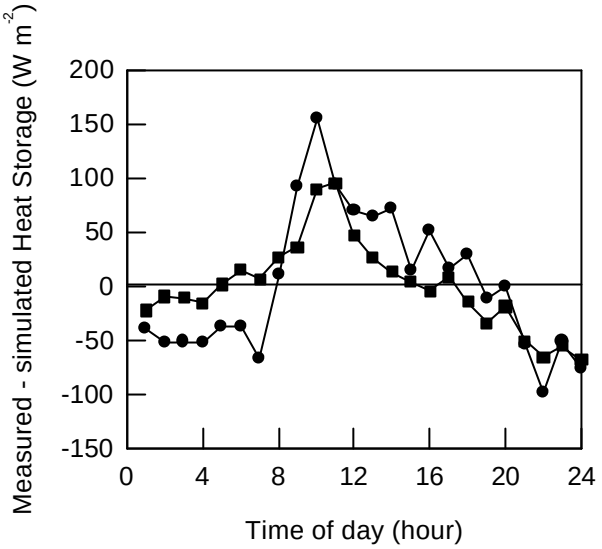

Figure 3.37 The diurnal pattern of the difference between measured and assumed (3% of R_n) total heat storage. Sample days are August 16 (clear-sky conditions)(closed circles) and August 18 (overcast conditions)(closed squares).

In Figure 3.38 the diurnal course of latent heat exchange lE is calculated from Equation 1.103 for August 16 and 18, and with S determined in the two different ways as explained above. During night there was a negligible difference between both methods. After sunrise the difference increased, with the lowest latent heat exchange observed for the calculations based on measured heat storage, and peaked for both days at 1000 h. Especially on the sunny day the maximal difference was rather large (>50 W m^{-2}), but was immediately followed by a very sharp decline. For the cloudy day, there was a deviation of about 10 W m^{-2} during several morning hours, which was almost completely reduced to 0 around 1500 h.

The difference in daily evapotranspiration sum for the period August 15 - 20, calculated by the two methods described, was almost negligible (0.12 ± 0.08 mm day^{-1}), with the calculations based on measured heat storage resulting in a somewhat lower evapotranspiration (3.09 ± 0.33 mm day^{-1}). Extrapolating the differences in latent heat exchange over an entire growing season (May - September) resulted in a difference in evapotranspiration of only 18.48 mm.

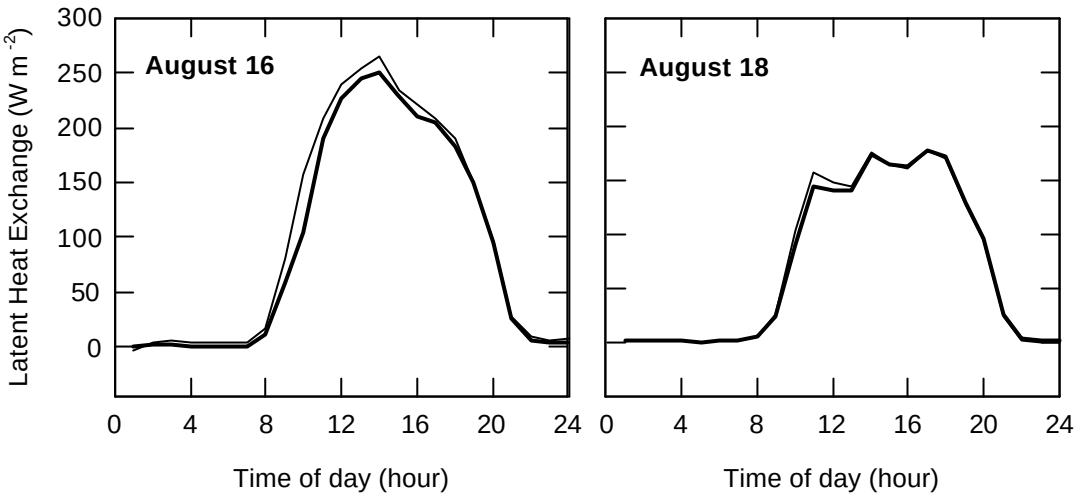

Figure 3.38 The diurnal patterns of latent heat exchange calculated using two different methods: (i) based on measured total heat storage (thick line), and (ii) based on an assumed heat storage (3% of R_n)(thin line). The selected sample days are: (a) August 16 (clear-sky conditions); and (b) August 18 (overcast conditions).

The contrasting results obtained so far (i.e. the rather large differences in heat storage on one hand (Figure 3.37), and the small differences in latent heat exchange on the other hand (Figure 3.38)), can be explained by the decoupling coefficient Ω (Jarvis & McNaughton, 1986)(see above § 1.1.2.5). The coupling (i.e. 1-Ω) between the forest 'Aelmoeseneie' and the atmosphere was rather strong, and amounted on average a value of 0.10 for the period August 15-20. This is within the range from 0.05 to 0.2 observed by Granier et al. (2000a) for a beech forest. Similar values were also found for a beech forest in Germany (Herbst, 1995; Herbst et al., 1999). A high coupling decreases the importance of the available energy to the overall evapotranspiration (see before § 1.1.2.5).

For ecosystems strongly coupled to the atmosphere, knowledge of the heat storage, and, hence, the amount of available energy, seems to be less important for the determination of latent heat exchange using the Penman-Monteith approach. For less coupled ecosystems (such as in greenhouses) an accurate determination of the heat storage, and more precisely of the available energy, will be much more necessary. The same is true when the Bowen-ratio is used for the calculation of the latent heat exchange as this ratio also contains the available energy as an input variable (Aston, 1985a,b).

3.6 Estimation of the latent heat flux at stand level with the Bowen ratio method

3.6.1 Introduction

The Bowen ratio-energy balance (BREB) method (Bowen, 1926) has become a standard technique for measuring latent and sensible heat fluxes from vegetated surfaces. The accuracy of this method has already thoroughly reviewed by e.g. Fuchs and Tanner (1970), Sinclair et al. (1975) and Spittlehouse and Black (1980). A general opinion is that latent heat flux can be estimated to within 10 % (Sinclair et al., 1975).

The BREB method (see above, § 1.1.2.3) estimates latent heat flux from a surface using measurements of vertical air temperature and humidity gradients, and of the net radiation and of the soil heat flux (Fritschen and Simpson, 1989). Unlike other flux-profile techniques, the Bowen ratio method does not require information on wind speed and aerodynamic properties of the surface. Also, the calculation of the fluxes is independent of atmospheric stability if equality of eddy diffusivities of heat and vapour transport is assumed (see above, § 1.1.2.2). The method assumes that water vapour and heat transport is one dimensional, with no horizontal gradients; and also similarity of humidity and temperature profiles. If different sources and sinks of water vapour and heat exist, dissimilar profiles may develop above the canopy. However, these profile differences may disappear at some elevation above the surface. Data from Garatt (1978a) indicate that the minimum elevation for measurements is three to five time the height of the roughness elements. A fetch (distance from the leading edge) to height-above-surface ratio of 100:1 is often considered a rule of thumb (Rosenberg et al., 1983), although a ratio as low as 20:1 was considered adequate when Bowen ratios were small and positive (Heilman et al., 1989). Sensors placed at different heights respond to different upwind source areas (Schuepp et al., 1990; Schmid 1997), and all sensors must have adequate fetch. Stannard (1997) confirmed theoretically that the Bowen ratio method requires less fetch than the eddy covariance method.

The Bowen ratio-energy balance (BREB) method has been frequently used to quantify water use (Fritschen, 1966; Malek et al., 1990; Wight et al., 1993), to calculate crop coefficients (Malek and Bingham, 1993b; Casa et al., 2000), to investigate plant-water relations (Grant and Meinzer, 1991; Malek et al., 1992) and to evaluate crop water use models (Ortefa-Farias et al., 1993; Todd et al., 2000). It is considered to be a fairly robust method, and it has compared favourably with other

methods for evapotranspiration measurements such as weighing lysimeters (Grant, 1975; Asktorab et al., 1989; Prueger et al., 1997; Todd et al., 2000), the eddy covariance technique (Cellier and Olioso, 1993) or water balance calculations (Malek and Bingham, 1993a). Most of the studies that showed agreement were conducted when Bowen ratios were mostly positive and sensible heat advection absent. Others showed less certain agreement (Blad and Rosenberg, 1974; Dugas et al., 1991).

The BREB-method is an indirect method, compared to methods such as eddy covariance which directly measures turbulent fluxes, or weighing lysimeters which measure the mass change of an isolated soil volume and the plants growing in it. The advantages include the straightforward and simple measurements. The method can integrate latent heat fluxes over large areas (hundreds to thousands of square meters); estimate fluxes on fine time scales (less than an hour) and provide for continuous, unattended measurements (Todd et al., 2000). Disadvantages are the sensitivity to errors from the biased instruments which measure the vertical temperature and humidity gradients and energy balance terms; and the requirement (which is common to many micro-meteorological methods) of an adequate fetch to ensure compliance to the assumptions of the method.

Different authors already applied the Bowen ratio method above temperate deciduous forests, e.g. a beech forest (Herbst, 1995), and an oak forest (Ogink-Hendriks, 1995). However, Bowen data have not yet been frequently compared to upscaled transpiration data from sap flow measurements in forest ecosystems. Eddy covariance data are most commonly used for this purpose (see Granier et al., 2000b).

The objectives of this study part of the study are to apply the Bowen ratio-energy balance method above the small heterogeneous temperate deciduous forest Aelmoeseneie. First, the Bowen ratio data will be analysed. From these Bowen ratio data the latent heat flux between the forest Aelmoeseneie and the atmosphere will be estimated. The sensitivity of estimations of the latent heat flux to heat storage in the forest (see § 3.5) will be described. Finally, the obtained latent heat fluxes will be compared with sap flow data scaled-up to the level of the forest Aelmoeseneie as described in § 3.4.

3.6.2 Material and methods

3.6.2.1 Micro-meteorological measurements, instrumentation and data collection

Micro-meteorological measurements above the forest were taken from an experimental tower at the right edge of the forest (see Chapter 2). Fetch was 100 and 200 m to the north and south respectively, and less than 100 m to the east (see above Figure 2.1). To the west fetch was approximately 500 m (see above Figure 2.1). Wind directions between 240° and 290° had the longest fetch of 500 m. Taking the upper measurement height z = 36.0 m and zero plane displacement d = 21.9 m (from wind profile measurements above the canopy, see also later § 4.2), the equivalent fetch to (z-d) ratio at the west side of the forest was at least 20:1, which is likely to be sufficient for representative micro-meteorological profile measurements over rough surfaces such as forests (e.g. Munro & Oke, 1975; Gash, 1986; Heilman et al., 1989).

The Bowen ratio was measured between height levels 36.0 and 28.6 m using wet and dry bulb psychrometers (H301, Vector Instruments, Rhyl, UK). Net Radiation at 36 m was determined with a REBS radiometer, type Q*7.1 (Seattle, WA). Soil heat flux was measured at both forest sites with self calibrating soil heat flux sensors (HFP01SC, Hukseflux, Delft, The Netherlands) installed 8 cm under the soil surface (see also § 2.2). Energy storage above these heat flux sensors was also taken into account by measuring soil temperature at a depth of 4 cm above each soil heat flux sensor (see § 3.5.2.1). As mentioned before (see § 2.2.3), a mean value of all measured variables was stored every ten minutes. Mean hourly values, calculated from these ten minute values, were used for the analysis.

Bowen ratio data were analysed for the period August 4 till 28, 1999. This period was characterised by sunny as well as rainy days, and was selected because of the availability of a complete climatic and physiological data set. Another reason was the fact that LAI was maximal and nearly constant (Samson and Lemeur, 2001). Daily sums of net radiation and precipitation during this period are shown in Figure 3.39. Prevailing wind direction was Southwest during the observation period (Figure 3.40), yielding a fetch of at least 300 m, and a fetch to (z-d) ratio of at least 20:1.

3.6.2.2 Theoretical background

The partition of the available energy between the sensible H and latent λE heat fluxes is obtained from the Bowen ratio (Kustas et al., 1996)(see § 1.1.2.3):

$$\beta = \frac{H}{\lambda E} \tag{1.80}$$

The Bowen ratio is combined with the energy balance:

$$R_n - S = H + \lambda E \tag{1.86}$$

yielding the following expression for H and λE:

$$H = \frac{\beta}{1+\beta}\left(R_n - S\right) \tag{3.33}$$

$$\lambda E = \frac{R_n - S}{1+\beta} \tag{1.87}$$

where R_n is the net radiation above the forest stand and S is the total heat storage in the forest. Total heat storage in the forest was calculated as explained in the preceding paragraph (§ 3.5.2)(see also Samson and Lemeur, 2001).

Using the assumption that the ratio of eddy diffusivities of sensible and latent heat fluxes is unity (§ 1.1.2.2, Equation 1.63), and measuring the temperature and vapour pressure gradients between two levels β is obtained as (see Equation 1.85)

$$\beta = \gamma \frac{\Delta T}{\Delta e} = \frac{c_p P_{atm}}{0.622\,\lambda} \cdot \frac{\left(T_2 - T_1\right)}{e_2 - e_1} \tag{3.34}$$

where ΔT and Δe are the temperature and vapour pressure differences between the two measurement levels z_1 and z_2 at respectively 36 and 28.8 m. The sign convention used for the energy fluxes is R_n being positive downward and S being positive when heat is stored in the forest. Sensible and latent heat fluxes are positive upward.

Energy advection represents the total energy advected to or away from the layer to which the energy budget is applied. Precipitation can be a source of vertical advection at the upper surface of the forest, and horizontal advection may be either

positive or negative. Rosenberg et al. (1983) defined advection as "the transport of energy or mass in the horizontal plane in the downwind direction". This term, which can be large in certain conditions, has been neglected in the energy balance equation used (Equation 1.86).

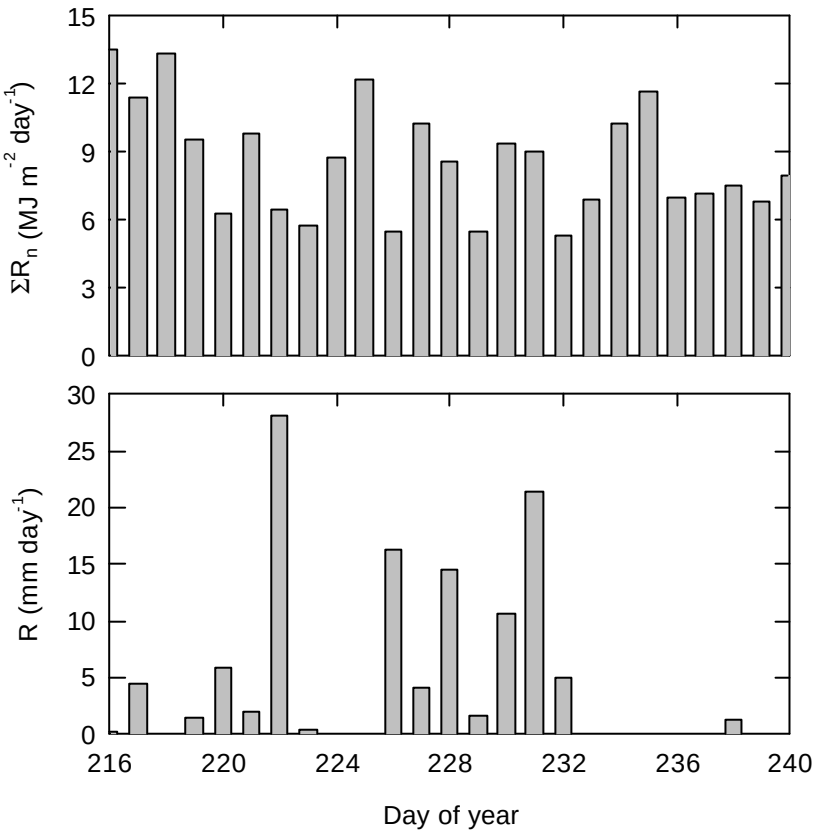

Figure 3.39 Daily net radiation sum (ΣR_n) and daily precipitation (R) during the period from 4 till 28 August, 1999.

An index that measures the combined effects of temperature, vapour pressure deficit, available energy and wind speed is the ratio of the climatic resistance r_{cl} (Monteith, 1965; Stewart and Thom, 1973) to the aerodynamic resistance r_a. Thom (1975) pointed out that this ratio will be very large if there is a strong, dry airflow over vegetation, which he called an 'oasis situation'. According to Todd et al. (2000) the resistance ratio becomes very large when the atmospheric conditions are warm, dry, and windy, as is encountered on days with evidence of sensible heat advection. As was done by Todd et al. (2000) the following formula is used:

$$\frac{r_{cl}}{r_a} = \frac{\rho_a c_p D\left[g\left(R_n - S\right)\right]^{-1}}{\left\{\ln\left[\left(z-d\right)/z_0\right]\right\}^2\left(k^2 u\right)^{-1}} \qquad (3.35)$$

where ρ_a is air density (kg m^{-3}), c_p the specific heat of moist air (1013 J kg^{-1} °C^{-1}), D is vapour pressure deficit of the air (kPa) measured at z = 28.6 m, g is the psychrometric constant (kPa °C^{-1}), d is the zero plane displacement height (m) calculated as 0.81h_c (h_c being the canopy height of 27 m), z_0 is the roughness length (m) calculated as 0.1h_c, k = 0.41 is von Karman's constant and u is the wind speed (m s^{-1}) at z = 28.6 m.

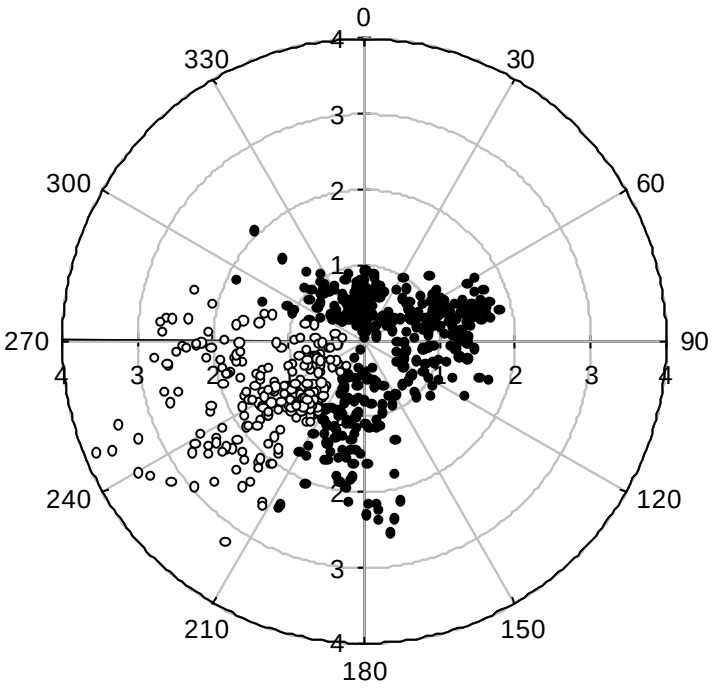

Figure 3.40 Polar representation of hourly wind direction (0-360°) and wind speed (0-4 m s^{-1}) during the period from 5 till 28 August. Wind directions between 210 and 290°, having a fetch of at least 300 m, are indicated as white circles. Other directions correspond with black circles.

3.6.2.3 Data analysis

In order to determine correct fluxes it is necessary to apply some set of criteria to select suitable Bowen ratio data. The simplest criterion for rejection of data may be to discard the surface flux values obtained when the differences of temperature and vapour pressure are of the same order of magnitude as the resolution limits of the sensors (Unland et al., 1996). However, this does not always imply that the flux values are incorrect.

A problem inherent in the BREB method arises when b approaches -1, since the denominator in Equations 3.33 and 1.87 approaches 0. The values $b \approx$ -1 can appear at sunrise and sunset, and also during precipitation when the direction of the temperature gradient changes to be opposite to that of the vapour pressure gradient. In these cases, with extremely inaccurate flux values, the problem is to find out which non-permissible range around -1 to consider (Perez et al., 1999). Some ranges have been proposed; for example, b values of less than -0.75 or values in the range $-1.3<b<-0.7$ (Ortega-Farias et al., 1993; Unland et al., 1996).

To calculate latent heat fluxes the Bowen ratio data were selected for periods: (i) without precipitation, (ii) with adequated fetch (wind direction between 210 and 290°), and (iii) with $\beta > -0.75$. Moreover, because night periods or periods of sunrise or sunset are characterised e.g. by small or changing temperature gradients, flux values at these moments are often inaccurate. Therefore only daylight hours between 1000 and 1800 h are used to calculate latent heat fluxes from the Bowen ratio data (e.g. Herbst, 1995).

3.6.3 Results and discussion

3.6.3.1 Data analysis

The main experimental requirement for the Bowen ratio method is that temperature and humidity gradients are measured within the internal boundary layer, and preferably in the portion of the boundary layer that is in equilibrium with the surface. Model calculations indicated that the lowest 10 % of the boundary layer is in equilibrium with the surface for an aerodynamically smooth-to-rough transition (Brutsaert, 1982). The thickness of the internal boundary layer above the forest Aelmoeseneie was calculated according to Munro and Oke (1975). The result yielded

that in this case the upper measurement level was not situated in the equilibrium sublayer. However, because Bowen ratio was small it was not sensitive to imperfect fetch conditions (Heilman et al., 1989).

In Figure 3.41 a mean diurnal course of the Bowen ratio for days without rain is illustrated. The Bowen ratio during nighttime was rather high, whereas during daytime the Bowen ratio was close to zero and sometimes even negative, indicating an opposite flux of latent and sensible heat exchange. Negative daytime Bowen ratio data were due to a mean negative De value of the vapour pressure gradient (-0.95 $\pm$ 0.02 hPa), which indicated that vapour pressure near the crown surface was lower compared to vapour pressure at the upper measurement level. During periods of active transpiration, as can be assumed during daytime, the reverse situation is expected. This unconventional humidity gradient was not due to a miscalibration of the Pt100 sensors as was revealed by calibration of the sensors in an (ice)-water bath. It could have been due to a malfunctioning of the psychrometers itself or to a non-ideal experimental set-up. Mean daytime ΔT was –0.23 $\pm$ 0.01 °C.

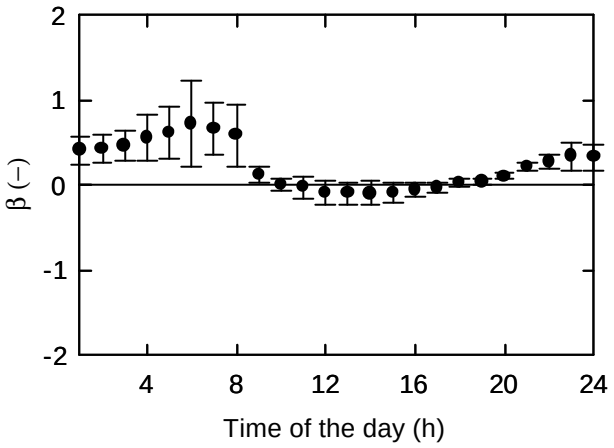

Figure 3.41 Mean diurnal course and error bars (±SE) of the hourly Bowen ratio (*b*) for all days without precipitation during the period 4-28 August, 1999.

The diurnal dynamics of the mean ratio of the climatic resistance r_{cl} to the aerodynamic resistance r_a is shown in Figure 3.42. The ratio is lowest during midday, and increases during the afternoon. Todd et al. (2000) pointed out that when r_{cl} is very large in comparison with r_a there is evidence of sensible heat advection. Although, Thom (1975) and Todd et al. (2000) both do not mention exact values from

which advection is considered, Todd et al. (2000) assumed advection with lower values of the ratio of r_{cl}/r_a as reported in this study. Therefore, there was a strong indication for situations of advection during daytime (Figure 3.42)(Thom, 1975; Todd et al., 2000). Todd et al. (2000) concluded from observations of Verma et al. (1978), Motha et al (1979) and Lang et al. (1983) that the behaviour of exchange coefficients in the presence of sensible heat advection is uncertain, and thus also the BREB. When advection of energy exists, as suggested by Figure 3.42, an advection term should be included in Equation 1.86, and must also be added to R_n-S in Equations 3.33 and 1.87.

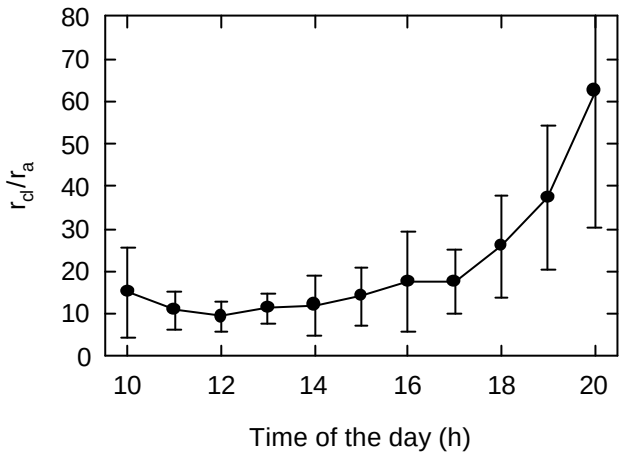

Figure 3.42 Mean hourly change of the ratio of the climatic resistance (r_{cl} to the aerodynamic resistance (r_a) during daytime, for all dry days during the period 4-28 August, 1999.

3.6.3.2 Estimation of the latent heat flux

As can be seen in Figure 3.43, Bowen data were generally close to zero, which caused the latent heat fluxes, according to Equation 1.87, to almost equal net radiation. Because of the applied criteria and difficulties when measuring Bowen ratio data, only a discontinuous data set was obtained. To overcome this problem, and to be able to determine latent heat fluxes for the entire measurement period, a relationship was described between R_n-S and the latent heat flux data ($lE_{Bowen,select}$) estimated from the selected Bowen ratio measurements (dry and fetch, see Table 3.12). The observed linear relationship (r^2=0.99, n=190) between R_n-S and the

latent heat flux $lE_{Bowen,select}$ was used to estimate the latent heat flux, $lE_{regression}$, for the period 5 till 27 August. Comparison of $lE_{regression}$ to the latent heat flux values calculated from the original Bowen ratio data (lE_{Bowen}) (Figure 3.44) showed a strong linear relationship (r^2=0.97, n = 552) for the period 5 till 27 August. At higher flux values (>400 W m^{-2}) lE_{Bowen} overestimated $lE_{regression}$. The similarity between both approaches showed that the selected data (dry and adequate fetch) did generally not yield different latent heat fluxes compared to the original Bowen ratio data set of the entire period. Therefore, all measured Bowen data were used to calculate latent heat fluxes, instead of only data measured during periods without precipitation and with adequate fetch. During the considered period lE_{Bowen} ranged between 1.6 and 5.4 mm between 1000 and 1800 h, with a mean value of 3.1 ± 0.2 mm (see Figure 3.45). High latent heat fluxes (Figure 3.45) were observed for days with high daily net radiation sums, and days without precipitation (see Figure 3.39), and on days with low Bowen ratio values (see Equation 1.87).

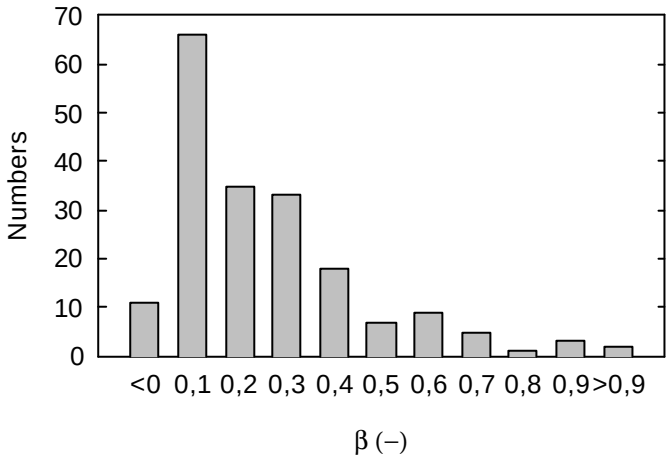

Figure 3.43 Distribution of the hourly Bowen data (*b*) measured between 4 and 28 August, 1999, for periods without precipitation and with adequate fetch.

Table 3.12 The number of Bowen ratio data during the period August 4-August 28, fulfilling following criteria: (i) no precipitation measured (dry) and a (ii) minimal fetch of 300 m (between the wind directions 210 and 290°)(fetch). The numbers of data fulfilling the two criteria (dry and fetch) are also shown. Day is defined as $R_n \geq 0$, night as $R_n < 0$.

	Data	Dry	Fetch	Dry and Fetch
Day	320	276	130	109
Night	265	232	92	81
Total	585	508	222	190

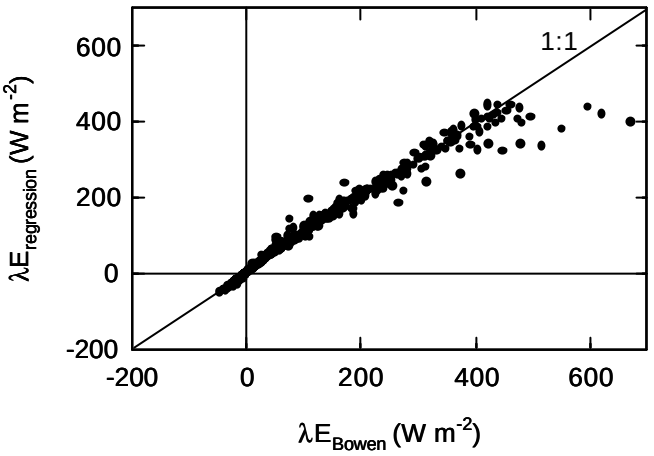

Figure 3.44 Comparison of the hourly latent heat flux derived from all Bowen data (lE_{Bowen}) measured between 5 till 27 August (n= 552) to the latent heat flux ($lE_{regression}$) derived from regression between R_n-S and $lE_{Bowen,select}$. $lE_{Bowen,select}$ is calculated from the Bowen ratio data measured during periods without precipitation and with adequate fetch.

The heat storage term S, important for the determination of the available energy (R_n-S)(see Equation 1.86), can be calculated in several ways. It can be calculated as described in Samson & Lemeur (2001)(see also § 3.5.2.1) or as 3 % of R_n, which is a typical value when the canopy is dry (McCaughey, 1985). For the selected Bowen ratio data (dry and fetch)(Table 3.12), the difference in latent heat flux for both mentioned methods to determine the available energy (R_n-S) only yielded a mean daily difference of 0.10 ± 0.03 mm, with the second method (S = 0.03 R_n) resulting in the lowest fluxes. This small difference between both methods was in contrast to what was expected (Aston, 1985a,b; Samson & Lemeur, 2001) and similar to the differences found for the Penman-Monteith approach (see § 3.5.3.4). This apparent

strange result was explained by the low and primarily positive values of b (Figure 3.43), and by the predominantly small difference in heat storage according to both calculation methods (Figure 3.46), and is illustrated in Figure 3.47. This last figure (Figure 3.47) shows that, at low and positive values of b, a difference in S for both determination methods will lead to small differences in lE, and this difference decreases as b increases. Only for negative b values the impact of both calculation methods for S on lE becomes more important.

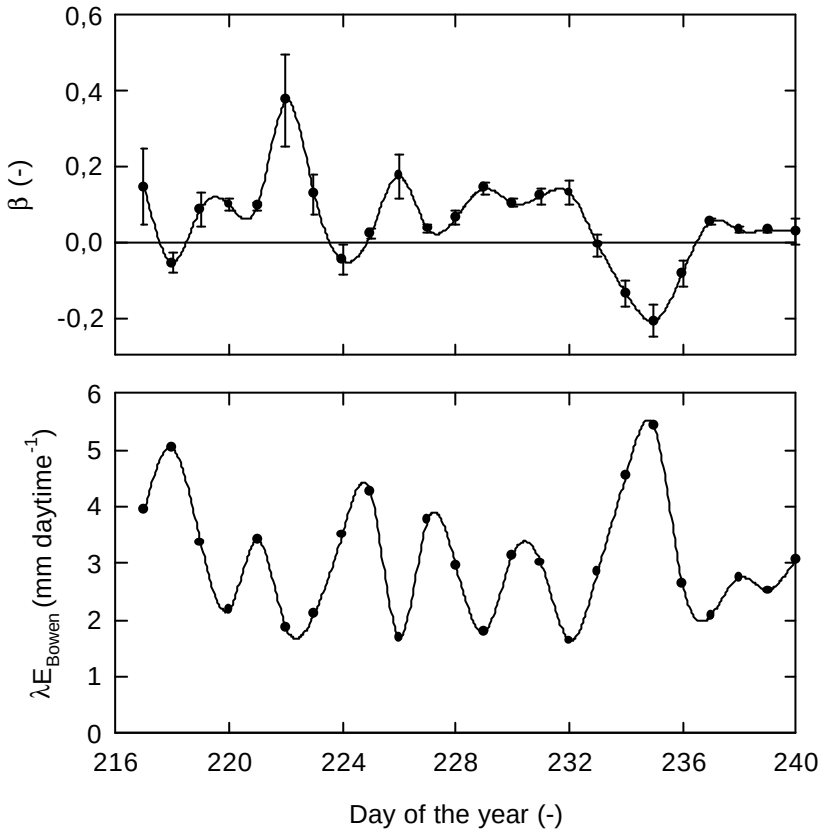

Figure 3.45 Daytime dynamics of mean (±SE) Bowen ratio (b)(above) and latent heat flux calculated from these Bowen ratio data (lE_{Bowen})(below) during the measurement period from 4 till 28 August, 1999. Daytime is defined as between 1000 and 1800 h.

3.6.3.3 Comparison between latent heat fluxes obtained from Bowen ratio and sap flow measurements

Figure 3.48 shows the diurnal behaviour of latent heat fluxes obtained from Bowen ratio (lE_{Bowen}) and upscaled sap flow ($lE_{F,L}$) measurements. Sap flow data of individual trees and species are scaled-up to the stand level as explained before (see § 3.4). As shown in Figure 3.48 the magnitude of $lE_{F,L}$ is sometimes very similar to lE_{Bowen} (Figure 3.48 right). Moreover, maximal and minimal values are observed at more or less the same time for both methods. However, the observed diurnal behaviour was not similar, and on most days there was a pronounced difference between both methods (Figure 3.48 left). Latent heat fluxes obtained from Bowen ratio (lE_{Bowen}) and sap flux ($lE_{F,L}$) measurements are confronted in Figure 3.49. As well for the selected period (dry and adequate fetch) as for the entire period the correlation between both methods was rather weak, but the highest correlation was calculated for the selected period (r^2 = 0.63)(Figure 3.49 right). Moreover, $lE_{F,L}$ underestimated lE_{Bowen} by more than 50 %. This underestimation was also observed when comparing daytime values of lE_{Bowen} and $lE_{F,L}$ (Figure 3.50).

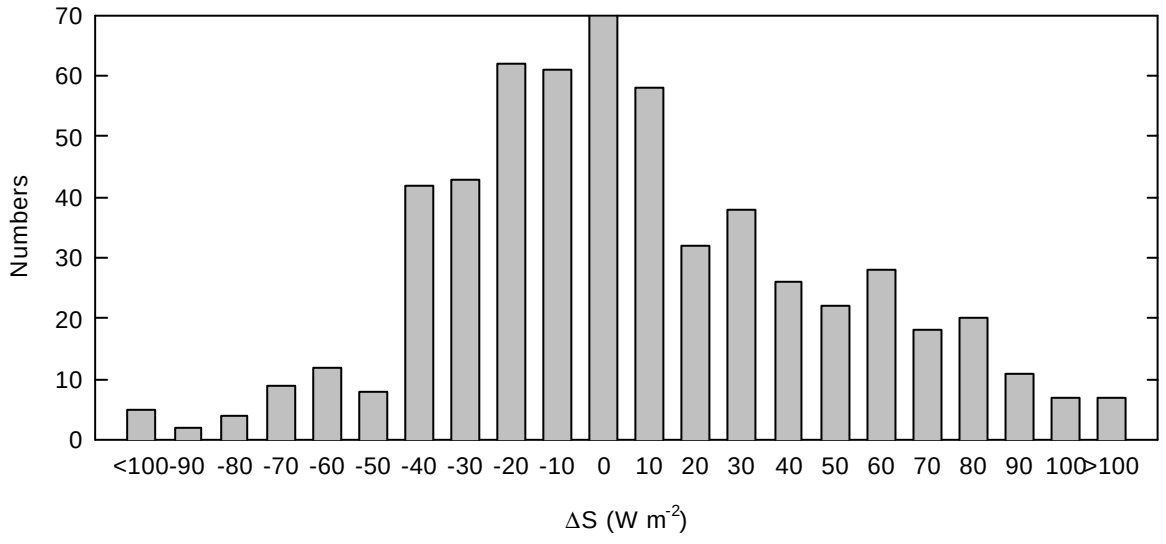

Figure 3.46 Distribution of the hourly difference in heat storage (*DS*)(*S* calculated according to Samson and Lemeur (2001) minus $S = 0.03R_n$) for the period 4-28 August, 1999.

The deviation between both methods can partly be explained by the fact that $\Delta E_{F,L}$ only takes the transpiration of upperstory and understory species into account and no herb layer transpiration and soil evaporation. Also, and probably more important, also evaporation of intercepted rain and dew from leaves, branches and stems is not considered. For a temperate deciduous forest, comparable to the forest Aelmoeseneie in terms of height and LAI, evaporation at the forest floor was typically less than 0.5 mm day^{-1} (Wilson et al., 2000), which does not explain the differences observed in Figures 3.48 till 3.50. So, also measurement errors in both methods (Bowen ratio and sap flow) and errors in the upscaling procedure (sap flow) will explain the differences in latent heat flux as observed in Figures 3.48 till 3.50. Another possible source of divergence between the sap flow and Bowen ratio data is

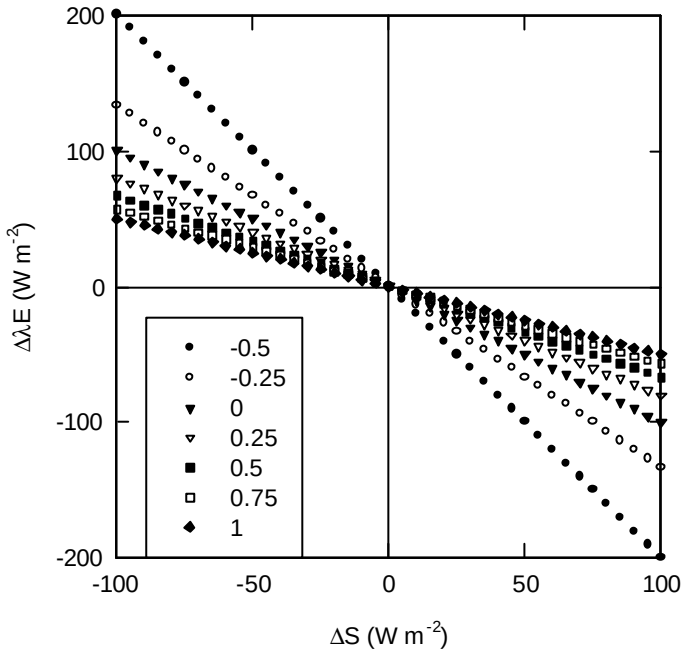

Figure 3.47 Sensitivity of the difference in latent heat flux ($\Delta\lambda E$)(latent heat flux calculated with S determined according to Samson and Lemeur (2001) minus latent heat flux calculated with S = 0.03R_n) to the difference in heat storage (ΔS) (S calculated according to Samson and Lemeur (2001) minus S = 0.03R_n), for different Bowen ratio values.

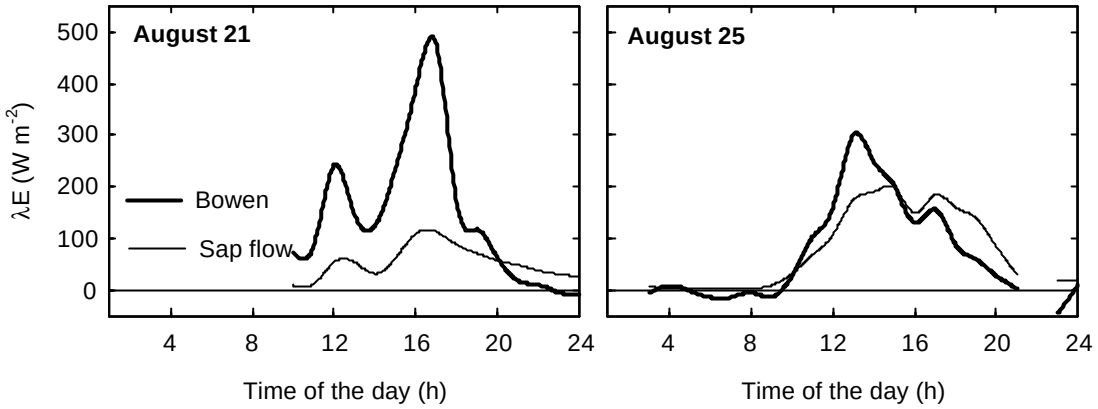

Figure 3.48 Diurnal behaviour of latent heat fluxes (*lE*) derived from Bowen ratio data (Bowen), and from sap flow measurements scaled-up to the level of the forest Aelmoeseneie (Sap flow), during two days without precipitation in August, 1999.

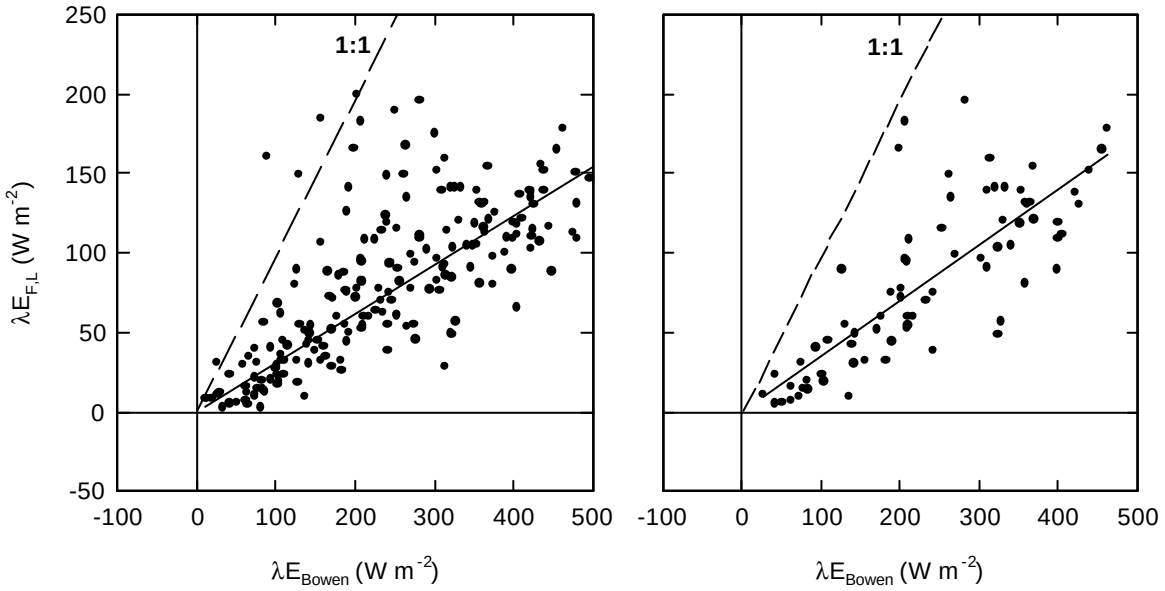

Figure 3.49 Comparison of hourly latent heat fluxes obtained from the measured Bowen ratio data (lE_{Bowen}) with latent heat fluxes scaled-up from sap flow measurements ($lE_{F,L}$), to the level of the forest Aelmoeseneie for: (left) the total measurement period, and (right) the measurement period without precipitation and with adequate fetch. The indicated data are measured from 4 till 28 August, 1999, and represent daytime data (between 1000 and 1800 h). The solid line is the fitted linear relationship.

the species composition used to scale up the sap flow estimates (see before § 2.1 and 3.4.2)(Wilson et al., 2001). Species composition is not constant within the tower footprint (Schmid, 1997), varying with wind direction and distance from the tower. As such, Wilson et al. (2001) observed a rather large difference between transpiration estimated from sap flow and evapotranspiration estimated from eddy covariance. These authors found that the ratio of transpiration estimated from sap flow over evapotranspiration estimated from eddy covariance amounted between 42 and 44 %. This is very close to the ratio of $lE_{F,L}$ over lE_{Bowen} observed in this study, i.e. this ratio was between 31 and 35 % (slopes of the linear relationships in Figure 3.49 and 3.50). In addition, and especially in case of the small forest Aelmoeseneie, the assumed advection (Figure 3.42) may also partly explain the observed differences between lE_{Bowen} and $lE_{F,L}$, as advection will influence the Bowen ratio measurements.

In general the BREB method seems to be a useful micro-meteorological method for estimating forest evapotranspiration on condition that the measurement system is improved. One of the possibilities to obtain more reliable data is the use of interchanging psychrometers, and using differential ventilated and shielded thermocouples for measuring air temperature.

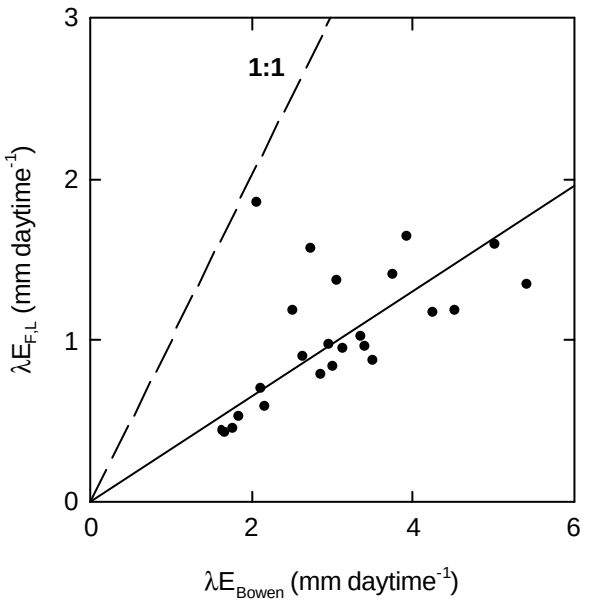

Figure 3.50 Comparison of daytime latent heat fluxes obtained from the measured Bowen ratio data (lE_{Bowen}) with latent heat fluxes derived from sap flow measurements ($lE_{F,L}$) scaled-up to the level of the forest Aelmoeseneie for the period 4 till 28 August, 1999. Daytime is defined as the hours between 1000 and 1800 h. The solid line is the fitted linear relationship.

Chapter 4
MODELLING APPROACH TO THE ACTUAL EVAPOTRANSPIRATION

Forest evapotranspiration is known to have an important impact on the regional and the global climate (Ogink Hendriks, 1995). Forest transpiration can be determined experimentally using various techniques (see Chapter 3). However, many of these techniques are labour intensive, require a large, expensive experimental set-up, and yield mostly discontinuous data sets. Although some techniques like sap flow measurements and eddy covariance measurements can be used during a long period of time (during several months or consecutive growing seasons), data are frequently missing due to e.g. technical malfunctions of sensors or to a non-valid footprint of the flux measurements. In these cases missing data can be interpolated. But if the time period of the missing data becomes too large, then extrapolation of data outside the measurement period can introduce serious errors (e.g. Cermak & Nadezhdina, 1998). Therefore, modelling forest evapotranspiration is very useful in order to scale up for missing data.

A basic stand inventory, together with eco-physiological information, and standard climatic data, often suffice to estimate forest transpiration with a model. The first two sets of input data only need to be established once. The model can yield continuous estimates of evapotranspiration and can also be used for prediction in specific, e.g. global change, situations. Such models can be very simple and consider the forest as one single layer, as is done with the big-leaf or the Penman-Monteith (Monteith, 1965) approach. More detail was introduced by Shuttleworth & Wallace (1985) as they developed a two-layer model consisting of both a canopy and a soil layer. However, a forest canopy is a very complex type of vegetation, with a vertical dimension that can easily reach 25 m of height. Baldocchi & Harley (1995), therefore, used a multi-layer model to describe CO_2-exchange in a temperate deciduous forest, assuming leaves with different physiological characteristics at different depths within the canopy.

In this fourth chapter, water use in the forest Aelmoeseneie will be determined by applying the one-layer Penman-Monteith approach to estimate evapotranspiration (see § 1.1.2.4 and § 1.2.2). A critical parameter in the Penman-Monteith approach is the canopy conductance which expresses the physiological control of water loss. Therefore, this parameter will be determined by inversion of sap flow measurements scaled up to the stand level. The dependence of this inverted canopy conductance on environmental factors will also be described. The canopy conductance determined

this way will allow realistic estimation of forest transpiration based on the one-layer approach.

Besides single-layer forest evapotranspiration, the forest (evapo)transpiration calculated from a multi-layer model (see § 1.2.3) will be evaluated, and a comparison between a single-layer versus a multi-layer model version will be analysed. In the multi-layer model the canopy conductance is replaced by the stomatal conductance. Therefore, also this parameter will be determined, but now from inversion of sap flow measurements at branch level. Model performance will also be evaluated in terms of its sensitivity to the driving climatic variables and to selected model parameters.

So, in the first part of this chapter as well canopy as stomatal conductance will be determined. In the second part of this chapter these conductances will be used as parameters in a single-layer and a multi-layer modelling approach respectively, to obtain forest evapotranspiration. Both model approaches will be evaluated and compared.

4.1 Forest canopy conductance and leaf conductance inverted from sap flow measurements of upperstory and understory species

4.1.1 Introduction

Transpiration fluxes from coniferous forests have been reported (e.g. Jarvis & McNaughton, 1986) to be largely controlled by canopy conductance (g_c). More recently, similar results were found for some deciduous forests such as beech forests (e.g. Herbst, 1995). This is because most forest canopies are aerodynamically rough and, hence, well ventilated. This minimises the control of transpiration by the aerodynamic conductance (Jarvis & McNaughton, 1986). The influx of carbon dioxide will be similarly constrained by g_c since both water vapour and CO_2 pass through the stomata. Therefore, the stomatal control is not only the key for the correct assessment of the transpiration rate and the water balance of forest stands. It is also an important determinant for estimation of carbon assimilation and net primary production. It is known that canopy conductance can be limited by high vapour pressure and soil water deficits (Cienciala et al., 1997).

Many evapotranspiration models contain conductance sub-models of various complexities. Variables such as solar radiation, vapour pressure deficit, soil water deficit or water potential, are considered as driving variables, and are commonly expressed as multiplicative factors which determine the value of g_c (e.g. Jarvis, 1976). Such “black box” models do not provide any ecophysiological information about mechanisms governing stomatal control, but, after calibration, they can mimic the actual conductance rather well for most modelling purposes. The specification of how the canopy conductance depends on the canopy micro-climate of the forest is a key element of a mechanistic modelling approach (Sakai et al., 1997).

Canopy conductance can be obtained from individual measurements of leaf conductance carried out at several layers in the canopy (Monteith, 1973; Lhomme, 1991), and complemented with the vertical distribution of leaf area and vertical gradients of climatic variables (Jarvis, 1995). However, the spatial variation of porometer measurements of leaf conductance is very large (Jarvis, 1995). Leverenz et al. (1982) calculated that, in a uniform monospecific Norway spruce canopy, the number of porometer readings required to produce an estimate of leaf conductance within 10 % of the mean value may exceed 150 readings at a particular moment of the day.

Another method to obtain surface conductance of a forest canopy relies on the inversion of the Penman-Monteith equation when (evapo)transpiration rate is known. Evapotranspiration rate can be estimated independently from micro-meteorological measurements, like the Bowen ratio as was done in Chapter 3 (§ 3.6)(see also Herbst, 1995; Ogink-Hendriks, 1995; Herbst et al., 1999; Granier et al., 2000b) and eddy covariance measurements (Köstner et al., 1992; Granier et al., 2000a,b). More recently, the canopy conductance has also been estimated from sap flow measurements which were scaled to the stand level (see § 3.4)(Köstner et al., 1992; Cienciala et al., 1997; Martin et al., 1997; Ewers & Oren, 2000; Granier et al., 2000a,b). These studies mainly focussed on monospecific stands (e.g. Granier et al., 2000a), or they compared canopy conductance of different species which were grown at different sites (e.g. Granier et al., 2000b).

The objectives of this part of the study are to estimate canopy and stomatal conductance by inversion of respectively transpiration rates at the canopy level and of transpiration rate at the branch level for several co-occurring species. The relationship between canopy and stomatal conductance and climatic variables will be described. Also, the coupling between the forest Aelmoeseneie and the atmosphere will be characterised by the decoupling and radiative decoupling coefficient, to estimate the role of stomatal control of forest transpiration. The study period is 4 till 31 August, 1999.

4.1.2 Material and Methods

4.1.2.1 Calculation of canopy and leaf conductance

The forest canopy conductance for water vapour (g_c, expressed in m s^{-1}) can be calculated from measurements of the transpiration rate of the stand and from climatic data, using the rearranged Penman-Monteith equation (see Granier & Loustau, 1994; Granier et al., 2000b, and Chapter 1, Equation 1.108)

$$r_c = \frac{r_{ah}}{\gamma \lambda E}\left[\Delta(R_n - S) + \frac{\rho_a c_p (e_s(T_a) - e_a)}{r_{ah}} - \lambda E(\Delta + \gamma)\right] \qquad (1.108)$$

which yields, knowing that $g = 1/r$,

$$g_c = \frac{g_{am}\,\lambda E\,\gamma}{\Delta(R_n - S) + \rho_a c_p (e_s(T_a) - e_a) g_{am} - \lambda E(\Delta + \gamma)} \qquad (4.1)$$

where E is the transpiration rate of the stand (kg m^{-2} s^{-1}), l is the latent heat of vaporisation (J kg^{-1}), g is the psychrometer constant (Pa °C^{-1}), D is the slope of the saturating vapour pressure with temperature (Pa °C^{-1}), (R_n-S) is the available energy of the forest canopy (W m^{-2}), r_a is the density of dry air (kg m^{-3}), c_p is the specific heat capacity of the air (J °C^{-1} kg^{-1}), $e_s(T_a)$ is the saturated vapour pressure (Pa) at air temperature (T_a, expressed in °C), e_a is the actual vapour pressure (Pa), and g_{am} is the aerodynamic conductance (m s^{-1}).

In Chapter 1 a theoretical distinction was made between the aerodynamic resistance for momentum (r_{am})(Equation 1.90) and sensible heat flux (r_{ah})(Equation 1.91). To be able to calculate r_{ah}, the roughness length for sensible heat flux z_{0h} should be known. Whereas z_0 can be inferred easily from the wind profile relationship (see below § 4.2.2.4), only an estimate of z_{0h} can generally be obtained (Troufleau et al., 1997). This means that the value of z_{0h}, and thus r_{ah}, is uncertain. Therefore, and also because it is commonly practice when calculating forest evapotranspiration (e.g. Herbst, 1995) r_{am} and r_{ah} are assumed to be equal, so that r_{ah} in Equation 1.108 was replaced by r_{am} (and thus g_{am}) in Equation 4.1.

The aerodynamic conductance (g_{am}) was calculated from (Thom, 1975):

$$r_{am} = \frac{\left[\ln\left(\frac{z-d}{z_0}\right)\right]^2}{k^2 u} \qquad (1.90)$$

which yields, knowing that $g_{am} = 1/r_{am}$,

$$g_{am} = \frac{k^2 u}{\ln^2\left[(z-d)/z_0\right]} \qquad (4.2)$$

with $z_0 = 0.1h_c$ and $d = 0.81h_c$, h_c being the height of canopy. The structural parameters z_0 and d are determined from wind speed measurements at four heights above the canopy (see below § 4.2.2.4, § 4.2.3.1, and De Bie, 1998). The measured values for z_0 and d are very close to those arbitrarily chosen by Herbst (1995) above a beech forest with a canopy height of 29 m. Available energy (R_n-S) was calculated as explained before (see § 3.5). Stand transpiration rate E is derived from sap flow measurements scaled up to the stand level for a uniform beech, oak and ash forest, and for the forest Aelmoeseneie (see § 3.4). Stand transpiration rate E includes as well upperstory as understory transpiration.

Leaf conductance to water vapour transport (g_v, m s^{-1}) can be calculated with Fick's law as was explained in Chapter 1 (Equation 1.8). Putting $g_v = 1/r_v$, Equation 1.8 becomes:

$$g_v = \frac{E_L}{\rho^\circ(T_l) - \rho_v} \qquad (4.3)$$

where E_L is the transpiration rate per unit leaf area (kg m^{-2} s^{-1}), and $\rho^\circ(T_l)$ is the saturated water vapour density of the substomatal cavity (kg m^{-3}) at leaf temperature (T_l, expressed in °C), and ρ_v the water vapour density of the air near the leaf surface (kg m^{-3}). When leaf and air temperature are similar, a condition that occurs for small leaves exposed to a sufficiently high wind speed (Herbst, 1995; Martin et al., 1999), which was observed in this forest (Samson & Lemeur, 2000), the vapour density deficit of the air can be used as an approximation of $\rho^\circ(T_l) - \rho_v$ (Monteith and Unsworth, 1990). In this situation the leaf boundary layer conductance (g_b) is very high compared to stomatal conductance (g_s), and thus can be neglected, so that g_v in Equation 4.3 can be approximated by the value of g_s. The vapour density deficit of the air was measured above the canopy. Transpiration rate (E_L) is obtained from sap flux density per unit leaf area (F_{LA}, kg m^{-2} s^{-1}) measured at the branch level (see above Chapter 3, § 3.1) of beech at three heights in the crown (21, 14 and 7 m), of ash (21 m), sycamore and hazel.

For computing g_c and g_s from transpiration rate and climatic variables, some precautions were taken (Herbst, 1995; Granier et al., 2000b):
-only complete hourly data sets were used;
-only data from the period in which leaves were fully expanded (July-September) were used;
-only data from daylight periods in which the canopy was dry were used. Periods during rainfall and for the 2 hours following rainfall were excluded in order to avoid the discrepancy between evaporation and tree transpiration;
-when either PAR or vapour pressure deficit of the air (D) were too low (< 5 % of the maximum value, data were eliminated, because of the large relative uncertainties in computing g_c from Equation 4.1 under these conditions (Granier et al., 2000b).
Typically, discarded data correspond to early morning and late afternoon periods. Furthermore, when D is low during the early morning, dew is quite likely to occur and affects tree transpiration and its measurements. The entire data set, ten minute values, was collected between 4 till 31 August, 1999, and data were selected according to the above listed criteria. From the remaining ten minute data set (n=1146), spread over 27 days, g_c and g_s were calculated as described above (Equations 4.1 and 4.3). The remaining values of g_c and g_s are referred to as measured values below.

According to Granier et al. (2000b), excluding the data as described above has only limited consequences on calibrating the g_c functions, because they represent periods of low transpiration rates. Modelling stand transpiration under conditions of maximum transpiration rates, i.e. when both D and g_c are high (and therefore the product $g_c.D$ is high), is more crucial.

A time lag between the sap flow measured in stems and canopy transpiration has been frequently reported (e.g. Granier & Bréda, 1996). This capacitance effect has often been reported for coniferous species (e.g. Granier & Loustau, 1994), the time lag being typically in the range of 1 to 2 h. The time lag seems to be less important for broadleaved species [e.g. 30 min for oak (Granier & Bréda, 1996) and 60 min for poplar (Hinckley et al., 1994)]. Tests of cross-correlation between data of E or F_{LA} and D in this study suggest a time lag of the same order as was mentioned by the last authors (see also § 3.1). For an accurate calculation of canopy and stomatal conductance, it is therefore necessary to take this time lag into account in order to improve the synchronism between sap flow and climatic demand (e.g. Granier et al., 2000b). Cross-correlation analyses were performed using SPSS Release 10.0.5 (SPSS Inc., Chicago, Illinois, USA). Increasing time lags (from 0 to 120 min in steps of ten minutes) were introduced in the calculation of g_c and g_s, so that sap flow was lagging behind climatic variables. The time lag was assumed to correspond to the highest correlation coefficient obtained.

4.1.2.2 The canopy conductance and leaf conductance submodel

According to Jarvis (1976), stomatal conductance is a function of solar radiation, specific humidity deficit, temperature, leaf water potential and ambient CO_2 concentration. He described the relation between the stomatal conductance and these variables in a synergistic model, where the maximum stomatal conductance is reduced by stress functions. These stress functions are assumed to act independently. The coefficients of the relationships are estimated from field data by a technique of non-linear least squares. Stewart (1988) modified this model to describe the surface conductance of a pine forest. This approach is now widely used (e.g. Dolman & van Den Burg, 1988; Granier & Loustau, 1994; Ogink-Hendriks, 1995; Granier & Bréda, 1996). The following models were described in Chapter 1 (see § 1.2.2 and 1.2.3), to describe canopy (g_c) and stomatal (g_s) conductance respectively:

$$g_c = g_{c,\max}\left(L/L_{\max}\right) f(PAR) f(\Delta q) f(T_a) f(\Delta \boldsymbol{q}) \quad (1.181)$$

and

$$g_s = g_{s,\max}\, f(PAR) f(\Delta q) f(T_a) f(\Delta \boldsymbol{q}) \quad (1.194)$$

where $g_{c,max}$ and $g_{s,max}$ are the maximum canopy and stomatal conductance respectively (m s^{-1}), *f(PAR)* is a visible radiation function (Equation 1.180), *f(Dq)* is a specific humidity deficit function (Equation 1.177), $f(T_a)$ is an air temperature function (Equation 1.178) and *f(Dq)* is a soil moisture deficit function (Equation 1.179)(see also § 1.2.2.3). All functions yield a value between 0 and 1, as they express a reduction with respect to the maximum conductance. For calculation of the canopy conductance (Equation 1.181) also the LAI was taken into account, with *L* the LAI of the forest at the considered moment in the growing season, and L_{max} the maximal LAI of the forest during the growing season (both expressed in m^2 m^{-2}). However, because applying these equations (Equations 1.181 and 1.194) to our data set resulted in very low correlation coefficients, other mathematical descriptions were fitted to the available data set.

For a mathematical description of the dependence of g_c and g_s on light and humidity conditions above the forest, which can be used to simulate g_c and g_s for other time periods and sites if light and *D* are available, Lohammar-type equations (Lohammar et al., 1980) were used for describing the combined effects of both variables. As Lohammar-type equations have already been applied successfully to several European forests (e.g. Halldin et al., 1984; Herbst, 1995; Granier et al., 2000b), it allows comparison with our data. In its general form these relationships can be written as:

$$g_i = g_{i\max} \cdot f(R_x) f(D) \cdot f(LAI) \cdot f(T_a) \quad (4.4)$$

where g_{imax} is the maximum g_i (the subscript *i* refers to the fact that Equation 4.4 can be used to calculate g_c and g_s), reduced by functions between 0 and 1 dependent of radiation (R_x), vapour pressure deficit of the air (*D*) measured above the stand, leaf area index (function as shown in Figure 1.11) and air temperature (T_a). Equation 4.4 does not include a soil moisture deficit function as was the case in Equations 1.181 and 1.194. Due to technical problems soil water content during the measurement period (4 till 28 August) could not be measured. However, precipitation during this period was 117 mm, so that soil water availability was assumed to be non-limiting. A comparable assumption was made by Cienciala et al. (1997).

Some of such relationships are listed below:

$$g_i = g_{i,\max}\frac{R_x}{R_x + a}\left(b - c\ln D\right) \quad (4.5)$$

$$g_i = g_{i,\max}\left(a + bR_x\right)\left(c + dD\right) - f \quad (4.6)$$

$$g_i = g_{i,\max}\frac{R_x}{R_x + a}\exp\left(-bD\right) \quad (4.7)$$

$$g_i = g_{i,\max}\left(a - bR_x\right)\left(c + d\exp\left(eD\right)\right) - f \quad (4.8)$$

where the subscript *i* refers to the fact that Equations 4.5 till 4.8 can as well be used for calculating g_c as g_s (m s^{-1}), *D* is the vapour pressure deficit of the air (hPa), *a* till *e* are coefficients found by fitting the equations to the data set, and R_x represents PAR (µmol m^{-2} s^{-1}). Just as Herbst (1995), we used PAR as input parameter in Equation 4.5 till 4.8, instead of short-wave radiation (e.g. Granier et al., 2000b) or R_n (e.g. Martin et al., 1997). A strong linear relationship was observed between PAR, short-wave radiation and R_n (r^2 = 0.99 in all cases).
As well to obtain canopy as stomatal conductance, the different forms of Equation 4.4 (i.e. Equations 4.5 till 4.8) were fitted to the data set. First, coefficients of $f(R_x).f(D)$ (Equations 4.5 till 4.8) were fitted under non-limiting temperature. Then $f(T)$ was separately fitted. The entire data set (see above § 4.1.2.1) was divided in two sub sets: one data set (data set I) was used for parameterisation of the model (i.e. Equations 4.5 till 4.8), while the other (data set II) was used for validation of the model. Just as Gash et al. (1989) and Ogink-Hendriks (1995) the two sub sets were obtained by dividing the complete data set in subsets of alternate days. Data set I (even days) contained 519 data, while data set II (odd days) contained 627 data.

4.1.3 Results and discussion

4.1.3.1 Effects of radiation, vapour pressure deficit and temperature on canopy conductance

The fitting of g_c needs to take into account the effect of water exchange between the sap flow in the xylem and the surrounding tissues. This creates a time lag between transpiration and sap flow (e.g. Martin et al., 1997; Ewers & Oren, 2000). The procedure to test such a capacitance effect was similar to the one described by Granier et al. (2000b), but now using ten minute time steps instead of half hourly time steps. For the fitting of g_c correlation coefficients increased when estimates of g_c were limited to conditions in which $D \geq 10$ hPa. Ewers & Oren (2000) found that

errors in mean stomatal conductance for the canopy decreased to less than 10 % at $D \geq 10$ hPa.

Transpiration of the forest Aelmoeseneie was calculated from the transpiration of a uniform beech, oak and ash forest, taking the respective time lag for these forests into account, and considering the contribution of these species in the forest Aelmoeseneie as explained in Chapter 3 (see § 3.4). The time lags found were very small, namely ten minutes, for the different uniform forests (beech, oak and ash), and thus also for the forest Aelmoeseneie. Granier et al. (2000a) did not observe any time lag for beech, but used half hourly values for the analysis, and did not include understory transpiration.

The relations between the canopy conductance g_c found by Equation 4.1 and the driving climatic variables is shown in Figure 4.1 for the forest Aelmoeseneie. Comparable patterns were observed by e.g. Ogink-Hendriks (1995). To describe the relation between g_c and the climatic variables Equation 4.5 yielded the best results. The coefficients of Equation 4.5 are shown in Table 4.1 for the different uniform forests and the forest Aelmoeseneie. When the response of g_c to both variables PAR and D was extracted, then no significant relationship between the g_c residuals and air temperature T_a was detected. This might result from the high correlation between air temperature T_a and vapour deficit D (as shown in Figure 4.2), or from the rather narrow range of air temperatures as the observations were made during a summer period with no warm nor cold spell. The correlations shown in Table 4.1 were not very high, especially for the ash forest, but they compared well to literature values (e.g. see Granier et al., 2000a,b). These low correlations can be attributed to errors in the estimation of the transpiration rate of the stand [errors in sap flow measurements and/or upscaling (see e.g. § 3.4)] and the other variables contained in Equation 4.1.

Table 4.1 The parameters and coefficients of Equation 4.5 as obtained by least-square analysis for data set I, and the variance explained by the equation for the determination of canopy conductance of a uniform beech, oak; ash forest and of the forest Aelmoeseneie (all forests including upperstory and understory transpiration).

Forest	$g_{c,max}$	a	b	c	r^2
Beech	0.0251	245	1.249	0.389	0.78
Oak	0.0125	30	1.276	0.376	0.77
Ash	0.0146	120	1.268	0.383	0.32
Aelmoeseneie	0.0176	119	1.259	0.383	0.80

Comparing our results of canopy conductance with literature data is not easy, but can best be done by comparing values of maximum conductance $g_{c,max}$. A major problem

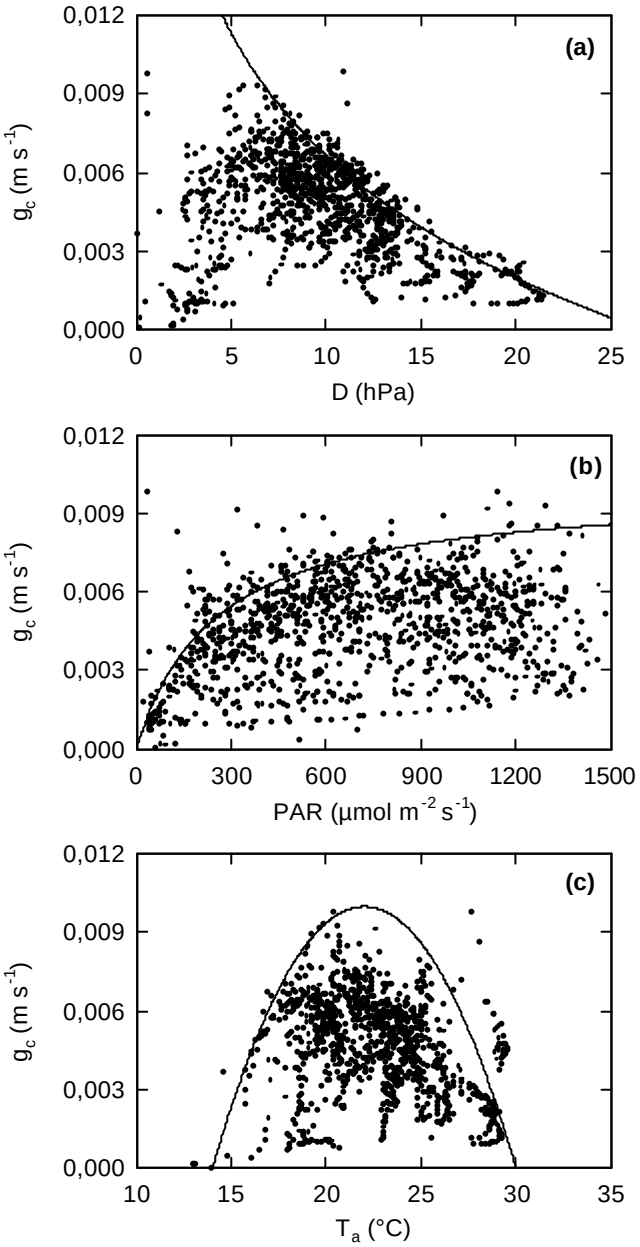

Figure 4.1 Scatterdiagrams showing the relation between ten minutes values of canopy conductance (g_c) of the forest Aelmoeseneie and (a) air vapour pressure deficit of the air (D), (b) PAR and (c) air temperature (T_a) for the period August 4-31, 1999. Fitted lines are for (a) and (b) from Equation 4.5 (see also Table 4.1), and for (c) from Equation 1.178.

is that $g_{c,max}$ obtained here (statistically derived $g_{c,max}$ values) are different in nature in comparison with directly observed values (Bernhofer & Gay, 1989). Moreover, $g_{c,max}$ values depend both on the type of the mathematical model and the particular data

set used. Ogink-Hendriks (1995) found when using different data sets that $g_{c,max}$ values for an oak forest ranged between 0.037 and 0.073 m s^{-1}. Another problem is that if conductances are inferred from micro-meteorological data (e.g. Bowen ratio data) instead of upscaled sap flow data, the bulk surface conductance rather than the canopy conductance is obtained. The former conductance also includes aspects of soil evaporation (Kelliher et al., 1995). If however, the leaf area index of the forest is large, then bulk surface conductance should be close to canopy conductance because soil evaporation tends to zero (Kelliher et al., 1995). Granier et al. (2000b) found for forest stands with a LAI of five a value of 0.0337 m s^{-1} for $g_{c,max}$, while Sakai et al. (1997) reported a $g_{c,max}$ value of around 0.0200 m s^{-1} for a deciduous forest in central Massachusetts. And a mean canopy conductance for temperate deciduous forests of 0.0207 $\pm$ 0.0070 m s^{-1} was found by Kelliher et al. (1995). As such the values of $g_{c,max}$ found in this study correspond rather well with the ones reported in literature.

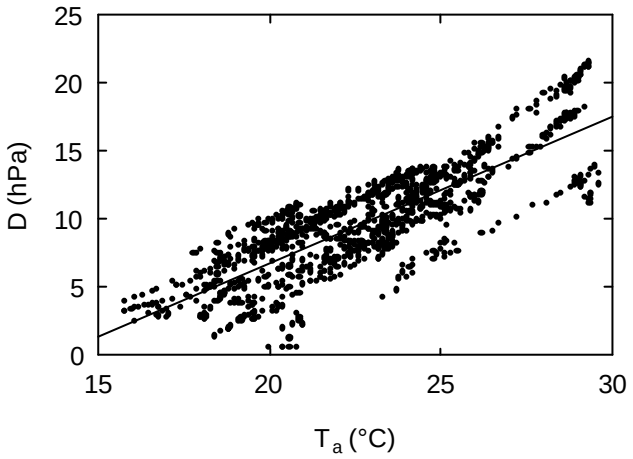

Figure 4.2 Relation between ten minute averages of air temperature (T_a) and vapour pressure deficit of the air (D) for the period August 4-31, 1999. The line represents the observed relationship: $D = 1.07T_a - 14.7$ ($r^2 = 0.71$)

Our canopy conductance function for beech forest (Table 4.1) matched closely (if D is not too high) with those reported by Herbst (1995) and Granier et al. (2000a) also for beech forests. Just as did Granier et al. (2000a) the estimates of g_c presented here are compared to the two models of Herbst (1995), and the one published by Granier et al. (2000a). This is shown in Table 4.2 for different combinations of the climatic variables PAR and D. For low values of PAR and D, the relative differences are of an order that would lead to differences in forest stand transpiration of less than 10 % (Granier et al., 2000a). Granier et al. (1996) previously reported such similarities in the diurnal pattern of g_c when comparing various forest ecosystems.

However, Granier et al. (2000a) mentioned that, when comparing canopy conductance in different forest stands, it seems that the LAI plays a more important role than species composition. For high values of *D* and PAR the model used here gives lower g_c values compared to the other models mentioned in Table 4.2. The model parameters found were obtained for conditions of high vapour pressure deficit (D > 10 hPa) and high values of PAR. Figure 4.3 thereby illustrates that during midday and afternoon, periods with high values of *D* and PAR, the simulated g_c values corresponded very well with the measured ones. Deviations increased during periods of low *D* although for these circumstances the model estimates corresponded rather well with the ones calculated with the models of Herbst (1995) and Granier et al. (2000a). This is shown in Table 4.2.

Table 4.2 Modelled canopy conductance (Equation 4.5) in comparison with the results obtained with the two models (H1 and H2) of Herbst (1995) and the model (G1) of Granier et al. (2000a). Conditions are full leaf expansion, adequate soil moisture availability, and different combinations of PAR and vapour pressure deficit of the air (*D*). All models were fitted for a beech stand.

PAR (μmol m^{-2} s^{-1})	D (hPa)	% difference H1	% difference H2	% difference G1
500	5	25	-4	7
500	10	29	-11	15
1200	10	50	72	39
1200	20	246	272	231

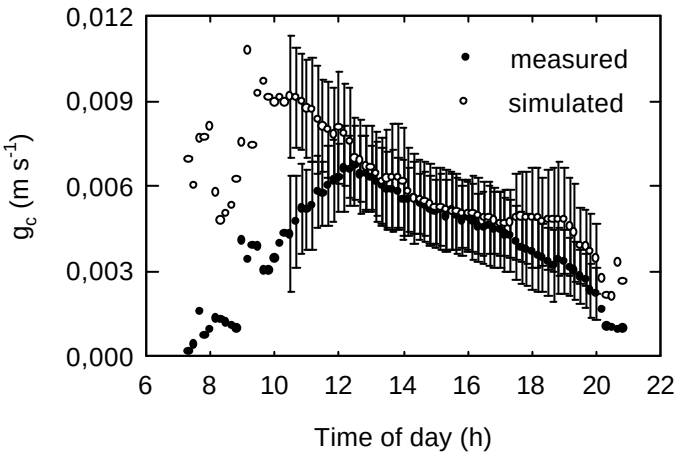

Figure 4.3 Mean diurnal course of ten minute averages of simulated (derived from data set I) and measured (data set II) canopy conductance (g_c) for the period August 4-31, 1999. Each vertical bar represents one SE of the mean.

4.1.3.2 Effects of radiation, vapour pressure deficit and temperature on stomatal conductance

Just as was done for the canopy conductance the capacitance effect in branches of beech, ash and for sycamore and hazel was tested using the cross correlation of the data of sap flux density per unit leaf area (F_{LA}) and the vapour deficit (D). This technique was also applied by Ewers & Oren (2000). The time lag now varied between 0 (middle and lower crown layer of beech, and the understory species) and 30 minutes (upper crown layer of beech and ash). After correction of F_{LA} by the obtained lag for the respective species, g_s was calculated with Equation 4.3.
The relationship between the stomatal conductance (g_s) and climatic variables is shown in Figure 4.4. The relationship between g_s and vapour pressure deficit is more scattered than the equivalent relationship for canopy conductance (g_c)(Figure 4.1). However, for D < 15 hPa the relationship between g_s and D becomes more or less linear. The relationship between g_s and PAR is also quasi-linear, suggesting that both D and PAR inside the crown canopy are the main factors limiting stomatal conductance and transpiration rate. The used equations, and the coefficients of these equations are shown in Table 4.3 for the different species and canopy layers. Just as was the case for g_c, considering air temperature as an extra variable influencing g_s did not improve the found relationships.

The correlation obtained for stomatal conductance (Table 4.3) was lower than the one found for canopy conductance (Table 4.1). These weaker relationship is explained by shading effects and a variable micro-climate deeper in the crown canopy compared to the micro-climate prevailing above the canopy (see e.g. Figure 2.5). Ewers and Oren (2000) found no vertical differences in air temperature and D with height, but their forest was less high (± 10 m) and also LAI was lower (between 1.8 and 3.6). For hazel no meaningful relationship was found between stomatal conductance and any of the considered climatic variables (D, PAR, T_a).

Values of maximal stomatal conductance ($g_{s,max}$) are an order of magnitude lower than the ones for canopy conductance. They are also lower compared to values found in literature. Dolman & Van Den Burg (1988) found $g_{s,max}$ values for oak between 0.0053 and 0.0106 m s^{-1}, and Kelliher et al. (1995), for temperate deciduous forests, reported a mean $g_{s,max}$ value of 0.0046 ± 0.0017 m s^{-1}. Separate measurements performed with a porometer (AP4, dynamic diffusion porometer) yielded direct values that were higher than those inferred from sap flow measurements. Maximal stomatal conductance measured with a porometer was 0.0093 m s^{-1} for ash, 0.0057, 0.0036 and 0.0025 m s^{-1} for respectively the upper, middle and lower crown layer of beech, and 0.0019 m s^{-1} for hazel (see also Table 1.10). These porometer data are closer to the literature values mentioned above.

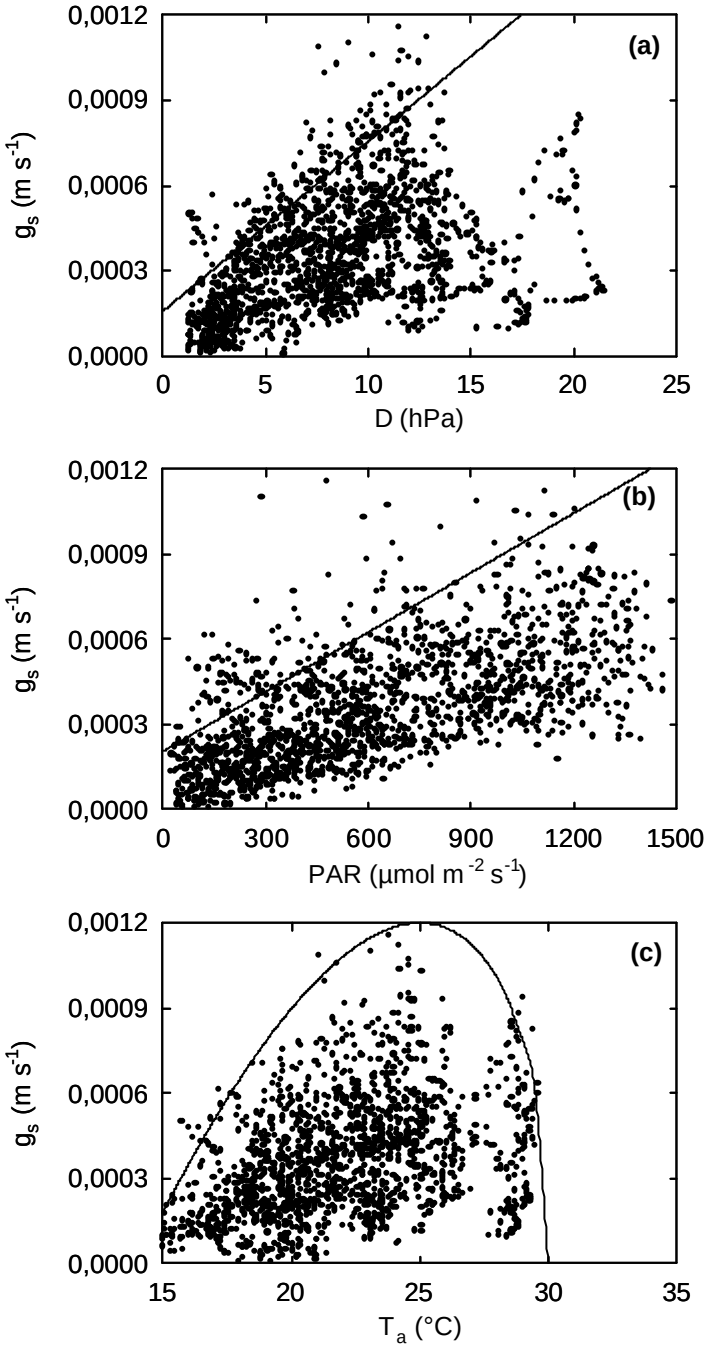

Figure 4.4 Scatterdiagrams showing the relation between ten minutes values of stomatal conductance (g_s) of beech at 21 m and (a) air vapour pressure deficit of the air (D), (b) PAR and (c) air temperature (T_a) for the period August 4-31, 1999. Fitted lines are for (a) and (b) from Equation 4.6 (see also Table 4.3), and for (c) from Equation 1.178.

The low $g_{s,max}$ values obtained from the sap flow measurements of this study (Table 4.3) can be explained by different reasons. The use of different equations makes comparison between the different $g_{s,max}$ values difficult. Moreover, the calculation of g_s uses a D value which is measured above the canopy, while the actual vapour pressure deficit at different crown levels is not the same. A lower D is observed closer to the ground level, and the introduction of this D into Equation 4.3 will result in a higher g_s and, hence, higher $g_{s,max}$ values. Another reason can be that the assumption of a negligible boundary layer conductance is not valid anymore at low crown levels. Even when the forest is highly coupled to the atmosphere (see below § 4.1.3.3), the wind speed will decrease with depth down the canopy (see Figure 1.13), this would mean that g_v in Equation 4.3 represents stomatal and boundary layer conductance ($1/g_v = 1/g_s + 1/g_b$). So, when this boundary layer would be taken into account, Equation 4.3 would result in higher g_s and, hence, $g_{s,max}$ values.

Table 4.3 Parameters and coefficients of the selected models as obtained by least square analysis for data set I, and the variance explained by the equation for the determination of stomatal conductance of beech at 21, 14 and 7 m (respectively B21, B14 and B7), ash at 21 m (A21) and sycamore (S).

Species	Parameter							
(model)	$g_{s,max}$	a	b	c	d	e	f	r^2
B21(A)	0.00121	0.0705	0.0001	1.559	0.60	-	0.00013	0.50
A21(B)	0.00189	1089	0.0015	-	-	-	-	0.36
B14(C)	0.00102	51.55	0.02	-0.0013	0.0018	0.195	0.00001	0.55
B7(C)	0.00063	47.91	0.01	-0.0080	0.0091	0.0092	0.00002	0.59
S(A)	0.00021	0.3412	0.0002	0.415	0.076	-	0.00002	0.55

Model A: $g_s = g_{s,\max}(a + bPAR)(c + dD) - f$ (Equation 4.6)

Model B: $g_s = g_{s,\max}\frac{PAR}{PAR + a}\exp(-bD)$ (Equation 4.7)

Model C: $g_s = g_{s,\max}(a - bPAR)(c + d\exp(eD)) - f$ (Equation 4.8)

Figure 4.5 illustrates the relationship between simulated and measured stomatal conductance. In early morning the measured stomatal conductance was higher than the simulated values, while at evening the reverse was observed. However, during these periods of the day vapour pressure deficit of the air is normally not very high, so that errors in the estimate of transpiration will be limited. In the second part of the afternoon measured stomatal conductance was again higher than simulated values, while during this period of the day the atmospheric demand for water vapour can be rather high, so that important errors can occur in the estimates of transpiration. However, during the largest period of the day there is a good agreement between measured and simulated stomatal conductance. In Figure 4.3 a sudden increase in

canopy conductance was observed during morning, and a slow decrease from midday till evening. More or less the reverse was observed for stomatal conductance (Figure 4.5). Moreover, maximal canopy conductance was obtained during midday, whereas stomatal conductance reached a maximum at the end of the afternoon. These different diurnal dynamics of stomatal and canopy conductance are explained by the totally different nature of both conductances, the different equations used to obtain them (Equation 4.1 versus Equation 4.3), and the different micro-climate in the canopy compared to the micro-climate prevailing above the canopy.

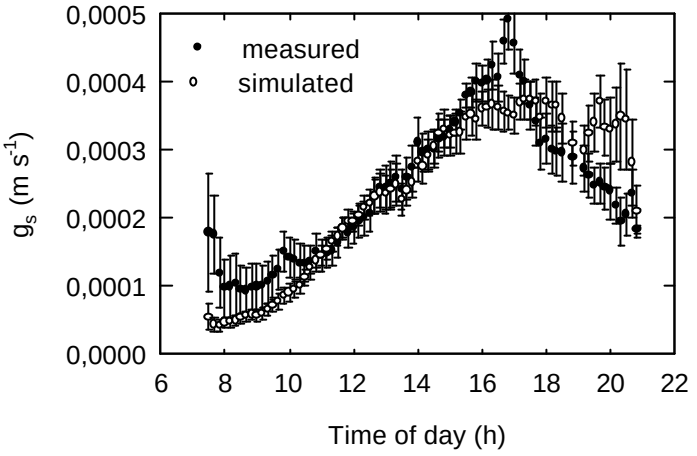

Figure 4.5 Mean diurnal course of ten minute averages of simulated (derived from data set I) and measured (data set II) stomatal conductance (g_s) for beech at 7 m for the period August 4-31, 1999. Each vertical bar represents one SE of the mean.

4.1.3.3 Stomatal control of transpiration

The canopy conductance can be used to describe the coupling between the canopy and the atmosphere in terms of the radiative decoupling coefficient (W_r). The decoupling coefficient (W) was introduced by Jarvis & McNaughton (1986), and can be expressed as (see also Chapter 1, § 1.1.2.5):

$$\Omega = \frac{\Delta/g + 1}{\Delta/g + 1 + g_{ah}/g_c} \qquad (4.9)$$

where g_{ah} and g_c are the aerodynamic conductance for sensible heat transfer and canopy conductance respectively, both expressed in m s^{-1}, g is the psychrometer constant (Pa °C^{-1}) and D is the slope of the saturating vapour pressure with temperature (Pa °C^{-1}). Martin (1989) redefined the decoupling coefficient W in terms of a radiative transfer conductance (g_r)(see § 1.1.2.5). Following Jarvis & McNaughton (1986) and Martin (1989), W_f was calculated as:

$$\Omega_r = \frac{\Delta/g + 1 + g_r/g_{ah}}{\Delta/g + 1 + g_{ah}/g_c + g_r/g_c + g_r/g_{ah}} \qquad (4.10)$$

The main difference between W and W_f is that the latter, besides the convective coupling, also describes how closely the vegetation is coupled radiatively to the air around it.
An W_f value close to 0 indicates a strong coupling of the canopy to the surrounding air, with transpiration being controlled mainly by the degree of opening of the stomata. On the other hand, a value for W_f close to 1 indicates a canopy which is decoupled from the atmosphere by a thick boundary layer and which leads to local equilibrium values of air humidity near the evaporating surfaces. In this circumstance, transpiration is no longer controlled by the stomata but by the net amount of absorbed energy.

Mean values of aerodynamic and canopy conductance, and of W_f and W for the forest Aelmoeseneie are given in Table 4.4. Values of W_f and W were calculated for the same period and data set as used to calculate canopy conductance, and the mean values reported in Table 4.4 are calculated from all these values. The mean aerodynamic conductance of the total forest was almost two orders of magnitude higher than the mean canopy conductance. The mean radiative decoupling coefficient was significantly lower (P = 0.002) than mean W (Table 4.2). However, both methods showed an almost identical mean diurnal pattern (Figure 4.6), and during some moments of the day values were almost identical. Therefore, it can be concluded that the radiative conductance does not seem to be of major importance to describe the coupling of the forest Aelmoeseneie to the atmosphere. This means that the forest Aelmoeseneie is well coupled radiatively to the air around it ($g_r \rightarrow 0$). This would indicate that the forest is in radiative equilibrium with the air around it, i.e. the long-wave radiative loss from the surface is small.

In Figure 4.6 it is shown that the dynamics of both W_f and W during morning and afternoon differs. A rather steep increase was observed in the morning, whereas during the afternoon the values were decreasing slowly. This diurnal dynamics can be explained by the diurnal dynamics of canopy conductance (Figure 4.3). In early morning the forest is strongly coupled to the atmosphere, which means, as was

mentioned before, that transpiration is mainly controlled by the degree of opening of the stomata. Indeed, in early morning stomata are (almost) closed, and consequently there is no or little transpiration. When atmospheric conditions in the morning start to become favourable for photosynthesis, stomata will open, and canopy conductance will sharply rise (see Figure 4.3). After this sharp rise, at higher values of canopy conductance, the same increase in the degree of stomatal opening will have less impact on transpiration as before, as the aerodynamic conductance will be somewhat more limiting for transpiration. The forest is then less coupled to the surrounding air (Figure 4.6). In the afternoon, when canopy conductance slowly decreases (Figure 4.3), canopy conductance will again slowly become a more limiting factor for transpiration. So, transpiration becomes again more sensitive to the degree of stomatal opening, and the forest again becomes more coupled to the atmosphere.

Table 4.4 Mean values of the canopy conductance (g_c) of the forest Aelmoeseneie, the aerodynamic conductance (g_a), the radiative decoupling coefficient (W_r) and of the decoupling coefficient (W). Results for daylight periods in which the canopy was dry during the period 4 till 31 August, 1999. Input data for the calculations were data set I and II.

	g_c (m s^{-1})	g_a (m s^{-1})	Ω_r (-)	Ω (-)
Mean	0.005	0.256	0.069	0.076
SE	0.001	0.004	0.001	0.002

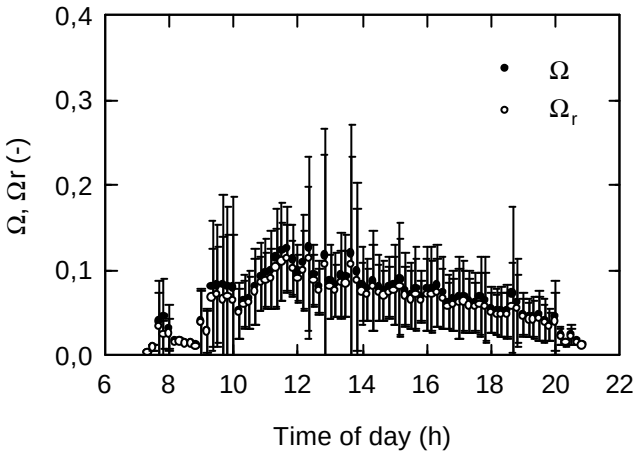

Figure 4.6 Mean diurnal pattern of the radiative decoupling coefficient W_r and the decoupling coefficient W for the period August 4-31, 1999. Each point represents a ten minute average, each vertical bar one SE.

Just as was found by Herbst (1995), Herbst et al. (1999) and Granier et al. (2000a) for beech forests, the average value of Ω remained lower than 0.2 throughout the day. Only for situations of very low wind speeds (u < 0.7 m s^{-1}), higher Ω-values were obtained (only 3 % of the cases). Granier & Bréda (1996) found also a low Ω for an oak forest. The average value of 0.92 for $(1-\Omega)$ indicates that the relative change of forest transpiration caused by the closing or the opening of the stomata will be 0.9 times the fractional change of the canopy conductance g_c. This shows that the canopy of the forest Aelmoeseneie is closely coupled to the atmosphere and that transpiration of this mixed forest ecosystem is mainly controlled by the stomata of the leaves.

4.2 Comparison of a single-layer and a multi-layer model approach for the calculation of forest evapotranspiration

4.2.1 Introduction

Models describing forest evapotranspiration have been developed in many scientific disciplines such as plant physiology, ecology, meteorology, hydrology and soil science. Each of these disciplines applies its own methodology and studies evapotranspiration at its own specific level of interest, resulting in a large diversity of forest evapotranspiration models. Other reasons for this large diversity are the different aims of the models, the different spatial and temporal scales, and the availability of data to parameterise the models (Dekker, 2000).

A group of models are based on the energy balance, sometimes enlarged with a stomatal conductance model. Models based on the energy balance are mostly derived from the Penman equation. Usually the models (e.g. Priestly & Taylor, 1972) contain several parameters, which are dependent on species, site and scale. Monteith (1965) extended the Penman model with a stomatal conductance model. In many cases, the canopy is described as a single big leaf where canopy conductance is composed of the bulk stomatal conductance and the remaining conductance when the stomata are closed.

A second line of thinking considers the details of the canopy micro-climate explicitly. Investigation at this level of detail is essential to the plant physiologist interested in the behaviour of plants in the field, or to the hydrologist wishing to partition evapotranspiration between soil and plant canopy. Attention is usually focussed on the vertical canopy structure, because the main direction for a systematic variation of the micro-climate is in the vertical (Raupach & Finnigan, 1988). Although the canopy varies continuously in the vertical direction, it has been common sense to consider the canopy as a finite number of horizontal layers : the so-called multi-layer models. These models aim to describe not only the evapotranspiration from the entire canopy, but also the partitioning of the evapotranspiration between various parts of the canopy-soil, understory and crown for example.

Of course the price of such detail is the increased complexity in both the physical content and the data requirement of a multi-layer as opposed to a single-layer model (Raupach & Finnigan, 1988). On the other hand, single-layer models are restricted to circumstances where the detailed and complex spatial structure of the actual canopy

micro-climate is irrelevant, which is doubtful in ecosystems with a height which can easily reach 20 to 30 m as is the case for temperate deciduous forests.

Objectives of this part of the study were to parameterise and validate a single-layer and multi-layer forest evapotranspiration model as described in Chapter 1 (see respectively § 1.2.2 and § 1.2.3). The parameters needed to determine aerodynamic resistance will be analysed in somewhat more detail. Moreover, the sensitivity of both models to some input variables and parameters will be analysed as to determine which variables and parameters should receive most attention when collecting field data. Forest evapotranspiration will be simulated using the single-layer and multi-layer model for an entire year (1997). These model results will be analysed and compared with each other, with reference evapotranspiration as defined by the FAO, with several definitions of potential evapotranspiration and with literature data.

4.2.2 Methodology

4.2.2.1 The single-layer evapotranspiration model

Evapotranspiration and interception were modelled using the Penman-Monteith equation (see § 1.2.2, Equations 1.100 and 1.103). The total single-layer model (SLM) is described in Chapter I (see § 1.2.2). Extending the original model, a formulation was introduced, for time steps when only a fraction of the considered time step the canopy is wet. Therefore, two values for canopy evapotranspiration were always calculated, using (i) the actual and (ii) an infinite canopy conductance, representing respectively (i) dry and (ii) wet leaf surfaces.
Driving variables for the model runs were incoming solar radiation (R_s), air temperature (T_a), relative humidity (RH), wind speed (u) and gross precipitation (R). Other radiation quantities necessary to run the model were estimated from these standard data as follows : (i) net radiation (R_n) above the forest could be related to short-wave radiation R_s as $R_n = 0.735R_s - 37$ (Equation 1.168), (ii) photosynthetic active radiation (PAR) could be related to R_s as $PAR = 0.398R_s$, (iii) heat flux into storage in the biomass and in the air between the trees was neglected according to Samson & Lemeur (2001), and (iv) heat flux into or out of the soil was considered to be 3 % of R_n (see also Samson & Lemeur, 2001). One unit of PAR expressed in $W\,m^{-2}$ was assumed equal to 4.61 $\mu mol\ m^{-2}\ s^{-1}$ of PAR. For the parameterisation and validation of the model meteorological and physiological data sets collected during the year 1999 were used. For the sensitivity analysis and model simulations a complete, hourly meteorological data set for the year 1997 was used. The

meteorological variables in this data set were measured on the tower in the forest Aelmoeseneie (see § 2.2) and missing data were derived from the nearby meteorological station at Melle operated by the Royal Meteorological Institute of Belgium.

4.2.2.2 The multi-layer evapotranspiration model

The multi-layer model (MLM) for calculation of transpiration, interception and soil evaporation is described in Chapter I (see § 1.2.3). Five different layers are considered, namely three upperstory layers, an understory layer and a soil layer. Just as done for the single-layer model two values for canopy evapotranspiration were always calculated, using (i) the actual and (ii) an infinite canopy conductance, again representing respectively (i) dry and (ii) wet leaf surfaces. The wet fraction of the canopy was calculated from rainfall data and the interception parameters (see § 1.2.3.3).
The multi-layer model is driven by the same variables as the single-layer model. For the vegetation layers heat flux into storage in the biomass and in the air between the trees was neglected according to Samson & Lemeur (2001)(see §1.2.3). For the parameterisation, validation, sensitivity analysis, and model simulation, the same data sets were used as for the single-layer model.

4.2.2.3 Parameterisation of the models

The parameterisation, or parameter estimation, of the single-layer and multi-layer model is based on the data analyses carried out and reported in previous chapters, and from literature. A summary of the used parameter values is presented in Table 4.5 and Table 4.6, for the SLM and MLM respectively.

Forest transpiration obtained from upscaled sap flow measurements (see § 3.4) during time periods when leaves were completely dry was used to calculate canopy conductance (g_c) by inverting the Penman-Monteith equation (see § 4.1). Most of the observed variation of g_c could be explained from actual light and humidity conditions above the forest using a Lohammar-type equation. Parameter estimation of the canopy conductance sub-model was done by adaptation of the $g_{c,max}$ value, because of the doubtful nature of this value (see § 4.1) and because of the difference between measured and reported literature values (see § 4.1.3). Also for the simulation of stomatal conductance in the MLM the same Lohammar-type equations as for simulation of g_c were used, in contrast to the equation reported in § 4.1. The use of

Lohammar-type equations facilitates the comparison of parameters with those reported in literature for other European forest sites. Because of the difference in $g_{s,max}$ between the fitted values reported in Table 4.3 and the experimentally obtained values reported in Table 1.10, and because of the doubtful nature of the former (see § 4.1), the stomatal conductance sub-model was initialised with the porometer values reported in Table 1.10. Further parameterisation of the stomatal conductance sub-model was done by validation of the transpiration results with upscaled sap flow data. This was done for a uniform (see Table 1.2 and § 3.4) beech, oak and ash forest separately. When the model was parameterised for each of these uniform forests, it was applied for the forest Aelmoeseneie. During parameterisation the relative difference in stomatal conductance between the different canopy heights, as reported in Table 1.10 for beech, was considered as a conservative value.

Table 4.5 Selected functions and parameter values for the calculation of evapotranspiration with the single-layer model. Symbols are: z_0: roughness length; d: zero plane displacement; h_c: canopy height; S_{cap}: interception capacity of the vegetation ; p: throughfall coefficient; c: coverage of the vegetation; $g_{c,max}$: maximal canopy conductance.

Parameter	Value and/or function		Reference
	Summer	Winter	Hörmann et al., 1996;
z_0/h_c (-)	0.10	0.09	De Bie ,1999,
d/h_c (-)	0.83	0.62	Samson & Lemeur, 2001
	Summer	Winter	Herbst et al., (1999)
S_{cap} (mm)	1.28	0.8	
p (-)	0.25	0.90	
c (-)	0.8	0.3	
Function for canopy conductance	$g_c = g_{c,\max}\frac{PAR}{PAR+a}(b - c\ln D)$		This work (see § 4.1)
$g_{c,max}$ (m s^{-1})	0.0165		
Parameter a (µmol m^{-2} s^{-1})	119		
Parameter b (m s^{-1})	1.259		
Parameter c (m s^{-1} hPa^{-1})	0.383		

The water vapour conductance of the soil surface (g_{soil}) in the forest was calculated based on a relationship reported by Herbst et al. (1999). This relationship was calculated from measurements of soil evaporation and micro-climate near the floor of a beech forest, and exhibited an exponential decrease with time since the last rainfall event. On average, the soil surface conductance was in the same order of magnitude as the canopy conductance.

Parameters for the interception sub-model were taken from literature, because (i) throughfall collectors were often blocked because of the high dust concentration at the forest floor, and because heavy rains were usually accompanied by high wind speeds causing leaves and branches to accumulate in the collectors; and (ii) because the experimental set-up for measuring stem flow (number of collectors and frequency of sampling) did not allow to accurately calculate the necessary parameters. Crockford & Richardson (2000) concluded from their review that it is difficult to draw general conclusions about the interception loss by a particular forest type because it usually depends on the type of rainfall and on other meteorological

Table 4.6 Selected functions and parameter values for the calculation evapotranspiration with the multi-layer model. Parameters of functions mentioned in Table 4.5 and not mentioned in this table, are identical. Symbols are: k_{Rn}: extinction coefficient for net radiation ; $g_{s,max}$: maximal stomatal conductance ; d_c : characteristic dimension ; d_{cs} : characteristic or effective dimension of the soil; t: time since last rainfall event.

Parameter	Value and/or function				References
	Beech	Oak	Ash	Underst.	
k_{Rn} (-)	0.592				Baldocchi et al., 1984
Function for stomatal conductance	$g_s = g_{s,\max}\frac{PAR}{PAR+a}(b - c\ln D)$				This work (see § 4.1)
$g_{s,max}$ (m s^{-1})	0.0049	0.0039	0.0093	0.0019	
Parameter a (µmol m^{-2} s^{-1})	245	30	120	119	
Parameter b (m s^{-1})	1.249	1.276	1.268	1.259	
Parameter c (m s^{-1} hPa^{-1})	0.389	0.376	0.383	0.383	
Function for leaf boundary layer resistance	$r_b = 307\sqrt{\frac{d_c}{u}}$				Vanoverbeke, 1998; This work
d_c (m)	0.050	0.045	0.035	0.050	
Function for the resistance of the soil-vegetation interface	$r_{sv} = 108\sqrt{\frac{d_{cs}}{u}}$				Personal communication M. Aubinet, Gembloux, 1999
d_{cs} (m)	0.040				
Function for soil surface conductance	$g_{soil} = a\,b^t$				Herbst et al., 1999
t (h)					
Parameter a (m s^{-1})	0.00347				
Parameter b	-0.0212 D + 0.8485				

conditions during the study period. The major difficulty is the reliable estimation of the throughfall (where it is not unusual for measured throughfall to exceed the rainfall value). In forests where stemflow volumes are large enough to significantly influence the interception values, the methodological approach is even more difficult.
As mentioned before, all relevant equations and parameter values are summarised in Table 4.5 and 4.6, for the SLM and MLM respectively. It was assumed that rainfall interception and soil evaporation were the same throughout the forest Aelmoeseneie. Model simulations are executed for the forest Aelmoeseneie, considering a similar species composition as was done in § 3.4 when scaling up sap flow measurements to the level of the forest Aelmoeseneie. Hourly time steps were used.

4.2.2.4 Estimation of zero plane displacement and roughness length

Just as was mentioned by Businger (1956), and as was explained in Chapter 1, the aerodynamic resistance for momentum (r_{am}, s m^{-1}) of the canopy can be calculated as:

$$r_{am} = \frac{\left[\ln\left(\frac{z-d}{z_0}\right)\right]^2}{k^2 u} \qquad (1.90)$$

where d is the zero plane displacement (m) and z_0 is the roughness length (m). In Chapter 1 a theoretical distinction was made between the aerodynamic resistance for momentum (r_{am})(Equation 1.90) and sensible heat flux (r_{ah})(Equation 1.91). To be able to calculate r_{ah}, the roughness length for sensible heat flux z_{0h} should be known. Whereas z_0 can be inferred easily from the wind profile relationship, only an estimate of z_{0h} can generally be obtained (Troufleau et al., 1997). This means that the value of z_{0h}, and thus r_{ah}, is uncertain. Therefore, and also because it is commonly practice when calculating forest evapotranspiration (e.g. Herbst, 1995) r_{am} and r_{ah} are assumed to be equal (see also § 4.1.2.1). Before it was already assumed that the aerodynamic resistance for sensible heat flux equals the aerodynamic resistance for latent heat flux (see § 1.1.2.4).

Wind speed was measured at four different heights above the canopy as well in foliated as in non-foliated conditions (Figure 4.7). Therefore a simple method could be used to calculate d

$$\frac{u_1 - u_2}{u_3 - u_4} = \frac{\ln(z_1 - d) - \ln(z_2 - d)}{\ln(z_3 - d) - \ln(z_4 - d)} \qquad (4.11)$$

where the subscript refer to measurement levels (Monteith, 1973; Landsberg & Jarvis, 1973). Equation 4.11 can be easily solved using an iterative procedure. When ln(*z-d*) is plotted against wind speed (*u*), the corresponding value of z_0 can be found from the intercept. Zero plane displacement and roughness length are estimated from ten minutes values for the period 3 till 31 August, 1999, and the period 3 till 22 December, 1999, respectively representing foliated and non-foliated conditions.

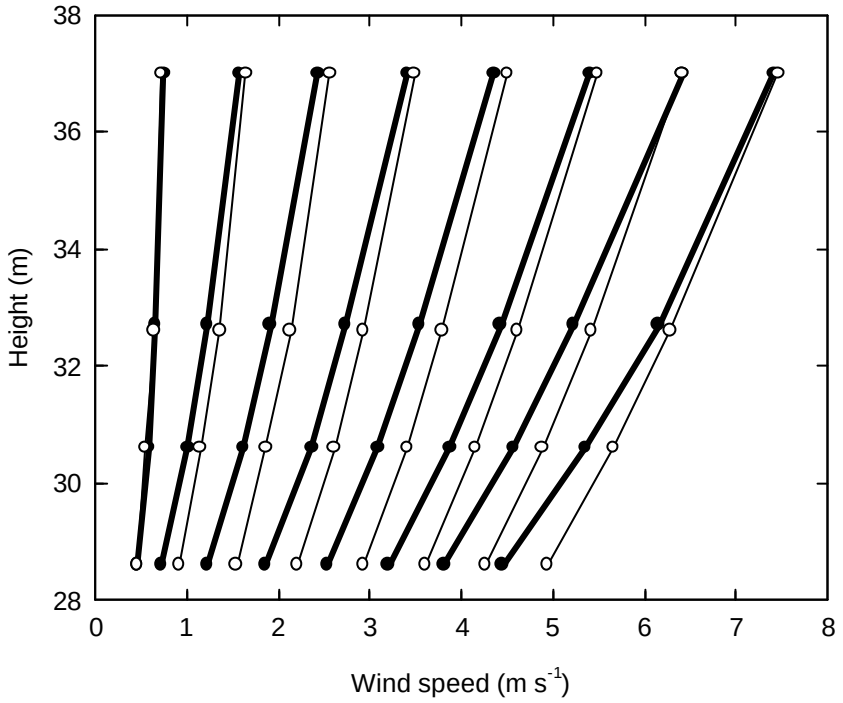

Figure 4.7 Mean wind profiles above the crown canopy (top of canopy is 27 m) for foliated and non-foliated conditions, and for different wind speed classes (measured at 37 m)(wind speed classes are: 0–1, 1-2, 2-3, 3-4, 4-5, 5-6, 6-7 and 7-8 m s^{-1}). Mean values are calculated from ten minutes values. Filled symbols and thick lines indicates foliated conditions, and open symbols and thin lines indicate non-foliated conditions. The measurement period was 3 till 31 August, 1999, and 3 till 22 December, 1999, for the foliated and non-foliated conditions respectively.

Because of the turbulence instigated by the height and roughness of the canopy surface, above forests temperature gradients are generally small (Dolman, 1986). As a result, Richardson numbers (see § 1.1.2.2) remain close to zero and “it is questionable whether any real improvement is obtained in the estimation of z_0 and *d* for forest by the application of empirical stability corrections (e.g. Dyer & Hicks, 1970; Pruit et al., 1973 see § 1.1.2.2) obtained for completely different kinds of surface such as grass and stubble” (Jarvis et al., 1976). Furthermore, stability corrections on aerodynamic resistances prove to be of little numerical importance in evaporation

modelling, according to Shuttleworth et al. (1984). In view of these arguments stability influences were ignored.

4.2.2.5 Calculation of reference crop evapotranspiration

Reference crop evapotranspiration (*ETo*) is the evapotranspiration rate from a reference surface, not short of water. The FAO assumes “a hypothetical reference crop with an assumed crop height of 0.12 m, a fixed surface resistance of 70 s m^{-1} and an albedo of 0.23”(Allen et al., 1998). For the calculation of the reference crop evapotranspiration, *ETo* (mm h^{-1}), the following formula was used (Allen et al., 1998):

$$ETo = \frac{0.408\Delta}{\Delta + g(1+0.34u)}(Rn - G) + \frac{g\left[37/(T_a + 273)\right]}{\Delta + g(1+0.34u)}u\left[e_s(T_a) - e_a\right] \qquad (4.12)$$

where R_n is the net radiation at the grass surface (MJ m^{-2} h^{-1}), G is the soil heat flux density (MJ m^{-2} h^{-1}), T_a air temperature (°C), D is the slope of the saturation water vapour pressure curve at T_a (kPa $°C^{-1}$)(Equation 1.165), g is the psychrometric constant (kPa $°C^{-1}$), $e_s(T_a)$ is the saturation vapour pressure of the air at T_a (kPa), e_a is the actual vapour pressure (kPa) and u is the wind speed measured 2 m above the grass surface (m s^{-1}).

The psychrometric constant was also calculated according to Allen et al. (1998) as:

$$g = \frac{c_p P_{atm}}{\varepsilon_{v/d}\, l} \qquad (4.13)$$

where c_p is the specific heat of the air at constant pressure (1010 J kg^{-1} $°C^{-1}$), P_{atm} is the atmospheric pressure (kPa)(Equation 1.161), $\varepsilon_{v/d}$ is the ratio of molecular weight of water vapour/dry air (0.622), and l is the latent heat of evaporation (J kg^{-1})(Equation 1.166).

According to Allen et al. (1998) hourly soil heat flux density G can be approximated during daylight and nighttime periods as 10 and 50 % of R_n respectively.

Short-wave radiation, air temperature, relative humidity and wind speed were measured at the most nearby meteorological station operated by the Royal Meteorological Institute of Belgium. This was the meteorological station at Melle at a distance of about 1 km of the experimental tower in the forest Aelmoeseneie. Net radiation was calculated from short-wave radiation as explained in § 1.2.2.2.

4.2.2.6 Sensitivity analysis

A simple sensitivity analysis was performed on both the SLM and MLM, in order to evaluate the relative sensitivity of both models with respect to their parameters and input variables. The relative sensitivity was expressed by a dimensionless index of sensitivity (b_{sens}) for each of the parameters and variables tested (Raupach & Finnigan, 1988; Friend, 1995; Lankreijer, 1998)

$$b_{sens} = \frac{\frac{X_I - X_o}{X_o}}{\frac{P_I - P_o}{P_o}} \qquad (4.14)$$

where X_I is the simulated evapotranspiration value corresponding with the changed parameter value P_I, and X_o is the simulated evapotranspiration value at the reference value P_o. A change in the parameter P will result in a directly proportional change in the simulated value X when b_{sens} = 1. Thus, an absolute value much less than one implies a low sensitivity of the model to that parameter or variable.

The parameters included in the model were tested for the effect of a 10 % change in their values (Table 4.7). For climatic input variables, a change of 10 % is in most cases unrealistic, and the change was set to the measurement accuracy of the corresponding sensor (Table 4.7).
The sensitivity analysis was performed for the whole year 1997, using hourly time steps.

Table 4.7 Imposed change on the climatic variables (R_s: short-wave radiation; T_a: air temperature; *RH*: relative humidity; *u*: wind speed), structural parameters (*LAI*: leaf area index; z_0: roughness length; *d*: zero plane displacement), and an ecophysiological parameter ($g_{s,max}$ or $g_{c,max}$ for the single-layer and the multi-layer model respectively) for the sensitivity analysis of the single-layer and multi-layer model.

Variable or parameter	Induced change
R_s	2.5 %
T_a	1 % (min 0.1 °C)
RH	10% (max 100 %)
u	1 % + 0.1 m s^{-1}
LAI	10 %
z_0	10 %
d	10 %
$g_{s,max}/g_{c,max}$	10 %

4.2.3 Results and discussion

4.2.3.1 Estimation of aerodynamic resistance

The wind profiles above the crown canopy for foliated and non-foliated conditions, and for different wind speeds classes is illustrated in Figure 4.7. At the lowest wind speeds no logarithmic wind speed profile was observed, and wind profiles did not differ in shape during foliated or non-foliated conditions. This observation was explained by the stalling errors of the anemometers. At higher wind speeds the wind profile differed for foliated and non-foliated conditions. As foliage density decreased, the mean area of momentum sink also decreased, causing the wind profile to evolve as observed in Figure 4.7. The measurements also illustrated that during winter the height of the anemometers should be lowered, as was done by Dolman (1986).

Wind profiles were selected by excluding values of d which were an artefact of the computing procedure. Thus, only values of d contained in the interval 0.0 – 27.0 m were used. This selection criterion was incorporated, because the physical interpretation of values lying outside this interval seems unclear. For foliated conditions 2032 profiles were used; for non-foliated conditions 2573. Figure 4.8 shows that estimates of d decreased as wind speed increased, where the reverse was observed for z_0. A general lowering of the profile during the non-foliated period, as can be inferred from Figure 4.7, can also be seen in the estimates of d and z_0 illustrated in Figure 4.8. A lowering of the profile means that the height in the canopy where wind speed theoretically would become zero (at $d + z_0$) decreases.

For the calculation of aerodynamic resistance in the SLM and MLM a dependence of d and z_0 on wind speed is not considered, because sensitivity analysis (see § 4.2.3.3) revealed that the models are not sensitive to these parameters. Moreover, wind speeds during the growing season 1999 were in 87 % of the time below 4 m s^{-1}, so that the variation in d and z_0 was not large (see Figure 4.8). So, considering all wind speed measurements together, calculations revealed that for the foliated period d and z_0 equals respectively 0.83 h_c and 0.1 h_c, with h_c being the canopy height (De Bie, 1998; Samson & Lemeur; 2001). Because during the non-foliated period the height of the anemometers was not lowered, d and z_0 were not calculated from experimental data collected during this period. For the determination of the values of d and z_0 during non-foliated conditions, the same ratio was considered, as found by Dolman (1986), for d and z_0 between foliated and non-foliated conditions. Values for d and z_0 during non-foliated conditions were thus 0.62 h_c and 0.09 h_c respectively.

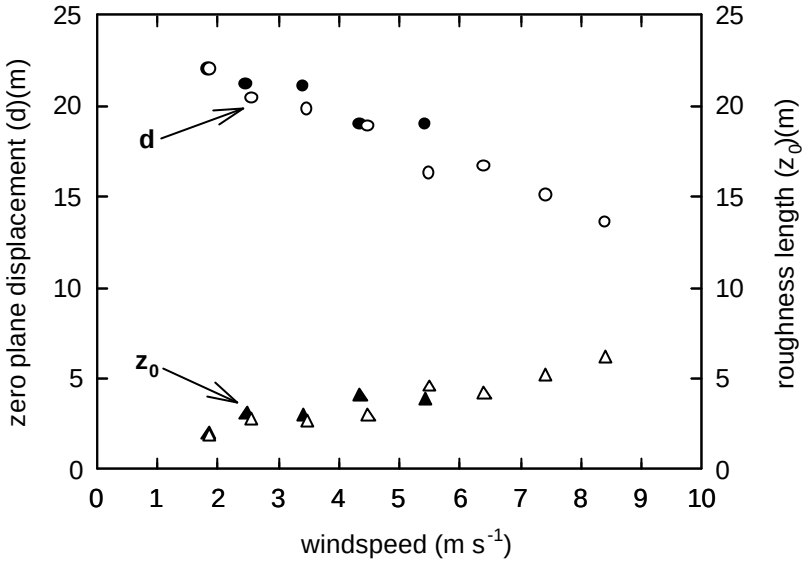

Figure 4.8 The change of zero plane displacement (*d*)(circles) and roughness length (z_0)(triangles) with wind speed for foliated (filled symbols) and non-foliated (open symbols) conditions. The measurement period was 3 till 31 August, 1999, and 3 till 22 December, 1999, for the foliated and non-foliated conditions respectively.

The rather high value found for d, 0.83 h_c for foliated conditions can probably be attributed to the structure of the forest that is very dense. Furthermore, the leaves are mainly concentrated in the top of the canopy (see Table 1.2), providing an effective momentum sink. From Figure 4.8 it can be seen that values of z_0 for foliated and non-foliated conditions do not differ. This was also observed by Dolman (1986) but was not what one would generally expect. Because, according to Thom (1976) the roughness length is a measure of the effectiveness of the canopy as a momentum absorber, it can be concluded that the leafless canopy acts thus as effective as momentum absorber as the foliated canopy.

The aerodynamic resistances in foliated and non-foliated conditions are of the same order of magnitude. This implies that, other environmental variables remaining the same, the evaporation rates from wet surfaces in summer and winter may be of the same order of magnitude.

4.2.3.2 Model validation

To validate the two models with independent field data, the same data set as was used for the validation of the inverted canopy conductance (see above § 4.1), and was obtained from sap flow measurements scaled up to the level of the forest Aelmoeseneie (see § 3.4). Only periods when leaf surfaces were dry were selected, because interception evaporation can not be measured with sap flow sensors. Neither was the model validated for the winter period, as no measurements of soil evaporation were available. For the validation of the MLM, soil evaporation was extracted from forest evapotranspiration (ET), as the sap flow sensors did not measure soil evaporation.

Values of hourly transpiration obtained from sap flow measurements scaled-up to the level of the forest Aelmoeseneie (see above § 3.4) were plotted against transpiration, simulated with the SLM and MLM (Figure 4.9). This figure (Figure 4.9) illustrates that the model predictions matched quite well the measured values. Only a slight, but obviously systematic overestimation at lower transpiration values and an underestimation at higher transpiration values remains unexplained, for as well SLM as MLM. Most likely, uncertainties in the modelling of canopy and stomatal conductance (see § 4.1) may have caused these deviations.

4.2.3.3 Model sensitivity

The relative sensitivity values, $\boldsymbol{b}_{sens}$, for the imposed changes on the variables and parameters as listed in Table 4.7 for the SLM and MLM are shown in Figure 4.10. Values presented in Figure 4.10 are for the evapotranspiration integrated over the year 1997. Both models showed a very low sensitivity for wind speed and air temperature. The models were somewhat more sensitive to short-wave radiation, but both models were very sensitivity to relative humidity (Figure 4.10). The difference in sensitivity of both models to R_s and RH indicated that the aerodynamic term, driven by the vapour pressure deficit of the air, is much more important than the energy term (see Equation 1.102) for the determination of forest evapotranspiration.

As was mentioned before the sensitivity of both models to parameters used in the estimation of the aerodynamic resistance, i.e. the roughness length and the zero plane displacement, was very low for both models. The models were somewhat more sensitive to the determination of the zero plane displacement. However, as mentioned before, for the most frequent wind speeds (see § 4.2.3.1), the variation in roughness length or zero plane displacement is rather limited (see Figure 4.8), and

thus also the variation in ET. This supports the use of one fixed value of d and z_0 when calculating ET. Although the low sensitivity of the models to the roughness parameters, it is recommended to lower the actual heights of the anemometers for non-foliated conditions. Both models seem to be more sensitive to variations in the value of total LAI, especially the multi-layer model. The importance of the LAI can be explained by its influence on the canopy conductance and the interception of rain (see e.g. § 1.2.2.3 and 1.2.2.4). Whereas the maximal LAI during the growing season is believed to be reasonably well estimated (Mussche, 1997; Samson et al., 1997a), deviations from the estimated seasonal LAI evolution (Figure 1.11) can occur, especially at the beginning and end of the growing season. Also LAI measurements at the end of the growing season do not necessarily yield physiological active LAI, and thus LAI during this period can be seriously overestimated. On the other hand the model output is rather independent of the assumed vertical LAI distribution (data not shown).

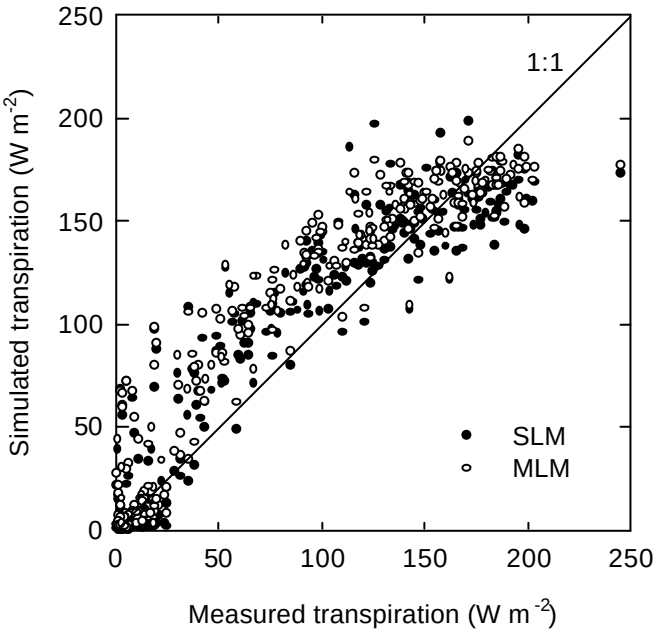

Figure 4.9 Upscaled sap flow measurements (measured) versus modelled hourly transpiration (T) of the forest Aelmoeseneie for selected days during the 1999 growing season. Filled circles indicate modelled ET with the single-layer model (SLM), and open circles indicate modelled ET with the multi-layer model (MLM). Observed relationships are: T_{SLM} = 1.01 T_{meas} (r^2 = 0.87); T_{MLM} = 1.07 T_{meas} (r^2 = 0.86)(n = 331).

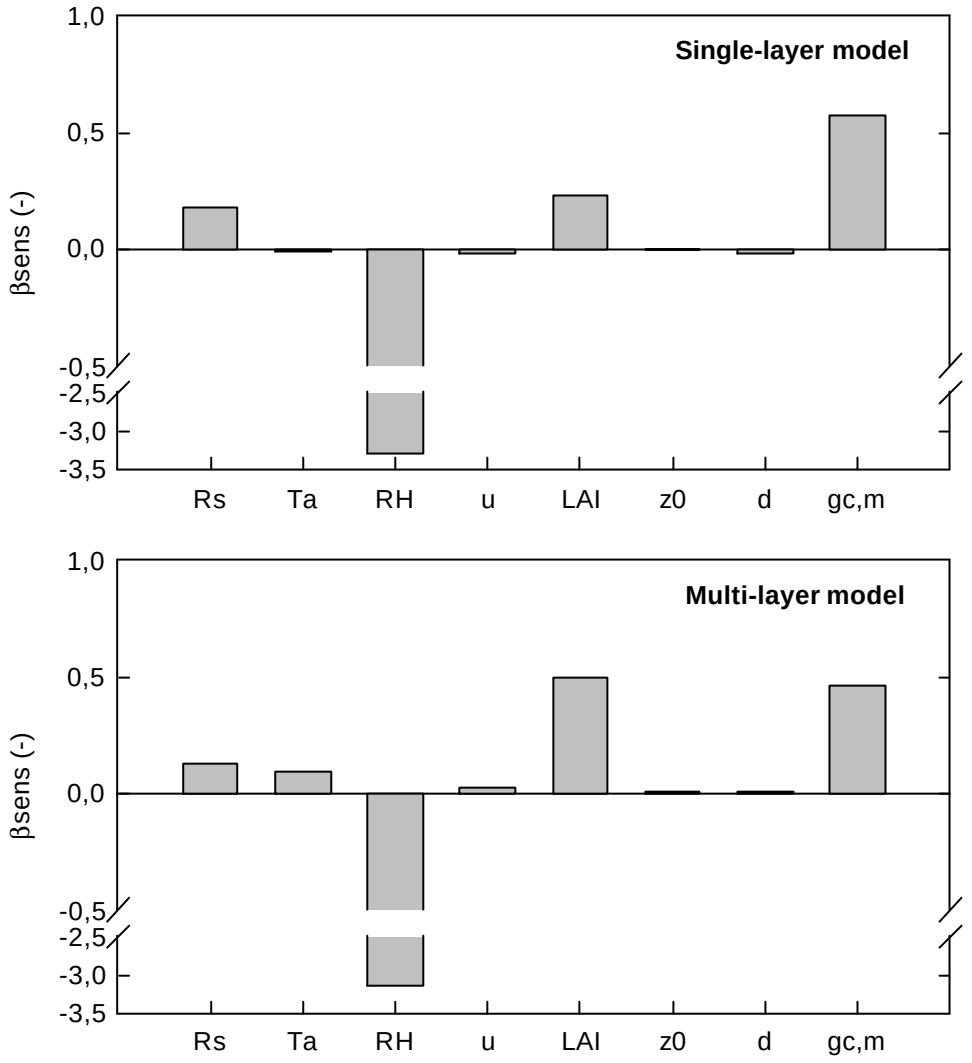

Figure 4.10 Relative sensitivity, *bsens* (-), of the single-layer (above) and multi-layer model (above) for the imposed variation, on the climatic variables (R_s: short-wave radiation; T_a: air temperature; *RH*: relative humidity; *u*: wind speed), structural parameters (*LAI*: leaf area index; z_0: roughness length; *d*: zero plane displacement), and an ecophysiological parameter ($g_{s,max}$ or $g_{c,max}$ for the single-layer and the multi-layer model respectively) as listed in Table 4.7. Presented results are for the year 1997.

Both models seem to be sensitive to the value of the maximal canopy/stomatal conductance, with the highest sensitivity observed for the single-layer model. The models were also rather sensitive (data not shown) to the other parameters of the canopy or stomatal conductance function (see Table 4.5 and 4.6). So, when estimating evapotranspiration, maximal canopy/stomatal conductance and the other

parameters of the used functions for the calculation of canopy/stomatal conductance are best derived from measurements collected in the forest under study.

The sensitivity of both models to the parameters and variables presented in Figure 4.10 is rather similar. For the variables (T_a,u) and parameters (z_0,d) for which the lowest sensitivity were measured, the signs of the observed sensitivity were reversed. However, because of the low sensitivities observed this will only be of minor importance to explain differences in model behaviour.

As is illustrated in Figure 4.10, sensitivity to certain parameters and variables depends largely on the model, e.g. Lankreijer (1998) found for the model he used a high dependency on air temperature and a very low dependency on air humidity, while for our models the reverse was observed. However, Lankreijer (1998) also found that transpiration strongly depended on parameters determining surface conductance. It should be mentioned that the sensitivity values (b_{sens}) mentioned by other authors are sometimes calculated for a single condition (fixed meteorological conditions)(e.g. Raupach & Finnigan, 1988; Lankreijer, 1998), whereas in this study, b_{sens} was calculated for a complete growing season (based on hourly time steps). The advantage of this approach is that a more general and reliable b_{sens} is obtained, as it is calculated for many different combinations of environmental input parameters.

Prior knowledge of the model that will be used and the sensitivity of this model to its parameters can help focussing field measurements. From our sensitivity analysis, it is clear that a lot of attention has to be paid to measurements of relative humidity of the air. Therefore, each platform should be equipped with ventilated psychrometers to obtain vapour pressure deficits and reliable air temperatures at different canopy heights. Although capacitive air humidity sensors are easier to keep operational, ventilated psychrometers are preferred. Moreover, the canopy conductance sub-model should be further checked, either by measurements on canopy level (e.g. Bowen ratio), individual tree level (sap flow), and the level of individual leaves (porometer or gas exchange measurements). Although a detailed analysis was already carried out (Mussche, 1997), a correct determination of LAI throughout the growing season still remains important.

4.2.3.4 Model predictions

Daily sums of simulated evapotranspiration, transpiration, soil evaporation and interception for 1997 are presented in Figure 4.11. Reference crop evapotranspiration (*ETo*) was calculated according to the FAO-methodology (Allen et al.; 1998) and was during periods out of the growing season (LAI=0) always

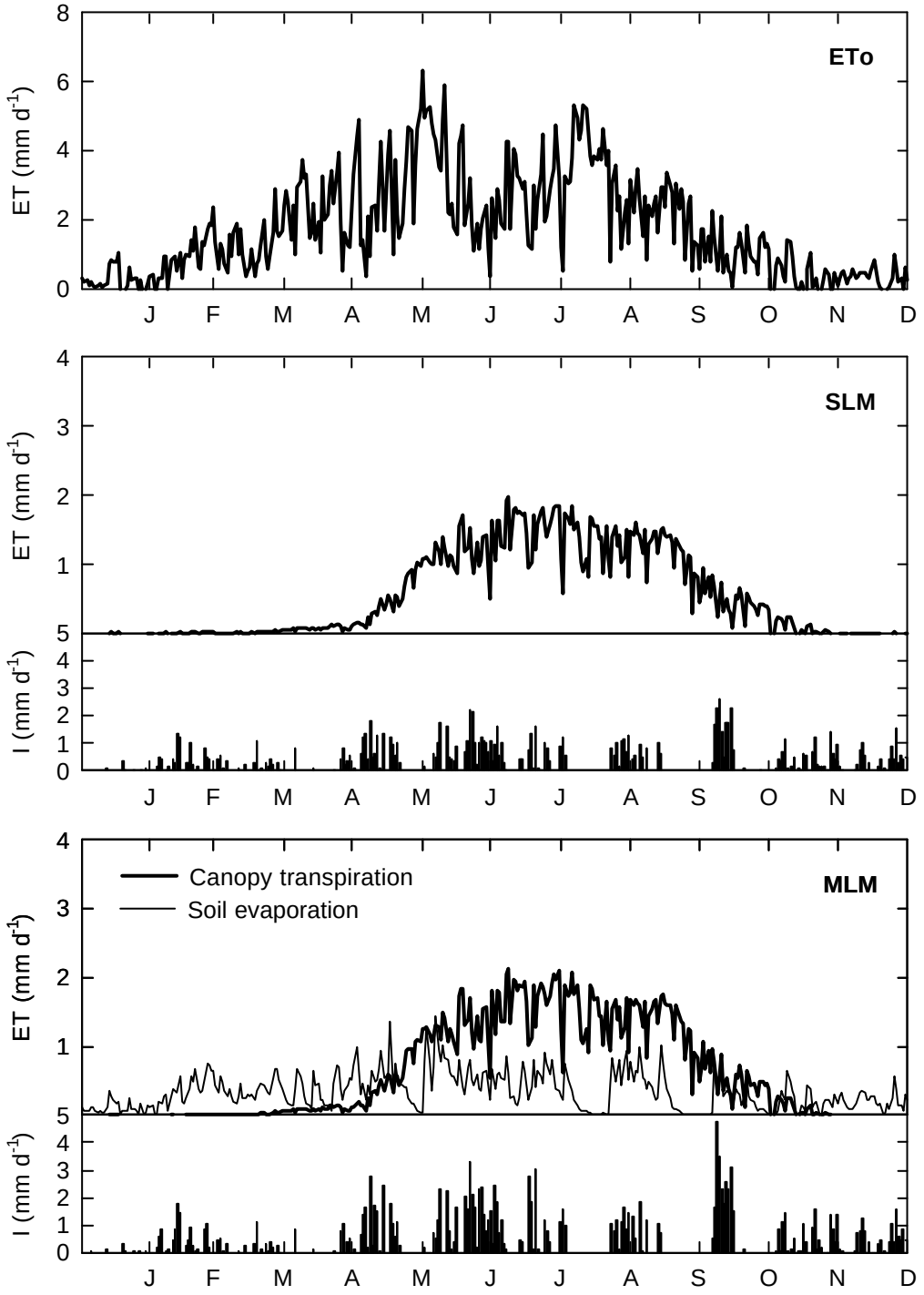

Figure 4.11 Modelled daily sums of reference crop evapotranspiration (*ETo*), evapotranspiration (ET) and interception evaporation (*I*) calculated with the single-layer model (SLM) and canopy transpiration, soil evaporation and interception evaporation calculated with the multi-layer model (MLM) for the year 1997. Values simulated with the SLM and MLM refer to the forest Aelmoeseneie.

higher than the values calculated with the SLM. The *ETo* does not include evaporation of intercepted rainfall. Maximum values of transpiration, as simulated with both the SLM and MLM are rather low. As was also seen in Figure 4.9, the transpiration simulated by both methods is very similar, indicating that a single-layer approach can suffice for modelling forest transpiration.

The difference in interception values was pronounced between the SLM and MLM, i.e. 110 and 151 mm y^{-1} respectively, which can be explained by the different layers taken into account in the MLM (three upperstory and one understory layer). The peak values of daily interception evaporation were in summer of similar range and sometimes higher compared to transpiration. This was also observed by Herbst et al. (1999). Interception should be studied in detail, as its contribution to total forest evapotranspiration is not negligible. In particularly more attention should be given to throughfall and stemflow measurements. Throughfall collectors should be intensively followed, i.e. cleaned at least several times a week, whereas more stemflow collectors should be installed and connected to automatically registering tipping bucket raingauges. Just as interception evaporation, also the soil evaporation seemed to be important throughout the whole year. In contrast, Herbst et al. (1999) mentioned that soil evaporation was insignificant during summer, but that it reached values higher than the ones observed in this study temporarily in spring prior to leaf unfolding. Although soil evaporation decreased during drier periods (e.g. during August in Figure 4.11), it is believed that daily soil evaporation is not correctly simulated as the amount of throughfall was not considered. Only the occurrence of a rain event was used to consider re-wetting of the soil. In future, also soil evaporation should be studied in detail.

Considering the annual sums of total evapotranspiration, i.e. *ETo* = 637 mm y^{-1}, *ET(SLM)* = 307 mm $y^{-1}$and *ET(MLM)* = 493 mm y^{-1}, it is clear that *ETo* results in the highest value, especially knowing that interception evapotranspiration was not taken into account. One reason for this high value is that in this case the value of the surface resistance is considered to be fixed at 70 s m^{-1}, for both day and night periods. This assumption is not realistic. On the other hand annual ET(SLM) is much lower than ET(MLM). From Table 4.8, showing the different components of the multi-layer forest evapotranspiration, it can be seen that this large difference can almost totally be attributed to soil evapotranspiration. Table 4.8 indeed illustrates that canopy transpiration calculated with the SLM and MLM is very comparable (see also Figure 4.11). From the above we may conclude that a single layer approach is not accurate enough to simulate forest ET, when canopy conductance is inverted from sap flow measurements, thus only taking into account transpiration values. And because in a dense forest the temporal dynamics of transpiration and soil evaporation is totally different; it is questionable whether one formula can be found which integrates and describes accurately the conductances that drive these two

processes. Therefore, a multi-layer approach, as developed in this study seems to be best suited, because at least a differentiation is made between canopy transpiration and soil evaporation.

Interception evaporation was sometimes higher than transpiration of the same layer. The amount of interception depends, among other variables, on the amount of precipitation and the characteristics of the rain events, and thus can be highly variable from year to year. Moreover, rainfall is not only intercepted during the growing season, but also outside this period, when precipitation is intercepted by twigs, branches and stems. These model simulations of understory transpiration are of the same magnitude than the understory transpiration estimated from sap flow measurements (see § 3.4).

With respect to the use of the SLM and MLM it can be concluded that the SLM suffice to estimate forest transpiration, because simulated transpiration rates are very comparable for the SLM and MLM approach (see Figure 4.11). The main advantages of a SLM are that it requires less input parameters, and that it is easier to apply than a MLM. On the other hand, when estimates of forest evapotranspiration (vegetation and soil) should be known at least a two layer approach is preferred. An alternative could be the use of a SLM with as input surface conductance instead of canopy conductance. However, as mentioned before, it is questionable whether surface conductance will accurately simulate the two totally different processes of soil evaporation and transpiration, especially in a dense forest. When the necessary input data are available a MLM approach is advisable, because it can explain intra-canopy differences and clarify overall canopy behaviour. Moreover, when water and carbon fluxes are estimated by using one coupled model, also a MLM is preferred. This is due to the radiation extinction in the canopy (see § 1.2.1) and the non-linearity of photosynthesis in response to this radiation (see § 1.1.1.3) requiring a MLM approach.

Table 4.8 Modelled annual sums of transpiration and interception evaporation (*I*) for the different canopy layers, soil evaporation and total evapotranspiration (ET) for the forest Aelmoeseneie simulated with the multi-layer model. All values in mm y^{-1}, for the year 1997. (-) indicates that this value was not calculated in the model. The canopy of the upperstory is divided in an upper, middle and lower layer.

	Upper	Middle	Lower	Understory	Soil	Total
ET	120	63	11	22	126	341
I	80	35	18	18	-	151

According to the FAO-methodology (Allen et al., 1998) true or actual crop evapotranspiration is calculated by multiplying reference crop evapotranspiration (*ETo*) with a crop factor (K_{crop}). As in this study both the *ETo* and the actual crop evapotranspiration (SLM and MLM calculations)(Figure 4.11 and Table 4.8) are known, K_{crop} values are found by the ratio. Monthly K_{crop} values were calculated and are presented in Table 4.9. Because *ETo* does not consider interception evapotranspiration, K_{crop} values were only calculated for dry periods and, hence, can only be used for these periods. At the beginning and end of the growing season K_{crop} values were lower than in the middle of the growing season which reflects the higher LAI and forest ET during this period. Also the crop coefficients mentioned in Allen et al. (1998) show the same seasonal trend. Outside the growing season, K_{crop} values indicate the conversion from *ETo* to forest soil evaporation.

Table 4.9 Mean monthly crop factors (K_{crop}), calculated from the ratio of actual forest evapotranspiration to reference evapotranspiration, for the deciduous forest Aelmoeseneie. (M: mean; SE: standard error). Values are for the cases of single and multi-layer models, respectively SLM and MLM.

Model		J	F	M	A	M	J	J	A	S	O	N	D
SLM	M	0.08	0.06	0.07	0.04	0.19	0.49	0.59	0.47	0.60	0.44	0.36	0.06
	SE	0.03	0.03	0.03	0.01	0.02	0.07	0.03	0.06	0.03	0.03	0.07	0.03
MLM	M	0.65	0.40	0.38	0.20	0.35	0.70	0.82	0.60	0.76	0.63	0.67	0.51
	SE	0.09	0.04	0.04	0.02	0.03	0.08	0.04	0.08	0.04	0.04	0.08	0.05

Reference crop evapotranspiration (*ETo*) is the evapotranspiration rate from a reference surface, not short of water. The FAO strongly discourages the use of other denominations such as potential ET, due to ambiguities in their definitions. These ambiguities are illustrated in Table 4.10 considering several definitions of potential ET. Especially, defining potential ET as ET under conditions of infinite forest canopy conductance yields unrealistic high values (more than an order of magnitude above annual gross precipitation). Therefore, when using potential ET, this parameter has to be precisely defined, and for comparison reasons the use of *ETo* should indeed be encouraged.

4.2.3.5 Model results in comparison with literature data

Roberts (1983) observed that mid-European forests transpire in a very 'conservative' range (333 ± 36 mm y^{-1}), independent of climate, species composition and forest structure. The value obtained in this study for the SLM is somewhat lower than the mean value reported by Roberts (1983). The transpiration value obtained with the MLM corresponds well with this mean value. Also Herbst et al. (1999) reported for a beech forest in Germany annual transpiration values ranging between 326 and 421 mm, and Roberts and Rosier (1994) found an annual transpiration for a beech and ash forest in Britain of respectively 393 and 407 mm. Herbst et al. (1999) refer to a publication by Peck and Mayer (1996) who reviewed nine evapotranspiration studies of European beech forests, and found a mean evapotranspiration value of 561 mm y^{-1}. Nizinski & Saugier (1989) found for an oak forest in France an annual ET of 529 mm y^{-1}, whereas Herbst et al. (1999) for their beech forest found an annual value of 517 mm. These latter values are rather close to the values simulated with the MLM. However, the somewhat lower transpiration values obtained here, can be explained by the underestimation of the model at higher transpiration values (Figure 4.9), due to errors in the canopy conductance sub-model. Another important possible reason are errors in the sap flow measurements and in the upscaling form individual tree to canopy (see § 3.4).

Table 4.10 Comparison of annual potential ET, calculated from different definitions of potential ET to crop reference evapotranspiration (*ETo*), during the 1997 growing season. Fr_c=0: in the single layer model the canopy conductance is assumed to be infinite; Gr_c=0: evapotranspiration of a grass canopy (height 0.12m) where canopy conductance is assumed to be infinite; Fr_{min}: in the single layer model the canopy conductance is assumed to equal $g_{c,max}$. All values are in mm growing $season^{-1}$.

	ETo	Gr_c=0	Fr_c=0	Fr_{min}
ET	591	998	13455	860

Figure 4.11 showed that peak values for daily interception evaporation were higher than canopy transpiration, although available energy on rainy days is clearly much lower than during phases of maximum transpiration. On September 1997 for example (see peak in Figure 4.11) the forest interception evaporation was around 5 mm d^{-1} according to our MLM, and this value was six times as high as the net radiation on that day of 1.94 MJ m^{-2} d^{-1}. However, these values are plausible when compared with other findings (Stewart & Thom, 1973; Herbst et al., 1999) that show downward fluxes of sensible heat above wet forest canopies, and evaporation rates that exceed net radiation severalfold. This corresponds also to our findings (Table 4.10) and the

study of Martin et al. (1997), where it was demonstrated that an infinite surface conductance (representing wet leaf surfaces) would increase evaporation severalfold under a given radiation input.

The simulated interception evaporation was somewhat higher for the MLM and somewhat lower for the SLM compared to the values (116-141 mm y^{-1}) reported by Herbst et al. (1999). However, Nizinski & Saugier (1989) reported for an oak forest in France a value of 241 mm y^{-1}. The review by Crockford & Richardson (2000) concluded that interception of rainfall by forests is extremely variable and difficult to measure. Moreover, they mentioned that it is difficult to draw a general conclusion about interception losses by a particular forest type and for a particular climate. They mention that interception always depends on the type of rainfall and other specific meteorological conditions during the study period.

Kelliher et al. (1992) reported that about 10 to 20 % of the total evaporation in a closed *Nothofagus* forest comes from the soil surface. Modelled annual values of soil evaporation were similar, although slightly higher, than the values (between 79 and 120 mm y^{-1} for a beech forest, and between 82 and 135 mm y^{-1} for a black alder stand) reported by Herbst et al. (1999). This is not surprising because the same sub-model for soil evaporation was used in the SLM and MLM as in the model developed by Herbst et al. (1999). Due to the important contribution of soil evaporation to total forest ET, this sub-model still needs to be validated for the forest Aelmoeseneie.

A factor that is only indirectly incorporated in the soil evaporation sub-model is the water storage capacity of the litter on the forest floor. Roberts et al. (1980) emphasised the important role of rainfall interception in and evaporation from the litter layer. According to Crockford & Richardson (2000) interception from the litter layer can be added to forest interception values when the rainfall is sufficiently large to saturate the litter layer. Herbst et al. (1999) mentioned that their modelled amount of soil evaporation corresponded to interception storage capacities of the litter layer on the order of 2.5 to 3.0 mm which is not negligible.

GENERAL CONCLUSIONS AND RESEARCH PERSPECTIVES

Forest evapotranspiration is supposed to have a large impact on regional and global climate (Ogink-Hendriks, 1995 ; Granier et al., 2000b). Although during the last decade a large number of studies have been conducted, quantifying forest evapotranspiration and its spatial and temporal variation, under various stand conditions, it remains difficult to estimate evapotranspiration from such a complex ecosystem as forests. Not only the water consumption of these ecosystems should be estimated correctly, but detailed knowledge of the main processes influencing the evapotranspiration is also necessary, to allow predictions of possible changes in water consumption under changing climatic conditions.

The meteorological sensors in the forest Aelmoeseneie

The measurement tower in the forest Aelmoeseneie is a unique instrument that allows measuring meteorological parameters above the canopy and at different heights in the crown. Because the crowns of a beech and ash growing near the tower are mingled with this tower, several eco-physiological parameters of these species can be monitored at different heights in the crowns.

However, the experimental set-up can be improved on some points. The scientific background of some of these improvements will be mentioned somewhat further in this part. Each platform should be equipped with ventilated psychrometers to obtain vapour pressure deficits and reliable air temperatures at different canopy heights. Although capacitive air humidity sensors are easier to keep operational, ventilated psychrometers are preferred. More attention should be given to throughfall and stemflow measurements. Throughfall collectors should be intensively followed, i.e. cleaned at least several times a week, whereas more stemflow collectors should be installed and connected with automatically registering tipping bucket raingauges. It would be interesting to measure, during a foliated and non-foliated period, the extinction of net radiation. When measuring wind speed at different heights above the canopy, to retrieve parameters describing the roughness of the forest, the heights of the anemometers should be changed during foliated and non-foliated periods. Also, continuous measurements of wind speeds at different heights in the canopy, during a limited period, would allow calculating boundary layer resistances. Again it would be advisable to distinguish between foliated and non-foliated conditions.

Sap flow dynamics of upperstory and understory species

Sap flow of several upperstory and understory species in the forest Aelmoeseneie was measured using different techniques, namely the thermal dissipation technique (TDP) and the stem heat balance (SHB) method. The TDP technique was applied in the stems of the beech, oak and ash surrounding the tower, whereas the SHB technique was applied on branches in the crown of beech (several heights) and ash, and on hazel and sycamore in the forest understory. Sap flow reacted differently to vapour pressure deficit during a dry compared to a wet period, indicating an active stomatal control. Sap flow and stomatal conductance were highest in the upper crown, and lowest in the understory. Nighttime sap flow contributed about 19 and 12 % to daily sap flow for beech and ash respectively. It is also suggested that these species keep their stomata open during night.

It should be tested whether stem heat storage influences the heat balance of the branches and thus has an effect on the calculated sap flow. This can be done according to the method of Grime et al. (1995). Until now, due to mainly financial restrictions; only one individual of each species was monitored using one sensor per individual, however, it should be interesting to increase the number of monitored individuals. To optimise the basal sap flow measurements, i.e. to obtain high quality data with a minimal equipment per tree, it is recommended to analyse the radial, azimuthal and longitudinal variation in sap flux density. Especially, the radial position and length of the used TDP is of major importance to obtain reliable sap flux densities. Also more measurements on understory species should be executed as, especially for this forest layer, the exposition of the monitored branches (sun exposed or not) seems to be of major importance. Nighttime sap flow can be checked with gas exchange apparatus applied on leaf or branch level.

Hydraulic conductance of the upperstory and understory species

Diurnal variation of leaf water potential (y_l) was most pronounced for the upper crown layer, and was smallest for the understory species. Predawn y_l was comparable for all species and crown layers, except for ash, which was attributed to nighttime transpiration. Hourly total hydraulic conductance of the soil-root-leaf pathway (G_t) could be calculated, and yielded stable values between 1200 h and 1600 h. For ash G_t was 12 10^{-9} m^3 m^{-2} s^{-1} MPa^{-1}, for beech G_t was between 8 and 15 10^{-9} m^3 m^{-2} s^{-1} MPa^{-1}, and for hazel G_t amounted 4 10^{-9} m^3 m^{-2} s^{-1} MPa^{-1}. The water potential gradient between the soil and the leaf was highest for the understory species, and lower for the upperstory species to avoid cavitation of the xylem. Just as

observed by Meinzer et al. (1995) and Andrade et al. (1998) an asymptotic curve between G_t and stomatal conductance g_s was observed, which could indicate that all (woody) species respond similarly, in view of g_s, to changes in water transport efficiency.

However, this last hypothesis should best be tested by independent measurements of G_t and g_s. Stomatal conductance should thus be measured with a porometer, or even better by measuring the water vapour exchange from a part of a branch, downstream of the sensor, enclosed in a branch bag.

Water storage in stems and branches

Because sap flow was as well measured in the stem as in the branches, water storage use (WSU) could be estimated for beech and ash. Results showed that measurements from only the upper crown layer suffice to calculate WSU. A different diurnal pattern of WSU was observed for beech as for ash. Total WSU differed between the two species, ranging from a mean daily value during the season of 50 ± 6 kg for beech and 15 ± 3 kg for ash, whereas maximum values reached 161 kg and 69 kg for beech and ash respectively. Daily WSU amounted 35 $\pm$ 2 % and 28 ± 4 % of daily transpiration of beech and ash respectively. However, the day to day variation of the contribution of WSU to transpiration was high.

It should be remarked that the validity of the calculation of WSU depends on the reliability of the applied sap flow methods. Therefore, WSU is best calculated when sap flow in the crown and stem is measured using the same sap flow technique, because it is not impossible that the totally different techniques used in this study respond differently to environmental changes, and therefore yield different diurnal responses of sap flow.

Upscaling from single tree to stand level

Scaling up sap flow measured at the stem level, using sapwood area as the scaling factor ($E_{F,S}$), and sap flow measured at the branch level, using leaf area as the scaling factor ($E_{F,L}$), to the stand level did result in different transpiration values. This difference was attributed to the different measurement techniques used at branch and stem level, and to errors in the upscaling parameters. Comparing our results to the mean seasonal transpiration for NW European forests, we may conclude that $E_{F,L}$

in the present study yields more reliable results than $E_{F,S.}$ These low $E_{F,S}$ results were associated with radial gradients in sap flow for as well the ring-porous species (oak and ash) as for the diffuse porous species (beech), and by the perceived inability of sap flow probes to adequately integrate observed rates of sap flow along their length (Phillips et al., 1996; Clearwater et al., 1999). Underestimation can especially be expected for ring-porous tree species. This study confirmed the findings of Hatton et al. (1995) that the main reason of potential errors in the estimation of stand transpiration is rather due to the error in the estimation of transpiration of a single tree, than due to errors in the upscaling procedure. The low contribution of understory transpiration to total forest transpiration in the oak-beech stand was attributed to the high upperstory LAI. Due to the higher LAI of the understory in the ash forest the contribution of this layer to overall stand transpiration was five times higher than in the oak-beech forest (25 mm yr^{-1}). Our results agreed with the idea that total forest transpiration remains equal, even when forest structure differs (high upperstory transpiration plus low understory transpiration or vice versa). Thus, the understory can be regarded as an effective buffer to canopy differences.

For scaling up sap flow to the stand level an accurate knowledge of sapwood area is required, as well in a radial, azimuthal and longitudinal direction. Determination of the active sapwood can best done by measuring the radial sap flow profile, and this should be done throughout the growing season because of the possible seasonal dynamics of sapwood area. When applying the TDP technique care should be given to an appropriate needle length so that the needles are in full contact with the conducting sapwood, to avoid over- or underestimation of sap flow.

Energy balance storage terms

Five different heat storage terms were studied in the forest Aelmoeseneie. The study revealed that all terms should be taken into account for the calculation of the overall heat storage, because they all can be significant during certain weather conditions and hours. Heat storage in the biomass was estimated using surface temperatures with an infrared radiometer, which seemed to be a good method. The often-neglected photosynthetic heat storage may not be omitted. On a seasonal basis soil heat storage seemed to be the most important term. The overall heat storage showed a small tendency for releasing heat to the atmosphere during fall. Fluctuations in overall heat storage are a result of complex changes of several climatic parameters. Due to the high degree of coupling of the forest to the atmosphere, accurate measurements of overall heat storage for the determination of big leaf forest evapotranspiration are not of the utmost importance.

It would be interesting to investigate the relationship between surface temperature and stem temperature. Stem temperature should hereby be measured for as well upperstory and understory species, at different depths in the stem, and at different heights. A distinction should also be made between branches and stems. Besides for the calculation of heat storage in the vegetation, this information will also be very useful for modelling respiration of the woody biomass.

The Bowen ratio-energy balance method

During daytime negative Bowen ratio values were measured. This was due to negative Δe values, which indicated that vapour pressure near the surface was lower compared to vapour pressure at the upper measurement level. However, during active transpiration, which can be assumed during daytime, the reverse is expected. During daytime there was a strong indication for advection, which made the Bowen ratio-energy balance (BREB) method uncertain. Because Bowen data were generally close to zero, latent heat fluxes estimated from the BREB method almost equalled net radiation. In contrast to what was expected and mentioned in literature, the calculation of latent heat storage was not very sensitive to the correct determination of heat storage, just as what was observed for the single-layer Penman-Monteith approach. Only for negative Bowen ratio values heat storage becomes important for the determination of latent heat fluxes. Latent heat fluxes derived from sap flow measurements underestimated those derived from Bowen ratio data by about 65 to 70 %. This large difference was partly explained by the fact that upscaled sap flow values did not consider soil and interception evaporation, and also by measurement errors in both (sap flow and BREB) techniques, and errors in the upscaling procedure. Also, the assumed advection may partly explain the observed underestimation.

The BREB method seems to be a useful micro-meteorological method for estimating forest evapotranspiration on condition that the measurement system is improved. One of the possibilities to obtain more reliable data is the use of interchanging psychrometers, and using differential ventilated and shielded thermocouples for measuring air temperature.

Canopy and leaf conductance

The relations between canopy conductance (g_c) and climatic variables are comparable with the relations reported in literature. Also, the obtained correlation

coefficients compared well with literature values, except for ash. The behaviour of both g_c and stomatal conductance (g_s) was described in function of PAR and vapour pressure deficit (D), but no significant relationship between g_c and g_s residuals and air temperature was pointed out. The values of maximal canopy conductance ($g_{c,max}$) corresponded well with those reported in literature, although $g_{c,max}$ values obtained by different methods are difficult to compare. For low values of D and for PAR, the relationship with g_s was near linear, suggesting that D and radiation inside the canopy are the main factors limiting stomatal conductance and thus transpiration. The obtained correlations between g_s and the climatic variables were lower than those observed for g_c. This was explained by shading effects and a different micro-climate deeper in the canopy compared to that prevailing above the canopy. Values of maximal stomatal conductance ($g_{s,max}$) were an order of magnitude lower than values of $g_{c,max}$, and were low compared to those found in literature. Porometer measurements yielded higher $g_{s,max}$ values than those inferred from sap flow measurements and were closer to literature values. For as well g_c as g_s simulated values compared rather well with measured values. Although the mean radiative decoupling coefficient Ω_r was significantly lower than the decoupling coefficient Ω, the radiative transfer conductance does not seem to be of major importance for describing the coupling of the forest Aelmoeseneie. The radiative decoupling coefficient Ω_r (0.069 ± 0.001) showed that the forest Aelmoeseneie is closely coupled to the atmosphere, and that transpiration of this forest is mainly controlled by the stomata of the leaves.

When reliable values of the exchange of water vapour between the forest and atmosphere are available, from e.g. Bowen ratio measurements, surface instead of canopy conductance can be calculated. The advantage of surface conductance is that it also includes aspects of soil evaporation.

Comparison of a single-layer and a multi-layer model

Forest evapotranspiration was simulated using a single- and a multi-layer model, or respectively SLM and MLM. Although, the zero plane displacement (d) and roughness length (z_0) varied with wind speed, for the calculation of aerodynamic resistance in the SLM and MLM a dependence of d and z_0 on wind speed is not considered. Both models seemed to be very sensitive to relative humidity, to the value of the maximal canopy or stomatal conductance and to LAI. Transpiration calculated by both models was very similar, indicating that only understory and upperstory transpiration was calculated with SLM, without taking soil evaporation into account. Therefore, when only values of forest transpiration are needed a SLM will suffice. However, when estimates of forest evapotranspiration are required, at least a

two layer approach (soil and vegetation) should be used. An alternative is the introduction of surface conductance instead of canopy conductance in the SLM. When intra-canopy processes have to be analysed, a MLM is required. Also when linking a water exchange model to a carbon exchange model, a MLM approach is needed. Peak values of interception evaporation during summer were sometimes higher than transpiration values. Just as interception evaporation, soil evaporation (simulated with the MLM) seemed to be important throughout the whole year. Simulated understory transpiration was similar to the transpiration derived from sap flow measurements. Calculated crop coefficients (*Kc*) showed a seasonal trend as mentioned in literature. It was shown that the meaning of potential evapotranspiration should be described carefully due to ambiguities in the different definitions.

Prior knowledge of the model that will be used and the sensitivity of this model to its parameters can help focussing field measurements. From our sensitivity analysis, it was clear that a lot of attention has to be paid to measurements of relative humidity of the air. Moreover, the canopy conductance sub-model should be further checked, either by measurements on canopy level (e.g. Bowen ratio), individual tree (sap flow), and individual leaves (porometer or gas exchange measurements). Although a detailed analysis was already carried out (Mussche, 1997), a correct determination of LAI throughout the growing season still remains important. Also, interception should best be studied in detail as its contribution to total forest evapotranspiration is not negligible. Also attention should be given to soil evaporation which also seemed to be an important contributing process to forest evapotranspiration.